Etude géochimique des magmas acides d'Islande : mode de genèse, implications sur l'évolution géodynamique islandaise et sur la formation de la proto-croûte continentale

Erwan Martin

N° d'Ordre : D.U. **1709**

Université Blaise Pascal
(U.F.R. de recherche Scientifique et Technique)

ECOLE DOCTORALE DES SCIENCES FONDAMENTALES
N° 515

THESE

Présentée pour obtenir le grade de

DOCTEUR D'UNIVERSITE
Spécialité : Géochimie-Volcanologie

Par

Erwan MARTIN

Diplômé d'études approfondies

Etude géochimique des magmas acides d'Islande : mode de genèse, implications sur l'évolution géodynamique islandaise et sur la formation de la proto-croûte continentale.

Soutenue publiquement le 8 décembre 2006, devant la commission d'examen.

Président :	**Pierre Schiano** – *Professeur – Univeristé Blaise Pascal – Clermont-Ferrand*
Rapporteurs :	**Maury René** – *Professeur – Université de Bretagne Occidentale – Plouzané*
	Cottin Jean-Yves – *Professeur – Université Jean Monnet – Saint Etienne*
Examinateur :	**Scaillet Bruno** – *Directeur de Recherche – Institut des Sciences de la Terre – Orléans*
Directeur de thèse :	**Sigmarsson Olgeir** – *Directeur de Recherche – Clermont-Ferrand*

Maro Pontkalek

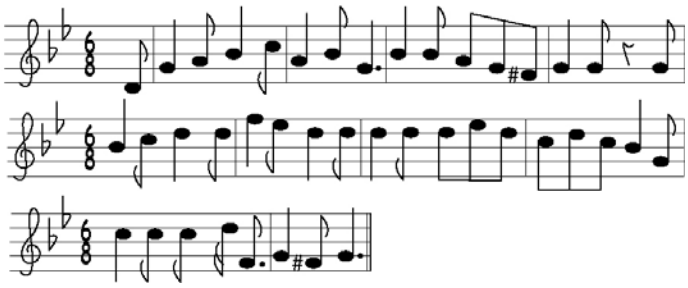

Chant populaire breton

Remerciements

En premier lieu, je tiens à remercier aussi chaleureusement que sincèrement Olgeir Sigmarsson, pour son encadrement et son amitié. Merci de m'avoir fait confiance et d'avoir bien voulu me consacrer du temps pendant ces quatre années (DEA + Thèse). Merci de m'avoir fait partager tes idées (foisonnantes) et tes façons de penser… qui bien souvent se basent sur la phrase que je garderai toujours dans mon esprit : « il n'y a pas de problème, il n'y a que des solutions ».
Enfin et surtout Merci de m'avoir fait connaître et aimer l'Islande.

Je remercie également Pierre Schiano, René Maury, Jean-Yves Cottin et Bruno Scaillet d'avoir bien voulu juger ce travail.

Un merci tout particulier à celui qui m'a également beaucoup soutenu, encadré et conseillé : Hervé Martin, pour qui j'ai une profonde admiration.

Je suis également extrêmement reconnaissant envers Chantale et Karine (les reines de la salle blanche), Delphine (la Miss Triton), Mireille, Michèle V., G.ROM, Mhammed, Jean Luc D, Jean Luc DP, Jean Marc, François et Christophe de m'avoir permis de réaliser l'ensemble de mes analyses au sein du LMV.
Un merci tout particulier à Valérie et Jean Louis pour les bons moments passés en leur compagnie sur le terrain ainsi que pour leurs performances de géochronologue.

Un grand merci à Serge Fourcade et au laboratoire « Géosciences Rennes » de m'avoir accueilli et encadré pour mes analyses des isotopes de l'oxygène. Merci également à Sylvain de m'avoir accueilli chez lui durant mon séjour breton.

Takk fyrir à Bergrún pour son accueil en Islande, son amitié et sa « Vikingur's attitude », Gudrun Larsen, Thor Thordarsson et Kristján Geirsson pour leur expérience de terrain et la famille d'Olgeir pour son accueil… sans oublier évidemment encore une fois Olgeir qui restera pour moi le meilleur guide islandais possible !!!

Evidemment l'ambiance géologique qui règne au sein du LMV est pour beaucoup dans le bon déroulement de cette thèse. Effectivement toutes les personnes animant ce laboratoire donnent une âme et une vie joviale au bâtiment n°5 de la rue Kessler… merci à tous !!!
Une mention toute spéciale à l'ensemble des thésards, DEA et autre « zami Comorien »… que j'ai pu côtoyer au LMV durant tout ce temps… « big up » à vous tous !!!
Je tiens tout particulièrement à mentionner Silvana et Nico, qui sont à mes yeux, bien plus que des collègues de bureau.

Un grand merci au sens large à l'ensemble de mes amis « extra LMV », qui me font voir la vie en rose… merci à toutes les Filles et Fils qui font de la LGS une merveille, merci à la BDVGDF2A avec qui les moments passés ensemble dépassent l'entendement et merci aux amis de lycées qui sont restés auprès de moi depuis tout ce temps.

Il me semble également important de remercier ma mie, Eloïse, sans qui ma vie ne serait que trop fade. Mon frère et ma belle-sœur qui savent prendre la vie dans le bon sens. Mon père qui joue sur tous les plans. Enfin je tiens tout particulièrement à remercier ma mère qui, au quotidien, sait tout bonnement me donner une vraie leçon de vie… me faisant ainsi relativiser beaucoup de petits soucis de tous les jours.

Merci à toutes les personnes qui sont entrées dans ma vie et avec qui mes rapports furent aussi divers qu'enrichissants.

Sommaire

Introduction générale

La distribution du magmatisme à la surface de la terre est étroitement contrôlée par la tectonique des plaques. De manière générale il se développe en limite de plaques, qu'elles soient divergentes (rides médio-océaniques) ou convergentes (zones de subduction et de collision). Seul le magmatisme de point chaud se met en place de manière intra-plaque. Parfois l'interaction entre deux de ces environnements géodynamiques peut résulter en des conditions thermiques singulières et en une activité magmatique elle aussi particulière. Il peut s'agir de la subduction d'une ride médio-océanique active, comme c'est le cas dans la presqu'île de Taitao en Patagonie et dont résulte la genèse de magmas adakitiques par fusion de la croûte subductée. Ou bien encore, il peut aussi s'agir de l'interaction d'un point chaud avec une ride médio-océanique, comme en Islande où un volume anormalement élevé de magma acide est engendré dans un environnement océanique.

Les magmas acides sont très difficilement recyclables dans le manteau du fait de leur faible densité, ce qui en fait les constituants majeurs de la croûte continentale. Aujourd'hui, les lieux privilégiés de production des magmas acides contribuant à la formation de la croûte continentale juvénile sont : 1) les zones de subduction, soit par fusion du coin de manteau métasomatisé, soit plus rarement par fusion directe de la croûte océanique et 2) de manière moins importante en termes de productivité, les plateaux océaniques tels que Hawaï ou Kerguelen, peuvent aussi donner naissance à de petits volumes de magmas acides d'affinité alcaline ou transitionnelle. L'Islande, en raison de l'interaction entre un point chaud et la ride médio-atlantique voit une production de grands volumes (10 %) de magmas acides, ce qui fait de cet environnement un site potentiellement efficace de genèse de croûte continentale. Il a d'ailleurs été souvent suggéré que le « modèle islandais » pourrait être un analogue de l'environnement de genèse de la proto-croûte continentale terrestre.

Avant d'aborder ce dernier point, il a semblé nécessaire de comprendre le détail des mécanismes mis en jeu lors de la genèse des magmas acides en Islande, qui représente actuellement l'un des rares endroit émergé sur Terre où s'observe la superposition d'un panache mantellique avec une ride médio-océanique. Après le prélèvement sur le terrain, les outils utilisés sont ceux de la pétrologie et surtout de la géochimie. Une démarche multi-méthodologique (éléments majeurs, en traces, isotopes radiogéniques et stables) a été favorisée afin de contraindre au maximum les modèles pétrogénétiques. Cette démarche n'a pas uniquement pour but de contraindre les mécanismes magmatiques mis en jeu actuellement au sein de l'île, mais également d'étudier leur évolution au cours du temps. Il s'agit finalement d'une étude spatio-temporelle du magmatisme acide islandais.

C'est cette approche qui a servi de fil conducteur à mes travaux de thèse et qui d'une certaine manière révèle la structure de ce manuscrit. D'autre part, les résultats principaux de mon activité de recherche en Islande font l'objet de cinq articles, dont un paru, un accepté, un soumis et deux à soumettre. C'est pourquoi ces publications, rédigées en anglais, constituent la trame principale de ce mémoire de thèse.

Le **premier chapitre**, consiste en une rapide présentation du contexte géologique et géodynamique de l'Islande. Par souci de clarté, seules les informations nécessaires à la compréhension de la suite du mémoire ont été présentées.

Le **second chapitre** traite de la différenciation quasi-complète, par cristallisation fractionnée, de magmas basaltiques au sein des coulées de laves dans lesquelles ont été générées des veines de ségrégation. Après une discussion portant sur le mode de formation de ces veines de ségrégation, il est discuté des implications que ce mode de différenciation peut avoir non seulement pour les roches acides d'Islande mais également pour la genèse des roches acides constitutives de la proto-croûte continentale terrestre. Ceci ayant fait l'objet de deux articles :

Martin, E. and Sigmarsson, O., 2006. *Segregation veins formed by in-situ differentiation of tholeiitic lavas from Reykjanes (Iceland), Lanzarote (Canary Islands) and Masaya (Nicaragu*a). Accepté avec correction à Contribution to Mineralogy and Petrology.

Martin, E. and Sigmarsson, O., 2005. *Trondhjemitic and granitic melts formed by fractional crystallization of an olivine tholeiite from Reykjanes Peninsula, Iceland.* Geological Magazine, 142(6): 651-658.

Le **troisième chapitre**, qui est le plus volumineux, propose une étude principalement géochimique des magmas acides d'Islande. Leurs mécanismes de genèse durant l'holocène ont été déterminés, quantifiés puis replacés selon leur localisation géographique et donc leur contexte géothermique. Le site de Hrafntinnusker (Torfakökull) a de plus fait l'objet d'une étude détaillée des processus pré- et post-éruptifs. Enfin, l'étude de l'évolution spatio-temporelle des processus pétrogénétiques et des contextes géodynamiques de genèse des magmas acides, au cours des 13 derniers millions d'années, a permis de proposer un modèle d'évolution géodynamique de l'Islande. Ceci ayant fait l'objet de deux articles :

Martin, E. and Sigmarsson, O. 2006. *Crustal thermal state and origin of silicic magma in Iceland: the case of Torfajökull, Ljósufjöll and Snæfellsjökull volcanoes.* Contribution to Mineralogy and Petrology, sous presse.

Martin, E and Sigmarsson, O. *Silicic rocks petrogenesis during the last 13 Ma, implications for the geodynamical evolution of Iceland.* À soumettre.

Enfin le **dernier chapitre** propose d'étendre la réflexion au rôle joué par le magmatisme acide des plateaux océaniques dans la genèse de la croûte continentale terrestre primitive. Ceci ayant fait l'objet d'un article :

Martin, E., Martin, H. and Sigmarsson, O. *Can Iceland be a modern analogue of Earth's early continental crust?* À soumettre.

En guise de **conclusion**, une synthèse des points importants mis en évidence dans ce manuscrit est proposée.

Chapitre I : Géologie de l'Islande

A. Aperçu de la géologie de l'Islande

1. Contexte général

Située entre 63°23' et 66°30' de latitude Nord, l'Islande se trouve à l'aplomb de la dorsale médio-Atlantique. Prolongée au Nord par la ride de Kolbeinsey et au Sud par celle de Reykjanes, l'île offre une spécificité exceptionnelle : c'est l'unique endroit au monde où une ride médio-océanique active est émergée et affleure (Figure I-1)

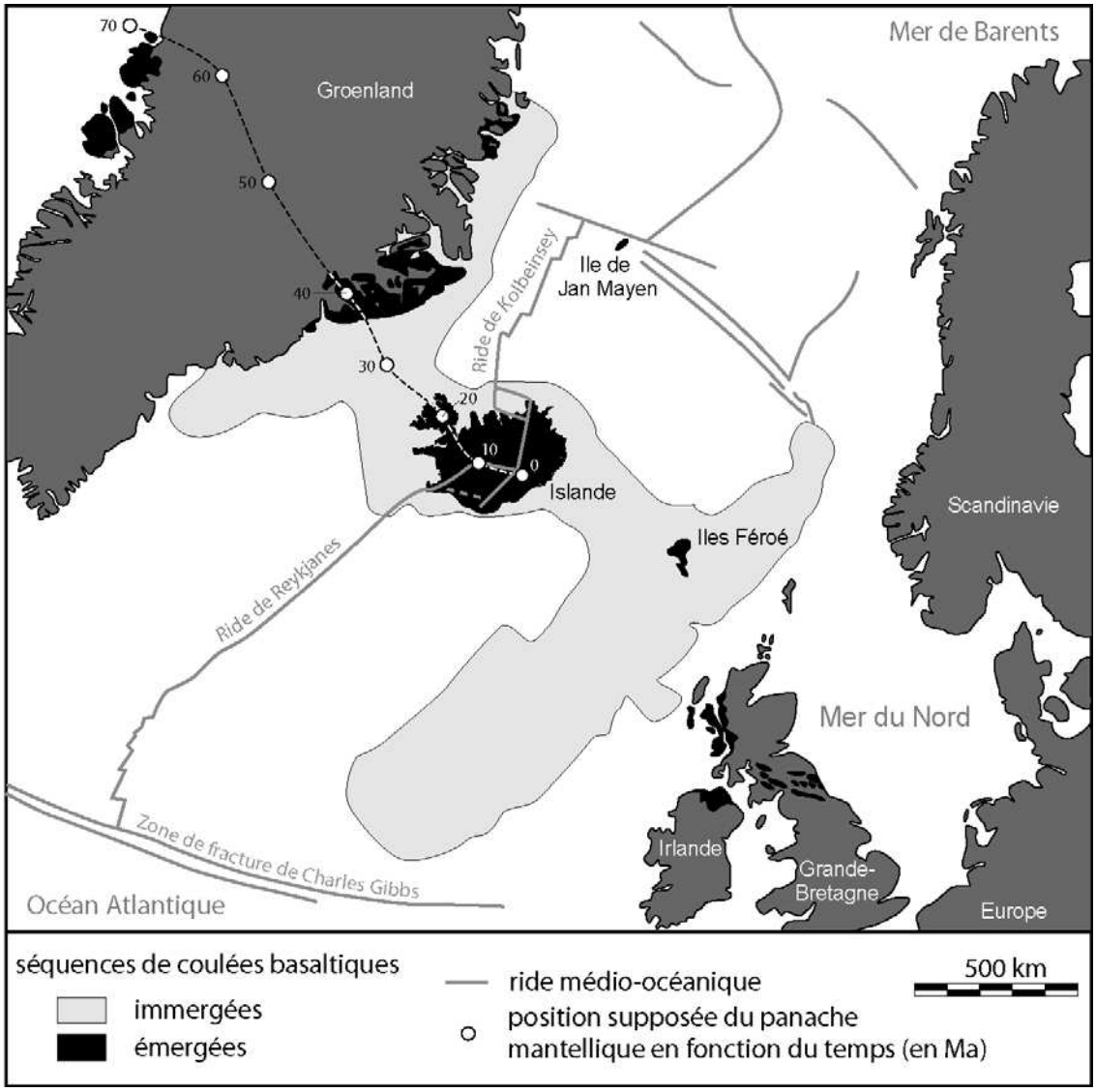

Figure I-1 : Localisée au sein de l'Atlantique Nord, l'Islande constitue une partie émergée du plateau océanique Groenland – Féroé, d'après Saunders et al. (1997) et modifié par Thordarson and Hoskuldsson (2002).

Depuis 36 Ma, le panache mantellique « islandais » est localisé sous la croûte océanique et coïncide avec la ride médio-Atlantique (par ex. Vink, 1984 ; Figure I-1). Cette dernière est une ride lente classique qui donne naissance à une croûte océanique de 6-7 km d'épaisseur (White et al., 1992). L'activité du point chaud superposé à la ride provoque une augmentation considérable de la production magmatique, induisant ainsi un épaississement important de la croûte océanique islandaise («socle Islandais »). En effet, l'excès de productivité magmatique ne pouvant pas être accommodé par la vitesse d'ouverture de la ride, il en résulte que la croûte islandaise s'épaissi considérablement. Selon les approches et les modèles proposés (Kaban et al., 2002 et références incluses), cette épaisseur est estimée entre 15 et 40 km ce qui est considérable en comparaison des 6-7 km d'une croûte océanique « normale ». Une telle accumulation de laves induit une surcharge de poids locale, qui va initier la subsidence rapide du cœur de la zone de rift. Comme la plupart des systèmes de ride, cette dernière est affectée par une activité géothermale intense qui va altérer et hydrater partiellement les empilements volcaniques lors de leur formation de leur enfouissement. Il en résulte un métamorphisme progressif de la croûte islandaise, depuis le faciès à zéolites, jusqu'au faciès amphibolite en passant par les faciès à chlorite – épidote et schiste vert. En d'autres termes, la croûte islandaise est le résultat de ces mécanismes auxquels s'ajoute son écartement progressif de part et d'autre de la zone de rift (Figure I-2 ; par ex. Pálmason, 1986 ; Pálmason, 1973 ; Oskarsson et al., 1982).

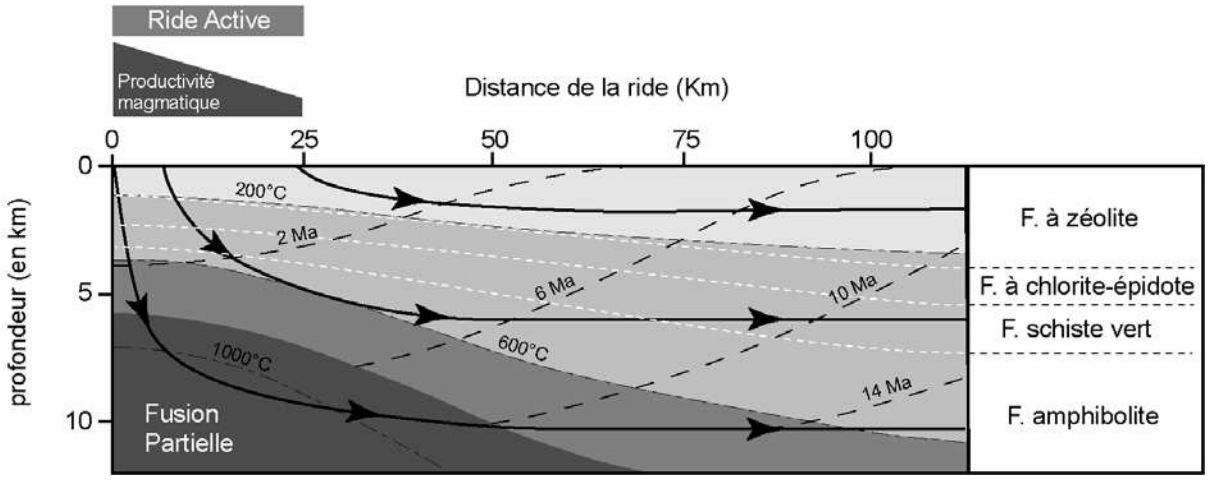

Figure I-2 : Modèle de formation de la croûte islandaise, d'après Pálmason (1973 ; 1986) et Oskarsson et al. (1982). Pointillés blancs = limite des faciès (F.) métamorphiques ; pointillés noirs = isochrones ; courbes noires et fléchées = trajets suivis par les roches au sein de la croûte islandaise

2. Age de l'Islande

L'âge du soubassement de l'Islande est mal connu, en revanche de nombreuses roches exposées en surface ont fait l'objet de datations. Les plus vieilles roches à l'affleurement proviennent de la Péninsule de Vestfirðir (les fjords ouest) et ont été datées à 16 Ma alors que d'autres issues des fjords Est à 13 Ma (par ex. Moorbath et al., 1968 ; Paquette et collaborateurs 2006, communication personnelle). Trois unités stratigraphiques majeures sont conventionnellement distinguées au sein des formations volcaniques : 1) les formations « tertiaires » âgées de plus de 3,3 Ma ; 2) les roches « plio-pléistocènes » dont l'âge va de 3,3 à 0,7 Ma et enfin 3) les formations d'âges « pléistocène supérieur » qui ont moins de 0,7 Ma forment la zone néo-volcanique (zone de rift) (Figure I-3 et Figure I-4). La dernière unité, dite « pléistocène supérieur » peut être divisée en deux sous-unités : les formations du pléistocène supérieur s.s. de 0,7 Ma à 0,01Ma et celles de l'holocène ou post-glaciaire (de 0,01Ma à aujourd'hui).

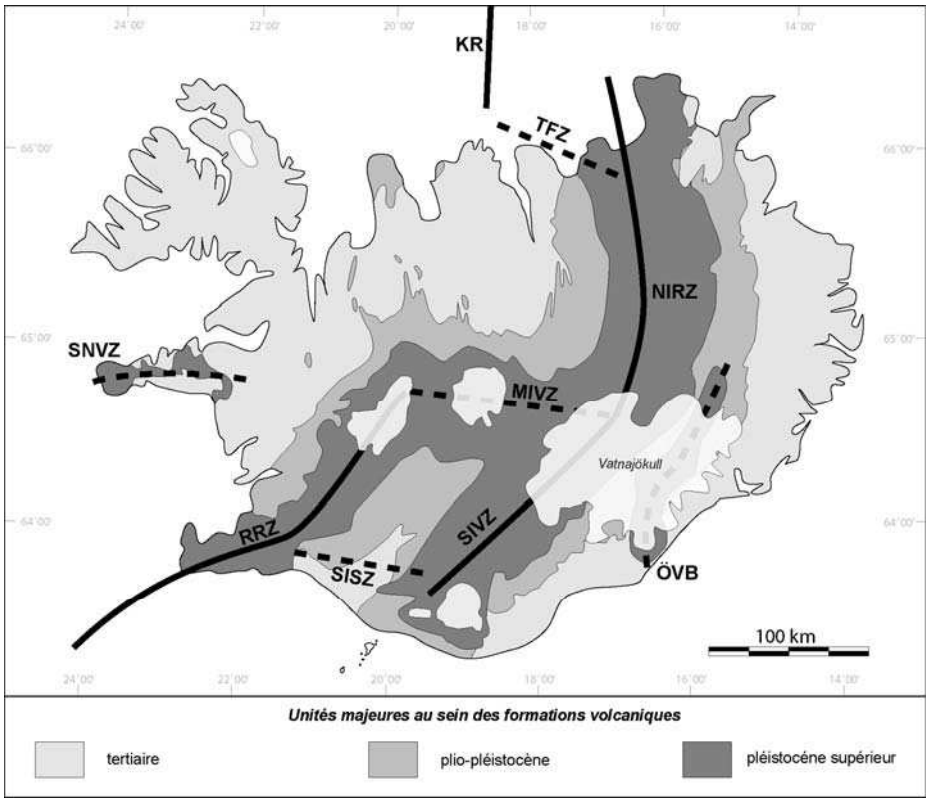

Figure I-3 : Carte des principaux éléments de la tectonique islandaise (zones volcaniques et failles majeures), d'après Sæmundsson (1979) et modifié par Thordarson and Hoskuldsson (2002). RRZ = Reykjanes Rift Zone ; NIRZ = North-Iceland Rift Zone ; SIVZ = South-Iceland Rift Zone ; SNVZ = Snæfellsnes Volcanic Zone ; ÖVB = Öræfi Volcanic Belt et zones de jeu de failles transformantes TFZ = Tjörnes Fracture Zone ; SISZ = South-Iceland Seismic Zone ; MIVZ = Mid-Iceland Volcanic Zone.

3. Activité volcanique actuelle

Aujourd'hui, l'activité volcanique islandaise est confinée le long de 3 zones de rift (Figure I-3 et Figure I-4), la RRZ (Reykjanes Rift Zone), NIRZ (North-Iceland Rift Zone) et la SIVZ (South-Iceland Rift Zone) ainsi que dans 2 zones volcaniques hors rift, la SNVZ (Snæfellsnes Volcanic Zone) et la ÖVB (Öræfi Volcanic Belt). Les zones de rift sont reliées entre elles par des jeux de failles transformantes à l'image de :

- la TFZ (Tjörnes Fracture Zone) qui relie la NIRZ à la ride de Kolbeinsey,
- la SISZ (South-Iceland Seismic Zone) qui joint la ride de Reykjanes à la SIVZ
- et enfin la MIVZ (Mid-Iceland Volcanic Zone) qui relie la RRZ à la NIRZ.

Le centre du panache mantellique est quant à lui localisé sous le nord-ouest du glacier Vatnajökull (Figure I-5 ; par ex. Eysteinsson and Gunnarsson, 1995; Wolfe et al., 1997).

Les zones axiales de rift qui contrôlent l'essentiel du régime tectonique de l'Islande (extension ONO – ESE), sont caractérisées par un magmatisme de type tholéiitique. En revanche, au sein des zones volcaniques hors rift (SNVZ et ÖVB), un volcanisme de type transitionnel à alcalin se met en place de façon discordante sur les formations tholéiitiques tertiaires. La zone axiale de rift SIVZ est quant à elle une zone singulière car la nature de son magmatisme évolue depuis des compositions tholéiitiques au Nord, jusqu'à des compositions alcalines au Sud. Cette configuration géographique de la SIVZ est interprétée comme résultant de l'initiation d'un nouvel axe de rift, ce qui est d'autre part parfaitement cohérent avec le fait que cette zone volcanique est aujourd'hui la plus active d'Islande (Jakobsson, 1972). Il est maintenant communément admis que la SIVZ correspond à la propagation vers le Sud de la NIRZ et que depuis 3 Ma, cet axe de rift est progressivement en train de remplacer la RRZ (par ex. Sæmundsson, 1979; Oskarsson et al., 1985). A l'échelle de l'histoire islandaise, cette relocalisation de la zone de rift correspond à un saut de rift vers l'Est.

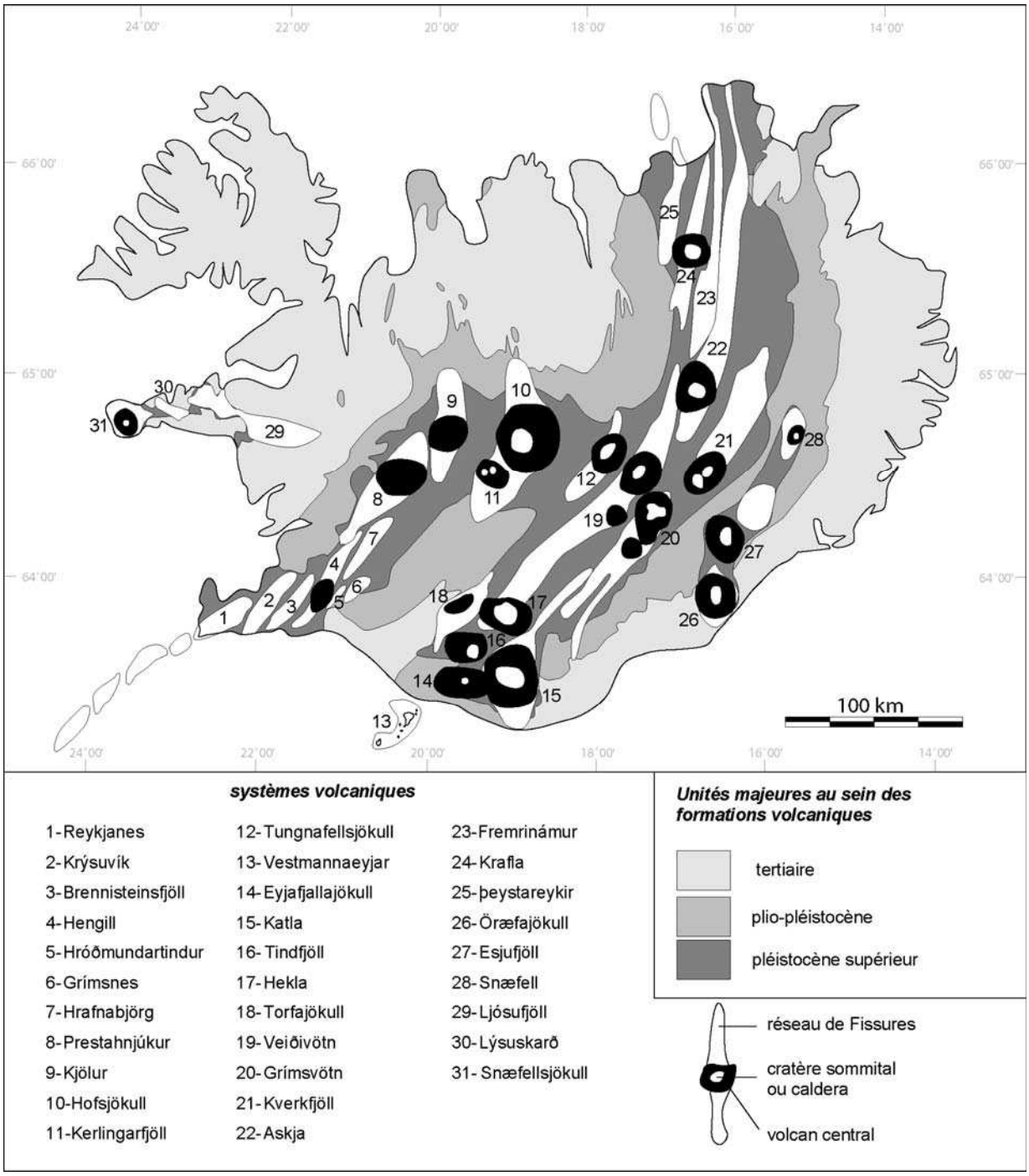

Figure I-4 : Carte des systèmes volcaniques actifs, d'après Sæmundsson (1979), modifiée par Thordarson and Hoskuldsson (2002).

4. Evolution de la zone de rift

Des sauts de ride, tels que celui observé actuellement entre la RRZ et la SIVZ, se sont déjà produit au moins une fois dans le passé, il y a 7 Ma (par ex. Jóhannesson, 1980 ; Sæmundsson, 1979) et probablement une fois encore avant il y a 15 Ma (Hardarson et al., 1997). En effet, par rapport au centre du panache, la dorsale océanique se déplace vers le NO. Lorsque la distance entre la ride et le centre du point chaud devient trop importante, une nouvelle zone de rift est alors recréée, au sein de la croûte océanique, à l'aplomb du centre du panache mantellique. L'ancienne zone de rift abandonnée, devient quant à elle inactive. Au niveau de l'Islande, la dorsale médio-Atlantique se trouve ainsi « capturée » et déviée vers l'Est, relativement à la position qu'elle devrait «normalement» occuper ; dans le prolongement direct de la Ride de Kolbeinsey au Nord et de la ride de Reykjanes au Sud (Figure I-1). Actuellement les reliques de ces différentes zones de rift abandonnées sont observables et sont localisées comme indiqué en Figure I-5. Il y a plus de 7 Ma, la zone de rift s'étendait de la péninsule Snæfellsnes (au Sud-ouest) à celle de Skagi (au Nord). Il y a environ 7 Ma, cette dernière est devenu inactive, laissant ainsi place à la zone de rift actuelle qui est localisée plus à l'Est (Sæmundsson, 1979; Jóhannesson, 1980; White et al., 1992). Hardarson et al. (1997) ont même suggéré qu'une zone de rift éteinte, localisée actuellement dans les Fjords Nord-ouest de l'Islande, a été active entre 24 et 15 Ma, avant de laisser la place à la zone de rift de Snæfellsnes-skagi.

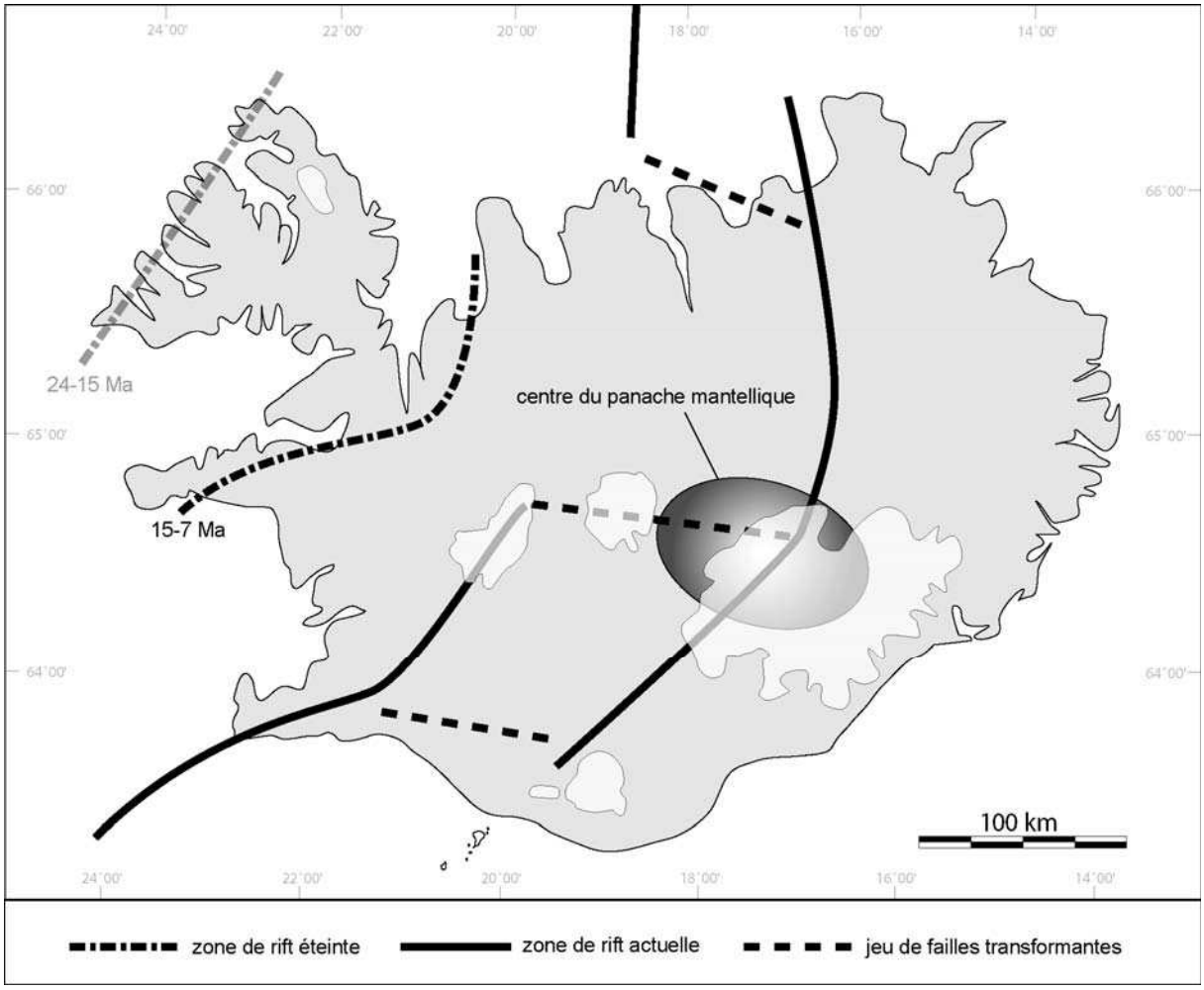

Figure I-5 : Carte d'Islande montrant l'évolution des zones de rift au cours de l'histoire islandaise d'après Jóhannesson (1980) et Sæmundsson (1979). La position du centre du panache (ellipse grise) correspond à celle proposée par Eysteinsson & Gunnarsson (1995) et Wolfe et al. (1997). La zone de rift éteinte du NO de l'île (en grisée) a été déduite des études de Hardarson et al. (1997) mais sa réelle existence entre 24 et 15 Ma reste toujours sujette à controverses.

5. Systèmes volcaniques

En Islande, chacune des zones volcaniques est constituée d'un ensemble de systèmes volcaniques (Figure I-4) dont la durée de vie active moyenne est typiquement de l'ordre de 0,5 à 1,5 Ma (par ex. Sæmundsson, 1979). Ces derniers se composent classiquement d'un réseau de fissures et d'un volcan central qui sont respectivement l'expression en surface de réservoirs magmatiques profonds et de sub-surface (Figure I-5). A son terme de maturation, le toit de la chambre magmatique sous le volcan central peut s'effondrer, formant ainsi une caldeira. Un ensemble de 31 systèmes volcaniques a été reconnu dans les zones actives

actuelles (Figure I-4) et de nombreux systèmes éteints ont aussi été identifiés dans les formations tertiaires (par ex. Walker, 1963; Sæmundsson, 1979; Jóhannesson and Saemundsson, 1998).

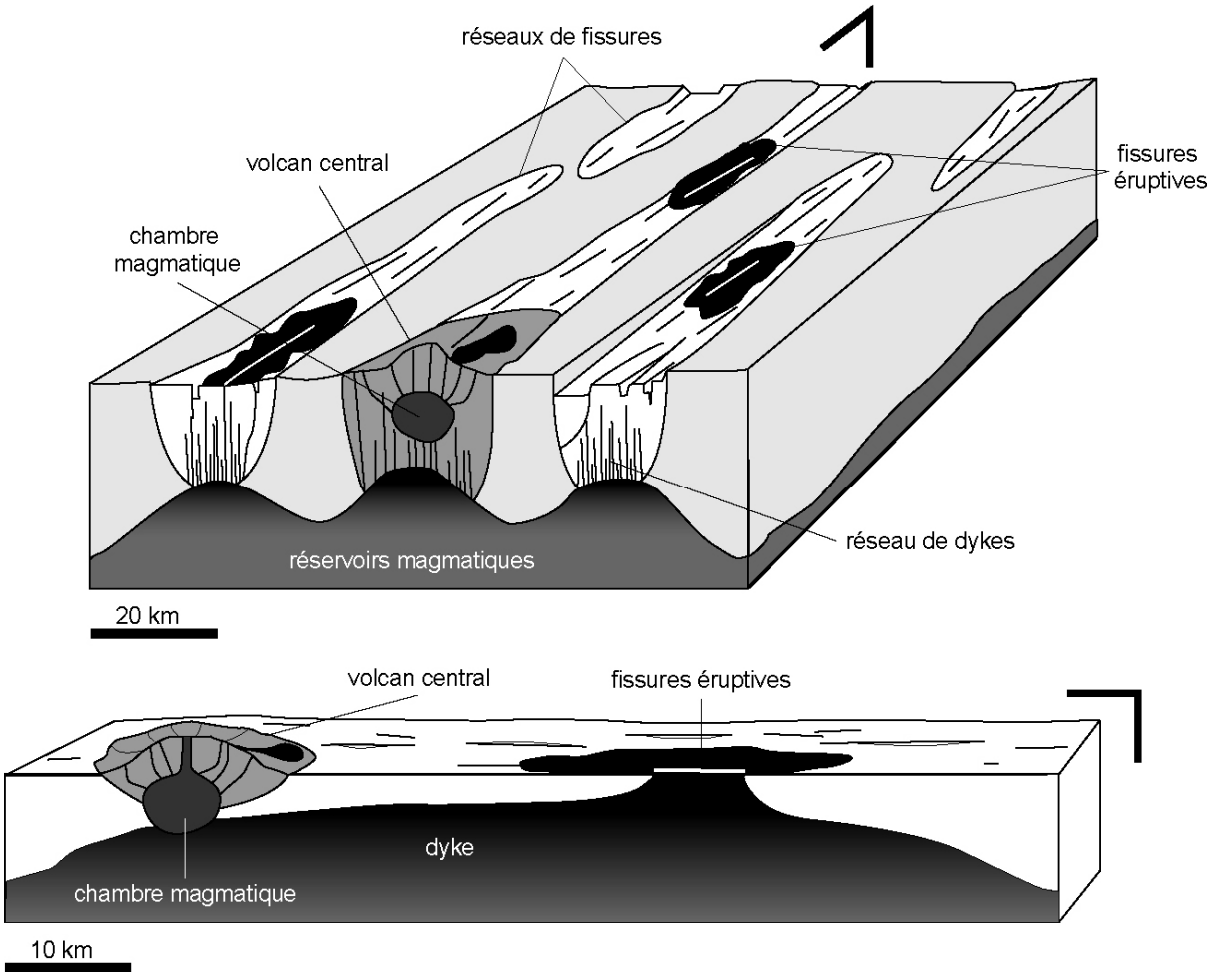

Figure I-6 : Eléments constitutifs d'un système volcanique islandais classique, d'après Gudmundsson (1995) et modifié par Thordarson and Hoskuldsson (2002).

Au cours de l'histoire de l'Islande, ces systèmes volcaniques ont essentiellement émis des basaltes. Toutefois, au sein des volcans centraux, des roches acides (rhyolite, dacite et trachyte) et plus rarement des laves de composition intermédiaires, ont pu se mettre en place. Le bilan volumétrique des magmas émis en Islande a été estimé à 90 % de basaltes et 10 % de magmas plus différenciés, dont une large majorité de roches acides (par ex. Sæmundsson, 1979).

6. Magmatisme acide

Bien que se trouvant en plein domaine océanique, le magmatisme islandais donne naissance à près de 10 % de roches acides. Cette proportion est anormalement élevée pour une île océanique, qui classiquement à l'image d'Hawaï, n'en présente qu'une infime proportion (par ex. Marsh et al., 1991). Cette grande productivité volcanique acide a suscité la curiosité de nombreux géologues qui se sont intéressé à son origine. Deux grands types de modèle ont alors été proposés afin de rendre compte de la genèse de ces roches :

- La cristallisation fractionnée de magmas basaltiques (par ex. Carmichael, 1964; Wood, 1978; Macdonald et al., 1990; Furman et al., 1992a; Prestvik et al., 2001). En remontant vers la surface, le magma basaltique issu de la fusion mantellique forme des réservoirs magmatiques, au sein desquels vont se former des magmas acides par cristallisation fractionnée.

- La fusion partielle de la croûte islandaise dont la composition est principalement basaltique (par ex. O'Nions and Gronvold, 1973; Oskarsson et al., 1982; Nicholson et al., 1991; Sigmarsson et al., 1991; Sigmarsson et al., 1992a; Jónasson, 1994; Lacasse et al., 2006). Suivant le modèle de Pálmason (1986) ; Figure I-2), la croûte islandaise est progressivement hydrothermalement altérée lors de sa formation au cœur de la zone de rift. Cette hydratation partielle a pour effet d'abaisser la température du solidus de la croûte basaltique. La remontée et la mise en place de magmas basaltiques issus de la fusion mantellique va permettre un réchauffement local de la croûte hydratée, permettant ainsi le franchissement de la température de son solidus. C'est donc la fusion de ces basaltes hydratés qui engendre le magmatisme acide. D'autres auteurs (par ex. Sigurdsson, 1977; Sigurdsson and Sparks, 1981; Marsh et al., 1991; Gunnarsson et al., 1998) proposent qu'au sein de la croûte islandaise résident des roches de composition acide, sous forme de « strates » (à l'échelle de la croûte islandaise) ou de veines (échelle plus locale) qui ont été formées par la cristallisation fractionnée de liquides basaltiques. C'est, selon eux, la fusion partielle de cette croûte hétérogène et par conséquent des roches acides qu'elle contient qui va permettre de générer et concentrer les grands volumes de magma felsique.

La plupart des travaux effectués sur la genèse des roches acides en Islande ont traité le sujet en se basant sur des formations holocènes. Dans le cadre de cette thèse, un échantillonnage plus représentatif de l'ensemble des roches siliceuses émises au cours de toute l'histoire géologique de l'Islande a été effectué (cf Annexes 1 et 7), le but étant d'étudier à l'échelle de l'ensemble de l'île l'évolution spatio-temporelle de la pétrogenèse de ces roches acides

Chapitre II : Mécanisme de cristallisation fractionnée

Les sources magmatiques les plus communes sont le manteau pour la plus importante et de façon plus exceptionnelle la croûte océanique et continentale. La fusion partielle de ces sources donne naissance à des magmas « primaire » de composition relativement comparable (pour une source donnée). C'est principalement la cristallisation fractionnée qui va permettre à ce magma « primaire » de générer la variété de roches magmatiques que nous connaissons sur terre. Par exemple la fusion mantellique ne peut pas donner naissance à des liquides de composition acide dans des conditions classiques, et c'est principalement la cristallisation fractionnée subséquente qui permet de différencier ces magmas jusqu'à une composition felsique. Bien que de nombreux indices pétrographiques attestent de la réalité de ce mécanisme, il n'en demeure pas moins qu'il reste rarement accessible dans son intégralité.

Toutefois, de petits « laboratoires naturels », existent dans toutes les provinces volcaniques du monde. Ils permettent d'étudier et de suivre le processus de différenciation dans sa totalité. En effet, au sein des lacs ou des coulées de laves il est possible de trouver des veines qui sont composées de magmas plus différenciés que la lave hôte. Ces veines dites « de ségrégation », ont depuis longtemps été décrites dans des lacs de laves comme au Kilauea Iki Lava Lake (par ex. Helz, 1980; Helz et al., 1989) ou au sein de coulées de laves de différentes tailles (par ex. Anderson et al. 1984; Goff 1996; Philpotts et al., 1996; Thordarson and Self, 1998; Caroff et al., 2000; Marsh 2002; Sigmarsson et al., 2006).

Les veines de ségrégation se forment au sein des coulées de laves, en conséquence, elles permettent d'avoir accès à la quasi totalité du processus de cristallisation fractionnée pour une pression proche de 1 atmosphère. En effet, quel que soit le mécanisme de ségrégation invoqué, le liquide magmatique constitutif de ces veines correspond à ~50 % de fractionnement de la lave hôte. Enfin, le verre interstitiel de ces veines représente les derniers incréments de liquide résiduel généré par fractionnement de la lave hôte. Le système « lave hôte – veine de ségrégation – verre interstitiel des veines » permet d'avoir accès aux liquides produits par respectivement 0%, 50 % et 75 à 98 %, de cristallisation fractionnée.

A. Veines de ségrégation formées par différenciation in-situ de laves tholéiitiques.

1. Article: “Segregation veins formed by in-situ differentiation of tholeiitic lavas from Reykjanes (Iceland), Lanzarote (Canary Islands) and Masaya (Nicaragua)” Accepté avec modifications à Contributions to Mineralogy and Petrology.

Segregation veins formed by in-situ differentiation of tholeiitic lavas from Reykjanes (Iceland), Lanzarote (Canary Islands) and Masaya (Nicaragua).

Martin, E.[(1)] and Sigmarsson, O.[(1,2)]

(1) Laboratoire Magmas et Volcans ; OPGC - Université Blaise Pascal – CNRS ; 5, rue Kessler ; 63038 Clermont-Ferrand Cedex (France).

(2) Institute of Earth Sciences, University of Iceland, 101 Reykjavik, Iceland.

E-mail: E.Martin@opgc.univ-bpclermont.fr

Keywords: Lava unit, segregation veins, interstitial glass, in-situ differentiation, fractional crystallisation, silicic melt.

Abstract

Segregation veins are common in lava sheets and result from internal differentiation during lava emplacement and degassing. They consist of evolved liquid, most likely, replace by gas-filter pressing from a ~50 % crystallised host lava. Pairs of samples, from host lavas and associated segregation veins, from the Reykjanes Peninsula (Iceland), Lanzarote (Canary Islands) and the Masaya volcano (Nicaragua) allow to show extreme mineralogical and compositional variations (MgO in host lava, segregation veins and interstitial glass ranges from 8-10 wt.%, 3-6 wt.% to less than 0.01 wt.% respectively). Based on chemical composition, temperature (~1250°C to ~950°C), oxygen fugacity (reduced condition), density (2.2-2.5 to 1.8-2.2) and viscosity (160-373 to 20-200 $Pa.s^{-1}$) of both host lavas and segregation veins were estimated. These physical parameters constrain the fractional crystallisation of olivine tholeiite at a pressure close to one atmosphere. The final products consist of silicic melts (SiO_2 = 70-80 wt.%), represented by interstitial glass in the segregation veins. Independently of the geodynamical environment, the fractional crystallisation evolution paths and the composition of the residual melts are controlled by the K_2O/Na_2O of the initial basaltic magma. The liquid line of descent, leads to the granitic minimum if the initial liquid has a high K_2O/Na_2O and to trondhjemitic composition for a low initial liquid K_2O/Na_2O.

Introduction

Lava cooling proceeds by two solidification fronts (SF): one from the top and another from the base of the lava unit, the core of which remains liquid during a longer period of time. At every cooling stage, each part of the lava displays different degrees of crystallisation that may result in internal chemical differentiation. One differentiation mechanism is the genesis and displacement of segregation veins. These are generally located in the upper half of the lava flow and form small (cm to dm sized) veins of porous rock, that are coarser grained and having a more differentiated composition than their host lava. Three sets of hypothesis are classically proposed to account for the origin of segregation veins: 1) In thick lavas (more than 70m), horizontal cracks in the upper half are filled with differentiated melts which segregated by compaction from the crystallizing lower SF (Philpotts et al. 1996). 2) The differentiated magma, formed by fractional crystallisation of the upper SF, is collected in-situ and due to instability (principally gravitational instability) of the upper SF, can concentrate in fractures and form veins (Marsh 2002). 3) The magma resulting from partial crystallisation of the lower solidification front is separated by gas filter pressing (Anderson et al. 1984), ascents by diapirism (Goff 1996; Helz 1980; Helz et al. 1989) and is finally emplaced into or just below the rigid upper SF. A good summary of this last can be found in Thordarson and Self (1998) or Caroff et al. (2000). Regardless of their exact origin, segregation veins represent a former melt phase separated from its host lava source that will evolve by crystallisation independently of the rest of main lava flow (Puffer and Horter 1993).

This study documents mineralogical, chemical and physical characteristics of segregation veins, in tholeiitic basalts from three different geodynamical environments: Reykjanes Peninsula (Iceland: ridge - mantle plume interaction), Lanzarote Island (Canary Islands: mantle plume) and Masaya volcano (Nicaragua: subduction zone). Furthermore, the conditions of genesis of these veins are discussed as well as the possibility to generate significant amounts of high silica magmas by simple fractional crystallisation as observed in segregation veins.

Geological setting

In Iceland volcanic activity is known to be high due to the association of both ridge and mantle plume systems (e.g. Schilling 1973). Recent lavas from the Reykjanes Peninsula are basaltic in composition, ranging from picrites through olivine tholeiites to tholeiites (Jakobsson et al. 1978) consistent with the geodynamical position of this peninsula, as the

prolongation of the Mid-Atlantic ridge (Fig.1). The influence of the Icelandic mantle plume is thought to be minimal in this region of Iceland and the Reykjanes Peninsula more akin to a typical ridge context. Segregation veins were extracted from a 5m thick Holocene lava unit from the Hrútagjá shield volcano (e.g. Jóhannesson and Saemundsson 1998).

Masaya volcano (Fig. 1) is a Quaternary caldera complex resulting from the subduction of the Cocos plate under the Caribbean plate (Carr et al. 1982). It produces tholeiitic lava flows (Walker 1989) and segregation veins were sampled from a ~30m thick lava flow forming the lower part of the southern caldera scarp.

Lanzarote island (Fig. 1) results from the mantle plume activity beneath the Canary Islands (Hoernle and Schmincke 1993). Lavas emitted during the 1730-36 eruption range in composition from basanite to tholeiitic basalt with time (Sigmarsson et al. 1998). The segregation veins of this study come from a 2m thick lava flow of the final phase of this peculiar eruption.

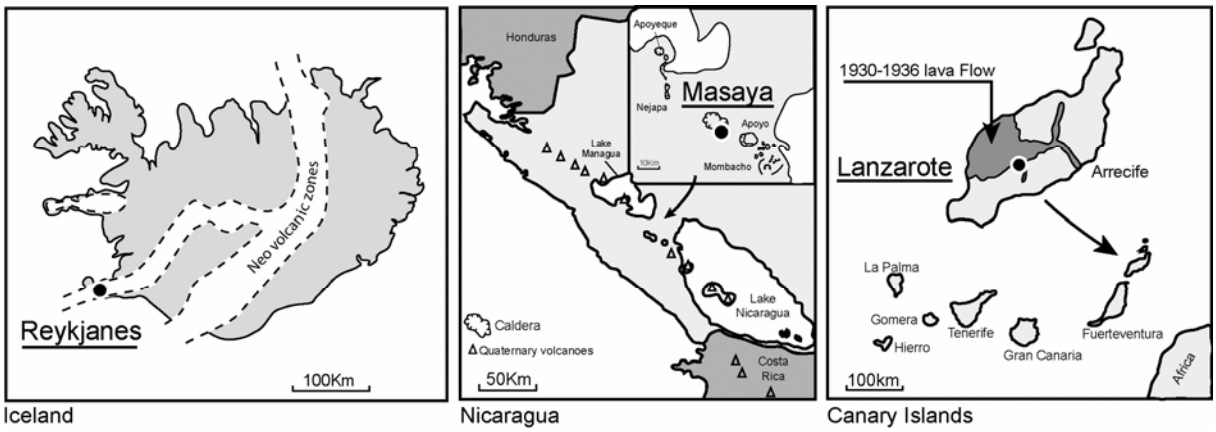

Figure 1: *Schematic maps showing the geographical location of studied areas: Reykjanes (Iceland), Masaya (Nicaragua) and Lanzarote (Canary), where segregation veins have been collected.*

Morphological characteristics of segregation veins

In the field, segregation veins can be easily distinguished from their host lava flow, due to coarser grains which sizes range from 0.5 to 2 mm whereas the host lava grain size never exceeds 0.5 mm (Table 1a). Porosity is 1.5 or 3 times greater in segregation veins (Table 1a), which indicates that important proportions of a gas phase were present during solidification. The veins are generally horizontal and located in the upper half of the lava flows. They are a few decimetres long and a few centimetres thick (Fig. 2a). In some cases, horizontal veins are prolonged below by a vertical cylinder which has a centimetre or

decimetre sized radius and can reach a few meters in length (Fig. 2b,c). These cylinders have exactly the same textural characteristics as horizontal veins and are interpreted in terms of feeding channels of the veins (Thordarson and Self 1998).

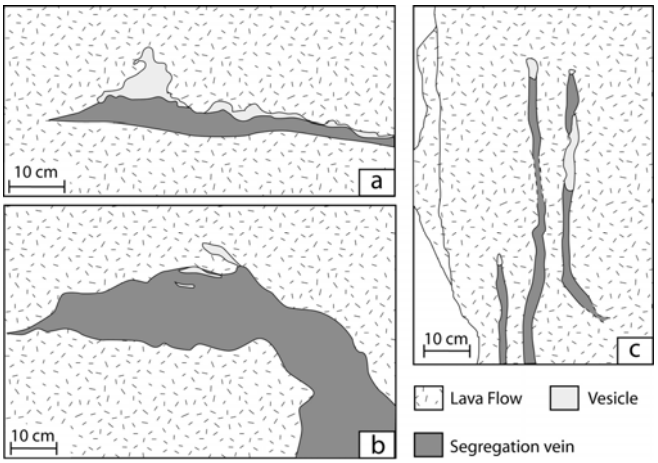

Figure 2: Drawing based on field observations showing the relationships between host lavas and segregation veins at Reykjanes: a) horizontal segregation vein, b) connection between horizontal segregation vein and vertical cylinder and c) vertical cylinder.

Analytical methods

Mineral and glass compositions were measured on a CAMECA SX 100 electron microprobe (EMP). The concentrations of major element were determined with a count time of 60 seconds per element. The EMP was calibrated on natural and synthetic mineral standards and raw data were corrected by an improved ZAF procedure. Mineral spot analyses used a current of 15 nA and an acceleration voltage of 15 kV. For glass analysis, beam diameter of 2-20 µm or rasters of 15 µm×15 µm with a current of 8 nA and an acceleration voltage of 15kV was used (see Martin and Sigmarsson 2005). Major and transitional element compositions of whole rock samples were obtained on ULTIMA C Jobin-Yvon ICP-AES, using purified lithium tetraborate fusion of rock powder. The ICP-AES analytical conditions are given in Cantagrel and Pin (1994) and international rock standards (BHVO-1, RGM-1, BIR-1 and JB-3) were used for instrument calibration. Trace element compositions were measured on VG PQ2+ ICP-MS, using same purified lithium tetraborate fusion of samples as for major element analyses and international standards (BR and BHVO-1) were used for instrument calibration (David, in prep.).

Table 1a: Table comparing the main textural characteristics and mineralogical composition of host lavas and vein from Reykjanes, Masaya and Lanzarote sites.

			Reykjanes			Masaya		Lanzarote	
			Host lava (HRG2)	**Vein** (HRG4)		**Host lava** (MA7)	**Vein** (MA8)	**Host lava** (MN3)	**Vein** (MN3s)
				core	**vesicle border**				
Rocks texture	**Phénocysts**	**Proportion**	15%	-	-	20%	-	10%	-
		Mineral phases	Pl (90%) - Ol (10%)	-	-	Pl	-	Ol	-
		crystal size	Pl (0.9-3.6mm) Ol (0.5-1.7mm)	-	-	1-3.2mm	-	0.3-0.5mm	-
	Matrix	**proportion**	75%	78%	89%	58%	72%	76%	64%
		Mineral phases	Pl (52%) - Cpx (39%) - Ol (6%) - Oxides (3%)	Pl (47%) - Cpx (40%) - Ol (3%) - Oxides (9%)- Apt (<1%)	Pl (43%) - Cpx (30%) - Oxides (15%)- Apt (<1%)	Pl (61%) - Cpx (23%) - Ol (7%) - Oxides (8%)	Pl (49%) - Cpx (40%) - Oxides (11%) - Apt (<1%)	Pl (43%) - Cpx (37%) - Ol (6%) - Oxides (14%)	Pl (43%) - Cpx (37%) - Ol (6%) - Oxides (14%) - Apt (<1%)
		crystal size	≤ 0.3mm	Pl (0.3-1.5mm) - Cpx (0.3-0.9mm) - Ol (≤ 0.5mm) - Oxides (≤ 0.6mm)	≤ 0.05mm exepted oxides (≤ 1mm)	≤ 0.3mm	Pl (0.3-2.5mm) - Cpx (≤ 2.2mm) - Oxides (≤ 2mm)	≤ 0.5mm	Pl (≤ 0.5mm) - Cpx (≤ 0.2mm) - Ol (≤ 0.3mm) - Oxides (≤ 0.5mm)
	Glass		3%	2%	5%	4%	4%	5%	6%
	porosity		7%	20%	6%	17%	24%	9%	30%
Minerals composition	**Plagioclase**		$An_{88}Ab_{12}Or_0$ to $An_{65}Ab_{34}Or_1$	$An_{63}Ab_{37}Or_0$ to $An_{43}Ab_{55}Or2$	$An_{36}Ab_{62}Or2$ to $An_5Ab_{54}Or_{41}$	An_{68} $Ab_{31}Or_1$ to $An_{40}Ab_{56}Or_4$	$An_{56}Ab_{42}Or_2$ to $An_6Ab_{51}Or_{43}$	$An_{57}Ab_{41}Or_2$ to $An_{46}Ab_{51}Or_3$	$An_{40}Ab_{58}Or_2$ to $An_7Ab_{65}Or_{28}$
	Clinopyroxenes		augite ($En_{48}Wo_{40}Fs_{12}$ to $En_{42}Wo_{37}Fs_{21}$) - pigeonite ($En_{48}Wo_{17}Fs_{35}$ to $En_{45}Wo_{16}Fs_{39}$)	augite ($En_{42}Wo_{41}Fs_{17}$ to $En_{28}Wo_{28}Fs_{44}$)	$En_{23}Wo_{39}Fs_{38}$ to $En_{13}Wo_{14}Fs_{73}$)	augite ($En_{44}Wo_{40}Fs_{16}$ to $En_{40}Wo_{39}Fs_{21}$) - pigeonite ($En_{42}Wo_9Fs_{49}$ to $En_{36}Wo_{13}Fs_{51}$)	augite ($En_{42}Wo_{34}Fs_{24}$ to $En_{11}Wo_{36}Fs_{53}$) - pigeonite ($En_{34}Wo_{12}Fs_{54}$ to En_{22} Wo_{13} Fs_{65})	augite ($En_{46}Wo_{42}Fs_{12}$ to $En_{46}Wo_{31}Fs_{23}$)	augite ($En_{41}Wo_{41}Fs_{18}$ to $En_{37}Wo_{35}Fs_{28}$) - pigeonite ($En_{45}Wo_{14}Fs_{41}$ to $En_{39}Wo_{14}Fs_{47}$)
	Olivine		Fo_{84} to Fo_{47}	Fo_{68} to Fo_{18}	-	Fo_{50} to Fo_{34}	-	Fo_{78} to Fo_{52}	Fo_{77} to Fo_{39}
	Oxides		$Usp_{66}Mt_{34}$ to $Usp_{75}Mt_{25}$	$Usp_{63}Mt_{37}$ to $Usp_{80}Mt_{20}$	$Usp_{40}Mt_{40}$ to $Usp_{77}Mt_{23}$ - $Ilm_{98}Hem_2$ to $Ilm_{94}Hem_6$	$Usp_{48}Mt_{52}$ to $Usp_{57}Mt_{43}$	$Usp_{97}Mt_3$ to $Usp_{90}Mt_{10}$ - $Ilm_{96}Hem_4$ to $Ilm_{92}Hem_8$	$Usp_{54}Mt_{45}$ to $Usp_{59}Mt_{41}$ - $Ilm_{85}Hem_{15}$	$Usp_{72}Mt_{28}$ to $Usp_{46}Mt_{54}$ - $Ilm_{92}Hem_8$ to $Ilm_{85}Hem_{15}$

Mineral phases proportion and porosity have been determined by point counting and abbreviations are as follows: Pl: plagioclase; Ol: olivine; Cpx: clinopyroxene; Apt: apatite; An: anorthite; Ab: albite; Or: orthoclase; En: enstatite; Wo: wolastonite; Fs: ferrosilite; Fo: forsterite; Usp: ulvöspinel; Mt: magnetite; Ilm: ilmenite; Hem: hematite.

Table 1b: Selected analyses of extreme compositions for the different mineralogical phases from Reykjanes: HRG2 (host lava), HRG4 (vein); Masaya: MA7 (host lava), MA8 (vein) and Lanzarote : MN3 (host lava), MN3s (vein).

Feldspar

	HRG2		HRG4 Core		HRG4 vesicle border		MA7		MA8		MN3		MN3s	
SiO_2	45.4	51.1	51.7	57.7	60.5	71.1	50.4	57.4	53.8	64.4	53.9	56.5	59.2	69.8
Al_2O_3	33.9	29.8	28.7	25.9	24.5	15.9	29.5	25.3	27.7	19.6	28.2	26.4	25.2	19.7
CaO	18.3	13.5	13.1	9.12	7.19	0.950	14.3	8.40	11.6	1.17	12.0	9.56	8.35	1.12
Na_2O	1.36	3.88	4.26	6.42	6.91	5.18	3.55	6.54	4.87	5.80	4.79	5.74	6.79	5.24
K_2O	0.004	0.122	0.098	0.259	0.407	5.90	0.184	0.770	0.366	7.47	0.259	0.467	0.443	3.40
Total	98.9	98.4	97.8	99.3	99.5	99.1	97.9	98.4	98.3	98.5	99.2	98.6	99.9	99.2
An	88.1	65.4	62.6	43.3	35.7	5.5	68.3	39.7	55.6	5.7	57.28	46.6	39.5	7.63
Ab	11.8	33.9	36.8	55.2	61.9	54.0	30.7	56.0	42.3	51.1	41.26	50.6	58.0	64.72
Or	0.0	0.7	0.6	1.5	2.4	40.5	1.0	4.3	2.1	43.2	1.47	2.7	2.5	27.65

Cliniopyroxenes

Augite	HRG2		HRG4 Core		HRG4 vesicle border		MA7		MA8		MN3		MN3s	
SiO_2	51.9	50.9	49.8	48.0	48.0	46.7	50.0	50.4	50.5	47.0	51.6	52.3	49.6	49.3
TiO_2	0.520	0.824	1.10	1.38	1.54	0.619	0.627	0.589	0.527	0.592	1.17	0.802	2.09	1.57
Al_2O_3	1.89	1.58	2.88	1.55	1.66	0.542	2.67	2.14	1.54	0.914	2.49	1.84	3.88	2.49
FeO*	7.45	12.8	10.7	25.5	22.9	40.8	9.95	13.1	14.8	29.9	7.63	13.9	10.9	16.2
MnO	0.199	0.288	0.309	0.680	0.564	1.12	0.314	0.389	0.531	1.07	0.154	0.440	0.194	0.478
MgO	17.3	14.8	14.5	9.07	7.63	4.06	15.5	14.0	14.5	3.40	16.0	15.2	13.6	12.2
CaO	19.9	18.2	19.8	13.0	17.9	5.96	20.0	18.8	16.5	15.8	20.2	14.6	19.4	16.2
Na_2O	0.225	0.302	0.314	0.194	0.229	0.120	0.298	0.305	0.298	0.301	0.404	0.528	0.569	0.437
K_2O	0.010	0.012	0.000	0.028	0.006	0.007	0.000	0.033	0.000	0.080	0.046	0.046	0.013	0.011
Total	99.4	99.7	99.4	99.3	100.4	99.8	99.3	99.7	99.3	99.1	99.6	99.7	100.2	98.9
Wo %	40.1	37.3	41.0	28.5	38.7	13.7	40.5	38.8	34.2	35.9	41.7	31.4	41.44	35.3
En %	48.3	42.3	41.7	27.7	22.9	13.0	43.7	40.1	41.8	10.8	46.0	45.4	40.40	37.1
Fs %	11.7	20.5	17.3	43.8	38.4	73.3	15.8	21.1	24.0	53.3	12.3	23.2	18.17	27.7

Pigeonite	HRG2		HRG4 Core		HRG4 vesicle border		MA7		MA8		MN3		MN3s	
SiO_2	50.3	50.0	-	-	-	-	50.0	49.9	48.7	47.9	-	-	50.8	49.3
TiO_2	0.904	0.871	-	-	-	-	0.295	0.500	0.514	0.294	-	-	0.736	1.18
Al_2O_3	1.30	1.04	-	-	-	-	0.525	0.523	0.744	0.652	-	-	1.03	1.39
FeO*	21.3	23.5	-	-	-	-	28.9	30.0	31.8	37.2	-	-	24.5	27.2
MnO	0.537	0.567	-	-	-	-	0.971	1.09	1.09	1.08	-	-	0.669	0.824
MgO	16.7	15.6	-	-	-	-	14.1	11.8	11.4	7.04	-	-	15.2	12.9
CaO	8.13	7.61	-	-	-	-	4.18	5.81	5.34	5.54	-	-	6.36	6.28
Na_2O	0.127	0.189	-	-	-	-	0.086	0.111	0.071	0.100	-	-	0.179	0.216
K_2O	0.031	0.011	-	-	-	-	0.014	0.063	0.019	0.041	-	-	0.041	0.075
Total	99.3	99.4	-	-	-	-	99.1	99.7	99.6	99.9	-	-	99.5	99.4
Wo %	16.9	16.0	-	-	-	-	9.0	12.7	11.6	12.5	-	-	13.64	13.80
En %	48.5	45.5	-	-	-	-	42.2	35.9	34.4	22.1	-	-	45.37	39.46
Fs %	34.6	38.5	-	-	-	-	48.7	51.3	53.9	65.5	-	-	40.99	46.74

Table 1b (continued):

Olivine

	HRG2		HRG4 Core		HRG4 vesicle border		MA7		MA8		MN3		MN3s	
SiO_2	39.0	34.0	36.8	31.0	-	-	34.4	32.9	-	-	38.9	35.1	39.4	33.7
FeO*	15.3	43.1	28.7	59.3	-	-	41.5	50.6	-	-	20.1	39.4	20.9	47.1
MnO	0.208	0.647	0.407	1.07	-	-	0.881	1.16	-	-	0.33	0.79	0.23	0.88
MgO	44.6	21.0	33.6	7.40	-	-	23.0	14.8	-	-	40.5	23.7	40.0	17.1
CaO	0.360	0.336	0.301	0.501	-	-	0.294	0.287	-	-	0.252	0.343	0.291	0.452
Total	99.5	99.1	99.9	99.3	-	-	100.0	99.7	-	-	100.1	99.3	100.9	99.3
Fo %	83.9	46.6	67.6	18.2	-	-	49.7	34.3	-	-	78.2	51.8	77.3	39.3

Oxides

Magnetite - ulvospinel	HRG2		HRG4 Core		HRG4 vesicle border		MA7		MA8		MN3		MN3s	
MgO	1.055	1.234	0.15	0.66	0.25	0.21	0.97	0.71	0.77	0.29	2.11	2.23	0.45	1.99
TiO_2	22.458	25.858	21.85	27.11	13.31	25.8	16.59	18.86	1.55	29.55	18.8	20.2	9.42	18.4
FeO*	69.339	67.265	71.99	64.42	76.92	65.73	75.85	70.69	84.84	61.46	71.8	69.8	80.4	71.5
MnO	0.476	0.382	0.6	0.57	0.34	0.58	0.48	0.33	1.08	0.3	0.52	0.49	0.36	0.44
Total	93.3	94.7	94.6	92.8	90.8	92.3	93.9	90.6	88.2	91.6	93.4	92.7	90.7	92.3
Usp %	66.0	75.0	63.0	80.0	39.7	77.2	47.7	56.8	2.9	89.7	54.2	58.7	27.8	53.7
Mt %	34.0	25.0	37.0	20.0	60.3	22.8	52.3	43.2	97.1	10.3	45.8	41.3	72.2	46.3

Ilmenite - hematite	HRG2		HRG4 Core		HRG4 vesicle border		MA7		MA8		MN3		MN3s	
MgO	-	-	-	-	0.300	0.150	-	-	0.844	0.713	1.08		1.99	1.22
TiO_2	-	-	-	-	50.4	48.6	-	-	50.6	46.1	44.2		48.5	44.4
FeO*	-	-	-	-	45.2	48.2	-	-	47.2	46.8	50.9		46.1	50.5
MnO	-	-	-	-	0.890	0.710	-	-	0.755	0.285	0.490		0.760	0.430
Total	-	-	-	-	96.8	97.7	-	-	99.4	93.8	96.7		97.3	96.5
Hem %	-	-	-	-	1.5	6.1	-	-	4.0	8.0	15.4		8.0	15.1
Ilm %	-	-	-	-	98.5	93.9	-	-	96.0	92.0	84.6		92.0	84.9

Petrology and mineralogy

Optical observation

All three sites show comparable mineralogy and will be described together. Petrological characteristics of vein samples are summarized in Table 1a. Host lavas (Fig. 3a), are microcrystalline and contain euhedral phenocrysts (10-20 % of the whole rock) of plagioclase and/or olivine. Groundmass (60-75 %) is composed of euhedral plagioclase (40-60 %) and Fe-Ti oxides (3-14 %) as well as anhedral clinopyroxene (22-38 %) and olivine (6-7 %). Plagioclase, clinopyroxene and olivine are compositionally zoned. Patches of silica-rich glass (3-5 %) are also present. Vesicles (often interconnected), represent between 7 and 17 % of the volume.

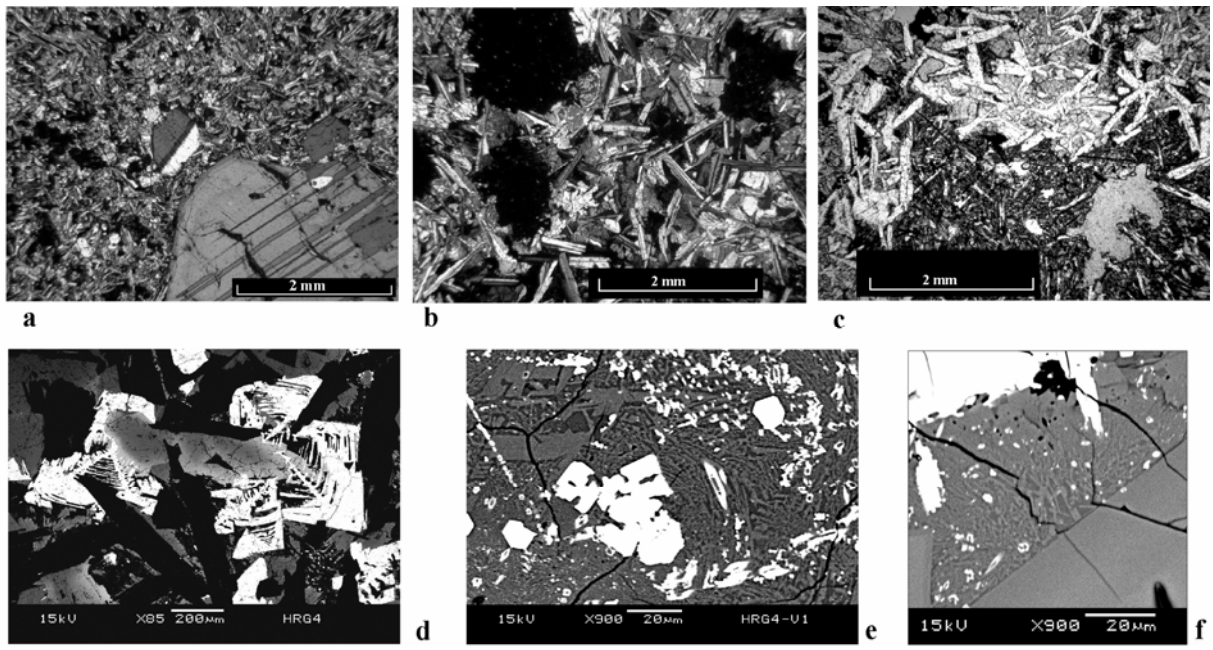

Figure 3: Microphotographs of thin sections from the Reykjanes lavas: a) Host lava with plagioclase phenocryst; b) Coarser grained segregation vein; c) Thinner crystallisation border of vesicle in segregation vein. Scanning electron microscope (SEM) images: d) Skeletal magnetite (white colours) around an olivine crystal in segregation vein, e) Micro-graphic texture in segregation vein (grey patches: albite, dark zones: quartz and white colours reflect Fe-Ti oxide), with occasional vesicles (black patches on f) reflecting the last gas exsolution stage (see text for further discussion). f) Porosity (black patches) in thin crystallisation glass from Reykjanes segregation vein.

In segregation veins (Fig. 3b), minerals have uniform size ranging between 2 mm and 0.5 mm. Exceptionally, crystal size is reduced at the border of the vesicle, as for instance in the veins of Reykjanes (Fig. 3c). Euhedral plagioclase (43-49 %) is most abundant and forms a crystalline network. A few crystals are deformed and have corroded edges, others present intergrowth, due to cotectic crystallisation together with clinopyroxene. Clinopyroxenes (30-40 %) and olivine (≤ 6 % or absent) are principally anhedral. Zoning is frequent in plagioclase, clinopyroxene and olivine crystals. Oxides usually have dendritic to skeletal shapes (Fig. 3d), which is interpreted to result from rapid crystallisation. Small, euhedral apatite crystals (< 1 %) are omnipresent. Interstitial glass patches (2-6 %), which are rarely higher than 100 μm in diameter, is considered as anhydrous (sum of oxide is always close to 100 %), it may contain vesicles (Fig. 3f) and occasionally is finely crystallised like in Reykjanes, forming graphic textures with an albite and quartz assemblage (Fig. 3e).

Mineralogical evolution

In the segregation veins, coarser grain size may reflect decreasing nucleation density during veins emplacement (Puffer and Horter 1993) and increasing diffusion rate due to water enrichment in the residual melt. The minerals in the veins systematically have more evolved chemical compositions than those of the host lava, i.e.: K-richer feldspar, Fe-richer clinopyroxenes and olivine (Table 1a and Table 1b). The evolution of mineral composition in the veins appears to be in continuity with that developed in the host lava (Fig. 4). This systematic variation of mineral composition is important, since it demonstrates that the crystallisation of the segregation veins is a direct continuity of host lava crystallisation. Consequently, segregation veins can be considered as representing more evolved degree of differentiation of the lava flow. The widespread mineral zoning of the host lavas and the veins reflects the role played by fractional crystallisation, rather than equilibrium crystallisation.

In the three studied lavas, feldspar composition shows similar evolution from anorthite-rich plagioclase ($An_{88}Ab_{12}Or_0$) to K-feldspar ($An_5Ab_{51}Or_{44}$) through more albitic compositions. Only in the Reykjanes basalt appears a small compositional gap between $An_{30}Ab_{70}Or_0$ and $An_5Ab_{54}Or_{41}$. Clinopyroxene presents similar compositional evolution for the three host lavas-veins pairs. In Lanzarote they are Fe-poorer than those from Masaya and Reykjanes. Augite and pigeonite form quasi-parallel trends in the pyroxene trapezoid with a almost constant CaO / (FeO+MgO). Pigeonite seems to crystallize later than augite as indicated by crystal zoning from an augitic core to pigeonitic rim. In Reykjanes, the pyroxene

compositions define trends that converge towards ferroaugite composition. Moreover, those from vesicle borders possess ferroaugitic cores while their rim is almost pure ferrosilite. Olivine presents the same mineralogical evolution from forsteritic (Fo_{84}) to fayalitic (Fo_{18}) composition in the three sites. In host lava, only solid solution of magnetite-ulvöspinel is present whereas in veins solid solution of ilmenite-hematite is also found. Therefore, ilmenite seems to appear after magnetite during fractional crystallisation. Finally, ilmenite is commonly exsolved in magnetite, probably due to subsolidus reequilibration of the veins.

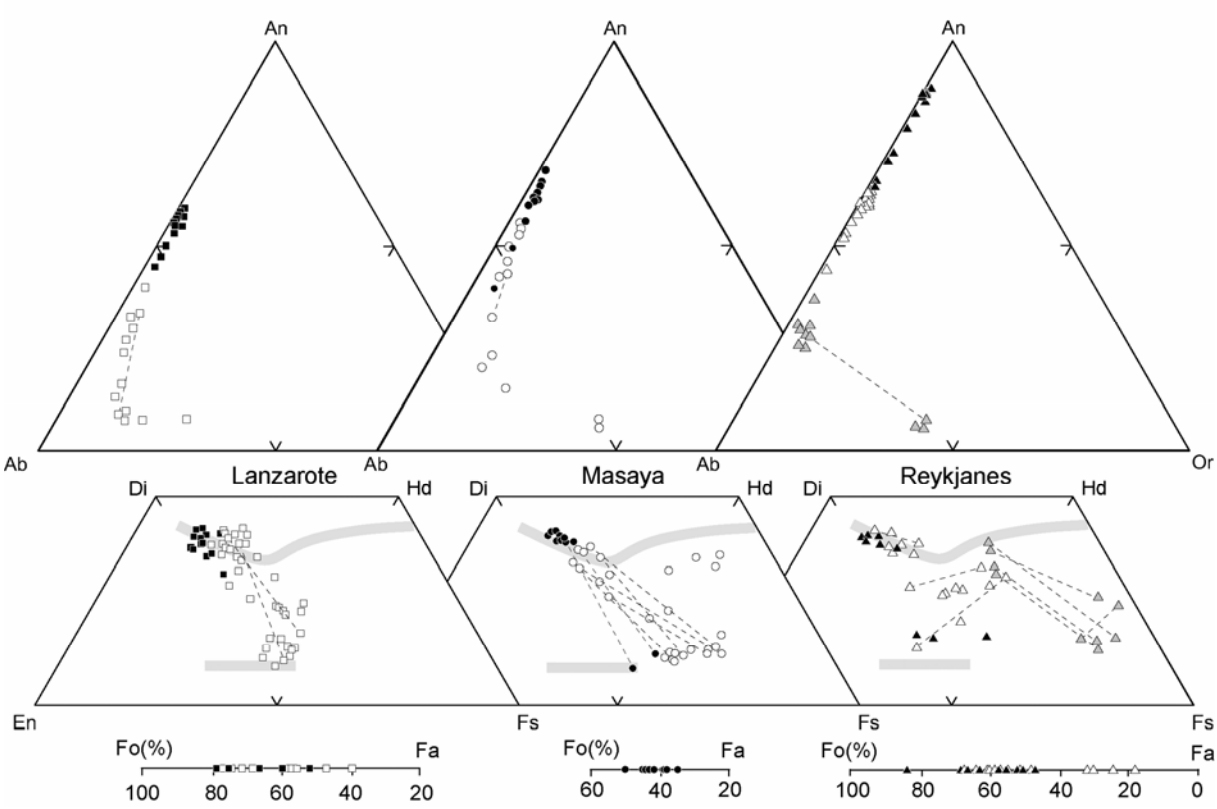

Figure 4: Feldspar (An-Ab-Or), pyroxene (En-Di-Hd-Fs) and olivine (Fo-Fa) diagrams showing the compositional evolution of minerals from both host lavas (filled symbols) and segregation veins (open symbols). Grey symbols for the Reykjanes vein, represent minerals located at the border of vesicles. Dotted lines connect extreme composition of mineral zoning. The grey large curve in the trapezoid represents the evolution trend observed at Skaergaard (Wager and Brown 1967), shown here for a reference.

Whole rocks composition

Major elements:

Host lavas of all three sites are of subalkalic basalt composition (~ 50 % SiO_2 and ~ 4.6-9.6 % MgO) with normative hyperstene and olivine (Table 2). In an AFM diagram, these basalts plot in the tholeiitic field (Fig. 5a). The principal difference between the lavas from the three sites is reflected in their K_2O content (Table 2) and the corresponding different K_2O/Na_2O, which is 0.07, 0.25 and 0.36 in Reykjanes, Lanzarote and Masaya lavas, respectively. Like their host lava, the veins plot in the tholeiitic field in Figure 5a. When compared to their host lavas, the veins are MgO-poorer but approximately two times K_2O-richer. Their K_2O/Na_2O is also significantly higher. The differences observed for this ratio between the host lavas is also present in the segregation veins (0.1, 0.34 and 0.63 in Reykjanes, Lanzarote and Masaya, respectively). Both the host lavas and veins are anhydrous with the sum of major element oxides close to 100 %.

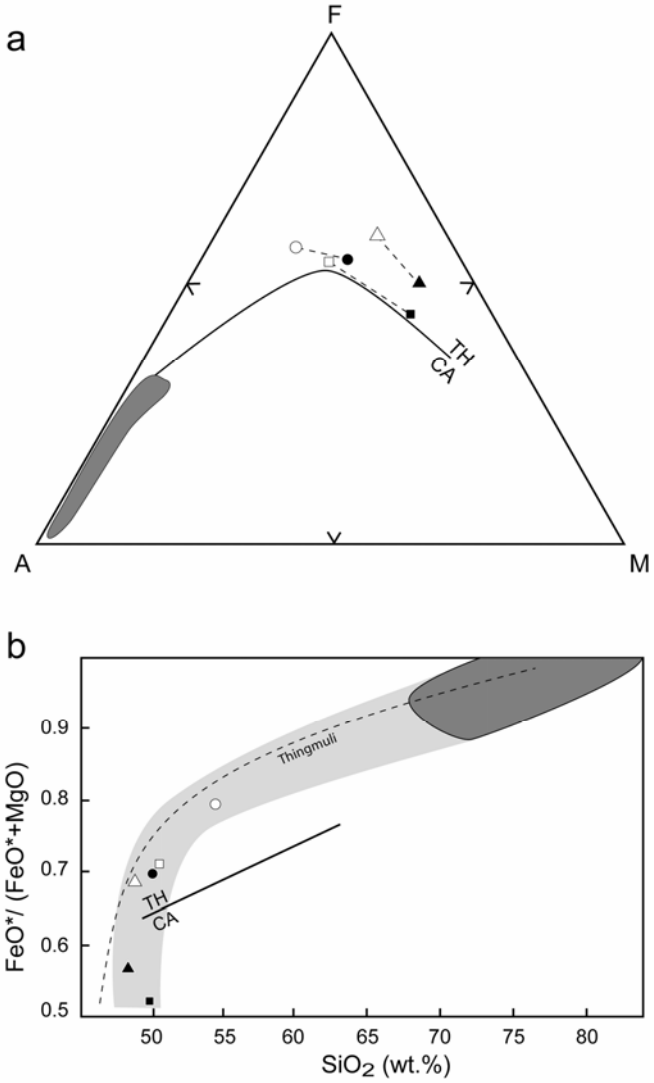

Figure 5: a) AFM diagram (A: Na_2O + K_2O, F: FeO, M: MgO in wt.%) and b) Harker diagram (FeO*/(FeO*+MgO) vs SiO_2) showing the tholeiitic character of the three studied sites. Triangle = Reykjanes; circle = Masaya; square = Lanzarote; filled symbols = host lavas; open symbols = segregation vein. The darker field represents glass compositions and grey area shows the tholeiitic trend defined by samples from this study. (Th: tholeiitic field; CA: calc-alkaline field from McBirney (1993) and the tholeiitic trend defined at Thingmuli by Carmichael (1964)).*

Table 2: Major and trace element compositions of host lavas and veins from Reykjanes, Masaya and Lanzarote.

	Reykjanes		Masaya		Lanzarote	
	Host lava	Vein	Host lava	Vein	Host lava	Vein
	HRG2	*HRG4*	*MA7*	*MA8*	*MN3*	*MN3s*
SiO_2	48.2	48.7	50.0	54.4	49.7	50.4
TiO_2	1.34	2.20	1.02	1.32	2.35	4.07
Al_2O_3	15.4	12.6	16.4	13.2	13.2	12.8
Fe_2O_{3*}	11.8	15.5	11.9	13.4	11.6	13.6
MnO	0.17	0.22	0.18	0.23	0.15	0.17
MgO	8.13	6.36	4.64	3.11	9.65	4.98
CaO	12.9	11.5	10.9	7.55	9.40	8.31
Na_2O	1.98	2.46	2.85	3.43	2.63	3.44
K_20	0.14	0.26	1.03	2.16	0.66	1.18
P_2O_5	0.13	0.21	0.22	0.51	0.45	0.94
Total	100.2	100.0	99.2	99.3	99.8	99.9
Estimation of Liquidus temperature	1210°C	1160°C	1200°C	1130°C	1270°C	1180°C
Quartz	0	0	0	4.25	0	2.51
Orthoclase	0.834	1.56	6.20	13.0	3.95	7.06
Albite	16.9	21.1	24.6	29.6	22.5	29.5
Anorthite	33.0	22.9	29.5	14.5	22.6	16.2
Nepheline	0	0	0	0	0	0
Diopside	25.0	27.8	20.1	17.2	17.5	15.9
Hypersthene	11.5	17.1	10.8	14.8	20.5	15.7
Olivine	7.32	1.40	3.75	0	4.82	0
Apatite	0.304	0.493	0.519	1.20	1.06	2.21
Ilmenite	2.57	4.23	1.97	2.55	4.52	7.83
Magnetite	2.59	3.39	2.61	2.95	2.54	2.98
Rb	2.22	3.90	18.2	40.6	14.2	26.2
Sr	160	162	447	373	531	514
Ba	37.8	62.4	754	1527	251	415
Y	22.1	35.9	24.3	46.9	21.3	35.4
Zr	61.1	102	81.3	178	206	370
Hf	1.67	2.78	2.24	4.69	4.69	8.40
Nb	6.83	11.7	2.96	6.28	42.9	78.3
Th	0.31	0.520	1.39	3.17	2.92	5.48
U	0.09	0.160	1.10	2.56	0.782	1.49
La	5.17	8.54	9.47	20.9	30.5	55.1
Ce	12.4	21.3	20.6	44.9	63.1	114
Pr	1.91	3.22	3.20	6.98	7.97	14.2
Nd	8.81	14.6	14.3	30.2	31	54.9
Sm	2.58	4.27	3.77	7.69	6.82	11.8
Eu	1.00	1.58	1.24	2.39	2.22	3.63
Gd	3.42	5.34	4.08	8.24	6.71	11.0
Tb	0.560	0.940	0.670	1.29	0.909	1.52
Dy	3.60	5.83	3.88	7.62	4.67	7.80
Ho	0.770	1.24	0.810	1.59	0.839	1.42
Er	2.06	3.49	2.24	4.34	1.98	3.31
Tm	0.330	0.540	0.350	0.690	0.268	0.427
Yb	2.14	3.47	2.32	4.55	1.54	2.64
Lu	0.340	0.530	0.350	0.670	0.213	0.370
Ni	112.7	69.1	17.3	6.2	259.9	70.7
Cr	293.5	19.3	34.1	n.d.	403.8	47.4
Sc	44.6	54.9	33.8	31.2	22.7	20.8
Degree of crystallisation (%)	0	44	0	57	0	48

In all samples, loss on ignition is negligible. CIPW normative composition was calculated assuming (Fe^{3+}/total iron) = 0.15. Liquidus temperatures are those calculated utilizing "Melts" algorithm (Ghiorso and Sack 1995). The degree of crystallisation was calculated from the ratio of highly incompatible elements in host lava and segregation veins.

Mass balance calculation, based on Störmer and Nicholls algorithm (1978), has been performed in order to quantify the crystallisation parameters that lead to the evolved composition of the veins relative to that of the host lavas (Table 3). Mineral compositions used are those analysed in the host lavas-veins pairs. In all cases mass balance modelling properly accounts for the vein compositions as judged from the low sum of the squares of residuals, which are systematically lower than 0.5. In all cases, the crystallizing assemblage consists of plagioclase + clinopyroxenes + olivine + oxides in proportions consistent with those observed in samples (Tables 1, 3). Finally, the estimated degree of crystallisation is 45 %, 48 % and 57 % for Reykjanes, Lanzarote and Masaya respectively.

Table 3: *Crystallizing assemblage estimated by the Störmer and Nicholls (1978) algorithm, forming the vein composition from that of the host lava and mineral/melt partition coefficient (D) calculated for Ni, Cr and Sc in olivine and clinopyroxene in the first ~50 % of fractional crystallisation of host lava from this study.*

Mass balance clculation		**Reykjanes**	**Masaya**	**Lanzarote**
Plagioclase		56% ($An_{80}Ab_{20}$)	60% ($An_{65}Ab_{35}$)	45% ($An_{50}Ab_{50}$)
Clinopyroxènes		29%	28%	29%
Olivine		14%	7%	23%
Fe-Ti oxide		1%	5%	3%
Degree of crystallisation (%)		45	57	48
Sum of the squares of residual (%)		< 0.01	0.04	0.45
Partition coefficient				
Ni	Clinopyroxene	2	4	2
	Olivine	7	15	10
	Magnetite [(1)]	31	31	31
Cr	Clinopyroxene	17	-	9
	Magnetite [(2)]	55	-	55
Sc	Clinopyroxene	2	3	3.5
	Magnetite [(2)]	4	4	4

Mass balance calculation: the fit acceptability is judged by the sum of the squares of residuals, which should be significantly lower than 1 %. (1) Shimizu and Kushiro (1975); (2) Leeman et al. (1978).

Trace elements:

Trace element compositions reported in a primitive mantle normalized multi-element diagram (Fig. 6-a), show patterns which are typical of the geodynamic environment of the studied samples (e.g. Hofmann 1988; Sun and McDonough 1989; Pearce 1983): (1) Reykjanes pattern displays depletion in the more incompatible elements (K, Ba, Rb, Th, U) indicative of depleted mantle source comparable to that of N-MORB. Nevertheless, while typical N-MORB have La/Yb < 1, the Reykjanes host lava has a value greater than 1 due to lower Yb contents. Such HREE impoverishment is classical in OIB magma genesis. In other words, it appears that Reykjanes lava has N-MORB characteristics for the most incompatible elements and OIB characteristics for the less incompatible elements, reflecting the influence of both mid-Atlantic ridge and Icelandic mantle plume (e.g. Gee et al. 1998; Schilling 1973; Zindler et al. 1979) (2) Lanzarote pattern present high concentrations of incompatible elements and depletion in less incompatible elements (La/Yb < 1) which is typical of OIB, generated in a mantle plume (3) Masaya, multi-element diagram shows enrichment in Rb, Ba, Th, U, K, and a pronounced negative Nb anomaly as is typical of a subduction related arc magmas where the magma source is a metasomatised mantle wedge.

When host lavas and segregation veins are compared, they display parallel patterns, which provide an additional evidence of their cogenesis. Systematically, veins are enriched in incompatible trace elements relative to the host lava. In Figure 6a, both Sr and Ti appears to be compatible during the formation of the veins, with Sr reflecting plagioclase fractionation (e.g. Drake and Weill 1975; Bindeman et al. 1998) and Ti that of Fe-Ti oxide. The lack of significant Sr depletion in the veins is most likely due to important Sr enrichment in the host lavas (Fig. 6a).

Figure 6-b better illustrates the behaviour of trace elements during the vein formation process. Both Eu and Sr are more compatible behaviour in Masaya magmas than in those of Lanzarote and even more so than the Reykjanes basalts. In the light of mass balance calculation (Table 3), this can be interpreted in terms of plagioclase fractionation which appears to be more important in Masaya's vein than in Lanzarote and in Reykjanes. Indeed arc basalts crystallizing under higher $P_{(H2O)}$ are expected to crystallize much plagioclase (e.g. McBirney 1993). Figure 6b also reveals a specificity of the Masaya vein, which is richer than those of Lanzarote and Reykjanes in highly incompatible elements and poorer in the less incompatible ones. This concurs with mass balance calculation (Table 3) showing that the Masaya vein corresponds to a liquid derived from higher degrees of crystallisation (57 %). Similarly, the more compatible behaviour for Ti in this vein request a higher activity of ferric

iron in the melt presumably due to relatively high oxygen fugacity as can be expected for subduction zone related magma. In summary, compared to Reykjanes and Lanzarote, the Masaya vein differentiated to a greater degree of crystallisation and resulted from a magma evolution under more oxidizing conditions, as expected from the subduction zone context of Masaya volcano.

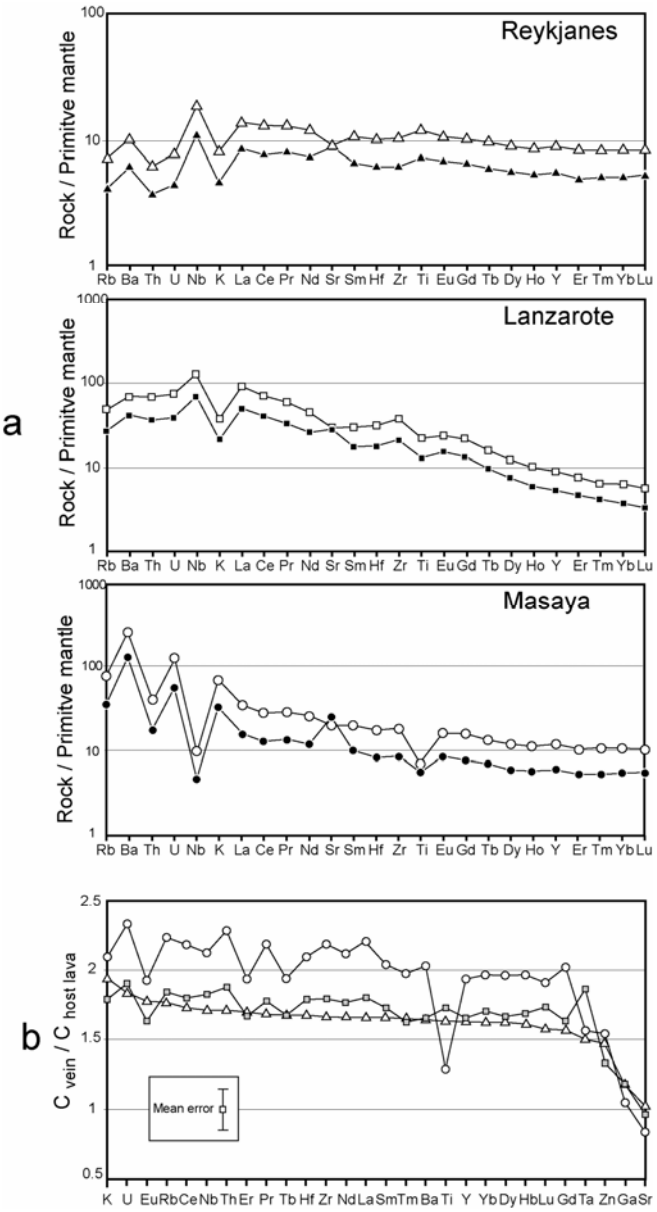

Figure 6: a) Primitive mantle normalized multi-elementary diagram (Hofmann 1988), showing the enrichment of veins when compared to their host lavas. Filled symbols = host lavas; open symbols = segregation vein. b) Diagram showing the relative enrichment of veins compared to host lavas (C_{vein}) / ($C_{host\ lava}$). Element order is established from incompatibility order of the Reykjanes samples. Triangle = Reykjanes; circle = Masaya; square = Lanzarote. (C_{vein}; $C_{host\ lava}$: concentration in vein and host lava respectively).

Partition coefficient of transitional elements:

The host lava – segregation vein pairs permit estimation of partition coefficients for a few transitional elements. These elements have specific compatible behaviour that often allow tracing the fractionation of individual minerals, such as Sc for clinopyroxene and Ni for olivine etc. The decreasing concentration of these elements in segregation veins compared to the host lavas (Table 2), reflects their elevated bulk partition coefficient. The estimated crystallizing assemblage of host lava producing the segregations can be used to calculate the D for Ni, Cr and Sc in clinopyroxene and olivine. By assuming incompatible behaviour of these elements for plagioclase and compatible one for Fe-Ti oxides, the D calculated for clinopyroxene and olivine (Table 3) are in agreement with those previously proposed (e.g. compilation from EarthRef database). The coherent behaviour of the transitional elements thus strongly supports the composition of the estimated fractionating assemblage before the vein formation.

Constraints on segregation veins formation

Mineral composition continuity from host lava to veins added to the fact that host lava and veins show parallel major and trace elements patterns, allows considering that both differentiated by fractional crystallisation independently of the geodynamical environment.

Degree of host lava crystallisation needed to generate segregation veins:

The most incompatible elements can be utilised to calculate the degree of fractionation forming the segregation veins. Both K and U display the most incompatible behaviour (Fig. 6b), consequently, the Rayleigh (1896) equation $C_l = C_o \, . \, F^{(D-1)}$ can be simplified into $F = (C_o/C_l)$ since D_K and D_U will be close to zero (C_o: initial liquid content; C_l: residual liquid content; F: degree of melting). The degree of fractional crystallisation is finally given by $X = (1-F) = 1- (C_o/C_l)$.

The whole rock host lava composition has been chosen as representative of the initial liquid (C_o). Calculation performed for all veins from three sites gives degree of fractional crystallisation X ranging between 44 % and 57 % (Table 2). These results are in perfect agreement with values established by mass balance from major element composition (Table 3) and close to the 50 % proposed for segregation vesicles and veins elsewhere (Anderson 1984).

Temperature:

Temperature of crystallisation has been estimated using the "Melts" algorithm (Ghiorso and Sack 1995), which allows to calculate the liquidus temperature of the host lava. The range 1270-1200°C is calculated for the three host lavas (highest for Lanzarote and lowest for Masaya; Table 2 and Fig 7a) whereas the maximum formation temperature of segregation veins is in the range 1180-1130°C. The calculated liquidus temperature of the residual glass patches in veins ranges from 1120°C to 950°C (Table4 and Fig 7a), which is close to the solidus temperature of the host-vein system. Figure 7a shows the temperature decrease from about 1250°C to 950°C during the differentiation process (from host lava: F=1 to interstitial glass: F=0.25-0.03 as discussed below).

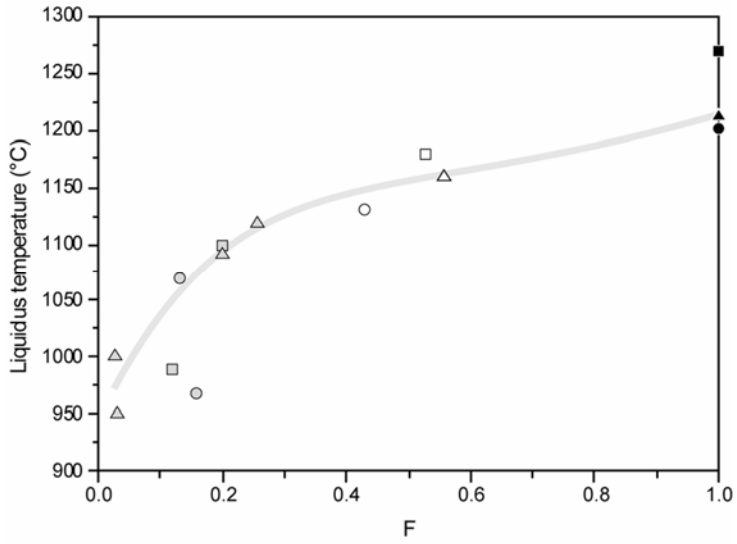

a

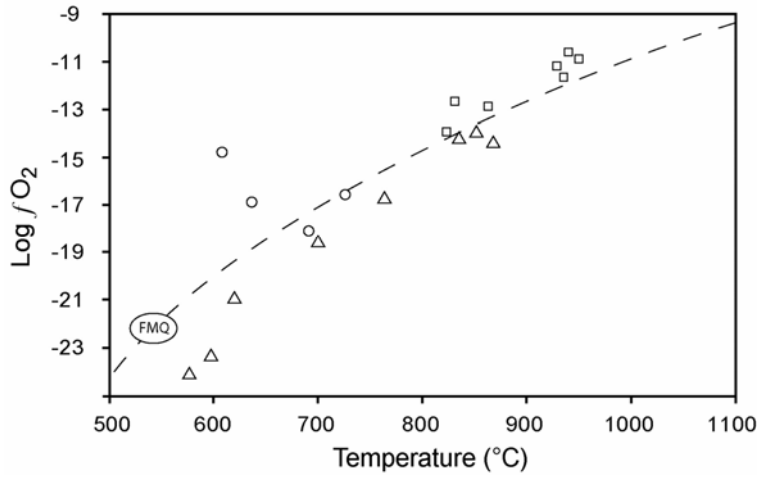

b

Figure 7: a) Temperature evolution during differentiation process, based on liquidus temperature estimated by "Melts" algorithm (Ghiorso and Sack 1995). The grey trend represents the Reykjanes evolution. b) Vein oxygen fugacity and temperature calculated from ilmenite – magnetite pairs at equilibrium using QUILF algorithm (Andersen et al. 1993). FMQ dotted line corresponds to the fayalite–magnetite–quartz buffer. Same symbols as in Figure 5, except grey symbols that represent glass.

Table 4: Selected analyses of extreme composition of glass from segregation veins.

	Reykjanes				Masaya		Lanzarote	
	"K_2O poor"		"K_2O rich"					
SiO_2	76.2	83.5	74.0	77.58	73.2	80.6	68.2	73.4
TiO_2	0.357	0.644	0.362	0.38	0.362	0.307	1.03	0.609
Al_2O_3	12.2	9.56	11.7	11.90	13.4	10.4	15.4	15.4
FeO*	0.691	1.03	4.43	0.83	1.23	0.459	3.71	1.57
MnO	0.026	0.054	0.125	0.02	0.00	0.030	0.085	0.068
MgO	0.055	0.00	0.295	0.01	0.00	0.00	0.235	0.153
CaO	4.72	1.05	1.28	0.38	0.32	0.242	1.23	0.472
Na_2O	5.35	3.97	2.62	1.67	2.95	1.96	7.44	1.95
K_20	0.569	0.717	5.59	5.54	8.06	6.60	3.34	5.70
Total	100.2	100.5	100.3	98.3	99.6	100.5	100.7	99.3
Estimation of Liquidus temperature	1120°C	1090°C	1000°C	950°C	1070°C	970°C	1100°C	990°C
CIPW norm, with no Fe correction								
Quartz	35.9	54.7	31.1	45.4	24.7	43.2	9.3	38.1
Orthoclase	3.36	4.21	32.9	32.7	47.8	38.8	19.6	33.7
Albite	45.3	33.4	22.1	14.2	24.3	16.5	60.3	16.5
Anorthite	7.51	5.17	3.53	1.88	0	0.063	0	2.34
Nepheline	0	0	0	0	0	0	0	0.00
Diopside	1.66	0	2.46	0	1.41	0.733	5.31	0.00
Hypersthene	5.46	0.914	7.18	0.955	0.917	0	3.04	2.38
Olivine	0	0	0	0	0	0	0	0.00
Ilmenite	0.68	1.22	0.685	0.729	0.690	0.580	1.94	1.16
Magnetite	0	0	0	0	0	0	0	0
Degree of crystallization (%)	75	80	97	97	87	84	80	88

Reykjanes has two types of glass compositions, one with low K_2O/Na_2O is called "K_2O poor" glass whereas the other has a higher K_2O/Na_2O and is called "K_2O rich" glass. Liquidus temperatures are those calculated utilizing "Melts" algorithm (Ghiorso and Sack 1995).

Oxygen fugacity:

Oxygen fugacity and temperature of the last oxide equilibration was estimated from the ilmenite-magnetite pairs (Bacon and Hirschmann 1988) in the veins, using the QUILF algorithm (Andersen et al. 1993). All data are plotted in Figure 7b and all three samples, record oxide temperatures significantly lower than calculated for the residual glass (around 1120-950°C). This is interpreted in terms of sub-solidus oxide re-equilibration. Both in the case of Reykjanes and Lanzarote, the oxides record reduced condition indicating that the veins cooled as closed systems, isolated from atmosphere, from 1000°C to 600°C. In contrast,

the Masaya oxides experienced a more complicated cooling history. Subduction zone calc-alkaline basalts generally have ΔLog fO2 (FMQ) of about +1 or +2 (Frost and Lindsley 1992), whereas in Masaya ΔLog fO2 (FMQ) ranges from -0.9 to +5.2. This indicates an open system behaviour around 650-700°C in the case of Masaya.

Origin of segregation veins

In lava flows, the pressure is close to atmospheric pressure (or does not exceed few bars). At such pressure, water is insoluble in magmatic melts (e.g. Wallace and Anderson 2000) which is attested by the anhydrous samples of this study (host lavas, veins and glass patches). Anderson et al. (1984) show that the gas volume increases sufficiently during crystallisation of anhydrous minerals (plagioclase, pyroxenes, olivine and oxides) to allow a residual liquid segregation by gas filter pressing (effervescent gas process). Assuming a pure incompatible behaviour of water, a degree of crystallisation of about 44 % to 57 % of anhydrous minerals in the lower SF should result in doubling water content in the residual liquid thus allowing "gas filter pressing" process to develop (Anderson et al. 1984; Goff 1996) and concentrate this differentiated liquid in sufficient volume to form a diapir. Indeed, gas phase associated with residual liquid allows decreasing density and viscosity of melt and consequently, as proposed in Kilauea Iki lava lake by Helz (1980) and Helz et al. (1989), it appears realistic to consider the diapiric ascent of these low density segregated melts in host lava which have higher density (Table 5). This vertical ascent could take place between the end of liquid lava movement and the deep penetration of columnar joints (Goff 1996).

Stockes' law has been used to estimate the velocity of diapiric ascent across lava units. The melts density and viscosity (Table 5) are estimated from the chemical composition of host lava and segregation vein. Density was calculated according to Bottinga and Weill (1970) and the viscosity according to the Shaw (1972) and Spera (2000) method. The volume of gas phase is taken equal to the whole rock porosity, in addition, it is assumed that all volatiles are exsolved in a gas phase. It is also considered that contrary to host lava, segregated liquid does not contain crystals during its emplacement. All other parameters are shown in Table 5.

The computed velocity for magma ascent through lava units ranges from 0.05 $m.day^{1}$ to 3 $m.day^{-1}$. In course of time, due to diapir feeding by new segregated liquids, its diameter increase, and ascent velocity reaches a few meters per day. These estimated rates are similar to those calculated by Goff (1996). Diapiric ascent stops at the rigid crust of the upper SF (>

55 % crystallinity) and the magma motion changes from vertical to horizontal, spreading out as veins.

Table 5: Parameters used for the computed diapiric ascent velocity of segregated melt though the lava unit.

		Reykjanes		Masaya		Lanzarote	
		Host lava	Vein	Host lava	Vein	Host lava	Vein
Crystal abundance (%)		15 - 44	0	20 - 57	0	10 - 48	0
Porosity (%)		7	20	17	24	9	30
Density	Host lavas liquidus	2.54	-	2.22	-	2.45	-
	Veins liquidus	2.55	2.21	2.23	2.00	2.47	1.88
Viscosity (Pa.s-1)	Host lavas liquidus	18	-	68	-	8	-
	Veins liquidus	158	20	373	200	304	32
Diapir radius		2-10cm					

The host lava temperature is considered as ranges between host lava and vein liquidus ones (~1230°C and ~1150°C) and segregation vein temperature as vein liquidus one (~1150°C). Density and viscosity were calculated using Bottinga and Weill (1970), Shaw (1972) and Spera (2000) methods.

Assessment of the fractional crystallisation efficiency

Compositional zoning of the minerals shows that equilibrium crystallisation is not a realistic process involved in the formation and differentiation of segregation veins. A differentiation mechanism similar to that of fractional crystallisation is thus more realistic. The ultimate product of this mechanism is preserved as the final interstitial glass in the segregation veins. The composition of these glasses represent the continuity of tholeiitic trend (Fig. 5a), defined by host lava and veins whole rock composition. In Figure 5b, the tholeiitic trend observed in our samples is similar to that of Carmichael (1964), established at Thingmuli. The tholeiitic trend defined here (Fig. 5a,b) shows a characteristic high FeO* increase in the first 50 % of fractional crystallisation (host lava to segregation veins) and in the second half (segregation veins to vein's glasses), the FeO* decreases but less rapidly than the MgO which decreases all along the fractional crystallisation. K_2O behaves as a very incompatible element during the whole crystallisation, (except during the very ultimate phases within the veins, where K-feldspar can crystallize). Consequently K_2O can be used to estimate the minimum degree of crystallisation or differentiation in vein glass. Using the simplified equation $F = (C_o/C_l)$, it appears that glass patches corresponds to magmatic liquids produced

by 75-98 % of crystallisation ranging. Glass patches thus record the final stage of fractional crystallisation and they can be considered as having the composition of the last magma drops generated by fractional crystallisation. Consequently, via the "host lava – segregation vein – vein's glasses" system we have access to the entire fractional crystallisation process at atmospheric pressure.

Glass composition:

Segregation vein glass patches from the three sites have different compositions, representative analyses are listed in Table 4 and the all of them in Appendix 1. Glass analysis from Reykjanes, discussed by Martin and Sigmarsson (2005) reveal a bimodal distribution: 1) The more abundant, (32/36 analysis), has an average K_2O/Na_2O of about 0.2 and is defined as a "K_2O poor" glass. This latter will be referred as trondhjemitic in composition (Barker 1979). 2) The second type, less represented, (4/36 analysis), has average K_2O/Na_2O of about 2.5 and is defined like "K_2O rich" glass. It will be referred to as granitic in composition (Barker 1979). All Masaya's glasses are homogeneous and granitic in composition having an average K_2O/Na_2O around 2.7, whereas those from Lanzarote are granitic or intermediate between granitic and trondhjemitic. They have an average K_2O/Na_2O of about 1.0.

Melt Evolution:

The entire evolution of liquid composition during fractional crystallisation can be discussed in two different systems at atmospheric pressure. During the first stage, the crystallizing assemblage is composed of plagioclase and clinopyroxenes (≥ 80 % volume). Consequently the melt evolution is clearly depicted in the Diopside-Anorthite-Albite (Di-An-Ab) system (basaltic system). Figure 8 shows that host lava compositions fall in the plagioclase stability field, whereas all veins plot on the plagioclase + clinopyroxene + liquid cotectic valley. This is in agreement with intergrowths of clinopyroxene and plagioclase observed in segregation veins. The liquid composition clearly evolves from the plagioclase field towards the cotectic valley and then down the thermal valley towards the albitic pole.

Close to the end of crystallisation, the liquid composition becomes granitic because of K-feldspar, albite, quartz and iron-titanium oxide crystallisation. Consequently its evolution must be discussed in Quartz-Albite-Orthoclase (Qz-Ab-Or) system. All "K_2O rich" glasses from Reykjanes, glasses from Lanzarote and Masaya, have a composition similar to the granitic system's minimum (Fig. 9). Only some glasses from Lanzarote form a less evolved

trend from the albitic pole towards the minimum. All "K_2O poor" glasses from Reykjanes plot close to the quartz + albite + liquid cotectic valley, far from the granitic minimum.

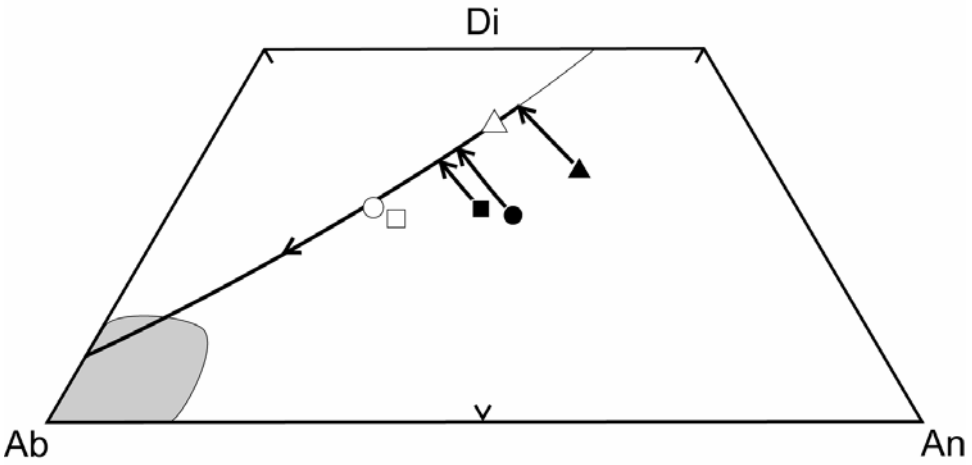

Figure 8: CIPW normative one-atmosphere Di-Ab-An diagram, from Morse (1980), showing that both host lavas and segregation veins, which present between 60 to 75 % of normative disopside + albite + anorthite, plot in the plagioclase field (at higher temperature than the cotectic valley) and in the cotecic valley respectively. Arrows show the compositional evolution of liquids from host lavas to residual glass patches (grey area) via segregation veins. Same symbols as in Figure 4 and Figure 5.

In Figure 9 is also shown evolution trends predicted by the "Melts" algorithm (Ghiorso and Sack 1995), for a fractional crystallisation under atmospheric pressure condition from segregation vein compositions of those from Lanzarote, Masaya and Reykjanes. It should be noted that this algorithm is mainly calibrated for basaltic to dacitic composition and it is assumed less accurate for granitic liquids. Therefore, we can only predict the hypothetical evolution of silicic liquids. Lanzarote and Masaya display a similar calculated evolution and the ultimate liquid composition should be granitic. In contrast, "Melts" algorithm prediction for Reykjanes does not lead to a granitic but trondhjemitic composition. As the main difference between the lavas is the K_2O/Na_2O, it seems that this initial ratio plays a significant role during fractional crystallisation. In fact, initial Lanzarote and Masaya's liquids which have a high K_2O/Na_2O (0.25 and 0.36, respectively) evolve towards granitic liquids by fractional crystallisation at atmospheric pressure, while that of Reykjanes have a low K_2O/Na_2O (0.07) and its last residual liquid is trondhjemitic in composition. At Reykjanes further local fractionation of Quartz and Albite (as observed in Fig. 3e), cause the liquid to

evolve from trondhjemitic composition towards the granitic minimum (Fig. 9). This very final composition corresponds to more than 98 % of fractional crystallisation, which appears too high to be faithfully predicted by the "Melts" algorithm.

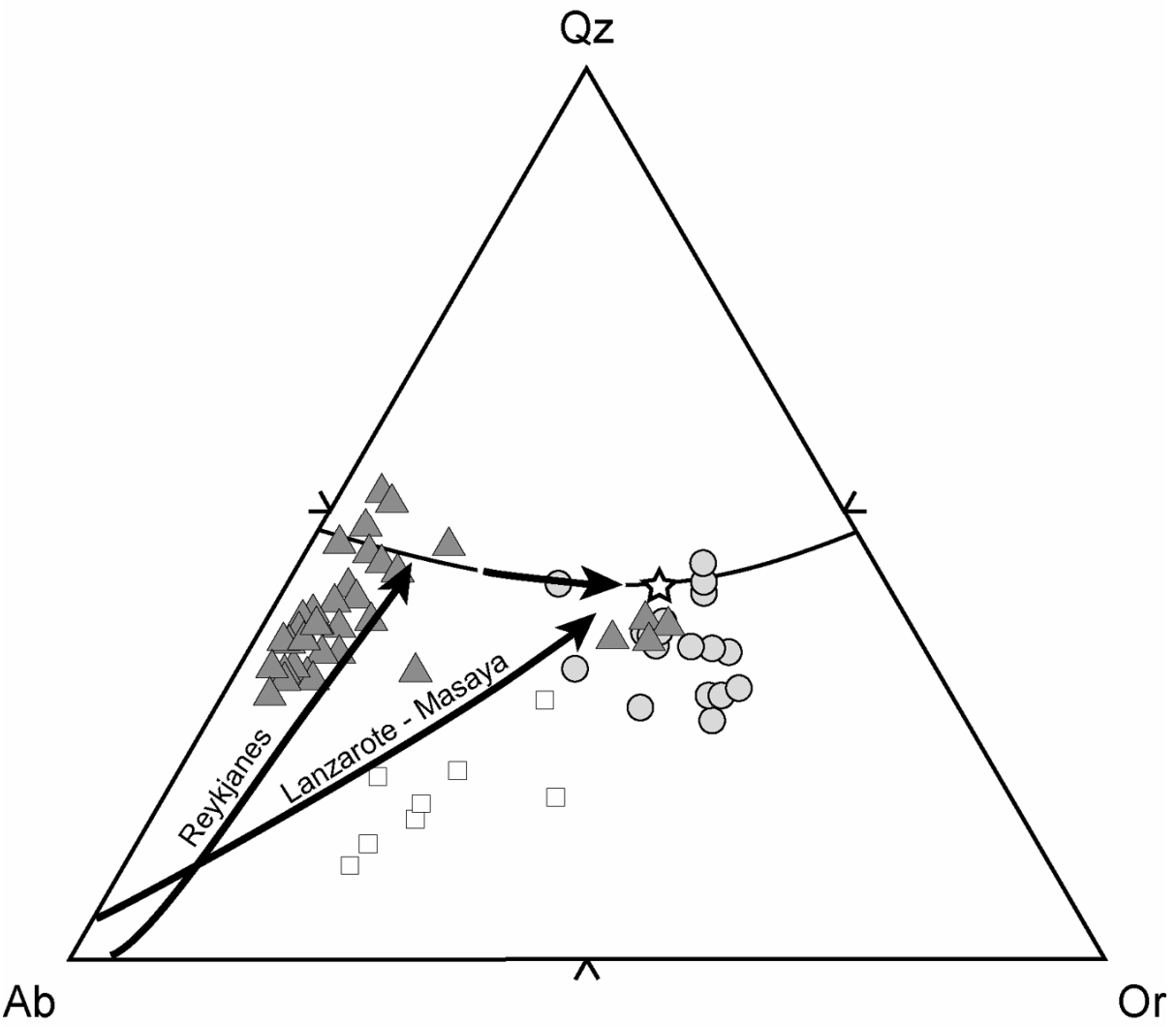

Figure 9: Projection of glass composition, which presents more than 80 % of normative quartz + albite + orcthoclase, in one atmosphere Qz-Ab-Or diagram using the scheme of Blundy and Cashman (2001). Most Reykjanes glasses (triangles) plot toward the cotectic valley between Ab and Qz poles (< 10-15 % Or), with only a few points close to the minimum of the system. Masaya (circle) glasses fall near the minimum, whereas at Lanzarote (squares) glass composition define a trend towards the system's minimum. Arrows show the liquid evolution tendency caused by atmospheric pressure fractional crystallisation, as estimated with the "Melts" algorithm (Ghiorso and Sack 1995). The Reykjanes and Lanzarote trends are calculated under FMQ oxygen fugacity condition and Masaya at two order of magnitude higher values (ΔLog fO_2 (FMQ) = +2; (Frost and Lindsley 1992). The smallest arrow, along the cotectic valley, indicates the liquid evolution by fractional crystallisation which leads to granitic melts genesis from trondhjemitic compositions in Reykjanes segregation vein after a second gas-filter pressing process (Martin and Sigmarsson 2005).

Summary and conclusions

The conditions during which segregation veins are generated are established. In tholeiitic lava flows, evolved basaltic liquid forms at temperature of about 1180-1130°C (~100°C lower than the lava liquidus temperature) and begin to segregate from the host lava when the latter has crystallised to approximately 50 % (44 - 57 %). This mechanism is independent of geodynamic environments. A diapiric origin for segregation veins appears most likely and magma ascent velocity from the lower SF to the upper SF would be close to 3 m per day. The host lavas and their associated segregation veins display a complete record of fractional crystallisation at 1 atmosphere both in the mineralogical evolution and by the highly evolved residual glass composition. Finally granitic liquids are formed by fractional crystallisation of tholeiitic basalt with a high initial K_2O/Na_2O (~0.2-0.4) whereas lower K_2O/Na_2O (<0.1) leads to the production of trondhjemitic melts.

Acknowledgment

We thank Michèle Veschambre, Karine David, Jean-Luc Devidal and Mhammed Benbakkar for their analytical assistance. We are grateful to Pierre Schiano, Pierre Boivin François Faure and Hervé Martin for fruitful discussions. This work was supported by the Icelandic Science Foundation and the French-Iceland “Jules Verne” programme.

References

Andersen DJ, Lindsley DH, Davidson PM (1993) QUILF: a PASCAL program to assess equilibria among Fe- Mg-Ti oxides, pyroxenes, olivine, and quartz. Computers in Geosciences 19:1333-1350

Anderson AT, George JR, Swihart H, Artioli G, Geiger CA (1984) Segregation vesicles, Gas filter-pressing, and igneous differentiation. J Geol 92:55-72

Bacon CR, Hirschmann MM (1988) Mg/Mn partitioning as a test for equilibrium between coexisting Fe-Ti oxides. Amer Mineral 73:57-61

Barker F (1979) Trondhjemites: definition, environment and hypothesis of origin. In: Barker F (ed) Trondhjemites, Dacites and Related Rocks, Elsevier, Amsterdam, pp 1-12

Bindeman IN, Davis AM, Drake M, J. (1998) Ion microprobe study of plagioclase-basalt partition experiments at natural coàncentration levels of trace elements. Geochim Cosmochim Acta 62:1175-1193

Blundy J, Cashman K (2001) Ascent-driven crystallisation of dacite magmas at Mount St Helens, 1980-1986. Contrib Mineral Petrol 140:631-650

Bottinga Y, Weill D (1970) Densities of liquid silicate systems csalculated from partial molar volumes of oxide components. Amer J Sci 269:169-182

Cantagrel F, Pin C (1994) Major, minor and rare-earth element determinations in 25 rock standards by ICP-atomic emission spectrometry. Geostandards Newsletter 18:123-138

Carmichael ISE (1964) The petrology of Thingmuli, a tertiary volcano in Eastern Iceland. J Petrol 5:435-460

Caroff M, Maury RC, Cotten J, Clement J-P (2000) Segregation structures in vapor-differentiated basaltic flows. Bull volcanol 62:171-187

Carr MJ, Rose WI, Stoiber RE (1982) Andesites: orogenic andesites and related rocks. In: Central america, Wiley, New-York, pp 149-166

Drake MJ, Weill DF (1975) Partition of Sr, Ba, Ca, Y, Eu^{2+}, Eu^{3+} and other REE between plagioclase feldspar and magmatic liquid: an experimental study. Geochim Cosmochim Acta 39:689-712

Frost BR, Lindsley DH (1992) Equilibria among Fe-Ti oxides, pyroxens, olivine, and quartz: Part II. Application. Amer Mineral 77:1004-1020

Gee MAM, Thirlwal MF, Taylor RN, Lowry D, Murton BJ (1998) Crustal processes: Major control on Reykjanes Peninsula lava chemistry, SW Iceland. J Petrol 39:819-839

Ghiorso MS, Sack RO (1995) Chemical mass transfer in magmatic processes. 4. A revised and internally consistent thermodynamic model for the interpolation of liquid-solid equilibria in magmatic systems at elevated temperatures and pressures. Contributions to Mineralogy and Petrology 119:197-212

Goff F (1996) Vesicle cylinders in vapor-differentiated basalt flows. J Volcanol Geotherm Res 71:167-185

Helz RT (1980) Crystallization history of Kilauea Iki lava lake as seen in drill core recovered in 1967-1979. Bull volcanol 43:675-701

Helz RT, Kirschenbaum H, Marinenko JW (1989) Diapiric transfer of melt in Kilauea Iki lava lake, Hawaï: a quick, efficient process of igneous differenciation. Geol Soc Am Bull 101:578-594

Hoernle K, Schmincke HU (1993) The petrology of the tholeiites through melilite nephelinites on Gran Canaria, Canary Islands: crystal fractionation, accumulation and depths of melting. J Petrol 34:573-597

Hofmann AW (1988) Chemical differentiation of the Earth: the relationship between mantle, continental crust, and oceanic crust. Earth Planet Sci Lett 90:297-314

Jakobsson SP, Jonsson J, Shido F (1978) Petrology of the Western Reykjanes Peninsula, Iceland. J Petrol 19:669-705

Jóhannesson H, Saemundsson K (1998) Geological map of Iceland. 1:500 000. Bedrock geology. In: Icelandic Institute of Natural History, Reykjavík

Leeman WP, Ma MS, Murali AV, Schmitt RA (1978) Empirical estimation of magnetite/liquid distribution coefficients for some transition elements - A correction. Contrib Mineral Petrol 65:269-272

Marsh BD (2002) On bimodal differentiation by solidification front instability in basaltic magmas, part 1: Basic mechanics. Geochim Cosmochim Acta 66:2211-2229

Martin E, Sigmarsson O (2005) Trondhjemitic and granitic melts formed by fractional crystallization of an olivine tholeiite from Reykjanes Peninsula, Iceland. Geol Mag 142(6):651-658

McBirney AR (1993) Igneous petrology, Jones and Bartlett Publishers, Boston, p 508

Morse SA (1980) Basalts and phase diagrams, Springer-Verlag, New-York

Pearce JA (1983) Role of the sub-continental lithosphere in magma genesis at active continental margins. In: Hawkesworth CJN (ed) Continental basalts and mantle xenoliths, Shiva Publishing, Nantwich, pp 230-249

Philpotts AR, Carroll M, Hill JM (1996) Crystal-mush compaction and the origin of pegmatitic segregation sheets in a thick flood-basalt flow in the mesozoic Hartford basin, Connecticut. J Petrol 34:811-836

Puffer JH, Horter DL (1993) Origin of pegmatitic segregation veins within flood basalts. Geol Soc Am Bull 105:738-748

Rayleigh JWS (1896) Theorical considerations respecting the separation of gases by diffusion and similar processes. Philos Mag 42:77-107

Schilling JG (1973) Iceland mantle plume: geochemical study of Reykjanes ridge. Nature 242:465

Shaw HP (1972) Viscosities of magmatic silicate liquids: an empirical method of prediction. Amer J Sci 272:870-893

Shimizu N, Kushiro I (1975) Partitioning of Rare-Earth Elements between Garnet and Liquid at High-Pressures - Preliminary Experiments. Geophys Res Lett 2 413-416

Sigmarsson O, Carn S, Carracedo JC (1998) Systematics of U-series nuclides in primitive lavas from the 1730-36 eruption on Lanzarote, Canary Islands and implications for the role of garnet pyroxenites during oceanic basalt formations. Earth Planet Sci Lett 162:137-151

Spera FJ (2000) Physical properties of magma. In: Sigurdsson H (ed) Encyclopedia of volcanoes, Academic press, London, pp 171-190

Stormer JC, Nicholls J (1978) XLFRAC: a program for interactive testing of magmatic differentiation models. Computer Geoscience 87:51-64

Sun SS, McDonough WF (1989) Chemical and isotopic systematics of oceanic basalts: Implications for the mantle composition and processes. In: Magmatism in the Ocean Basin, vol 42. Geol. Soc. Sp. Publi., pp 313-345

Thordarson T, Self S (1998) The Roza member, Columbia basalt group: a gigantic pahoehoe lava flow field formed by endogenous processes? J Geophys Res 103:27411-27445

Wager LR, Brown GM (1967) Layered igneous rocks, vol., San Fransisco

Walker JA (1989) Caribbean are tholeiites. J Geophys Res 94:10539-10548

Wallace P, Anderson AT (2000) Volatiles in magmas. In: Sigurdsson H (ed) Encyclopedia of volcanoes, Academic press., London, pp 149-170

Zindler A, Frey FA, Jakobsson SP (1979) Nd and Sr isotope ratios and rare earth element abundances in Reykjanes Peninsula basalts: evidence for mantle heterogeneity beneath Iceland. Earth Planet Sci Lett 45:249-262

Appendix 1: Major element composition of all analyzed glass patches in the segregation veins. Reykjanes has two types of glass compositions, one with low K_2O/Na_2O is called "K_2O poor" glass whereas the other has higher K_2O/Na_2O and is called "K_2O rich" glass

	Lanzarote							
	#2	#5	#17	#2	#6	#10	#11	#15
SiO_2	71.31	70.96	70.64	69.93	73.17	69.73	68.20	70.14
TiO_2	0.56	0.95	0.88	0.93	0.71	0.93	1.03	0.66
Al_2O_3	15.75	15.37	15.13	15.82	13.90	14.32	15.40	15.03
FeO*	1.83	2.22	2.74	2.16	0.96	3.61	3.71	1.74
MnO	0.04	0.01	0.02	0.01	0.04	0.03	0.09	0.07
MgO	0.11	0.23	0.21	0.14	0.07	0.15	0.24	0.17
CaO	0.83	0.71	0.74	0.83	0.81	0.75	1.23	0.38
Na_2O	5.73	5.91	6.51	7.16	3.49	4.81	7.44	4.49
K_2O	4.78	3.68	4.07	3.62	5.87	4.82	3.34	6.53
Total	100.9	100.1	101.0	100.6	99.0	99.2	100.7	99.2
Quartz	16.84	19.48	14.43	12.05	28.55	19.39	9.33	17.17
Corundum	0.00	0.36	0.00	0.00	0.33	0.00	0.00	0.00
Orthoclase	28.23	21.73	24.03	21.28	35.04	28.73	19.58	38.90
Albite	48.47	50.03	55.11	60.26	29.82	41.04	60.27	38.26
Anorthite	3.14	3.53	0.03	0.30	4.07	3.29	0.00	1.59
Diopside	0.86	0.00	3.19	3.32	0.00	0.42	5.31	0.27
Hypersthene	2.33	3.08	2.48	1.04	0.82	5.34	3.04	2.53
Ilmenite	1.06	1.80	1.67	1.75	1.37	1.79	1.94	1.27

	Masaya																
	#3	#4	#5	#6	#7	#8	#10	#54	#55	#56	#63	#67	#70	#86	#89	#93	#95
SiO_2	80.55	79.70	77.98	77.05	77.24	76.80	76.99	77.35	73.25	74.87	74.93	76.36	74.18	74.65	78.19	72.83	77.03
TiO_2	0.31	0.52	0.26	0.32	0.56	0.28	0.51	0.43	0.36	0.34	0.40	0.48	0.30	0.19	0.44	0.60	0.20
Al_2O_3	10.39	11.09	12.36	12.15	11.64	12.82	12.52	11.97	13.43	13.25	12.97	13.13	12.87	12.92	11.43	13.09	11.75
FeO*	0.46	0.86	0.41	0.63	1.20	0.56	0.90	0.55	1.23	0.82	0.96	0.42	0.65	0.60	0.47	1.62	0.66
MnO	0.03	0.01	0.00	0.05	0.00	0.01	0.05	0.07	0.00	0.06	0.03	0.04	0.05	0.00	0.00	0.03	0.04
MgO	0.00	0.02	0.01	0.00	0.00	0.01	0.01	0.00	0.00	0.00	0.01	0.02	0.02	0.00	0.02	0.04	0.00
CaO	0.24	0.24	0.30	0.30	0.25	0.26	0.33	0.31	0.32	0.20	0.20	0.44	0.25	0.24	0.49	0.88	0.24
Na_2O	1.96	2.06	2.92	2.70	2.51	1.89	1.97	2.62	2.95	2.79	2.98	3.55	2.65	2.73	3.12	2.93	3.07
K_2O	6.60	6.97	6.77	6.56	6.57	8.10	7.83	6.68	8.06	8.48	7.64	5.93	7.96	7.77	4.58	7.02	6.23
Total	100.5	101.5	101.1	99.8	100.0	100.7	101.1	100.0	99.6	100.8	100.1	100.4	98.9	99.1	98.7	99.0	99.2
Quartz	43.45	40.35	34.47	35.24	36.43	33.97	34.45	35.77	25.84	29.03	34.55	31.90	28.27	28.65	41.91	26.87	35.05
Corundum	0.00	0.00	0.00	0.06	0.00	0.47	0.21	0.00	0.00	0.00	0.00	0.07	0.00	0.00	0.45	0.00	0.00
Orthoclase	38.99	41.17	40.00	38.79	38.82	47.85	46.24	39.51	47.33	48.74	42.54	34.91	47.56	46.36	27.42	41.86	37.10
Albite	16.58	17.41	24.71	22.88	21.20	16.02	16.69	22.14	24.07	20.35	22.78	29.95	22.13	23.32	26.73	25.04	25.95
Anorthite	0.06	0.45	0.63	1.46	1.10	1.28	1.61	1.18	0.00	0.00	0.00	2.18	0.00	0.03	2.46	1.86	0.00
Diopside	0.74	0.66	0.67	0.00	0.11	0.00	0.00	0.32	0.00	0.00	0.00	0.00	1.09	1.04	0.00	2.25	1.05
Hypersthene	0.00	0.44	0.00	0.72	1.22	0.60	0.93	0.27	1.65	1.03	1.11	0.10	0.26	0.24	0.17	0.98	0.42
Ilmenite	0.58	0.98	0.50	0.61	1.06	0.54	0.96	0.81	0.68	0.63	0.72	0.90	0.58	0.37	0.85	1.14	0.37

Appendix 1 (continued):

	Reykjanes " *K2O poor*"																			
	#28	#29	#36	#41	#42	#1	#7	#8	#1	#4	#5	#12	#13	#19	#52	#55	#56	#57	#3	#8	#9
SiO_2	79.06	79.92	76.07	81.85	79.90	76.25	79.48	79.36	81.86	83.52	81.64	83.23	80.79	80.31	77.69	79.25	78.21	76.14	77.20	79.40	77.07
TiO_2	0.27	0.21	0.28	0.39	0.35	0.36	0.42	0.43	0.62	0.64	0.58	0.39	0.26	0.41	0.31	0.20	0.11	0.34	0.42	0.29	0.28
Al_2O_3	12.49	12.48	13.13	10.93	11.79	12.17	12.40	12.68	10.71	9.56	10.65	10.38	11.31	10.73	13.03	12.15	12.64	13.61	12.92	12.47	12.78
FeO*	0.52	0.56	0.50	0.63	0.94	0.69	0.54	0.66	0.77	1.03	0.76	0.82	0.86	0.91	1.42	0.54	0.63	1.07	1.28	0.72	0.79
MnO	0.01	0.02	0.03	0.04	0.00	0.03	0.00	0.03	0.04	0.05	0.04	0.01	0.00	0.00	0.04	0.00	0.04	0.00	0.02	0.07	0.04
MgO	0.00	0.03	0.02	0.01	0.01	0.06	0.00	0.02	0.02	0.00	0.01	0.00	0.00	0.00	0.04	0.01	0.01	0.00	0.01	0.00	0.03
CaO	1.78	1.50	0.54	1.26	1.26	4.72	1.75	1.49	1.14	1.05	1.16	1.19	1.33	1.11	2.68	1.69	2.64	2.35	1.29	1.81	1.93
Na_2O	5.57	5.47	5.61	4.69	5.31	5.35	5.46	5.55	4.35	3.97	4.83	3.77	4.20	4.46	4.77	4.68	4.65	5.20	5.31	4.93	5.12
K_2O	0.76	0.82	2.94	0.80	0.96	0.57	0.75	0.66	0.69	0.72	1.10	0.94	1.31	1.64	0.48	1.61	1.09	1.15	1.81	0.67	0.71
Total	100.5	101.0	99.1	100.6	100.5	100.2	100.8	100.9	100.2	100.5	100.8	100.7	100.1	99.6	100.5	100.1	100.0	99.9	100.3	100.4	98.8
Quartz	40.25	41.56	31.03	48.63	42.44	35.99	41.40	41.18	51.37	55.18	47.10	54.92	48.16	45.69	41.73	42.30	41.53	36.27	36.12	43.97	40.07
Corundum	0.00	0.00	0.00	0.06	0.00	0.00	0.00	0.13	0.73	0.34	0.00	1.00	0.58	0.00	0.00	0.00	0.00	0.00	0.00	0.34	0.10
Orthoclase	4.43	4.85	17.37	4.73	5.67	3.37	4.43	3.90	4.08	4.25	6.44	5.50	7.68	9.63	2.84	9.51	6.44	6.80	10.70	3.96	4.20
Albite	47.13	46.29	47.47	39.69	44.93	45.27	46.20	46.96	36.81	33.59	40.87	31.90	35.54	37.74	40.28	39.52	39.35	44.00	44.93	41.72	43.32
Anorthite	6.86	7.08	1.96	6.25	5.50	7.51	7.11	7.39	5.66	5.21	4.16	5.90	6.60	4.44	12.77	7.43	10.40	10.37	6.07	8.98	9.53
Diopside	0.58	0.32	0.62	0.00	0.67	1.11	0.14	0.00	0.00	0.00	0.47	0.00	0.00	0.95	0.46	0.80	1.55	1.15	0.29	0.00	0.00
Hypersthene	0.00	0.39	0.00	0.36	0.41	0.00	0.00	0.35	0.19	0.49	0.00	0.54	0.80	0.11	1.44	0.05	0.00	0.37	1.04	0.67	0.81
Wollastonite	0.55	0.00	0.00	0.00	0.00	6.08	0.59	0.00	0.00	0.00	0.44	0.00	0.00	0.00	0.00	0.00	0.40	0.00	0.00	0.00	0.00
Ilmenite	0.51	0.40	0.53	0.74	0.66	0.68	0.80	0.80	1.18	1.22	1.08	0.74	0.49	0.78	0.59	0.38	0.21	0.63	0.80	0.55	0.53
Magnetite	0.13	0.13	0.12	0.16	0.23	0.17	0.13	0.16	0.19	0.25	0.19	0.20	0.20	0.22	0.35	0.13	0.16	0.26	0.30	0.17	0.19

	Reykjanes" K2O poor"										*Reykjanes" K2O rich"*			
	#15	#16	#26	#27	#29	#30	#37	#55	#97	#99	#101	#50	#19	#31	#6
SiO_2	77.55	77.06	75.51	78.24	77.11	76.41	78.54	76.28	79.37	75.72	76.06	76.79	75.89	74.69	73.96
TiO_2	0.20	0.33	0.49	0.16	0.29	0.55	0.22	0.08	0.34	0.18	0.21	0.32	0.56	0.40	0.36
Al_2O_3	12.47	13.94	13.08	13.27	11.56	13.07	11.65	13.99	11.22	13.73	13.53	12.87	11.94	12.91	11.65
FeO*	0.67	1.12	1.20	0.63	2.38	2.35	0.86	0.79	0.78	0.84	0.71	1.29	1.16	1.24	4.43
MnO	0.01	0.00	0.01	0.00	0.01	0.02	0.07	0.00	0.05	0.02	0.00	0.00	0.00	0.07	0.13
MgO	0.00	0.00	0.02	0.00	0.12	0.01	0.00	0.00	0.00	0.03	0.02	0.00	0.00	0.02	0.30
CaO	1.78	2.23	1.73	2.25	2.29	1.93	1.57	3.37	1.54	2.23	2.36	0.24	1.40	0.39	1.28
Na_2O	5.44	5.46	5.63	5.49	4.70	5.26	4.64	5.64	4.65	5.34	5.04	2.58	2.42	2.77	2.62
K_2O	0.55	0.58	1.16	0.57	0.63	0.76	1.16	0.72	0.99	0.71	0.73	6.49	6.28	6.10	5.59
Total	98.7	100.7	98.8	100.6	99.1	100.4	98.7	100.9	98.9	98.8	98.7	100.6	99.6	98.6	100.3
Quartz	39.87	37.81	34.51	39.29	41.51	37.65	43.33	34.33	45.12	36.69	38.59	35.83	35.24	33.79	32.05
Corundum	0.00	0.28	0.00	0.00	0.00	0.10	0.00	0.00	0.00	0.12	0.17	1.17	0.00	1.04	0.00
Orthoclase	3.25	3.43	6.86	3.37	3.72	4.49	6.86	4.25	5.85	4.20	4.25	38.35	37.11	36.05	33.03
Albite	46.03	46.20	47.64	46.45	39.77	44.42	39.26	47.72	39.35	45.19	42.65	21.83	20.48	23.44	22.09
Anorthite	7.95	11.06	6.99	9.88	8.58	9.57	7.53	10.73	6.82	11.06	11.71	1.14	3.17	1.93	3.56
Diopside	0.78	0.00	1.41	1.14	2.44	0.00	0.23	1.86	0.69	0.00	0.00	0.00	1.38	0.00	2.44
Hypersthene	0.25	1.04	0.21	0.02	1.95	2.50	0.87	0.00	0.27	1.00	0.71	1.32	0.00	1.27	5.37
Wollastonite	0.00	0.00	0.00	0.00	0.00	0.00	0.00	1.63	0.00	0.00	0.00	0.00	0.93	0.00	0.00
Ilmenite	0.36	0.63	0.93	0.30	0.53	1.04	0.42	0.15	0.65	0.34	0.40	0.61	1.06	0.74	0.68
Magnetite	0.16	0.28	0.29	0.14	0.58	0.57	0.20	0.19	0.19	0.20	0.17	0.30	0.28	0.30	1.07

B. Magmas trondhjemitiques et granitiques générés par cristallisation fractionée d'une tholeiite à olivine de la péninsule de Reykjanes, Islande.

1. Article "Trondhjemitic and granitic melts formed by fractional crystallization of an olivine tholeiite from Reykjanes Peninsula, Iceland" paru en 2005 dans Geological Magazine, 142 (6) 651-658.

Geol. Mag. **142** (6), 2005, pp. 651–658. © 2005 Cambridge University Press
doi:10.1017/S0016756805001160 *Printed in the United Kingdom*

Trondhjemitic and granitic melts formed by fractional crystallization of an olivine tholeiite from Reykjanes Peninsula, Iceland

E. MARTIN*† & O. SIGMARSSON*‡

*Laboratoire Magmas et Volcans, OPGC – Université Blaise Pascal – CNRS, 5 rue Kessler, 63038 Clermont-Ferrand, France
‡Institute of Earth Sciences, University of Iceland, 101 Reykjavik, Iceland

(*Received* 18 October 2004; *accepted* 3 May 2005)

Abstract – A pair of samples, from host lava and an included segregation vein from the Reykjanes Peninsula, Iceland, allows the assessment of a complete fractional crystallization of an olivine tholeiite at low pressure. The final product consists of silicic glasses with bimodal composition: trondhjemitic and more rarely granitic. Compilation of data on major element compositions of Icelandic silicic rocks reveals a clear difference from those of the segregation glasses. Fractional crystallization of basalts at low pressure is therefore not the most likely mechanism for the origin of silicic magmas in Iceland. Similar conclusions have been reached in studies on O- and Th-isotope compositions. On the other hand, the trondhjemitic compositions of the glasses in the segregation vein from Reykjanes Peninsula suggest that fractional crystallization of olivine tholeiites could have played a significant role during the formation of the very early continental crust.

Keywords: Iceland, fractional crystallization, trondhjemite, segregation vein, interstitial glass.

1. Introduction

The question of how the primitive continental crust was formed is not readily answered because of the lack of rock record older than the Archaean. Today, continental crust is generated in subduction zones, principally by partial melting of the metasomatized mantle wedge yielding ordinary calc-alkaline magmas (e.g. Wyllie & Sekine, 1982; Tatsumi, 1989) and, more rarely, by direct melting of the subducted slab, which generates adakites (e.g. Defant & Drummond, 1990; Martin, 1999). Similarly, the TTG (tonalite, trondhjemite and granodiorite) association, typical of Archaean continental crust, has also been suggested to be related to subduction zones (e.g. Martin, 1986; Rapp, 1995; Martin *et al.* 2005). In a very different tectonic setting, relatively large amounts of silicic magmas are erupted in Iceland, where a mid-ocean ridge and a mantle plume interact. Such a context might have been frequent on the early and hotter Earth during the Hadean eon. Early existence of continental crust is indeed suggested by the discovery of 4.4 Ga old zircons (Mojzsis, Harrison & Pidgeon, 2001; Wilde *et al.* 2001), although very little is known about its character. The same holds for the formation of extraterrestrial 'continental crust' such as on Mars (see Sotin, 2005 for review). If the interaction of mantle plumes and mid-ocean ridges was frequent in the past, then an understanding of the origin of silicic magmas in Iceland would be relevant for an improved comprehension of the origin of these early crusts.

The origin of silicic magma in Iceland has long been debated, and the proposed models fall into three categories, as follows:

(1) Dacites and rhyolites are derived from basaltic magmas through fractional crystallization processes (e.g. Carmichael, 1964; Wood, 1978; Macdonald *et al.* 1990; Furman, Frey & Meyer, 1992).

(2) Silicic magmas result from partial melting of hydrated metabasalts (e.g. O'Nions & Gronvold, 1973; Oskarsson, Sigvaldason & Steinthorsson, 1982; Nicholson *et al.* 1991; Sigmarsson *et al.* 1991; Sigmarsson, Condomines & Fourcade, 1992; Jónasson, 1994). In this case, mantle-derived and more evolved basalts interact with water in geothermal systems and are transformed into amphibolites or lower-grade metamorphic assemblages. Subsequent dehydration melting gives rise to silicic melts.

(3) A third group of models is in many respects a combination of the two previous ones. In a first stage, fractional crystallization of basaltic magma produces silicic or intermediate intrusive rocks and, in a second stage, intrusion of hotter basaltic magmas melts the more differentiated rocks and thus produces large volumes of silicic magma (Sigurdsson, 1977; Sigurdsson & Sparks, 1981; Gunnarsson, Marsh & Taylor, 1998).

The aim of this study is to address the problem of the origin of silicic magma in Iceland from a different

† Author for correspondence: E.Martin@opgc.univ-bpclermont.fr

angle. It summarizes major element constraints from a detailed investigation of segregation veins in tholeiitic lava flows on a more global scale (Martin & Sigmarsson, unpub. data). In these veins, very high degrees of fractional crystallization are reached, producing interstitial silica-rich glasses. Here, we discuss the mechanisms of formation of two distinct glasses, having trondhjemitic and granitic compositions, in a single olivine tholeiite lava sheet from the Reykjanes Peninsula, and compare their compositions with those of Icelandic silicic rocks. Finally, we speculate about the implications of our results for primitive continental crust formation.

2. Geological setting

The interaction of a mid-ocean ridge and a mantle plume in Iceland results in magmatism displaying variable characteristics on the island. For instance, the influence of the Iceland mantle plume is less pronounced on the Reykjanes Peninsula where magma productivity is lower and silicic magmas are absent, compared to Central Iceland with four to five times higher productivity (Jakobsson, 1972) and several mature central volcanoes producing highly evolved silicic magmas. The Reykjanes Peninsula is characterized by picrites and olivine tholeiites forming small and large shield volcanoes, respectively, and quartz-normative tholeiites produced from fissure eruptions during post-glacial time (Jakobsson, Jonsson & Shido, 1978). The samples of this study, host lava (HRG2) and a segregation vein (HRG4), come from an olivine tholeiite lava shield of early Holocene age (Fig. 1).

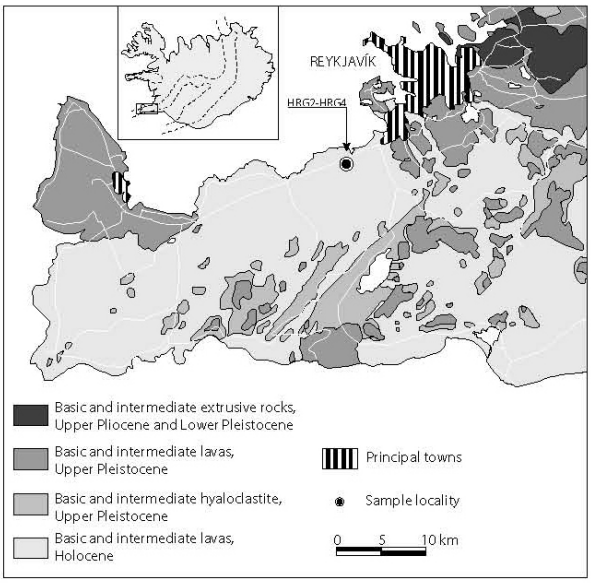

Figure 1. Simplified geological map of Reykjanes Peninsula (Iceland) showing samples location (host lava: HRG2 and segregation vein: HRG4). Modified from Jóhannesson & Saemundsson (1998).

Somewhat different models have been proposed for the formation of segregation veins in lava flows (Anderson *et al.* 1984; Goff, 1996; Marsh, 2002). Regardless of the details of vein formation, all authors agree that they result from internal differentiation of the host lava after approximately 50 % crystallization. After formation, the veins evolve as thermodynamically closed systems. This point is crucial, as it implies that the chemical composition of the magmatic liquid in the segregation veins evolved independently of that of the host lava.

3. Analytical methods

Glass compositions were measured with a CAMECA SX 100 electron microprobe (EMP). The concentrations of major elements were determined with a count time of 60 s per element, the EMP was calibrated on natural and synthetic mineral standards and raw data were corrected by an improved ZAF procedure. In order to avoid possible loss of Na during analysis, the beam was defocused with a current of 8 nA and an acceleration voltage of 15 kV. Most glass patches permitted only a beam defocusing to 2–3 μm in width, but in a few patches a larger beam (20 μm in diameter) was used, and in rare cases rasters of 15 μm $\times$ 15 μm could be analysed. The results of the three approaches are shown in Table 1. In total, 37 analysis with total oxides in the range of 98.5–101 % were obtained and are discussed here. Major element compositions of whole rock samples were measured on ULTIMA C Jobin-Yvon ICP-AES, using a purified lithium tetraborate fusion of rock powder. The ICP-AES analytical conditions are given in Cantagrel & Pin (1994) and international rock standards (BHVO-1, RGM-1 and JB-3) were used for instrument calibration.

4. Major element composition

The whole-rock compositions of both the host lava and the segregation vein are hypersthene- and olivine-normative (Table 1), illustrating their tholeiitic affinities. When compared to the host lava, the vein is MgO-poorer and FeO*-richer (FeO*/MgO equal to 1.45 and 2.44, respectively). The vein is about two times richer in K_2O with higher Na_2O concentrations and K_2O/Na_2O increases from 0.073 in the host lava to 0.1 in the segregation veins. The composition of the segregation vein falls on the extrapolation of the compositional trends defined by Jakobsson, Jonsson & Shido (1978) for Holocene basalts from Reykjanes Peninsula.

The production of the magmatic liquid forming the veins from host lava through fractional crystallization can be modelled by mass-balance (e.g. Stormer & Nicholls, 1978). Mineral compositions used for the calculation are those measured on crystals in our samples. The computed crystallizing assemblage consists of 56.5 % plagioclase ($An_{80}Ab_{20}$), 27 % clinopyroxene

Table 1. Major element composition of host lava, segregation vein and representative glass patches

			Glass				
	Host lava	Segregation vein	'K$_2$O-poor'			'K$_2$O-rich'	
Sample	HRG2	HRG4	15 × 15 μm	20 μm	3 μm	10 μm	2 μm
SiO_2	48.2	48.7	76.1	76.4	79.1	76.8	74.0
TiO_2	1.34	2.20	0.34	0.55	0.27	0.32	0.36
Al_2O_3	15.4	12.6	13.6	13.1	12.5	12.9	11.6
FeO*	11.8	15.5	1.07	2.35	0.52	1.29	4.43
MnO	0.17	0.22	–	0.02	0.01	–	0.13
MgO	8.13	6.36	–	0.01	–	–	0.30
CaO	12.9	11.5	2.35	1.93	1.78	0.24	1.28
Na_2O	1.98	2.46	5.20	5.26	5.57	2.58	2.62
K_2O	0.15	0.26	1.15	0.76	0.76	6.49	5.59
P_2O_5	0.13	0.21	n.d.	n.d.	n.d.	n.d.	n.d.
Total	100.2	99.9	99.9	100.4	100.5	100.6	100.3
Degree of crystallization (wt %)	–	44.2	87.4	80.9	80.8	97.8	97.4
Quartz	–	–	36.1	37.1	40.0	35.4	31.2
Orthoclase	0.83	1.56	6.81	4.47	4.44	38.1	33.0
Albite	16.9	21.1	44.0	44.3	46.9	21.7	22.1
Anorthite	33.0	22.9	10.4	9.54	6.81	1.16	3.54
Nepheline	–	–	–	–	–	–	–
Diopside	25.0	27.8	1.16	–	0.98	–	2.46
Hypersthene	11.5	17.1	0.80	3.47	–	1.83	7.21
Olivine	7.32	1.40	–	–	–	–	–
Apatite	0.30	0.49	–	–	–	–	–
Ilmenite	2.57	4.23	0.64	1.04	0.51	0.61	0.69
Magnetite	2.59	3.39	–	–	–	–	–

Normative composition of host lava and segregation vein is calculated assuming (Fe^{3+}/total Fe) = 0.15. No correction for Fe was applied to the glass patches due to low concentrations. For the glass analysis, raster surface and EMP beam diameters are listed. n.d. – not determined.

($Wo_{40}En_{48}Fs_{12}$), 16 % olivine (Fo_{71}), and 0.5 % FeTi-oxides ($Usp_{37}Mt_{63}$). The estimated degree of crystallization necessary to account for the segregation vein composition is thus approximately 44 %, with a sum of the squares of residuals close to 0.001.

Most of the segregation vein is crystallized (approximately 95 % of the volume), but small interstitial glass patches still remain (around 5 %). These glass patches, whose typical compositions are listed in Table 1, are highly silicic ($SiO_2 > 73$ %) and with low Al_2O_3 concentrations (~ 11–14 %). They are also characterized by a strong depletion in MgO, FeO*, TiO_2 and CaO. Surprisingly, the analyses reveal a bimodal distribution of Na_2O and K_2O. The majority of the glass analyses (32 out of a total of 37) have an average K_2O/Na_2O of about 0.2 and they are defined here as 'K_2O-poor' glasses. Based on the O'Connor (1965) classification, modified by Barker (1979), this Na-rich and K-poor silicic glass is referred to as trondhjemitic (Fig. 2). The second group of glasses is less frequent (5/37 analyses), with an average K_2O/Na_2O of about 2.5, and these are here referred to as 'K_2O-rich' glasses. According to the O'Connor–Barker classification, they have a typical granitic composition (Fig. 2).

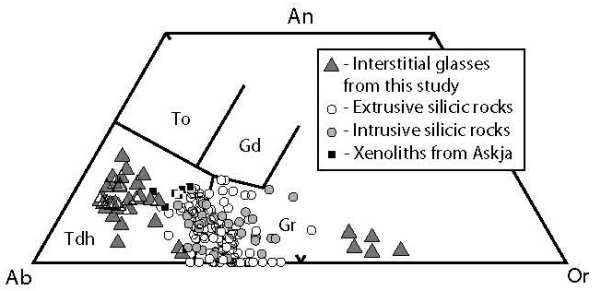

Figure 2. CIPW normative albite–anorthite–orthoclase (Ab–An–Or) classification diagram of O'Connor (1965), modified by Barker (1979), valid for > 10 % quartz normative rocks (Gr – granite, Tdh – trondhjemite, To – tonalite and Gd – granodiorite). Glasses from the segregation vein of Reykjanes Peninsula present a bimodal distribution of composition, mostly trondhjemitic and less frequently granitic. Extrusive and intrusive silicic rocks from Iceland have composition intermediate between trondhjemitic and granitic (144 samples compiled from the GEOROC database (http://georoc.mpch-mainz.gwdg.de/georoc/)). Trondhjemitic xenoliths from the 1875 eruption of Askja (Sigurdsson & Sparks, 1981) are also shown.

5. Differentiation mechanism

In both the host lava and the segregation vein, plagioclase and clinopyroxene are always normally zoned, excluding equilibrium crystallization as a realistic process for their differentiation. Fractional crystallization is a more likely differentiation mechanism for producing the segregation veins. As the differentiation takes place inside a lava flow at surface, it can be assumed to occur

at a low pressure (less than a few 10^5 Pa, or bars), and in the following discussion the fractional crystallization of host lava and segregation vein liquids is taken to have proceeded close to atmospheric pressure.

Glass patches in the vein represent the last and most evolved liquids formed by the fractional crystallization of a segregation melt, which in turn has an intermediate composition due to host lava differentiation. Throughout the whole process, K_2O behaves as a strongly incompatible element (except during the very last phase of solidification, where K-feldspar crystallized). Potassium can therefore be used to estimate the degree of crystallization (1−F) necessary to generate the segregation melt and the final liquid, using the $F = (C_0/C_l)$ equation (where F is melt fraction, C_0 and C_l are concentrations of potassium in host lava and evolved melts, respectively). This gives a degree of crystallization of the host lava of 44–45 % producing the segregation melt, which is in perfect agreement with the crystallization extent estimated from major element mass-balance calculations. The same method applied to the glass compositions yields a degree of fractionation of approximately 80 % (≥ 75 %) for the 'K_2O-poor' glass and of about 97 % for the 'K_2O-rich' glass. It must be noted that in the very last stages of crystallization, during which potassium may exhibit less incompatible behaviour, the calculated values are minimum estimates of the degree of crystallization. In summary, this olivine–tholeiitic lava from the Reykjanes Peninsula, together with its segregation vein, provides a record of up to 97 % fractional crystallization at very low pressure.

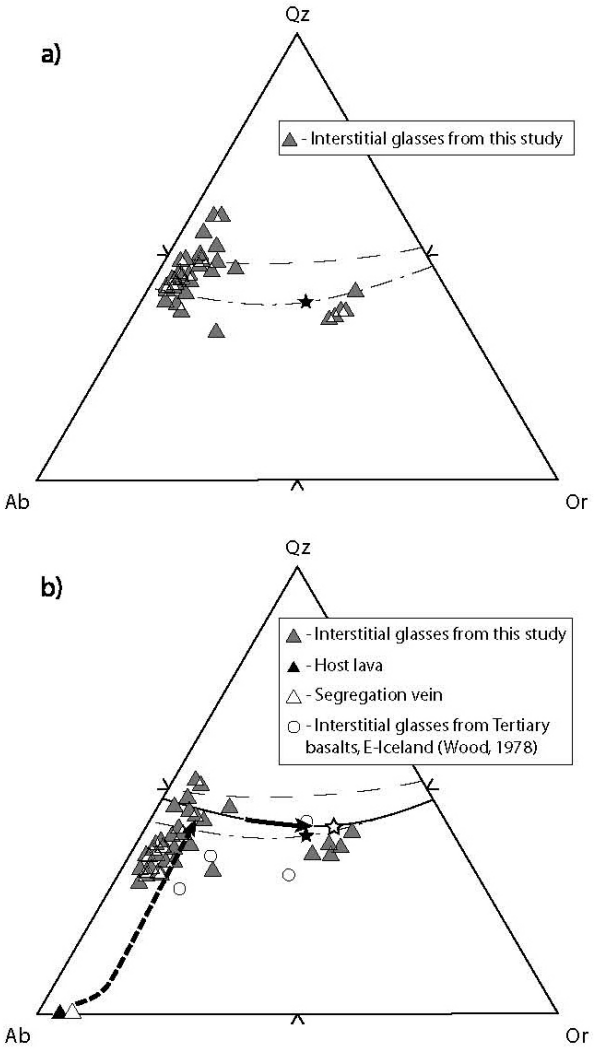

Figure 3. The one-atmosphere pressure quartz–albite–orthoclase phase diagram (CIPW-normative Qz–Ab–Or) showing: (a) the analysed glass composition from Reykjanes Peninsula, (b) recalculated compositions after corrections for the An-effect (see text for further details). Dashed curve corresponds to the experimental quartz + feldspar + liquid cotectic valley proposed by Tuttle & Bowen (1958). Dot-and-dash curve and black star represent respectively the cotectic valley and the system's minimum proposed by Brugger, Johnston & Cashman (2003). Also shown in (b) are An-corrected interstitial glasses from Tertiary basalt lavas of eastern Iceland (Wood, 1978). Continuous curve and the open star correspond to the most likely position, for the Reykjanes glasses, of the cotectic valley and the minimum of the Qz–Ab–Or system, respectively. The dashed arrow shows the liquid-line-of-descent as calculated by the *Melts* algorithm (Ghiorso & Sack, 1995) under FMQ and 1 atm pressure conditions. Solid arrow indicates the evolution from trondhjemitic liquids to granitic melts.

6. Differentiation products

Most of the melt evolution of the basaltic lava flow can be described in the diopside–anorthite–albite (Di–An–Ab) system, due to the nature of the crystallizing minerals (≥ 80 % plagioclase and clinopyroxene), but the ultimate liquid evolution in the vein must be discussed in the quartz–albite–orthoclase (Qz–Ab–Or) system. When projected onto the Qz–Ab–Or phase diagram for 1 atmosphere pressure (Fig. 3a), the 'K_2O-rich' glasses plot close to the composition of the minimum of the granitic system proposed by Brugger, Johnston & Cashman (2003). In contrast, the 'K_2O-poor' glasses record a different behaviour and plot between the Qz and Ab corners far from the granitic minimum and straddle the quartz + feldspar + liquid cotectic valley proposed by Tuttle & Bowen (1958) and Brugger, Johnston & Cashman (2003). Several 'K_2O-poor' glasses plot well above the cotectic curve in the Qz field, since the effect of variable anorthite content of the plagioclase is not considered in the projection in Figure 3a. Indeed, variations of Ab/An ratios result in displacements of the cotectic valley and the granitic minimum projection. For instance, it is well established that at 0.2 GPa (or 2 kbar: e.g. Winkler, 1974) a decrease of the Ab/An ratio shifts the granitic minimum towards Ab-poorer values, whereas the cotectic valley moves towards the Qz corner. Increase in water pressure would have exactly the opposite effect (e.g.

Johannes & Holtz, 1996). Figure 3b shows plots of the glass analyses corrected for this 'anorthite-effect' by assuming similar changes, from variable Ab/An at 1 atmosphere as established at 0.2 GPa, on the cotectic valley and the minimum positions in the Qz–Ab–Or phase diagram. After this correction, the 'K_2O-poor' glasses form a coherent evolution trend (liquid-line-of-descent) from more Ab-rich compositions to the cotectic valley, whereas the 'K_2O-rich' glasses still plot close to the minimum of the ternary system. It is worth noting that the compositional gap between the two glass groups exists regardless of which of the two projection schemes is used.

The *Melts* algorithm (Ghiorso & Sack, 1995) allows estimation of the theoretical evolution of liquid compositions during fractional crystallization at atmospheric pressure with the oxygen fugacity close to the FMQ buffer. It must be noted that this algorithm is mainly calibrated for basaltic to dacitic melts and that it is less accurate for granitic liquids. Consequently, the evolution calculated for more silicic liquids yields only semi-quantitative results. Models computed with the *Melts* algorithm and applied to crystallization of the Reykjanes host lava never lead to granitic but only to trondhjemitic compositions (Fig. 3b). They closely mimic the trend of the 'K_2O-poor' glasses from Ab-rich compositions to the cotectic valley. However, this leaves unanswered the question of how the 'K_2O-rich' glasses formed and why a bimodal composition is observed at the last stage of olivine tholeiite differentiation. In principle, the two types of final liquids could reflect the process of liquid immiscibility. Such immiscibility is well known in Si- and Fe-rich liquids (e.g. Philpotts, 1979) but is unknown between liquids that differ only in their alkaline and alkaline-earth metals. A more likely explanation is a two-stage evolution (Fig. 3b). The first stage consists of a liquid-line-of-descent similar to that predicted by the *Melts* algorithm. The second stage is a more local fractionation of quartz and albite-rich plagioclase from the 'K_2O-poor' liquid at the Or-poor end of the cotectic valley that would lead to an increased concentration of potassium and final volatiles. Volatile over-saturation in the final liquid would form a gas phase that may expel the resulting granitic glass to a different location in the final crystal framework. This would correspond to a repeated gas-filter pressing (Anderson *et al.* 1984) similar to the mechanism displacing the segregation vein liquid from the host lava.

Several arguments support the latter explanation for the formation of the final granitic liquid. The liquidus temperature, as estimated by the *Melts* algorithm, is significantly higher for the 'K_2O-poor' glasses compared to the 'K_2O-rich' ones (*c.* 1100 and 970°C, respectively). Consequently, it appears realistic that during a cooling process, 'K_2O-poor' liquids formed prior to 'K_2O-rich' liquids. The crystallizing assemblage causing the compositional changes of the final

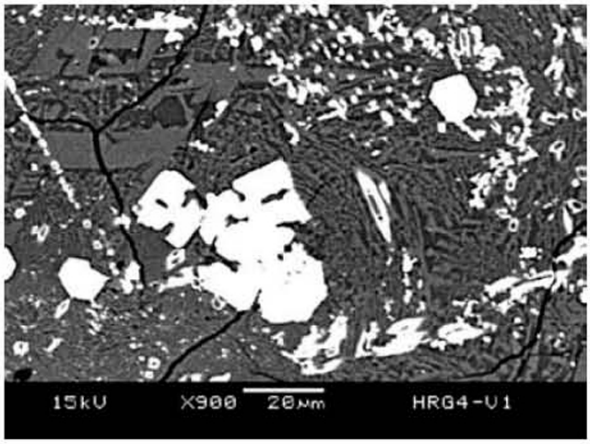

Figure 4. Scanning electron microscope (SEM) image, showing micrographic texture in a former glass patch of the segregation vein. Dark zones represent quartz, grey patches are albite and white colours reflect Fe–Ti oxide.

liquid can be estimated by mass balance calculation. It consists of plagioclase $An_{20}Ab_{80}$ (56 %) + quartz (42 %) + Fe–Ti oxides (2 %) and the degree of crystallization is 89 % with a sum of the squares of residual about 0.32. Indeed, albite and quartz intergrowths (graphic texture) are frequently observed in devitrified glass patches (Fig. 4). Moreover, vesicles which could represent the gas expulsion process are observed in 'K_2O-poor' glasses having albite and quartz intergrowths.

Taken together, the low-K_2O/Na_2O (< 0.1) olivine–tholeiitic basalt from Reykjanes Peninsula generates trondhjemitic liquids by more than 75 % (around 80 %) low-pressure fractional crystallization. Subsequently, and more exceptionally, small amounts of granitic liquid are formed. Most importantly, the silicic glasses represent bimodal compositions rather than a continuous evolution trend. Similar results can be deciphered from interstitial glass analyses in Tertiary basaltic lavas from eastern Iceland by Wood (1978), when only pristine glass analyses are considered and the anorthite effect in Qz–Ab–Or system is taken into account (Fig. 3b). The bimodality in the final silicic melt compositions is in stark contrast with observations on silicic formations in Iceland.

7. Implications for the origin of Iceland silicic rocks

Dacites and rhyolites represent between 3 and 10 % of the volcanic rocks produced in Iceland (Sigurdsson, 1977; Jakobsson, 1979). They are thought to be formed by either fractional crystallization of basalts or partial melting of hydrothermally altered basaltic crust. If they formed through a high degree of fractional crystallization at low pressure, their composition should be similar to those of the glasses in the Reykjanes segregation.

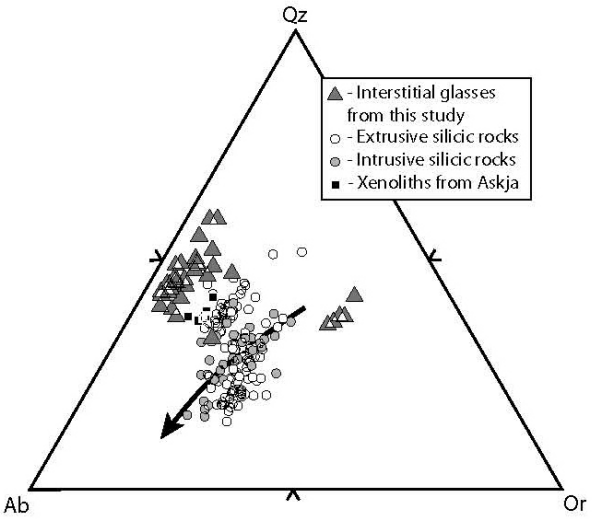

Figure 5. Comparison between glass patches from the Reykjanes Peninsula vein and silicic rocks from Iceland in the Qz–Ab–Or system. Extrusive and intrusive silicic rocks (144 samples compiled in GEOROC database (http://georoc.mpch-mainz.gwdg.de/georoc/)) as well as trondhjemitic xenoliths from Askja (Sigurdsson & Sparks, 1981) have composition intermediate between trondhjemitic and granitic glasses of this study. The arrow indicates the migration of minimum point of the system when pressure increases in a water-saturated system (Johannes & Holtz, 1996; see text for further discussion).

In Figure 5 are shown all available analyses of silicic rocks from Iceland containing more than 80 % of normative Qz + Ab + Or, like the Reykjanes glasses. It is clear that the Icelandic silicic rocks are different from the glasses analysed in this study, having compositions intermediate between the 'K_2O-poor' and 'K_2O-rich' glasses. This is further illustrated in Figure 2 where the silicic rocks from Iceland plot between trondhjemitic and granitic compositions and do not present the bimodal distribution observed in this study. Therefore, the silicic magma of Iceland is not formed by low-pressure fractional crystallization of an olivine tholeiitic magma like those erupted on the Reykjanes Peninsula.

The silicic rocks form trends towards lower Qz and higher Ab compositions in Figure 5 that concur with experimental results showing migration of the cotectic valley and the minimum point towards the Ab corner with increasing pressure (e.g. Johannes & Holtz, 1996). Trondhjemitic xenoliths from Askja volcano in central Iceland have been suggested to represent fractional crystallization products at depth (Sigurdsson, 1977; Sigurdsson & Sparks, 1981) and their compositions are plotted in Figures 2 and 5. These intrusive rocks are not as low in potassium as the 'K_2O-poor' glasses from the segregation vein, perhaps due to the pressure effect. However, these xenoliths have a significantly different composition compared to those of other intrusive silicic rocks from Iceland (Fig. 5). Therefore, based on the Qz–Ab–Or system, the fractional crystallization of basalts is not likely to have produced the silicic magmas, regardless of the exact pressure conditions. This conclusion applies to basalts having low K_2O/Na_2O such as those erupted on the Reykjanes Peninsula. Moreover, the total absence of differentiated rocks from this southwestern periphery of Iceland, and the northern extreme of the active rift-zone, compared to their abundance in the centre of the island and much higher magma productivity there, suggests a link with the presence of the mantle plume. Indeed, the thermal influence from the plume is expected to be highest in central Iceland where basalts with the least radiogenic He isotope ratios are erupted (Breddam, Kurz & Storey, 2000), a gravity low is observed (Eysteinsson & Gunnarsson, 1995) and the crust may be too hot to significantly cool down the high flux of incoming basalts. Instead, the hot mantle plume-derived basalts are likely to induce partial crustal melting.

Partial melting of hydrothermally altered basaltic crust has been shown capable of producing the silicic magmas of Iceland. For instance, fluid-absent melting of amphibolites at 0.3 GPa produces silicic liquid with composition indistinguishable from Icelandic silicic rocks (Sigmarsson, Condomines & Fourcade, 1992). Similar liquid compositions were also obtained from melting experiments at water pressure lower than 0.1 GPa and in the total pressure range of 0.1 to 0.3 GPa (Thy, Beard & Lofgren, 1990 and references therein). Finally, strong evidence for the melting model comes from O- and Th-isotope studies that observed higher isotope ratios in basalt lavas compared to contemporaneous silicic magmas from individual volcanoes (Nicholson *et al.* 1991; Sigmarsson *et al.* 1991; Sigmarsson, Condomines & Fourcade, 1992).

8. Differences between Archaean and Icelandic trondhjemites

Partial melting of metabasalts is classically thought to be at the origin of the Archaean crust with its well-known trondhjemitic, tonalitic and granodioritic (TTG) composition. In that case, a subducted oceanic crust transformed under amphibolite facies condition melts at such a depth that garnet is stable in the melting residue (see Martin *et al.* 2005 for review). The resulting trondhjemitic melt has a strongly fractionated REE pattern with high La/Yb due to the residual garnet. However, recent high-pressure experimental results reveal that water-saturated basalt melt crystallizes garnet and amphibole upon cooling (e.g. Müntener, Kelemen & Grove, 2001), which could produce similar REE patterns as observed in the Archaean trondhjemites. The mechanism of fractional crystallization may therefore have played a significant role during the formation of these trondhjemites.

Our study clearly shows that trondhjemites are generated from basalt via fractional crystallization. However, the olivine tholeiites on the Reykjanes Peninsula all have flat REE patterns (e.g. Zindler *et al.* 1979) and a similar flat pattern is expected for trondhjemitic glasses in the segregation vein. The principal difference between Archaean and Icelandic trondhjemites is the degree of fractionation of their REE pattern. Nevertheless, the different trace element ratios (e.g. La/Yb) could be explained by fractional crystallization at higher pressure forming Archaean trondhjemites compared to the near-atmosphere conditions recorded in the segregation vein on Reykjanes Peninsula. Due to the lack of rock samples, magmatic processes during Hadean times are not well known. However, as suggested for the Moon, an important magmatic ocean stage is thought to have characterized the Earth shortly after its accretion (e.g. Warren, 1985; Boyet *et al.* 2003; Caro *et al.* 2003). The progressive cooling and crystallization of the enormous volume of such a basaltic magma ocean could well have led to high degrees of fractional crystallization producing significant volumes of trondhjemitic magma and thus contributed to the formation of the very primitive continental crust.

9. Conclusions

Evolved glasses in a segregation vein hosted by olivine tholeiite lava on the Reykjanes Peninsula reveal a bimodal composition: trondhjemitic and granitic. These glasses were formed respectively by over 75 % and 97 % fractional crystallization of basaltic liquid at low pressure. The silicic magmas of Iceland have compositions that differ from those measured in the segregation vein. Consequently, major element constraints support the conclusion drawn from trace element and isotope studies that have proposed partial melting of hydrothermally altered basalts in order to account for the relatively large volume of silicic magmas in Iceland. The similarities of the trondhjemite glasses in the segregation vein and TTG may suggest that the formation of these glasses could be a modern analogue for the differentiation processes participating in the generation of trondhjemitic continental crust on the very early Earth.

Acknowledgements. We thank Hervé Martin for fruitful discussions about the primitive continental crust. Discussions with Pierre Schiano, Pierre Boivin and François Faure are also acknowledged. We are grateful to Michèle Veschambre, Mhammed Benbakkar and Jean-Luc Devidal for their analytical assistance and to Sigurdur Steinthorsson and John Maclennan for their constructive reviews. This work was supported by the French-Icelandic 'Jules Verne' programme and the Icelandic Centre for Research.

References

ANDERSON, A. T., GEORGE, J. R., SWIHART, H., ARTIOLI, G. & GEIGER, C. A. 1984. Segregation vesicles, gas filter-pressing, and igneous differentiation. *Journal of Geology* **92**, 55–72.

BARKER, F. 1979. Trondhjemites: definition, environment and hypothesis of origin. In *Trondhjemites, Dacites and Related Rocks* (ed. F. Barker), pp. 1–12. Amsterdam: Elsevier.

BOYET, M., BLICHERT-TOFT, J., ROSING, M., STOREY, M., TÉLOUK, P. & ALBARÈDE, F. 2003. ^{142}Nd evidence for early earth differentiation. *Earth and Planetary Science Letters* **214**, 427–42.

BREDDAM, K., KURZ, M. D. & STOREY, M. 2000. Mapping out the conduit of the Iceland plume with helium isotopes. *Earth and Planetary Science Letters* **176**, 45–55.

BRUGGER, C. R., JOHNSTON, A. D. & CASHMAN, K. V. 2003. Phase relations in silicic systems at one-atmosphere pressure. *Contributions to Mineralogy and Petrology* **146**, 356–69.

CANTAGREL, F. & PIN, C. 1994. Major, minor and rare-earth element determinations in 25 rock standards by ICP-atomic emission spectrometry. *Geostandards Newsletter* **18**, 123–38.

CARMICHAEL, I. S. E. 1964. The petrology of Thingmuli, a tertiary volcano in eastern Iceland. *Journal of Petrology* **5**, 435–60.

CARO, G., BOURDON, B., BIRCK, J.-L. & MOORBATH, S. 2003. ^{146}Sm–^{142}Nd evidence from Isua metamorphosed sediments for early differentiation of the Earth's mantle. *Nature* **423**, 428–32.

DEFANT, M. J. & DRUMMOND, M. S. 1990. Derivation of some modern arc magmas by melting of young subducted lithosphere. *Nature* **347**, 662–5.

EYSTEINSSON, H. & GUNNARSSON, K. 1995. *Maps of gravity, bathymetry and magnetics for Iceland and surroundings.* Report, OS-95055/JHD-07, National Energy Authority.

FURMAN, T., FREY, F. A. & MEYER, P. S. 1992. Petrogenesis of evolved basalts and rhyolites at Austurhorn, Southeastern Iceland: the role of fractional crystallization. *Journal of Petrology* **33**, 1405–45.

GHIORSO, M. S. & SACK, R. O. 1995. Chemical mass transfer in magmatic processes. 4. A revised and internally consistent thermodynamic model for the interpolation of liquid–solid equilibria in magmatic systems at elevated temperatures and pressures. *Contributions to Mineralogy and Petrology* **119**, 197–212.

GOFF, F. 1996. Vesicle cylinders in vapor-differentiated basalt flows. *Journal of Volcanology and Geothermal Research* **71**, 167–85.

GUNNARSSON, B., MARSH, B. D. & TAYLOR, J. H. P. 1998. Generation of Icelandic rhyolites: silicic lavas from the Torfajökull central volcano. *Journal of Volcanology and Geothermal Research* **83**, 1–45.

JAKOBSSON, S. P. 1972. Chemistry and distribution pattern of recent basaltic rocks in Iceland. *Lithos* **5**, 365–86.

JAKOBSSON, S. P., JONSSON, J. & SHIDO, F. 1978. Petrology of the Western Reykjanes Peninsula, Iceland. *Journal of Petrology* **19**, 669–705.

JAKOBSSON, S. P. 1979. Outline of the petrology of Iceland. *Jökull* **29**, 57–73.

JOHANNES, W. & HOLTZ, F. 1996. *Petrogenesis and Experimental Petrology of Granitic Rocks.* Berlin, Heidelberg: Springer-Verlag, 335 pp.

JÓHANNESSON, H. & SAEMUNDSSON, K. 1998. *Geological Map of Iceland 1:500 000 Bedrock Geology, 2nd ed.* Reykjavík: Icelandic Institute of Natural History.

JÓNASSON, K. 1994. Rhyolite volcanism in the Krafla central volcano, north-east Iceland. *Bulletin of Volcanology* **56**, 516–28.

MACDONALD, R., MCGARVIE, D. W., PINKERTON, H., L. S. R. & PALACZ, Z. A. 1990. Petrogenetic evolution of the Torfajökull volcanic complex, Iceland I. Relation between the magma types. *Journal of Petrology* **31**, 461–81.

MARSH, B. D. 2002. On bimodal differentiation by solidification front instability in basaltic magmas, part 1: Basic mechanics. *Geochimica et Cosmochimica Acta* **66**, 2211–29.

MARTIN, H. 1986. Effect of steeper Archaean geothermal gradient on geochemistry of subduction-zone magmas. *Geology* **14**, 753–6.

MARTIN, H. 1999. The adakitic magmas: modern analogues of Archaean granitoids. *Lithos* **46**, 411–29.

MARTIN, H., SMITHIES, R. H., RAPP, R., MOYEN, J. -F. & CHAMPION, D. 2005. An overview of adakite, tonalite-trondhjemite-granodiorite (TTG), and sanukitoid: relationships and some implications for crustal evolution. *Lithos* **79**(1–2), 1–24

MOJZSIS, S. J., HARRISON, M. T. & PIDGEON, R. T. 2001. Oxygen-isotope evidence from ancient zircons for liquid water at the Earth's surface 4,300 Myr ago. *Nature* **409**, 178–81.

MÜNTENER, O., KELEMEN, P. B. & GROVE, T. L. 2001. The role of H_2O during crystallization of primitive arc magmas under uppermost mantle conditions and genesis of igneous pyroxenites: an experimental study. *Contributions to Mineralogy and Petrology* **141**, 643–58.

NICHOLSON, H., CONDOMINES, M., FITTON, J. G., FALLICK, A. E., GRÖNVOLD, K. & ROGERS, G. 1991. Geochemical and isotopic evidence for crustal assimilation beneath Krafla, Iceland. *Journal of Petrology* **32**, 1005–20.

O'CONNOR, J. T. 1965. A classification for quartz-rich igneous rocks based on feldspar ratios. *United States Geological Survey Professional Paper* **525-B**, 79–84.

O'NIONS, R. K. & GRONVOLD, K. 1973. Petrogenetic relationships of acid and basic rocks in Iceland: Sr-isotopes and rare-earth elements in late and postglacial volcanics. *Earth and Planetary Science Letters* **19**, 397–409.

OSKARSSON, N., SIGVALDASON, G. E. & STEINTHORSSON, S. 1982. A dynamic model of rift zone petrogenesis and the regional petrology of Iceland. *Journal of Petrology* **23**, 28–74.

PHILPOTTS, A. R. 1979. Silicate liquid immiscibility in tholeiitic basalts. *Journal of Petrology* **20**, 99–118.

RAPP, R. P. 1995. Recycling of hydrated basalt of the oceanic crust and growth of early continents. In *Volatiles in the Earth and Solar System* (ed. K. A. Farley), pp. 261–9. American Institute of Physics. New York: AIP Press.

SIGMARSSON, O., HEMOND, C., CONDOMINES, M., FOURCADE, S. & OSKARSSON, N. 1991. Origin of silicic magma in Iceland revealed by Th isotopes. *Geology* **19**, 621–4.

SIGMARSSON, O., CONDOMINES, M. & FOURCADE, S. 1992. A detailed Th, Sr and O isotope study of Hekla: differentiation processes in an Icelandic volcano. *Contributions to Mineralogy and Petrology* **112**, 20–34.

SIGURDSSON, H. 1977. Generation of icelandic rhyolites by melting of plagiogranites in the oceanic layer. *Nature* **269**, 25–8.

SIGURDSSON, H. & SPARKS, R. S. J. 1981. Petrology of rhyolitic and mixed ejecta from the 1875 eruption of Askja, Iceland. *Journal of Petrology* **22**, 41–84.

SOTIN, C. 2005. Thermal evolution of the earth during the first billion years. In *Lectures in Astrobiology* (eds M. Gargaud, B. Barbier, H. Martin and J. Reisse), pp. 165–93. Springer-Verlag.

STORMER, J. C. & NICHOLLS, J. 1978. XLFRAC: a program for interactive testing of magmatic differentiation models. *Computer Geoscience* **87**, 51–64.

TATSUMI, Y. 1989. Migration of fluid phase and genesis of basalt magma in subduction zones. *Journal of Geophysical Research* **94**, 4697–707.

THY, P., BEARD, J. S. & LOFGREN, G. E. 1990. Experimental constraints on the origin of Icelandic rhyolites. *Journal of Geology* **98**, 417–21.

TUTTLE, O. F. & BOWEN, N. L. 1958. Origin of granite in the ligth of experimental studies in the system $NaAlSi_3O_8$–$KAlSi_3O_8$–SiO_2–H_2O. *The Geological Society of America Memoir* **74**, 153 pp.

WARREN, P. H. 1985. The magma ocean concept and lunar evolution. *Annual Review of Earth and Planetary Sciences* **13**, 201–40.

WILDE, S. A., VALLEY, J. W., PECK, W. H. & GRAHAM, C. M. 2001. Evidence from detrital zircons for the existence of continental crust and oceans on the Earth 4. 4 Ga ago. *Nature* **409**, 175–8.

WINKLER, H. G. F. 1974. *Petrogenesis of metamorphic rocks*. New York: Springer Verlag, 320 pp.

WOOD, D. A. 1978. Major and trace element variations in the tertiary lavas of eastern Iceland and their significance with respect to the Iceland geochemical anomaly. *Journal of Petrology* **19**, 393–436.

WYLLIE, P. J. & SEKINE, T. 1982. The formation of mantle phlogopite in subduction zone hybridization. *Contributions to Mineralogy and Petrology* **79**, 375–80.

ZINDLER, A., HART, S. R., FREY, F. A. & JAKOBSSON, S. P. 1979. Nd and Sr isotope ratios and rare earth element abundances in Reykjanes Peninsula basalts: evidence for mantle heterogeneity beneath Iceland. *Earth and Planetary Science Letters* **45**, 249–62.

C. Synthèse sur la genèse des roches acides par cristallisation fractionnée

Les compositions en éléments majeurs des laves acides étudiées précédemment diffèrent les unes des autres (à teneur semblable en SiO_2) par le rapport K_2O/Na_2O qui pour SiO_2~ 70-80 % varie de 0,2 dans les verres de Reykjanes à 2,7 dans ceux de Masaya. Il apparaît alors qu'au cours du déroulement d'un seul et même mécanisme : la cristallisation fractionnée, c'est le rapport K_2O/Na_2O du magma parent qui contrôle l'évolution par différenciation. En effet, des magmas parents possédant des rapports K_2O/Na_2O faibles, tels ceux mesurés dans les laves de Reykjanes (Islande) vont donner naissance, par cristallisation fractionnée, à des magmas trondhjémitiques alors que des laves ayant un rapport plus élevé pourront conduire à la différenciation de liquides de type granitique et ce, sans jamais former de trondhjémite.

.

Dans le cas de l'Islande, la cristallisation fractionnée d'une tholéiite à olivine (faible teneur en K_2O), analogue à l'échantillon HRG4 prélevé dans la Presqu'île de Reykjanes ne permet aucunement d'expliquer la composition en éléments majeurs des roches acides Islandaises. En effet, ces dernières ont des compositions intermédiaires entre purement granitique et trondhjémitique (Martin and Sigmarsson 2005). Toutefois, si l'on fait l'hypothèse que ces roches acides proviennent de la différenciation d'un magma basaltique contemporain provenant du même système volcanique, il apparaît alors que la cristallisation fractionnée peut tout à fait expliquer la composition en éléments majeurs des roches acides en Islande.

La Figure II-1 permet d'illustrer cela. Elle montre en effet que la cristallisation fractionnée des basaltes transitionnels du volcan central de Torfajökull, qui possèdent un rapport K_2O/Na_2O de l'ordre de 0.28 - 0.29, explique la composition en éléments majeurs des rhyolites de ce même volcan central. Il en va de même pour les roches acides formées au sein des volcans centraux de Askja et Krafla (zone de rift), dont la composition en éléments majeurs peut être également expliquée par la cristallisation fractionnée des basaltes associés, ayant un rapport K_2O/Na_2O de l'ordre de 0.16 - 0.22.

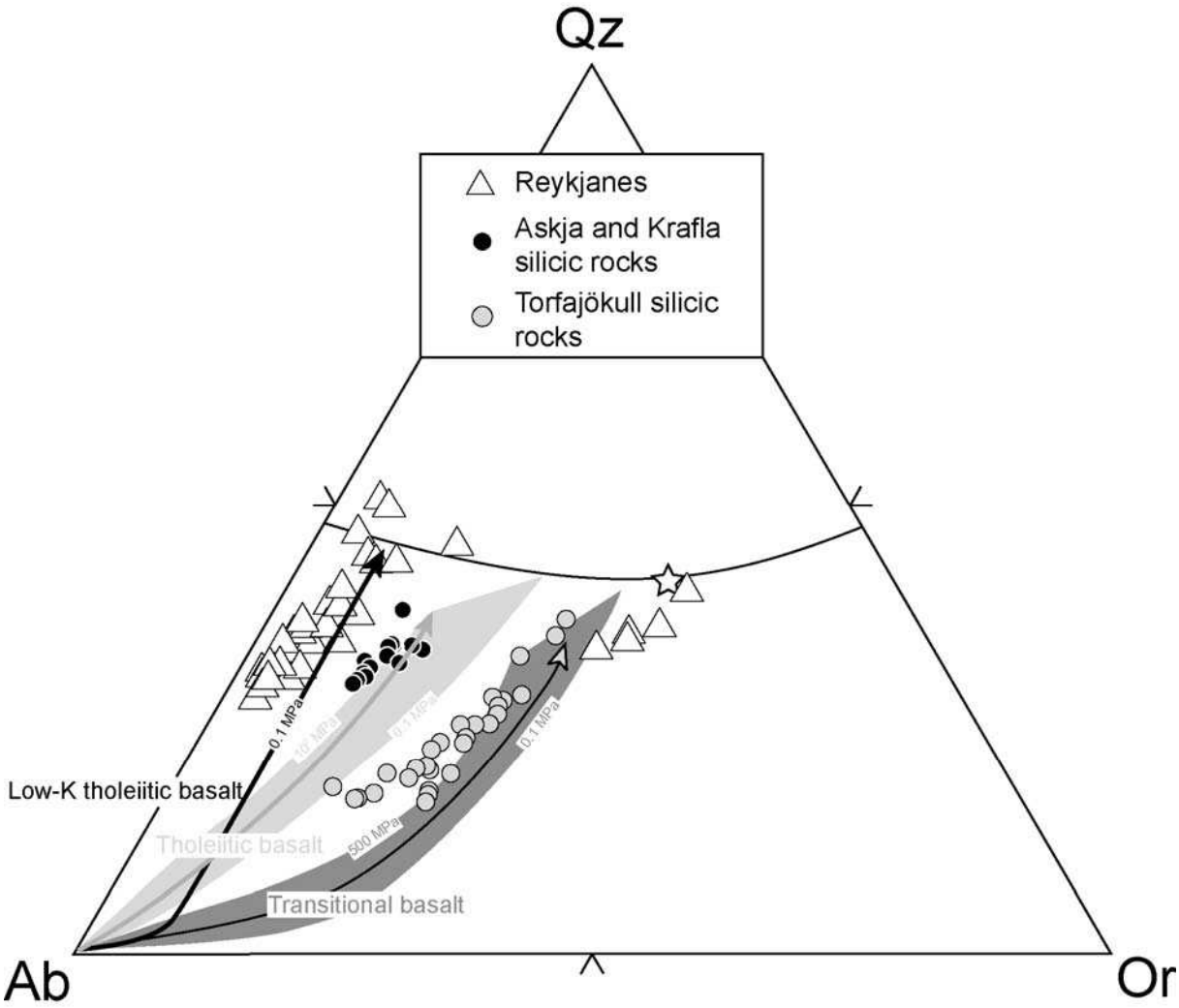

Figure II-1 : Projection des compositions normatives de roches acides d'Islande (Sigurdsson and Sparks, 1981; Oskarsson et al., 1982; McGarvie, 1984; Macdonald et al., 1990; McGarvie et al., 1990; Hemond et al., 1993; Gunnarsson et al., 1998; Sigvaldason, 2002a) dans le diagramme Qz-Ab-Or à 1 atmosphère, en utilisant la méthode de Blundy and Cashman (2001). Les flèches correspondent aux évolutions estimées par le logiciel « Melts » (Ghiorso and Sack, 1995) à différentes pressions par cristallisation fractionnée des basaltes issus des mêmes systèmes éruptifs que les roches acides considérées (basalte transitionnel de Torfajökull ; basalte tholéiitique de Askja et Krafla ; basalte tholéiitique à faible teneur en K de Reykjanes). Diagramme tiré de Martin and Sigmarsso (2006c)

En conclusion de ce chapitre, il apparaît donc que :

1) La composition du magma basique parent est un paramètre fondamental dont dépendra, après différenciation, la nature trondhjémitique ou granitique des laves acides.

2) La cristallisation fractionnée est un mécanisme simple qui permet d'expliquer la composition en éléments majeurs de l'ensemble des roches acides d'Islande.

3) Les mécanismes de « gas filter pressing » observés en détail dans les veines de ségrégation sont tout à fait susceptibles d'être extrapolés à plus grande échelle (chambre magmatique) afin de rendre compte de la genèse du magmatisme acide.

Toutefois, ce travail a montré que la cristallisation fractionnée était un mécanisme de différenciation possible, capable d'expliquer la composition en éléments majeurs des roches acides islandaises. Il convient maintenant de vérifier si, dans tous les cas, ce mécanisme est aussi capable de rendre compte des compositions en éléments en trace et en isotopes. En effet, dans le cas de plusieurs volcans centraux, des modèles de fusion partielle de la croûte métabasaltique islandaise (faciès amphibolite) ont été proposés afin d'expliquer la composition isotopique de l'oxygène, ainsi que le comportement du thorium et de l'uranium, (par ex. Nicholson, 1991 ; Sigmarsson et al. 1991, 1992a).

Chapitre III : L'origine des roches acides : implications sur l'évolution géodynamique de l'Islande

Dans le chapitre précédent il a été montré que la composition en éléments majeurs des roches acides d'Islande était compatible avec une genèse par cristallisation fractionnée. En revanches d'autres études ont montré que ce seul mécanisme ne permettait pas d'expliquer certains rapports isotopiques (par ex. Nicholson et al., 1991; Sigmarsson et al., 1991; Sigmarsson et al., 1992a). Le but de ce chapitre consistera à envisager ces autres possibilités et hypothèses, et ce en se basant, non seulement sur les données pétrologiques et la géochimie en éléments majeurs, mais également en utilisant le comportement des éléments en trace et des isotopes (cf. Annexes 2 à 5 pour les techniques et protocoles analytiques). Cette approche tentera non seulement d'établir la nature des mécanismes pétrogénétiques, mais aussi de les quantifier, afin de mettre en évidence d'éventuelles évolutions géographiques et temporelles.

En Islande les roches acides récentes (pléistocènes et holocènes) sont localisées non seulement au sein des zones de rift (NIRZ et MIVZ) et de la zone de propagation du rift (SIVZ), mais également en domaine hors rift (SNVZ et OVB). Cette distribution dans plusieurs domaines géodynamiques différents devrait permettre de discuter du mode de genèse de ces roches en fonction de leur répartition géographique, et par conséquent de leur contexte géodynamique.

Les plus vieilles roches datées en Islande ont 16 Ma au Nord-Ouest dans la péninsule de Vestfirðir et 13 Ma dans l'Est de l'île (par ex. Moorbath et al., 1968 ; Paquette et al. 2006, communication personnelle). Dans ces formations tertiaires ont été identifiés des volcans centraux ayant émis d'importants volumes de roches acides (par ex. Walker, 1963; Sæmundsson, 1979). Ceci démontre que la genèse de laves acides en Islande n'est pas exclusivement un phénomène actuel ou récent mais qu'il a eu lieu tout au long de l'évolution de l'île. En se basant sur notre connaissance des mécanismes de genèse des roches acides récentes, nous allons tenter de les extrapoler afin de mettre en lumière leur(s) mode(s) de formation tout au cours de l'évolution islandaise. Pour cela, il est nécessaire de connaître aussi précisément que possible l'âge des laves que l'on étudie. C'est la raison pour laquelle ce travail a été mené en collaboration avec V. Bosse et J-L. Paquette qui ont daté les échantillons soit par la méthode Ar-Ar sur roche totale soit par la méthode U-Th-Pb sur zircon (Annexe 6).

Le but ultime de ce chapitre est de proposer et de discuter un modèle d'évolution géodynamique de l'Islande.

A. La genèse des roches acides holocènes d'Islande

1. Article: "Crustal thermal state and origin of silicic magma in Iceland: the case of Torfajökull, Ljósufjöll and Snæfellsjökull volcanoes" Contributions to Mineralogy and Petrology, sous presse.

Crustal thermal state and origin of silicic magma in Iceland: the case of Torfajökull, Ljósufjöll and Snæfellsjökull volcanoes.

Martin, E.[1], Sigmarsson, O. [1,2]

1) Laboratoire Magmas et Volcans, OPGC - Université Blaise Pascal – CNRS, 5 rue Kessler, 63038 Clermont-Ferrand, France.

2) Institute of Earth Sciences, University of Iceland, 101 Reykjavik, Iceland.

E-mail: E.Martin@opgc.univ-bpclermont.fr

Abstract

Pleistocene and Holocene peralkaline rhyolites from Torfajökull (South Iceland Volcanic Zone) and Ljósufjöll central volcanoes and trachytes from Snæfellsjökull (Snæfellsnes Volcanic Zone) allow the assessment of the mechanism for silicic magma genesis as a function of geographical location and crustal geothermal gradient. The low $\delta^{18}O$ (2.4‰) and low Sr concentration (12.2 ppm) measured in Torfajökull rhyolites are best explained by partial melting of hydrated metabasaltic crust followed by major fractionation of feldspar. In contrast, very high $^{87}Sr/^{86}Sr$ (0.70473) and low Ba (8.7 ppm) and Sr (1.2 ppm) concentrations measured in Ljósufjöll silicic lavas are best explained by fractional crystallisation and subsequent ^{87}Rb decay. Snæfellsjökull trachytes are also generated by fractional crystallisation, with less than 10% crustal assimilation, as inferred from their $\delta^{18}O$.

The fact that silicic magmas within, or close to, the rift zone are principally generated by crustal melting whereas those from off-rift zones are better explained by fractional crystallisation clearly illustrates the controlling influence of the thermal state of the crust on silicic magma genesis in Iceland.

Introduction

The proportion of silicic rocks in Iceland is exceptionally high for an oceanic island, representing about 5-10 % of the exposed lavas (e.g. Walker 1966; Thordarson and Larsen, 2006). Together with the geochemical arguments of O- and Th isotope ratios, which are found to be lower in the silicic magmas than in contemporaneous basalts for a given volcano, this strongly suggests a crustal melting origin for the silicic rocks (e.g. Nicholson et al. 1991; Sigmarsson et al. 1991). However, generation of silicic magma by fractional crystallisation is still favoured for some Icelandic volcanoes (e.g. Carmichael 1964; Macdonald et al. 1990; Furman et al. 1992; Prestvik et al. 2001). The question remaining to be answered is whether or not these two contrasting mechanisms of silicic magma formation are mutually exclusive and, if not, what determines which of the two mechanisms is dominant.

The model of crustal partial melting developed for Krafla, Askja and Hekla volcanoes (e.g. Sigmarsson et al. 1991; Jónasson 1994), which are located in central Iceland, may not be realistic at the periphery of the island where the crustal thermal gradient is lower. Variable geothermal gradients have been measured in geothermal boreholes and clearly reflect a stronger influence of the Iceland mantle plume inland, as well as higher gradients in the presence of the rift system, while there are colder regions closer to the coast, and away from the spreading axis (Flovenz and Saemundsson 1993). Genesis of silicic magma by partial melting of the altered basaltic crust requires an elevated geothermal gradient so that incoming basaltic melts can raise the crustal temperature above its solidus. This condition is most likely to be met in central Iceland, whereas around the coast away from the rift zones the geothermal gradient is relatively low and the crustal temperature is likely to cool down incoming basaltic mantle melts. The lower geothermal gradient away from the rift zones is principally due to significantly lower volumes of incoming basalts. In this context, it would not be surprising to find different mechanisms for the generation of silicic magmas in regions with contrasting thermal gradients. Such an effect of the geothermal gradient on silicic magma has recently been discussed by Christiansen and McCurry (2006).

This study focuses on Pleistocene and Holocene felsic magmas from Torfajökull and Ljósufjöll and Snæfellsjökull volcanoes located respectively at the centre and the periphery of Iceland. The difference in geographical location of these volcanoes allows the potential influence of thermally contrasted settings on the mode of silicic magma formation in Iceland to be tested.

Geological setting

Iceland is located at a point of interaction between the Mid-Atlantic ridge and the Iceland mantle plume (Figure 1). The centre of the mantle plume is deduced from seismic and gravity anomalies characterized by the location of high $^{3}He/^{4}He$ volcanics (e.g. Eysteinsson and Gunnarsson 1995; Wolfe et al. 1997; Breddam et al. 2000). The influence of the mantle plume on the geothermal gradient of the crust is most likely induced by higher basalt productivity at the centre of Iceland compared to the coastal areas. Jakobsson (1972) estimated that the volume of basalts erupted during the Holocene in central Iceland was 2-3 times greater than in the coastal areas. This concurs with significantly higher geothermal gradients inland, as expressed by the shallower depth to the inferred 1200 °C isotherm (Fig. 1; Flovenz and Saemundsson 1993). To the extreme east and north-west the maximum depth of the inferred 1200 °C isotherm is observed in the oldest regions of Iceland, but this isotherm is not symmetrical around the rift axis due to change in the ridge position in the past. For example, the anomalously shallow depth of this isotherm to the north of the Snæfellsnes Volcanic Zone (SNVZ) represents a relatively high geothermal gradient that coincides with the site of a former rift axis, before it relocated to the Reykjanes Rift Zone (RRZ; Fig. 1).

Torfajökull volcano, located in the propagating rift zone in South Central Iceland (T in Fig. 1), is the largest silicic complex in Iceland, covering an area of more than 400 km^2 (Gunnarsson et al. 1998). A large part of this complex was formed during the Pleistocene and several subglacial and silicic table mountains, such as Laufafell, are thought to represent syn-caldera eruptions on a ring fracture (e.g. McGarvie 1984). Its post-glacial activity is characterized by the formation of obsidian lava flows following an initial explosive phase and tephra production. One such eruption occurred approximately 8000 years ago when the ca. 80 m-thick tephra pile and the Hrafntinnusker obsidian hill formed, while another one took place during the 9^{th} century when the obsidian lava flow was erupted (Hrafntinnuhraun). Silicic magmas at Torfajökull are characterized by their peralkaline composition (e.g. Macdonald et al. 1990; Gunnarsson et al. 1998 and references therein).

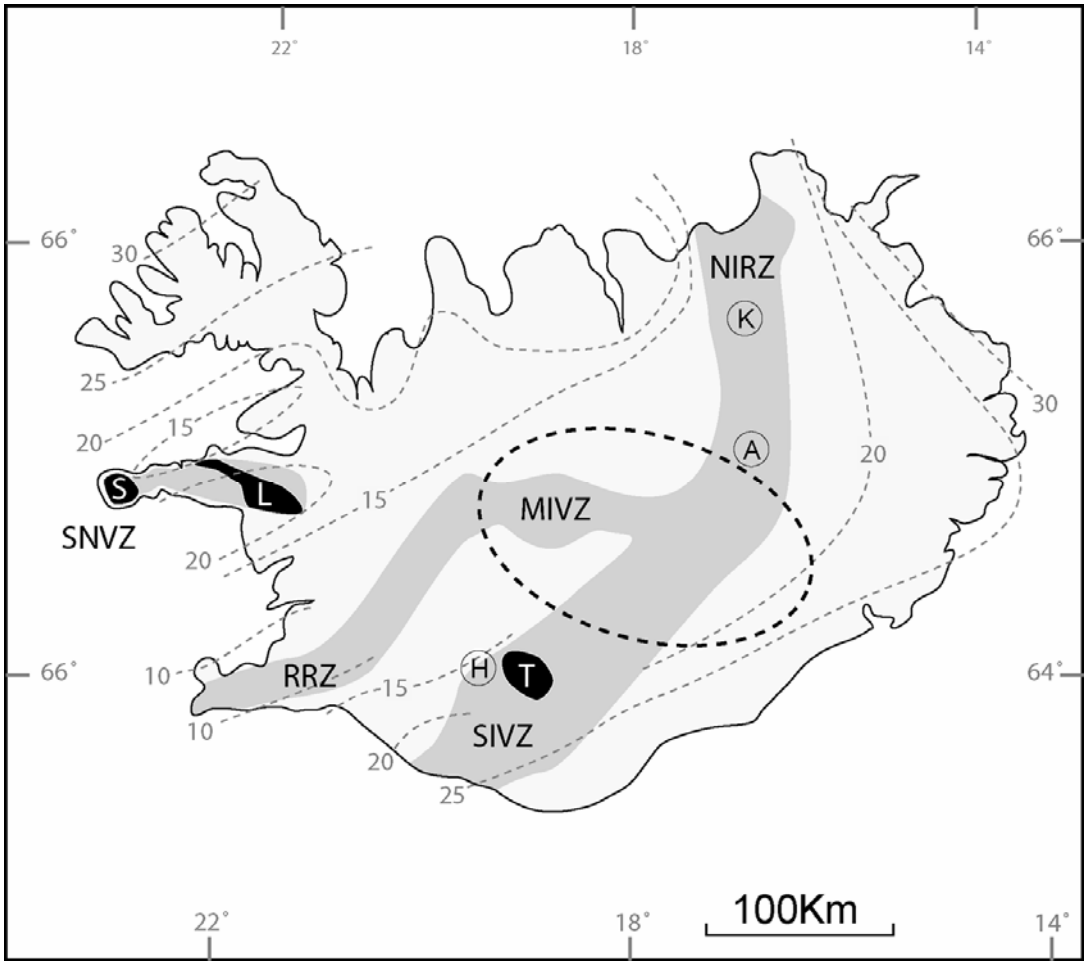

***Figure 1**: Map of Iceland showing the location of Snæfellsjökull (S), Ljósufjöll (L) and Torfajökull (T) volcanoes. The stippled ellipse corresponds to the location of the gravity and seismic velocity anomalies, which are interpreted as being the mantle plume centre (Eysteinsson and Gunnarsson 1995; Wolfe et al. 1997). Dashed grey lines correspond to inferred isobaths (km) of the 1200°C isotherm (Flovenz and Saemundsson 1993) and illustrate the decreasing thermal gradient away from the rift zones. A noteworthy exception is observed north of the Snæfellsnes volcanic zone (SNVZ). MIVZ: Mid-Iceland volcanic zone; SIVZ: South-Iceland volcanic zone; NIRZ: North-Iceland rift-zone; RRZ: Reykjanes rift-zone; K: Krafla; A: Askja and H: Hekla volcanoes.*

Snæfellsjökull and Ljósufjöll volcanoes, in the Snæfellsnes Volcanic Zone (SNVZ; Fig. 1), are located in western Iceland. Snæfellsjökull is a stratovolcano that has produced a complete alkaline magma series, with three Plinian eruptions releasing trachytic tephra layers of Postglacial age (Jóhannesson et al. 1982). To the east, the Ljósufjöll complex is principally composed of silicic extrusives with a few lavas of intermediate composition, all of which were formed in subglacial eruptions during the Pleistocene. Their age is estimated to be in the range of ~100 to ~800 ka (Flude et al. 2004; Gudmundsdóttir and Sigmarsson, 2006) and all

known silicic formations known have peralkaline compositions. In contrast to Torfajökull, Snæfellsjökull, and even more so Ljósufjöll, are constructed on a crust with a significantly lower geothermal gradient (Fig. 1).

Sample description

The Torfajökull samples come from three eruptive units: the subglacial table mountain Laufafell (Lauf, Table 1), the Hrafntinnuhraun eruption (HRN-21) and the early Holocene Hrafntinnusker (Hsk). The Lauf and Hsk8 samples consist of slightly porphyritic obsidians (3-5% phenocrysts: 80% plagioclase and 20% clinopyroxene) whereas all other samples are aphyric pumices. Hrafntinnusker samples come from a single 80m-thick tephra section formed during a single eruptive phase shortly after, or contemporaneous with, deglaciation in this region (Martin et al in prep.). Sample Hsk1 represents the first tephra emplaced during this eruption, whereas Hsk 3 and Hsk4 sample the middle of the profile and Hsk7 the top. An obsidian lava flow (Hsk8) covers the tephra pile, forming a summit cap on the Hrafntinnusker mount, and represents the last stage of the eruption.

Samples from Snæfellsjökull volcano are pumices greater than 1 cm in diameter, collected from two tephra layers approximately 10 km NE of the volcano. The pumices (SN1, SN2) contain a few plagioclase phenocrysts as well as clinopyroxene (less than 5%) and, more rarely, a few phenocrysts of amphibole. In contrast, all samples from Ljósufjöll are compact lava samples from subglacial extrusive units; domes and lava flows. Their mineralogy is characterized by 1-2% feldspar phenocrysts that frequently form glomerocrysts showing signs of resorption, with trace amounts of Fe-Ti oxides, clinopyroxene, amphibole, zircon, monazite and quartz (Flude, personal communication). All samples look fresh under the microscope, with no visible alteration products.

Analytical techniques

Major element compositions of whole rock samples were measured on ULTIMA C ICP-AES, using purified lithium tetraborate fusion of rock powder. The ICP-AES analytical conditions are given in Cantagrel and Pin (1994) and international rock standards (BHVO, BR, GH and DRN) were used for instrument calibration. Trace element compositions were obtained on a PQ2+ ICP-MS instrument, on the same solution as the major element analyses. The ICP-MS analytical conditions will be given elsewhere. Internal standards (BR and BHVO) were used for instrument calibration. The Th and U concentrations were measured by isotopic dilution method on a CAMECA TSN 206 mass spectrometer using a mixed ^{235}U-^{230}Th spike (Condomines et al. 1982). Analytical error is estimated at 0.5% (2σ) for Th and U concentrations. The Sr and Nd isotope ratios were measured on a Thermo-Finnigan TRITON TI mass spectrometer and normalized to $^{86}Sr/^{88}Sr = 0.1194$ and $^{146}Nd/^{144}Nd = 0.7219$. During this study, the $^{87}Sr/^{86}Sr$ of NBS-987 was equal to 0.710258 ±6 (2σ; n= 8) and $^{143}Nd/^{144}Nd$ of the AMES standard equal to 0.511960 ±4 (2σ; n=9). External error is about 2.10^{-5} (2σ) for both Sr and Nd isotopic ratios. For oxygen isotope measurements, 5-10 mg of whole rock powder was reacted overnight with BrF_5 at 680°C in Ni reaction vessels (Clayton and Mayeda 1963). After conversion to CO_2 gas, the O isotope ratios were analyzed on a VG SIRA 10 dual inlet instrument at "Géosciences Rennes" and normalized to NBS-28 = 9.6‰ (the mean value of the NBS 28 found during the experiments was 9.36‰). Total analytical uncertainties on $\delta^{18}O$ are estimated at 0.15 ‰ based on duplicate analysis.

Table 1: *Major- and trace element compositions together with $^{143}Nd/^{144}Nd$, $^{87}Sr/^{86}Sr$ and $\delta^{18}O$ isotope compositions of samples from Torfajökull, Ljósufjöll and Snæfellsjökull volcanoes.*

		SiO_2	TiO_2	Al_2O_3	Fe_2O_3*	MnO	MgO	CaO	Na_2O	K_20	P_2O_5	H_2O -	H_2O +	total
Torfajökull	HRN-21	70.2	0.28	14.5	2.80	0.08	0.27	0.98	5.63	4.52	0.10	0.17	1.02	100.5
	Lauf	72.1	0.34	13.3	2.95	0.11	0.06	0.72	5.83	3.66	0.03	0.10	0.37	99.6
	Hsk8	72.6	0.19	12.3	3.36	0.07	0.07	0.40	5.63	4.44	0.02	0.16	0.37	99.6
	Hsk8	*73.3*	*0.20*	*12.4*	*3.39*	*0.07*	*0.07*	*0.40*	*5.68*	*4.48*	*0.02*			*100.0*
	Hsk7	71.4	0.20	11.9	3.41	0.08	0.09	0.44	5.08	4.29	0.03	0.34	3.71	101.0
	Hsk7	*73.6*	*0.20*	*12.3*	*3.52*	*0.08*	*0.09*	*0.45*	*5.25*	*4.43*	*0.03*			*100.0*
	Hsk4	70.9	0.20	12.1	3.49	0.07	0.08	0.42	4.66	4.51	0.03	0.37	3.62	100.4
	Hsk4	*73.5*	*0.21*	*12.5*	*3.61*	*0.08*	*0.09*	*0.43*	*4.83*	*4.67*	*0.03*			*100.0*
	Hsk3											0.94	4.42	
	Hsk1	68.5	0.22	12.9	3.75	0.07	0.23	0.47	2.83	4.31	0.03	0.88	5.22	99.4
	Hsk1	*73.4*	*0.23*	*13.9*	*4.01*	*0.08*	*0.25*	*0.51*	*3.04*	*4.62*	*0.03*			*100.0*
Ljósufjöll	L-1	70.0	0.25	13.6	4.20	0.16	0.02	0.45	5.72	4.86	0.05	0.08	0.19	99.6
	L-4	71.6	0.22	13.1	4.00	0.14	0.03	0.49	5.90	4.74	0.02	0.07	-0.05	100.2
	L-6	71.5	0.21	12.8	3.88	0.13	0.03	0.43	5.96	4.60	0.02	0.24	0.19	100.0
	L-5	71.3	0.21	12.7	3.87	0.13	0.03	0.43	5.86	4.58	0.02	0.06	0.24	99.4
	L-2	54.9	1.64	16.3	9.04	0.21	3.89	7.41	4.18	2.66	0.34	0.10	-0.35	100.3
	L-3	53.0	1.72	16.2	9.33	0.20	4.83	8.77	3.61	2.20	0.35	0.13	-0.14	100.2
	7640 (1),(2)	47.5	1.96	13.4	11.4	0.16	11.2	11.9	2.27	0.67	0.30			100.8
	7637 (1),(2)	47.2	2.49	14.9	12.4	0.18	6.81	11.8	2.95	0.76	0.52			100.0
Snæfellsjökull	SN-1	65.6	0.31	14.9	3.95	0.15	0.16	1.31	5.59	4.40	0.06	0.38	2.72	99.5
	SN-2	64.9	0.38	15.1	4.51	0.17	0.27	1.61	5.59	4.20	0.08	0.28	2.08	99.1
	SN89-23(1),(2)	45.8	2.60	13.8	12.6	0.17	10.5	11.6	2.25	0.74	0.42			100.5
	SN89-27(1),(2)	46.3	4.04	14.8	15.4	0.22	5.17	10.2	3.35	1.11	0.85			101.4

In italics are major element concentrations for Hrafntinnusker samples recalculated to 100%. Underlined values are for results obtained by isotopic dilution mass spectrometry. HRN: Hrafntinnuhraun; Lauf: Laufafell; Hsk: Hrafntinnusker. (1) Sigmarsson et al. (1992b) and (2) Carpentier (2003).

Table 1 (continued):

		Rb	Sr	Y	Zr	Nb	Ba	La	Ce	Pr	Nd	Sm	Eu	Gd	Tb	Dy
Torfajökull	HRN-21	105.8	53.5	60.2	551.0	95.7	421.4	87.1	174.4	18.4	64.8	12.6	1.61	10.1	1.78	11.0
	Lauf	80.9	76.3	107.3	989.2	133.4	573.2	106.1	228.8	25.8	100.9	20.8	4.95	17.0	3.07	19.8
	Hsk8	119.8	12.2	116.9	1067.0	140.3	172.4	120.6	246.8	28.1	102.0	21.5	1.88	18.5	3.33	20.6
	Hsk7	110.4	14.1	111.4	1026.3	133.5	203.2	113.9	232.0	26.3	96.2	20.2	1.74	17.4	3.12	19.5
	Hsk4	114.0	13.8	115.9	1093.3	140.2	163.8	118.1	242.4	27.7	100.8	21.4	1.89	18.6	3.33	20.7
	Hsk3															
	Hsk1	102.2	14.5	112.2	1189.3	135.6	139.5	118.4	247.5	27.6	100.8	21.3	1.89	18.4	3.24	20.2
Ljósufjöll	L-1	*161.72*	*1.79*	91.3	1350.1	251.1	17.7	353.4	552.8	68.4	219.1	34.3	1.18	20.9	3.10	17.1
	L-4	*178.85*	*1.17*	86.7	1320.1	253.6	8.72	170.4	355.8	37.0	127.7	22.9	0.77	15.9	2.73	17.2
	L-6	*184.17*	*1.31*	111.3	1524.2	281.7	9.30	180.4	329.5	40.0	140.1	27.1	0.95	19.6	3.64	22.5
	L-5	*184.94*	*1.60*	141.9	1446.4	274.8	9.52	184.8	340.4	39.5	138.8	26.9	0.95	19.7	3.63	22.6
	L-2	*46.28*	*345.35*	36.9	357.2	74.9	691.5	82.9	161.4	17.8	63.9	10.7	2.74	7.93	1.17	6.85
	L-3	*41.28*	*356.80*	31.5	281.1	61.5	595.8	59.2	118.0	13.3	49.1	8.72	2.55	6.86	1.01	5.97
	7640 [(1),(2)]	15.6	368.0	-	129.0	24.5	233.0	22.2	47.8	6.22	24.5	5.14	1.72	4.97	0.72	3.95
	7637 [(1),(2)]	14.5	398.0	-	147.0	29.4	282.0	24.8	54.6	7.26	29.4	6.33	2.21	6.32	0.92	5.14
Snæfellsjökull	SN-1	98.7	83.3	61.0	646.9	117.6	1214.6	87.5	177.5	19.4	69.3	13.0	2.51	11.2	1.75	10.9
	SN-2	91.3	118.5	58.6	666.8	113.9	1216.8	85.0	172.6	19.0	68.1	12.7	2.75	10.9	1.71	10.7
	SN89-23[(1),(2)]	15.8	453.0	-	152.0	38.1	309.0	25.1	54.2	7.13	28.0	5.79	2.01	5.39	0.79	4.25
	SN89-27[(1),(2)]	23.4	546.0	-	242.0	61.6	534.0	42.0	91.4	12.0	47.3	9.55	3.33	8.84	1.28	6.83

		Ho	Er	Tm	Yb	Lu	Hf	Ta	Th	U	Th/U	$^{87}Sr/^{86}Sr$	$^{143}Nd/^{144}Nd$	$\delta^{18}O$
Torfajökull	HRN-21	2.24	6.21	0.91	5.83	0.86	15.4	8.11	*17.6*	*5.09*	3.46	0.70345		
	Lauf	4.19	11.0	1.53	10.3	1.38	25.9	11.5	*13.9*	*4.22*	3.29	0.70332	0.51298	2.44
	Hsk8	4.19	11.4	1.60	10.9	1.60	28.6	12.2	*20.0*	*5.96*	3.36	0.70338	0.51298	3.87
	Hsk7	3.94	10.7	1.51	10.3	1.50	26.8	11.1	*19.7*	*5.77*	3.41	0.70355	0.51297	
	Hsk4	4.22	11.4	1.60	11.0	1.61	29.3	12.6	*20.3*	*5.73*	3.54	0.70353	0.51297	
	Hsk3								*21.4*	*5.68*	3.77	0.70341	0.51298	
	Hsk1	4.07	11.0	1.53	10.5	1.54	31.3	12.8	*21.9*	*5.17*	4.24	0.70386	0.51297	
Ljósufjöll	L-1	3.16	8.52	1.28	9.38	1.49	29.1	17.6	*23.7*	*5.39*	4.40	0.70473	0.51291	6.30
	L-4	3.66	10.3	1.57	11.3	1.81	31.8	18.7	*24.9*	*7.06*	3.53	0.70435	0.51293	6.15
	L-6	4.63	12.6	1.84	12.8	2.00	34.5	20.6	*26.3*	*6.84*	3.85	0.70463	0.51292	5.84
	L-5	4.75	13.0	1.88	12.8	1.99	32.4	19.4	*24.9*	*6.56*	3.80	0.70442	0.51292	
	L-2	1.36	3.62	0.51	3.52	0.59	7.69	5.45	*6.16*	*1.59*	3.87	0.70338	0.51292	5.67
	L-3	1.19	3.18	0.46	3.06	0.48	6.34	5.20	*5.43*	*1.52*	3.57	0.70347	0.51290	5.84
	7640 [(1),(2)]	0.78	2.05	0.30	1.87	0.28	3.03		*1.96*	*0.586*	3.34	0.70334	0.51296	5.39
	7637 [(1),(2)]	1.03	2.69	0.40	2.46	0.38	3.50		*1.97*	*0.590*	3.34	0.70330	0.51295	5.20
Snæfellsjökull	SN-1	2.30	6.37	0.95	6.79	1.09	15.3	8.64	*12.3*	*3.50*	3.51	0.70338	0.51297	5.10
	SN-2	2.24	6.27	0.95	6.55	1.04	15.5	8.29	*11.5*	*3.29*	3.50	0.70337	0.51296	4.92
	SN89-23[(1),(2)]	0.83	2.16	0.31	1.99	0.30	3.41	2.37	*1.85*	*0.537*	3.45	0.70336		5.40
	SN89-27[(1),(2)]	1.35	3.51	0.50	3.20	0.49	5.37	3.82	*2.69*	*0.779*	3.45	0.70336	0.51297	5.30

Results

Major and trace elements

Major and trace element compositions are listed in Table 1 together with the isotope ratios of Sr, Nd and O for Torfajökull, Snæfellsjökull and Ljósufjöll samples. All samples are silicic with SiO_2 ranging from 70.2 to 73.6 wt% (on an anhydrous basis) for Torfajökull rhyolites, 70 to 71.6 wt% for Ljósufjöll samples, and 67 to 68.1 wt% for the trachytes of Snæfellsjökull (Fig. 2). The Torfajökull samples are all peralkaline rhyolites (except Hsk1) with an agpaitic index (molecular $[(Na_2O+K_2O)/Al_2O_3]$) higher than 1 (from 1.02 to 1.15) and between 1.13 and 1.5 wt% of CIPW normative acmite. The same holds for the peralkaline rhyolites of Ljósufjöll, which have an agpaitic index of ~1.1, and 0.9% - 2% normative acmite. In contrast, the Snæfellsjökull trachytes have an agpaitic index of less than 1 (0.91 and 0.94).

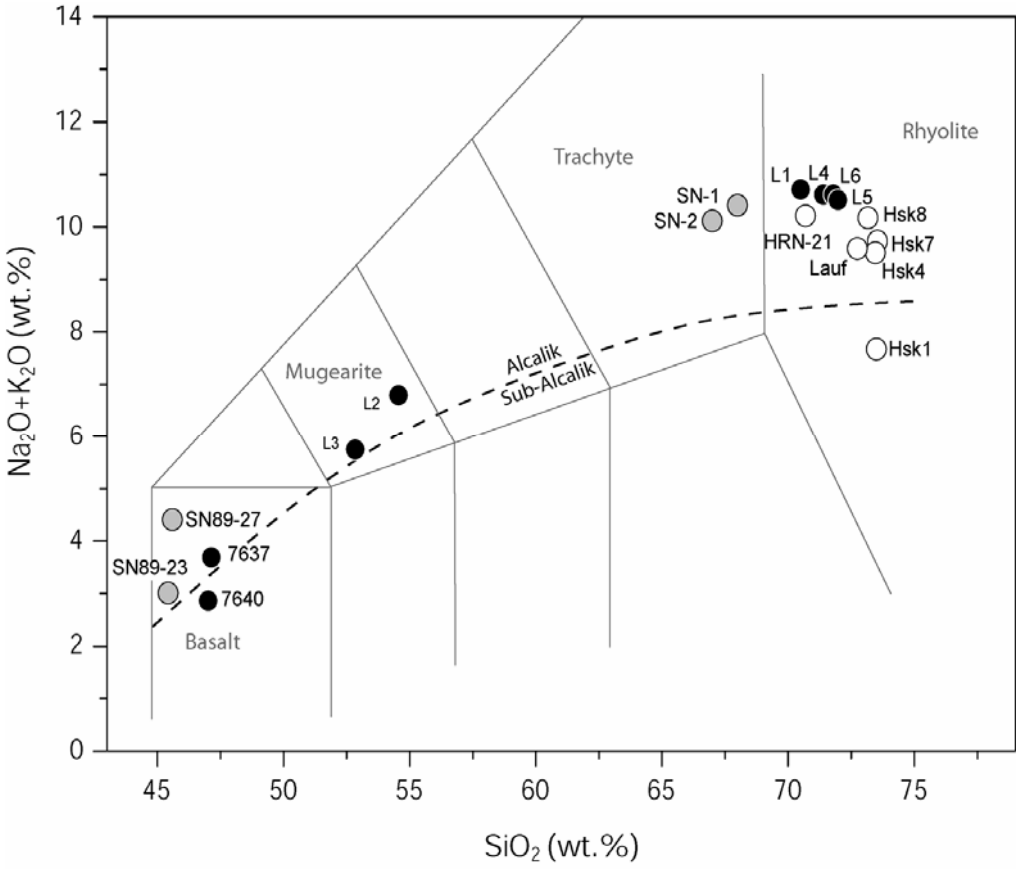

Figure 2: *Total alkali vs. SiO_2 diagram with rock classification boundaries from Le Bas et al., (1986). The limit between alkalic and sub-alkalic fields (dashed line) is that of Miyashiro (1978). Filled, grey and open circles represent samples from Ljósufjöll Snæfellsjökull and Torfajökull respectively.*

The compositional similarity between Torfajökull and Ljósufjöll rhyolites is also observed in their trace element patterns. In a primitive mantle normalized multi-element diagram (Fig. 3) rhyolites from both volcanoes display important negative anomalies for Ba, Sr and, to a lesser extent, for Eu, whereas the Snæfellsjökull trachytes display a strong negative anomaly for Sr and a weak one for Eu. Incompatible trace elements, such as Th, have concentrations reaching record high values in the peralkaline rhyolites, up to 21.9 ppm and 26.3 ppm in Torfajökull and Ljósufjöll rhyolites, respectively, whereas silicic rocks elsewhere in Iceland rarely exceed 11 ppm Th (Sigmarsson et al. 1991). The trachytes of this study have 11.5 - 12.3 ppm.

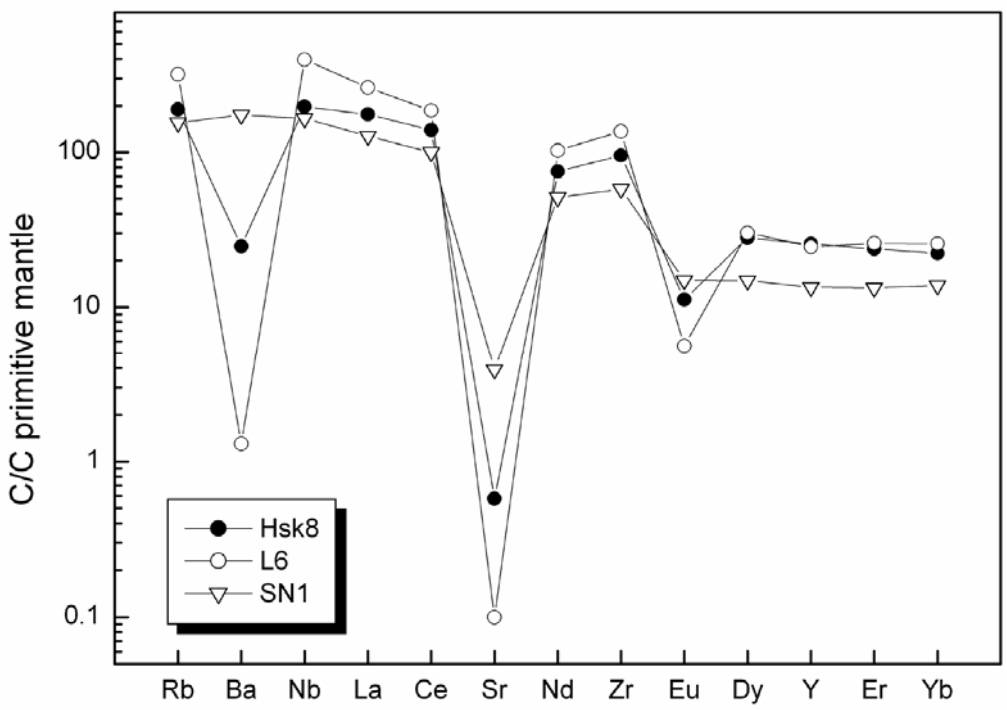

Figure 3: *Primitive mantle normalized (Sun and McDonough 1989) multi-element diagram for Torfajökull (Hsk8) and Ljósufjöll (L6) peralkaline rhyolites and Snæfellsjökull trachyte (SN1). These patterns illustrate the strong Ba, Eu and Sr anomalies in typical samples from the first two volcanoes.*

The very high water concentrations in some of the Hsk samples from Torfajökull (Table 1) are most probably due to water absorption of the volcanic glass during, or shortly after, their emplacement. The detailed process of glass hydration and consequences for trace and isotopic composition is outside the scope of this paper and will be discussed elsewhere. Nevertheless, the concentrations of Al_2O_3, Fe_2O_3*, CaO, Zr (Fig. 4a), Hf and Th decrease from sample Hsk1 to Hsk7, that is from the base of the profile to the top. In contrast, Na_2O,

Ba, Rb and U concentrations increase upwards through the profile. Other elements show insignificant variations throughout the profile. Since Th and U concentrations are negatively correlated, the Th/U strongly decreases from bottom (Th/U = 4.24 in Hsk1) to top (Th/U = 3.36 in Hsk8) of the Hrafntinnusker section (Fig. 4b). As a result, only those elements from the Torfajökull samples, that are not fluid-mobile will be discussed in this paper.

The lava samples from Ljósufjöll contain little water despite their subglacial origin (Table 1). When compared with basalts from the same volcanic system (7637 and 7640) and mugearites (L2, L3; Fig. 2), all the peralkaline rhyolites are depleted in TiO_2, Fe_2O_3*, CaO, P_2O_5 and Sr but enriched in alkalis (Na_2O and K_2O) and in the most incompatible trace elements. Only Ba deviates from this general behaviour, since the highest Ba contents are observed in the mugearites (Table 1). The rhyolites have very similar compositions except L1 which has significantly higher La/Yb and Th/U (37 and 4.41 compared to 14-15 and 3.53-3.85, respectively; Fig. 4b-c).

O, Nd and Sr isotopes

The whole-rock $\delta^{18}O$-values measured in Hsk8 and Lauf are 3.9‰ and 2.4‰, respectively. The latter value is significantly lower than those measured by Gunnarsson (1987) and Gunnarsson et al. (1998) in Laufafell (4.2‰). In stark contrast, the peralkaline rhyolites from Ljósufjöll have $\delta^{18}O$-values ranging from 5.8‰ – 6.3‰, and the mugearites have values of 5.8‰. The trachytes of Snæfellsjökull have slightly lower $\delta^{18}O$-values of 4.9‰ to 5.1‰.

$^{143}Nd/^{144}Nd$ does not show any significant variation in the samples of this study (Torfajökull: 0.51296-0.51298, Ljósufjöll: 0.51290-0.51296, Snæfellsjökull: 0.51296-0.51297; Table 1). The results for Torfajökull fall within the range observed for a larger sample set by Stecher et al. (1999), whereas those from Ljósufjöll, together with those for the Öræfajökull rhyolites, SE Iceland (Prestvik et al. 2001), display the lowest Nd isotope ratios measured in Icelandic rocks.

$^{87}Sr/^{86}Sr$ ratios show large variations from 0.70332 at Laufafell, through 0.70337 at Snæfellsjökull to 0.70386 in the first tephra (Hsk1) of the Hrafntinnusker eruption (Torfajökull) and up to 0.70473 at Ljósufjöll. This last value is by far the highest $^{87}Sr/^{86}Sr$ ever measured in Icelandic rocks.

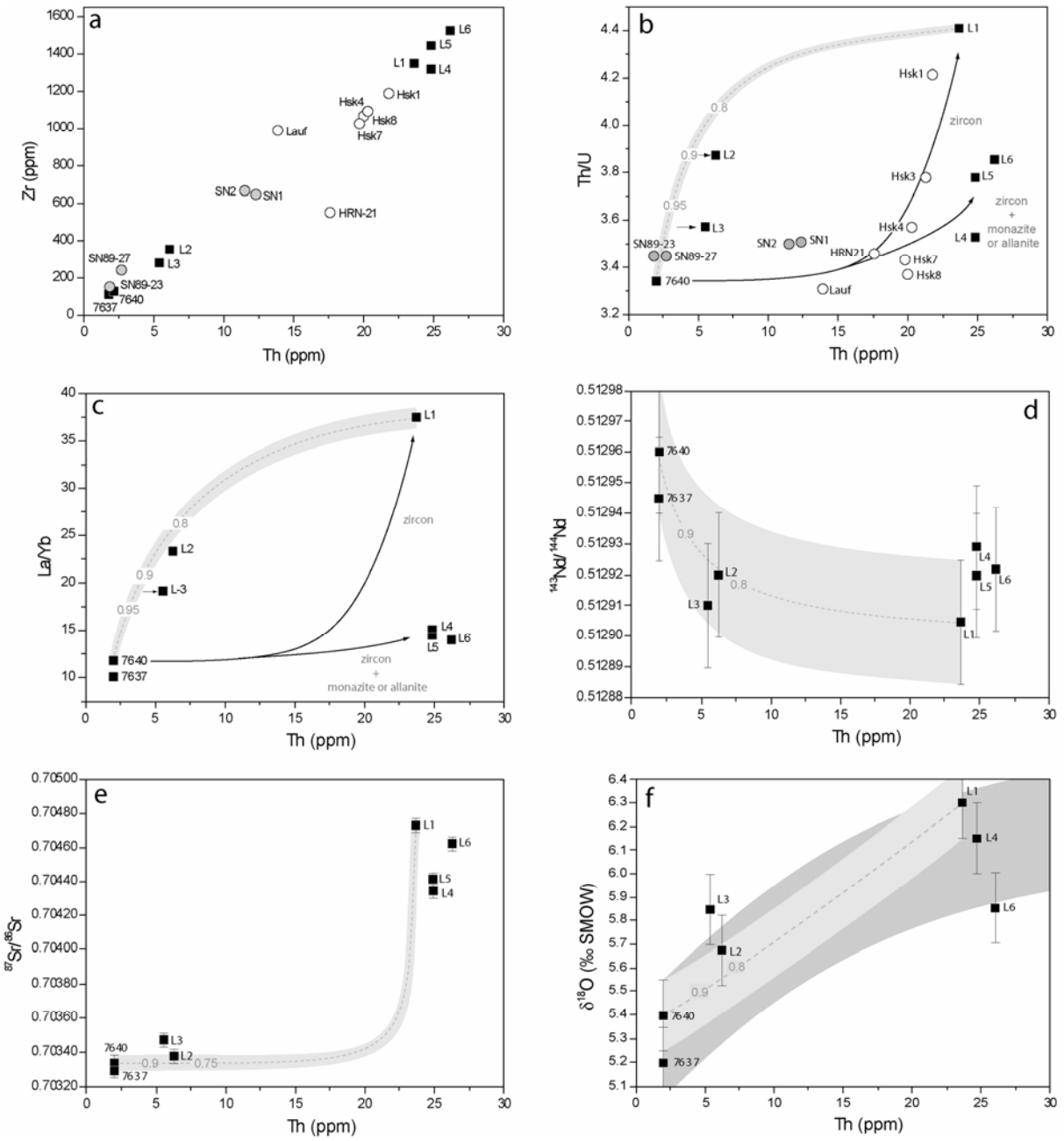

Figure 4: *The Th concentration vs. (a) Zr concentration, (b) Th/U, (c) La/Yb, (d) $^{143}Nd/^{144}Nd$, (e) $^{87}Sr/^{86}Sr$ and (f) $\delta^{18}O$. Open and grey circles represent samples from Snæfellsjökull and Torfajökull respectively and black squares the Ljósufjöll ones. a) The observed linear correlation precludes important fractionation of zircon during magma differentiation. High zirconium in the Lauf sample suggests an accumulation of zircon whereas the low concentrations in HRN21 may reflect significant zircon fractionation. b-c-d-e-f) Solid arrows or dark grey areas show the computed fractional crystallisation evolutions and light grey shaded area represent the calculated mixing curve between basalt 7640 and rhyolite L1. The curve width represents the 2σ analytical uncertainty.*

Discussion

Petrogenesis

Deciphering which of the two principal mechanisms of silicic magma production, crustal melting or crystal fractionation, is dominant is important to be related to the thermal state of the crust. A cold crust would need a large input of heat from basalts to reach its solidus, whereas hotter crust is more easily melted. At the same time, cold crust cools down basaltic intrusions more than hotter crust, thus favoring the formation of evolved magma. The arguments for or against each mechanism of silicic magma production will be evaluated for each volcanic system studied.

Torfajökull

The most recent studies of the petrogenesis of the large Torfajökull silicic complex are those of Macdonald et al. (1990) and Gunnarsson et al. (1998). The former reached the conclusion that fractional crystallisation explains the compositions of the silicic lavas whereas the latter prefer partial melting of a silicic intrusion produced by fractional crystallisation. The relatively low $\delta^{18}O$ of the silicic rocks are interpreted as resulting from partial melting of hydrothermally altered crust, which may contain plagiogranites (Gunnarsson et al. 1998; Sigurdsson 1977) or be in the amphibolite facies (Oskarsson et al. 1982). Our Hrafntinnusker obsidian has similar $\delta^{18}O$ to those of Gunnarsson et al. (1998) whereas the low value for Laufafell (2.4‰) is clearly lower than those published for the basalts of Torfajökull (4.5 – 5‰). A lower $\delta^{18}O$-value in silicic compared to mafic magma is similar to that which has been observed for Krafla and Askja volcanoes (Nicholson et al. 1991; Sigmarsson et al. 1991). Application of the crustal melting model based on results from the neighbouring volcano, Hekla (Sigmarsson et al. 1992a), is therefore appropriate to the Torfajökull case. In this model, the hydrothermally altered basalts in the amphibolite facies experience amphibole dehydration melting to produce a dacitic melt. This melt separates from its source and fractionates towards a rhyolitic composition upon cooling during ascent through the crust.

The magmatic evolution of the Torfajökull volcanic system is faithfully recorded by the concentrations of the highly incompatible element Th. The Th concentration varies by over an order of magnitude, from 2.65 ppm in basaltic inclusions in the Hrafntinnuhraun obsidian lava (Sigmarsson unpublished results), to 21.9 ppm in the first emitted silicic pumice of the Hrafntinnusker eruption (Hsk1). The ca. 80 m-thick tephra sequence of this eruption has Th concentrations that decrease only slightly down to 19.7 ppm in the most recent tephra at the

top of the sequence. Thorium shows a very good correlation with Zr (Fig. 4a), which suggests that no or very limited zircon fractionation has taken place, in agreement with the high zirconium solubility in peralkaline magmas (Watson 1979). The slightly decreasing Th concentration of the crystal-free pumice during the Hrafntinnusker eruption imply both a small and finely stratified liquid magma layer that was inverted upon eruption, together with a very efficient method of liquid-crystal separation. This situation is comparable to that proposed for high-silica rhyolites elsewhere, for which a gas-filter pressing mechanism is advocated for liquid-crystal separation (e.g. Sisson and Bacon 1999; Bachmann and Bergantz, 2004).

In a primitive mantle normalized multi-element diagram (Fig. 3) Hrafntinnusker peralkaline rhyolites show important negative anomalies for Ba, Sr and to a lesser extent, for Eu. These anomalies can be shown to be inconsistent with crustal partial melting alone, whereas feldspar fractionation can readily account for the observed Ba, Sr and Eu depletions (Fig.5). In Figure 5 two compositional fields are shown for an evolved magma derived from: 1) fractional crystallisation of a transitional basalt (sample 7637) and 2) partial melting of a hydrothermally altered basalt the latter being considered as a representative average of the Icelandic basaltic crust. In addition, in order to access the model boundaries, the highest and the lowest partition coefficients of Sr and Ba (Table 2) have been considered for plagioclase and orthoclase. Figure 5 clearly demonstrates that in Hrafntinnusker rhyolites the Ba anomaly can be produced by both mechanisms, whereas the Sr anomaly reflects either high degrees (85-90%) of fractional crystallisation or partial crustal melting with subsequent crystal fractionation. Hence, fractional crystallisation is an important process during the formation of the silicic magma at Torfajökull. However, the O-isotope ratios clearly show that, prior to the overprint of the final crystal fractionation stage, the magmas were originated from crustal partial melting. Thus, a two-stage process can be envisaged: 1) partial melting of hydrated metabasaltic crust generating a silicic magma having $^{143}Nd/^{144}Nd$ and $^{87}Sr/^{86}Sr$ more or less comparable to those of contemporaneous and spatially related basalts, but with lower $\delta^{18}O$-values; 2) subsequent fractional crystallisation of plagioclase and/or orthoclase accounting for the strong Sr depletion (as well as Ba and Eu) observed in Hrafntinnusker rhyolites. The principal difference with the case of Hekla (Sigmarsson et al. 1992a) is that, during the second stage, the role of zircon fractionation is significantly reduced because of the peralkaline nature of the silicic magma in Torfajökull.

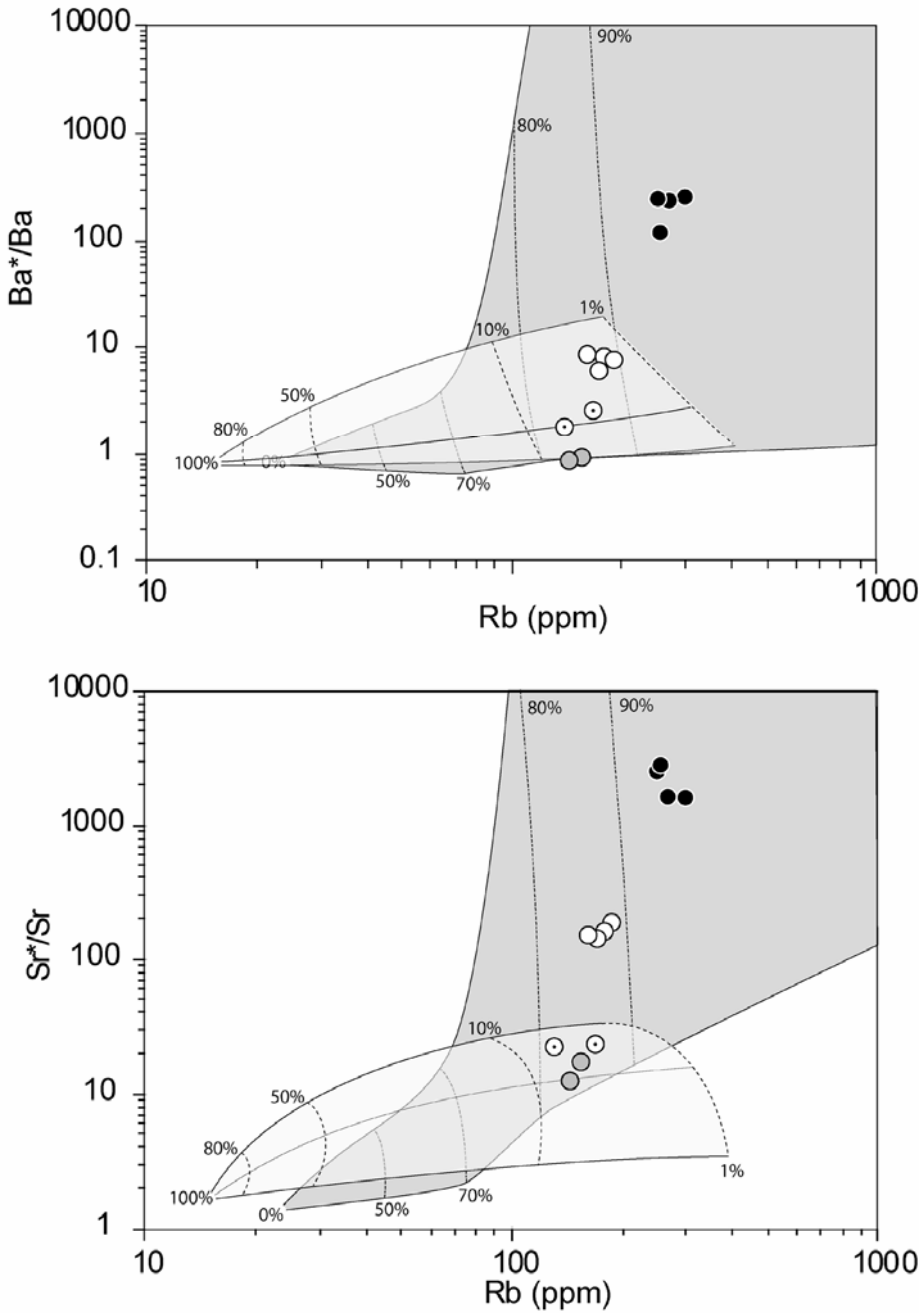

Figure 5: Diagrams of Ba*/Ba and Sr*/Sr vs. Rb concentration showing different compositional fields for fractional crystallisation and crustal partial melting. Light grey area is the domain for evolved melts generated by partial melting of the Iceland basaltic crust, whereas the dark grey area represents the domain formed by fractional crystallisation from a basalt of Ljósufjöll. The value for the average crust is taken from drill cuttings at 800 m depth in the geothermal field of Krafla, N-Iceland (Ingvarsson and Sigmarsson, in prep.). The Ba* is defined as $10^{(Log[Rb]+Log[Nb])/2}$ and Sr* as $10^{(Log[Ce]+\ Log\ [Nd])/2}$ and all concentrations are normalized to primitive mantle values (Sun and McDonough 1989). Symbols as in Fig. 2 except open circles with a central point for Lauf- and HRN- samples (see text for further discussion).

Table 2: *Partition coefficients used in trace element modelling (from Brooks et al. 1981; Fujimaki et al. 1984; Mahood and Hildreth 1983; Nash and Crecraft 1985; Paster et al. 1974).*

	Olivine	Clinopyroxene	Plagioclase	Orthoclase	Ilmenite	Zircon	Alanite
La	0.0067	0.056-0.19	0.302-0.38	0.08	0.098-1.223	4.18-16.9	820-2362
Ce	0.006	0.15-0.5	***0.005***-0.221-0.27-***0.62***	***0.017***-0.037-***0.095***	0.11-1.64	4.31-16.75	635-2063
Nd	0.0059	0.31-1.11	***0.008***-0.149-0.21-***0.29***	***0.009***-0.035-***0.093***	0.14-2.267	4.29-13.3	463-1400
Sm	0.007	0.5-1.67	0.102-0.13	0.025	0.15-2.833	4.94-14.4	205-756
Eu	0.0074	0.51-1.56	0.376-1.4	2.6	0.1-1.013	3.31-16	81-122
Gd	0.01	0.61-2	0.067-0.097	0.025	0.14-2.3	6.59-12	130
Dy	0.013	0.68-1.93	0.05-0.064	0.055	0.145-3.267	47.4-101.5	50-123
Er	0.0256	0.65-1.8	0.045-0.055	0.006	0.15-2.2	99.8-135	25-60
Yb	0.0491	0.62-1.8	0.041-0.049	0.03	0.17-1.467	128-527	8.9-24.5
Rb	0.0098	0.013-0.032	***0.016***-0.04-0.07-***0.46***	***0.11-1.75***			
Ba	0.0099	0.026-0.131	***0.03***-0.16-2.5-***19.5***	**1-44**	0.00034		
Nb	0.01	0.005-0.8	***0.008***-0.025-0.035-***0.27***	***0.01-0.15***	0.8-6.58		
Sr	0.014	0.06-0.516	***1.3***-1.8-4.7-***33***	**1.6-22**	0.1-0.5		
Zr	0.012	0.1-0.6	0.01-0.135	0.03	0.28-1.38		
Y	0.01	0.9-4	0.06-0.13	0.03	0.0045-0.3		
Th		0.36-2.89	0.01-0.048	0.023	0.00055-0.463	62-91	168-420
U		0.12-0.33	0.01-0.09	0.048	0.0082-0.517	298-383	6-14

Values in bold characters correspond to the highest and the lowest partition coefficients as compiled in the Earth Science reference data and models (http://www.earthref.org) and were used for the models in Figure 5.

Ljósufjöll

Rhyolite genesis

The peralkaline rhyolites of Ljósufjöll have several characteristics in common with those of Torfajökull. In a primitive mantle normalized multi-element diagram (Fig. 3) they display very strong depletions in Ba, Sr and, to a lesser extent, in Eu, due to feldspar fractionation. In contrast with Torfajökull volcano, the $\delta^{18}O$ is higher in the silicic lavas (5.8‰ to 6.3‰, Table 1) than in associated basalts from the Ljósufjöll volcanic system (5.2‰ to 5.4‰). In this case, there is no reason to invoke crustal partial melting since fractional crystallisation can fully explain the observed geochemical variations.

The genesis of rhyolites by fractional crystallisation of a basaltic magma can be tested and modelled in two ways. The mechanism is first verified using mass balance calculations (Stormer and Nicholls 1978). Based only on major elements, this algorithm calculates both the modal and chemical compositions of the crystallizing assemblage which fractionated from the magma, as well as the degree of crystallisation. The mass balance calculation relates the genesis of a rhyolite (L4) to a basaltic parental magma (7637) with a fractionating mineral

assemblage of plagioclase (50%) + clinopyroxene (28%) + Fe-Ti oxides (15%) + olivine (4%) + orthoclase (3%), yielding a low sum of squared residuals ($\Sigma r^2 = 0.06$). The necessary degree of fractional crystallisation is very high, at 94 %. When the mineralogical composition of the fractionating mineral assemblage is reintroduced into trace element modelling, the outcome fits perfectly with the analytical data of the rhyolites for degrees of fractionation ranging from 90 to 97% (Fig. 6a). However, slight differences appear when the REE are considered. For example, sample L1 is LREE-richer and HREE-poorer than other rhyolites (L4, L5 and L6) and has higher Th/U (Fig. 4b-c and Fig. 7). Fractionation of accessory mineral phases must therefore be taken into consideration. Only a very small amount of zircon fractionation (0.05%) is needed in order to account for the observed REE, without causing much decrease in Zr (Fig. 7), and it also accounts for the observed Th/U in sample L1, if $D_{Th}^{zircon/melt}$ and $D_{U}^{zircon/melt}$ are as high as 76 and 340, respectively (Table 2). However, the REE patterns, specifically the LREE, of the other rhyolites (samples L4, L5 and L6) require the fractionation of a different accessory mineral such as monazite or allanite. The high U and Th partition coefficients for allanite ($D_{Th}^{allanite/melt}$ and $D_{U}^{allanite/melt}$ are ~283 and ~12 respectively; Table 2) reduce the Th/U ratio in the melt. Figure 7 illustrates the effect of 0.02% allanite fractionation on REE patterns when added to the same fractionating mineral assemblage as for L1 (including 0.05% of zircon). This modified model fits the REE compositions of samples L4, L5 and L6. It also predicts a Th/U of ~3.7 (Th~25.4 and U~6.8) which is consistent with the Th and U content of these rhyolites (24.9-26.3 and 6.56-7.06 respectively). Monazite is similar to allanite, in that it has a Th/U typically between 5 and 50 (e.g. Deer, et al. 1963; Förster, 1998). When monazite is considered instead of allanite, a smaller proportion (around 0.002%) is required to provide the same effect. Such low fractionation rates are coherent with the high monazite solubility in peralkaline magmas (Montel, 1986).

The results from the major and trace element modelling can be tested for the O isotope results on the same samples. The minimal $\delta^{18}O$ increase ($\leq$ 1‰) from the basalts to the peralkaline rhyolites can be accounted for by the 94 % fractional crystallisation, using the phase proportions (assumed to be constant during the differentiation process) from the major and trace element modelling and mineral-magma isotopic fractionation coefficients estimated from Harris and Smith (2000) and Eiler (2005) ($\Delta_{plagioclase\text{-}melt} = 0.2$, $\Delta_{clinopyroxene\text{-}melt} = -0.2$, $\Delta_{orthoclase\text{-}melt} = 0.4$, $\Delta_{olivine\text{-}melts} = -0.6$, $\Delta_{Magnetite/Ilmenite\text{-}melts} = -2$; Fig. 4f).

The high degree of fractional crystallisation at the origin of the rhyolites in Ljósufjöll results in very low Sr contents and the highest Rb/Sr ever analysed in Icelandic rocks (90 to

150). Considering the large variability in Rb/Sr between rhyolites and basalts and the K-Ar ages (~100 to ~800 ky) obtained on the Ljósufjöll central volcano by Flude et al. (2004), the time corrected $^{87}Sr/^{86}Sr$ of rhyolites and basalts are similar, as would be expected with the fractional crystallisation mechanism.

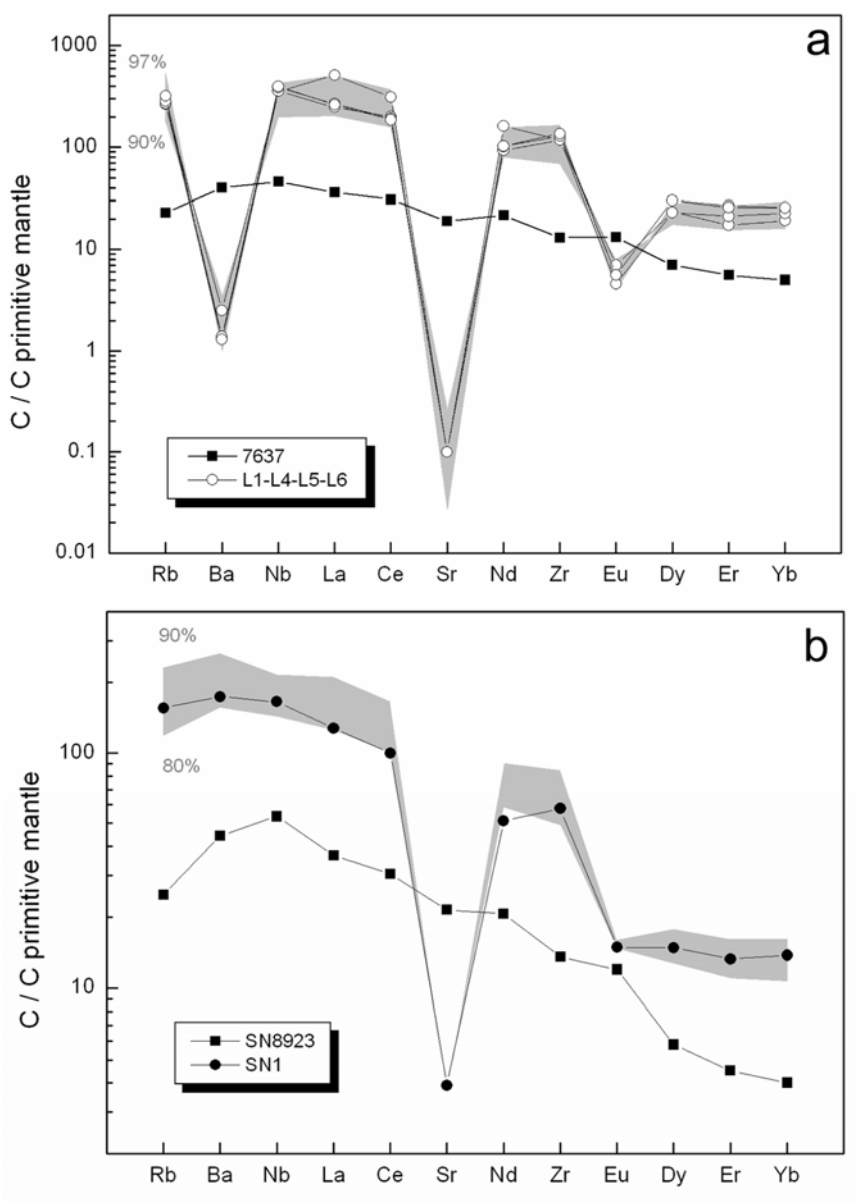

Figure 6: Primitive mantle normalized (Sun and McDonough 1989) multi-element diagram comparing a) samples L1-L4-L5-L6 with the calculated trace elements composition (grey area) of liquid obtained by 90-97% fractional crystallisation from the 7637 basalt. b) Trachyte SN1 compared with calculated trace element compositions for 80-90% fractional crystallisation of SN89-23 basalt from the vicinity of Snæfellsjökull volcano. The good fit between calculated and measured concentrations suggests that fractional crystallisation fully accounts for the compositional variability of the silicic rocks of Ljósufjöll and Snæfellsjökull.

An interesting corollary of the Sr-isotope results from Ljósufjöll is that old silicic formations in Iceland which were formed by fractional crystallisation should have elevated $^{87}Sr/^{86}Sr$ if their Rb/Sr has been increased by plagioclase fractionation. This could be a useful criterion when discussing the petrogenesis of Tertiary volcanoes.

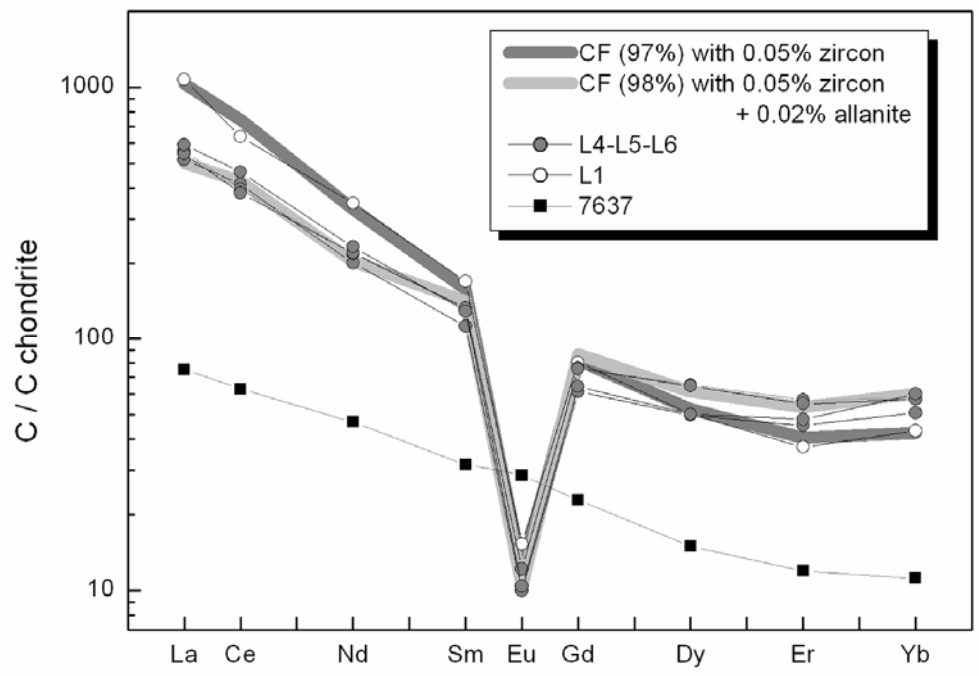

Figure 7: Chondrite normalized REE patterns comparing rhyolites L1-L4-L5-L6 with the calculated trace element compositions of liquid obtained by 97-98% fractional crystallisation including small proportions of zircon and allanite.

Intermediate rocks genesis

The intermediate compositions of samples L2 and L3 are not readily explained by a simple fractional crystallisation scenario. This is especially true for their relatively high Th/U (3.57 – 3.87) compared to those of the basalts (Th/U=3.34, Sigmarsson et al., 1992). However, magma mixing between previously formed rhyolites and incoming basalts of a similar composition to that presented in Table 1, appears to satisfy all geochemical parameters. Figure 4 shows the results of a mixing model between a basaltic magma (7640) and rhyolite L1. In order to account for the Th/U, La/Yb, $^{87}Sr/^{86}Sr$, $^{143}Nd/^{144}Nd$ and $\delta^{18}O$ of the intermediate samples, mixing proportions of 80-95% basalt with 5-20% rhyolite are required. However, the composition of the rhyolite end-member must have been slightly less affected by feldspar fractionation than sample L1, in order to match the Ba, K, Na and Eu variations. Complex zonation and resorption edges of the feldspars are compatible with such magma mixing.

Snæfellsjökull trachytes

Both basic and acid magmas from Snæfellsjökull have identical Sr and Nd isotopes compositions ($^{143}Nd/^{144}Nd$ ~0.51297±1 and $^{87}Sr/^{86}Sr$ ~0.70337±1; Table 1), which could indicate that they derived from a common source. As for the Ljósufjöll samples, the genesis of trachyte SN-1 by fractional crystallisation of alkali basalt was tested for both major and trace elements. The extracted mineral assemblage which best fits the data consists of Plagioclase (39%) + Clinopyroxene (37%) + Olivine (13%) + Fe-Ti oxides (11%). The Σr^2 is low (0.2) and the degree of fractional crystallisation is 87 %. This mineralogical assemblage is without alkali feldspar and the extracted plagioclase is of a smaller amount than in Hrafntinnusker and Ljósufjöll samples. When the mineralogical composition of the crystallising assemblage is reintroduced into trace element modelling, it appears that the model fits analytical data for degrees of fractionation ranging from 80 to 90% (Fig. 6b). In the same way as at Ljósufjöll, very small amounts (0.01%) of fractionating zircon are required to adjust the Th and U concentrations. This results in the calculated Th and U concentrations (Th~12.3ppm U~3.5ppm and Th/U~3.5) being consistent with SN-1 and SN-2 concentrations (Th=12.3ppm and 11.5ppm, U=3.5ppm and 3.29ppm, Th/U=3.51 and 3.50 respectively). A closed system differentiation mechanism operating from basalts to trachytes is thus likely to be the case for Snæfellsjökull volcano.

The $\delta^{18}O$-values of the trachytes (4.9 to 5.1‰) are slightly lower than those of the Holocene basalts (5.3 to 5.4 ‰; Sigmarsson et al., 1992b and references therein) erupted around the Snæfellsjökull stratovolcano. As already discussed for Ljósufjöll magmas, large degrees of fractional crystallisation are expected to slightly increase the $\delta^{18}O$ in the derived magma when significant amounts of Fe-Ti oxides fractionation takes place. The O-isotopes of Snæfellsjökull lavas cannot, therefore, be explained by a closed-system fractional crystallisation process alone. However, slight crustal contamination from the metabasaltic crust of the ancient rift zone in Snæfellsnes is capable of explaining the $\delta^{18}O$. In an assimilation-fractional crystallisation (AFC) process, assuming an average crustal $\delta^{18}O$ of 1-3‰ (Gautason and Muehlenbachs 1998) the mass ratio of crystal extract to assimilated crust would be in the range of 10-30 depending on the exact O-isotope fractionation factors between minerals and liquid. Such a high mass ratio of fractionating crystals over assimilated melt reflects a differentiation process occurring in a relatively "cold" environment. This illustrates the importance of the role of crystal fractionation compared to that of crustal partial melting. Accordingly, we propose that the compositions of the Snæfellsjökull trachytes are

best explained by fractional crystallisation with minor crustal assimilation. Thus it appears that the genesis of the silicic magma at Snæfellsjökull is likely to lie between the contrasting mechanisms inferred for Ljósufjöll and Torfajökull, namely crustal cooling effect leading to fractional crystallization and crustal melting due to a hotter environment.

Geodynamic environment

Figure 1 depicts the depth to a inferred 1200°C isotherm, which is estimated to be 20-25 km beneath Ljósufjöll and only 15-20 km beneath Snæfellsjökull. For Torfajökull, this isotherm can be assumed to be even shallower due to the influence of the propagating rift zone entering the silicic complex (e.g. Oskarsson et al. 1982). Partial melting of hydrated metabasaltic crust would only occur where the geothermal gradient is high and large degrees of a fractional crystallisation would be restricted to areas with low geothermal gradient.

Existing work on the genesis of silicic rocks supports the model presented in this paper. For instance, Sigmarsson et al. (1991; 1992a) proposed that the central volcanoes within or close to the rift zone resulted from partial melting of basaltic crust. Whereas, Prestvik et al. (2001) suggested that the silicic melts of the off-rift Öræfajökull central volcano (South-East Iceland) were generated by fractional crystallisation of basaltic magmas. Both these explanations are fully consistent with the geothermal gradient controlling which mechanism prevails.

Conclusion

The interaction between the mid-Atlantic ridge and a mantle plume beneath Iceland gives rise to high magma productivity, resulting in an elevated geothermal gradient. The lower amphibolitic crust is likely to cross its hydrous solidus at depth and will consequently undergo partial melting, generating silicic magmas within, or close to, the rift-zone. In contrast, at a distance from the rift zones or the plume centre, the geothermal gradient is significantly lower; there, the crust is unlikely to cross its hydrous solidus. Under the latter conditions, silicic magmas are generated by a high degree of fractional crystallisation of basaltic magmas in an off-rift context, as in the Ljósufjöll and Öræfajökull areas. The intermediate geothermal gradient beneath Snæfellsjökull is best explained by a combined magma differentiation mechanism, namely assimilation-fractional crystallisation with less than 10% of crustal assimilation. Therefore a clear link between the mode of silicic magma formation and the thermal state of the Icelandic crust appears to exist.

Acknowledgement

We greatly appreciate the guidance and help from Serge Fourcade at "Géosciences Rennes" during the O-isotope analysis, in addition to his pertinent remarks on an earlier version of this manuscript. Analytical assistance from Delphine Auclair, Chantal Bosq, Karina David and Mhammed Benbakkar is also gratefully acknowledged. Fruitful discussions on trace element modelling with Hervé Martin were very useful. We could not have had better company than Gudrun Larsen and Bergrun A. Oladottir during the fieldwork at Hrafntinnusker. Efficient English corrections by Fran Van Wyk de Vries were much appreciated. Constructive comments from two anonymous reviewers improved the manuscript. Finally, a grant from the Icelandic Science Foundation and the French-Icelandic Jules Verne collaboration program is acknowledged.

References

Bachmann O, Bergantz GW (2004) On the origin of crystal-poor rhyolites: extracted from batholithic crystal mushes. J Petrol 45:1565-1582

Breddam K, Kurz MD, Storey M (2000) Mapping out the conduit of the Iceland mantle plume with helium isotopes. Earth Planet. Sci. Lett. 176:45-55

Brooks CK, Henderson P, Ronsbo JG (1981) rare earth element partitioning between allanite and glass in the obsidian of Sandy Braes, northern Ireland. Miner. Mag. 44:157-160

Cantagrel F, Pin C (1994) Major, minor and rare-earth element determinations in 25 rock standards by ICP-atomic emission spectrometry. Geostandards Newsletter 18:123-138

Carmichael ISE (1964) The petrology of Thingmuli, a tertiary volcano in Eastern Iceland. J. Petrol 5:435-460

Carpentier M (2003) Variabilité géochimique des basaltes Holocène islandais. Université Blaise Pascal, Clermont Ferrand, p 53

Christiansen EH, McCurry M (2006) Contrasting Origins of Cenozoic Silicic Volcanic Rocks from the Western Cordillera of the United States. Bulletin of volcanology, in press.

Clayton R, N., Mayeda TK (1963) The use of bromine pentafluoride in the extraction of oxygen from oxides and silicates for isotopic analysis. Geochim. Cosmochim. Acta 27:43-52

Condomines M, Tanguy JC, Kieffer G, Allègre CJ (1982) Magmatic evolution of a volcano studied by 230 Th- 238 U disequilibrium and trace elements systematics: The Etna case Geochim. Cosmochim. Acta 46:1397-1416

Deer WA, Howie RA, Zusmna J (1963) Rock-Forming Minerals, vol. Longmans, Green and co LTD, London

Eiler J (2005) Oxygen isotope variations of basaltic lavas and upper mantle rocks. In: Walley JW, Cole DR (eds) Reviews in Mineralogy and geochemistry, vol 43. The mineralogical society of america, Washington, pp 319-364

Eysteinsson H, Gunnarsson K (1995) Maps of gravity, bathymetry and magnetics for Iceland and surroundings. In, vol. Orkustofnun, National Energy Authority, Geothermal division,

Flovenz OG, Saemundsson K (1993) Heat flow and geothermal processes in Iceland. Tectonophysics 225:123-138

Flude S, Burgess R, McGarvie DW (2004) Volcanism at Ljósufjöll central volcano, western Iceland: chemostratigraphy and geochronology. In: IAVCEI, vol., Pucón-Chile

Förster H-J (1998) The chemical composition of the REE-Y-Th-U-rich accessory minerals in peraluminous granites of the Erzgebirge-Fichtelgebirge region, Germany, PartI: The monazite-(Ce)-brabantite solid solution series. Amer Mineral 83:259-272

Fujimaki H, Tatsumoto M, Aoki K (1984) Partition coefficients of Hf, Zr, and REE between phenocrysts and groundmasses. Journal of Geophysical Research 89: 662-672. J. Geophys. Res. 662-672

Furman T, Frey FA, Meyer PS (1992) Petrogenesis of evolved basalts and rhyolites at Austurhorn, Southeastern Iceland: the role of fractional crystallisation. J. Petrol 33:1405-1445

Gautason B, Muehlenbachs K (1998) Oxygen isotopic fluxes associated with high-temperature processes in the rift zones of Iceland Chem. Geol. 145:275-286

Gudmundsdóttir LS, Sigmarsson O (2006) Highest measured strontium isotope ratios in Icelandic rocks: Rb and Sr systematics in Ljósufjöll volcanics, Snæfellsnes peninsula. Natural Science Symposium, Reykjavik.

Gunnarsson B (1987) Petrology and petrogenesis of silicic and intermediate lavas on a propagating oceanic rift. The Torfajökull and Hekla central volcanoes south-central Iceland. Johns Hopkins University, Baltimore, Maryland, p 432

Gunnarsson B, Marsh BD, Taylor JHP (1998) Generation of Icelandic rhyolites: silicic lavas from the Torfajökull central volcano. J. Volcanol. Geotherm. Res. 83:1-45

Harris C, Smith HS, Le Roex AP (2000) Oxygen isotope composition of phenocrysts from Tristan da Cunha and Gough Island lavas: variation with fractional crystallization and evidence for assimilation. Contrib. Mineral. Petrol. 138:164-175

Jakobsson SP (1972) Chemistry and distribution pattern of recent basaltic rocks in Iceland. Lithos 5:365-386

Jóhannesson H, Flores RM, Jónsson J (1982) A short account of the Holocene tephrochronology of the Snaefellsjökull central volcano, Western Iceland. Jökull 31:23-30

Jónasson K (1994) Rhyolite volcanism in the Krafla central volcano, north-east Iceland. Bull volcanol 56:516-528

Le Bas MJ, Le Maitre Rw, Streckeisen A, Zanettin B (1986) A chemical classification of volcanic rocks based on the total alkali-silica diagram. J. Petrol 22:745-750

Macdonald R, McGarvie DW, Pinkerton H, Smith RL, Palacz ZA (1990) Petrogenetic evolution of the Torfajökull volcanic complex, Iceland I. Relation between the magma types. J. Petrol 31:461-481

Mahood G, Hildreth W (1983) Large partition coefficients of trace elements in high-silica rhyolites. Geochim. Cosmochim. Acta 47:11-30

McGarvie DW (1984) Torfajökull: a volcano dominated by magma mixing. Geology 12:685-688

Miyashiro A (1978) Nature of alkalic volcanic rock series. Contrib. Mineral. Petrol. 66:91-104

Montel J-M (1986) Experimental determination of the solubility of Ce-monazite in SiO_2-Al_2O_3-K_2O-Na_2O melts at 800°C, 2kbar, under H_2O-saturated conditions. Geology 14:659-662

Nash WP, Crecraft HR (1985) Partition coefficients for trace elements in silicic magmas. Geochim. Cosmochim. Acta 49:2309-2322

Nicholson H, Condomines M, Fitton JG, Fallick AE, Grönvold K, Rogers G (1991) Geochemical and isotopic Evidence for Crustal Assimilation Beneath Krafla, Iceland. J. Petrol 32:1005-1020

Oskarsson N, Sigvaldason GE, Steinthorsson S (1982) A dynamic model of rift zone petrogenesis and the regional petrology of Iceland. J. Petrol 23:28-74

Paster TP, Schauwecker DS, Haskin LA (1974) The behavior of some trace elements during solidification of the Skaergaard layered series. Geochim. Cosmochim. Acta 38:1549-1577

Prestvik T, Goldberg S, Karlsson H, Grönvold K (2001) Anomalous strontium and lead-isotope signatures in the off-rift Öraefajökull central volcano in south-east Iceland, Evidence for enriched endmember(s) of the Iceland mantle plume? Earth Planet. Sci. Lett. 190:211-220

Sigmarsson O, Condomines M, Fourcade S (1992a) A detailed Th, Sr and O isotope study of Hekla: differentiation processes in an Icelandic volcano. Contributions to Mineralogy and Petrology 112:20-34

Sigmarsson O, Condomines M, Fourcade S (1992b) Mantle and crustal contribution in the genesis of recent basalts from off-rift zones in Iceland: constraints from Th, Sr and O isotopes. Earth Planet. Sci. Lett. 110:149-162

Sigmarsson O, Hémond C, Condomines M, Fourcade S, Oskarsson N (1991) Origin of silicic magma in Iceland revealed by Th isotopes. Geology 19:621-624

Sigurdsson H (1977) Generation of icelandic rhyolites by melting of plagiogranites in the oceanic layer. Nature 269:28-28

Sisson TW, Bacon CR (1999) Gas-driven pressing in magmas. Geology 27:613-616

Stecher O, Carlson RW, Gunnarsson B (1999) Torfajokull: a radiogenic end-member of the Iceland Pb-isotopic array. Earth Planet. Sci. Lett. 165:117-127

Stormer JC, Nicholls J (1978) XLFRAC: a program for interactive testing of magmatic differentiation models. Computer Geoscience 87:51-64

Sun SS, McDonough WF (1989) Chemical and isotopic systematics of oceanic basalts: Implications for the mantle composition and processes. In: Magmatism in the Ocean Basin, vol 42. Geol. Soc. Sp. Publi., pp 313-345

Thordarson T, Larsen G (2006) Volcanism in Iceland in historical time: Volcano types, eruption styles and eruptive history. J. Geodyn. doi:10.1016/j.jog.2006.09.005

Walker GPL (1966) Acid rocks Iceland. Bull. volcanol. 29:375-406

Watson EB (1979) Zircon saturation in felsic liquids: experimental results and applications to trace element geochemistry. Contrib. Mineral. Petrol. 70:407-419

Wolfe CJ, Bjarnason IT, VanDecar SC, Solomon SC (1997) Seismic structure of the Iceland mantle plume. Nature 385:245-247

2. Etude des mécanismes pré- et post-éruptifs du magmatisme acide de Hrafntinnusker, Torfajökull.

Comme cela a déjà été mentionné dans la partie précédente (Partie III-A-1), les rhyolites peralcalines de Hrafntinnusker ont été échantillonnées au sein du même dépôt de téphra. Ce dernier fait environ 80 mètres d'épaisseur et il est surmonté d'une coulée d'obsidienne qui forme ainsi le sommet du mont Hrafntinnusker (Figure III-1). L'absence de paléosol au sein de ce dépôt semble indiquer que l'ensemble s'est mis en place dans un laps de temps relativement court c'est-à-dire probablement au cours d'une phase éruptive unique, il y a environ 8 000 ans (Larsen, 2006, communication personnelle).

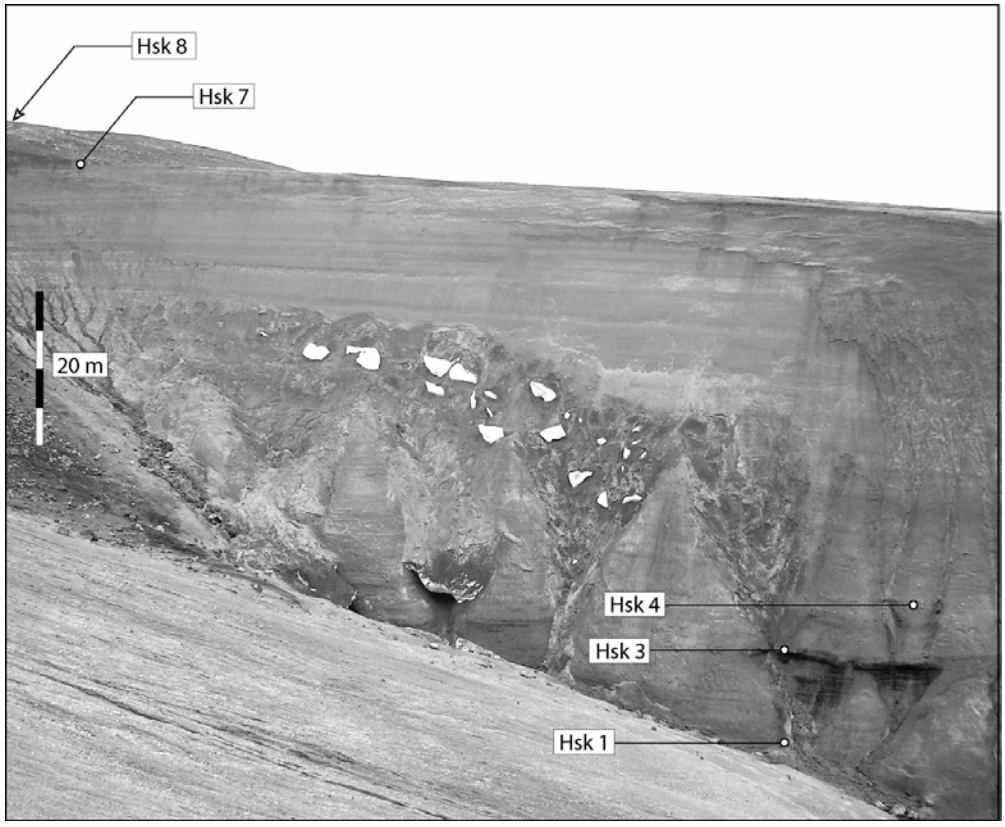

Figure III-1 : Dépôt de tephra de Hrafntinnusker au sein duquel sont localisés les échantillons analysés.

La composition chimique (roche totale) des ponces de ce dépôt (Tableau III-1) semble être corrélée avec la position de l'échantillon dans la colonne stratigraphique. En effet, en remontant le dépôt volcanique (Hsk1 jusqu'à Hsk8-7 via Hsk3 et Hsk4) les teneurs en TiO_2, Al_2O_3, Fe_2O_3*, MgO, CaO, Zr, Hf, Th et H_2O et le $^{87}Sr/^{86}Sr$ diminuent alors que celles en Na_2O, Ba, U et dans une moindre mesure en Rb, augmentent. Les autres éléments majeurs et

en traces ainsi que le rapport $^{143}Nd/^{144}Nd$ sont quant à eux, relativement constant quelque soit la position stratigraphique de l'échantillon. Le caractère alcalin des échantillons est lui aussi lié à l'emplacement des échantillons, il augmente du bas (0,72 pour Hsk1) vers le haut (1,15 pour Hsk8) du dépôt.

Tableau III-1 : Composition en éléments majeurs et en trace des échantillons de Hrafntinnusker

	Hsk8		**Hsk7**		**Hsk4**		**Hsk3**	**Hsk1**	
SiO_2	72,6	*73,3*	71,4	*73,6*	70,9	*73,5*		68,5	*73,4*
TiO_2	0,19	*0,20*	0,20	*0,20*	0,20	*0,21*		0,22	*0,23*
Al_2O_3	12,3	*12,4*	11,9	*12,3*	12,1	*12,5*		12,9	*13,9*
Fe_2O_3*	3,36	*3,39*	3,41	*3,52*	3,49	*3,61*		3,75	*4,01*
MnO	0,07	*0,07*	0,08	*0,08*	0,07	*0,08*		0,07	*0,08*
MgO	0,07	*0,07*	0,09	*0,09*	0,08	*0,09*		0,23	*0,25*
CaO	0,40	*0,40*	0,44	*0,45*	0,42	*0,43*		0,47	*0,51*
Na_2O	5,63	*5,68*	5,08	*5,25*	4,66	*4,83*		2,83	*3,04*
K_2O	4,44	*4,48*	4,29	*4,43*	4,51	*4,67*		4,31	*4,62*
P_2O_5	0,02	*0,02*	0,03	*0,03*	0,03	*0,03*		0,03	*0,03*
H2O -	0,2		0,3		0,4		0,9	0,9	
H2O +	0,4		3,7		3,6		4,4	5,2	
total	99,6	*100,0*	101,0	*100,0*	100,4	*100,0*	5,4	99,4	100,0
Rb	120		110		114			102	
Sr	12,2		14,1		13,8			14,5	
Y	117		111		116			112	
Zr	1067		1026		1093			1189	
Nb	140		133		140			136	
Ba	172		203		164			140	
La	120		114		118			118	
Ce	246		232		242			248	
Pr	28,1		26,3		27,7			27,6	
Nd	102		96,2		101			101	
Sm	21,5		20,2		21,4			21,3	
Eu	1,88		1,74		1,89			1,89	
Gd	18,5		17,4		18,6			18,4	
Tb	3,33		3,12		3,33			3,24	
Dy	20,6		19,5		20,7			20,2	
Ho	4,19		3,94		4,22			4,07	
Er	11,4		10,7		11,4			11,0	
Tm	1,60		1,51		1,60			1,53	
Yb	10,9		10,3		11,0			10,5	
Lu	1,60		1,50		1,61			1,54	
Hf	28,6		26,8		29,3			31,3	
Ta	12,2		11,1		12,6			12,8	
Th (DI)	20,0		19,7		20,3		21,3	21,8	
U(DI)	5,93		5,74		5,69		5,64	5,17	
Th/U	3,37		3,43		3,57		3,78	4,22	
$^{87}Sr/^{86}Sr$	0,70338		0,70355		0,70353		0,70341	0,70386	
$^{143}Nd/^{144}Nd$	0,51298		0,51297		0,51297		0,51298	0,51297	

Les données en italiques correspondent à la composition en éléments majeurs recalculée à 100 % (base anhydre). Perte au feu H_2O- : 100°C et H_2O+ : 1100°C. DI : dilution isotopique. Les conditions analytiques sont détaillées dans le Chapitre III-A-1 et Annexes 2 à 5.

Une chambre magmatique finement stratifiée

Au sein des liquides magmatiques, toutes les phases minérales majeures ont des $D_{Th}^{\text{minéral/liq}} << 1$ et $D_{Zr}^{\text{minéral/liq}} << 1$ (par ex. GEOROC database ; http://georoc.mpch-mainz.gwdg.de/georoc/). Seules des minéraux accessoires tels que le zircon, monazite, allanite etc. possèdent des $D_{Th}^{\text{minéral/liq}} > 1$ et $D_{Zr}^{\text{minéral/liq}} > 1$. Toutefois, il semble que dans les magmas peralcalins, la cristallisation de ces minéraux reste mineure (par ex. Watson 1979), de telle sorte que dans ces magmas les $D_{Th}^{\text{minéral/liq}}$ et $D_{Zr}^{\text{minéral/liq}}$ demeurent < 1, attestant ainsi du caractère très incompatible du Th et du Zr. Pour cette raison, les teneurs en ces éléments peuvent être utilisées comme de bons indicateurs du degré de différenciation des laves hôtes. La variation de concentration au sein des échantillons de Hrafntinnusker indique que les produits situés à la base du dépôt de téphra sont plus différenciés (riches en Th et Zr) que ceux situés au sommet (Figure III-2). En d'autres termes, les produits les plus différenciés ont été émis les premiers, suivis de magmas de moins en moins différenciés. Une telle configuration de mise en place, au cours d'une phase éruptive unique, implique que la chambre magmatique d'où sont issus les magmas était déjà préalablement finement stratifiée. Cette hypothèse est d'autant plus raisonnable que l'étude des magmas acides de Hrafntinnusker (Partie III-A-1) a montré que ceux-ci ont pour origine la fusion de la croûte basaltique hydrothermalement altérée suivie par de la cristallisation fractionnée (principalement de feldspaths alcalins). Il apparaît donc réaliste de considérer que cette cristallisation fractionnée tardive se soit produite dans un (ou plusieurs) réservoir(s) magmatique(s). Le caractère aphyrique des magmas acides de Hrafntinnusker suggère un mécanisme de « gas filter pressing » associé à cette cristallisation fractionnée tardive, permettant ainsi de parfaitement séparer les cristaux formés du liquide résiduel. Ce mécanisme peut ainsi engendrer une stratification compositionnelle fine au sein du réservoir hôte, avec un liquide plus différencié (plus riche en Th et Zr) et riche en gaz en sommet de chambre magmatique, et le liquide « originel » (moins différencié) et dégazé en base de réservoir. Au cours de la phase éruptive, le magma situé en sommet de réservoir sera le premier mis en place (Hsk1) et ceux de la base seront les derniers à s'épancher (Hsk8).

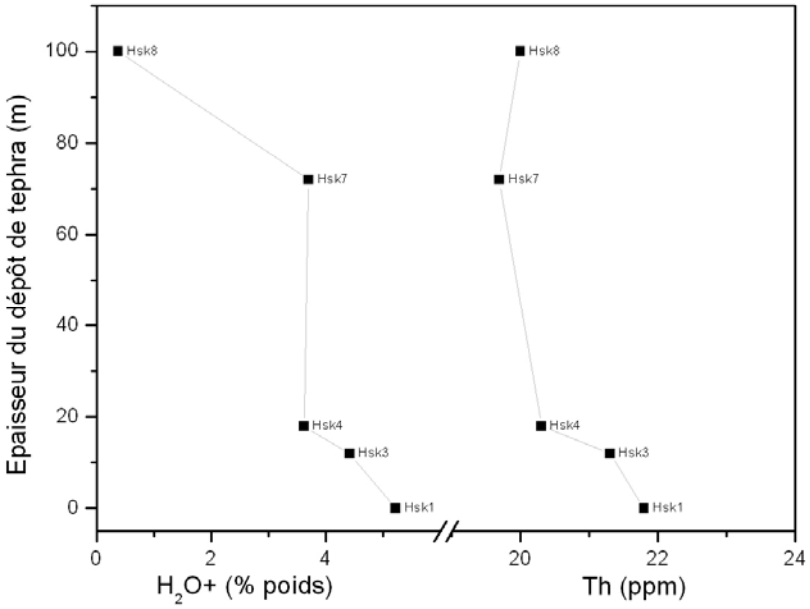

Figure III-2 : Teneur en eau et en Th des échantillons de Hrafntinnusker en fonction de leur position dans le dépôt de téphra.

Teneur en eau des ponces

Les ponces provenant de Hrafntinnusker présentent des fortes teneurs en eau allant de 3,6 à 5,2 % poids (H_2O+ ; Tableau III-1). Seule l'obsidienne sommitale (Hsk8) est quasi-anhydre (0,4 % poids H_2O+ ; Tableau III-1). Les observations réalisées aux microscopes optique et électronique à balayage (MEB ; Figure III-3) indiquent que les ponces ne présentent aucun signe d'altération ni ne contiennent aucun minéral hydraté (primaire ou secondaire). Ce qui tend à montrer que l'intégralité de cette eau (et autres éléments volatils) est contenue dans le verre constitutif des ponces.

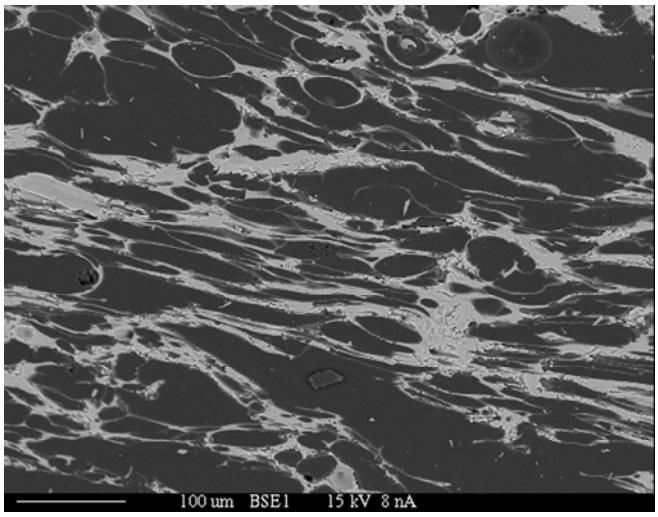

Hsk1

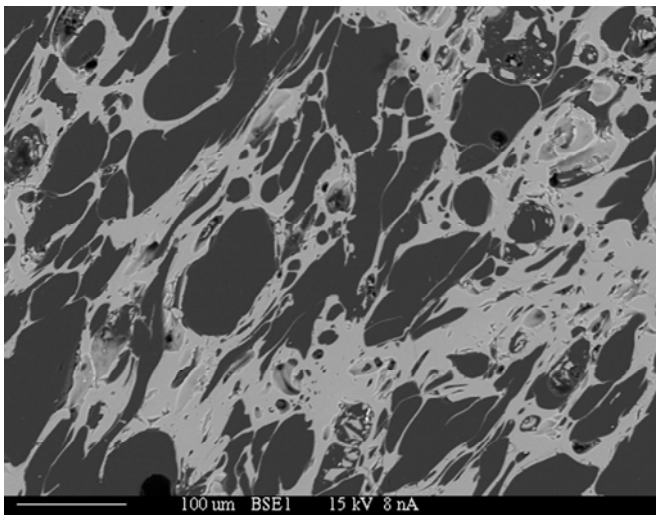

Hsk7

Figure III-3 : Photos prises au microscope électronique à balayage (MEB) montrant les structures (vésicularité) des échantillons Hsk1 et Hsk7. Hsk1 présente des vésicules très étirées avec des parois très fines alors que Hsk7 présente des vésicules plus sphériques avec des parois beaucoup plus larges.

Les analyses in situ (éléments majeurs) du verre des échantillons Hsk1 et Hsk7 ont été effectuées à la microsonde électronique (Tableau III-2). La somme des oxydes est de 96,4 % pour Hsk1 et de 97,3 % pour Hsk7. La différence entre la somme des oxydes analysés et 100 % fournit ainsi une indication sur la teneur maximale en eau (et autres éléments volatils) du verre. Au vu de ces résultats, il apparaît que le verre constitutif de la ponce Hsk1 est plus hydraté (et plus riche en éléments volatils) que celui de Hsk7. Cette observation est en parfait accord avec la tendance générale de la série qui indique que la teneur en eau (LOI) du verre décroît dans les échantillons depuis la base vers le haut du dépôt de tephra (Figure III-2).

	Hsk1		Hsk7	
	Moyenne (n=11)	± (2σ)	Moyenne (n=13)	± (2σ)
SiO_2	71,31	*0,57*	71,92	*0,37*
TiO_2	0,19	*0,01*	0,19	*0,01*
Al_2O_3	12,09	*0,14*	12,30	*0,09*
Fe_2O_3*	3,29	*0,10*	3,19	*0,09*
MnO	0,09	*0,04*	0,08	*0,02*
MgO	0,05	*0,01*	0,04	*0,01*
CaO	0,37	*0,01*	0,38	*0,01*
Na_2O	3,53	*0,25*	4,65	*0,39*
K_20	5,40	*0,15*	4,53	*0,14*
P_2O_5	0,02	*0,01*	0,02	*0,01*
total	96,4		97,3	

Tableau III-2 : Analyses faites à la microsonde électronique du verre des échantillons Hsk1 et Hsk7. Intensité : 8 nA ; tension d'accélération : 15 kV et diamètre du faisceau d'électron : 5 µm ; temps de comptage : 60 s.

Eau juvénile ou eau météorique ?

Les fortes teneurs en eau de ces ponces permettent de s'interroger sur son origine. En effet, il existe au moins deux manières de rendre compte de cette hydratation: 1) il s'agit d'une eau juvénile (magmatique) ou 2) d'une eau d'origine météorique.

Dans l'hypothèse d'une eau juvénile en équilibre avec son magma hôte, le $^{87}Sr/^{86}Sr$ de cette eau devra être sensiblement comparable à celui du magma (~0,7033 - 0,7034) alors que le $^{87}Sr/^{86}Sr$ de l'eau météorique sera bien plus élevé (0,7091 pour l'eau océanique). Une forte concentration en eau juvénile ne modifiera en rien le $^{87}Sr/^{86}Sr$ du magma. En revanche une hydratation du magma (pré-éruptive) ou de la roche (post-éruptive) par de l'eau météorique (pluie, neige ou directement par des embruns océaniques) engendrera une augmentation du $^{87}Sr/^{86}Sr$ du magma hôte ou de la roche hydratée. La Figure III-4 révèle que la teneur en eau des échantillons est corrélée avec le $^{87}Sr/^{86}Sr$ (à l'exception de l'échantillon Hsk3), observation qui va plutôt à l'encontre d'une eau d'origine magmatique (juvénile). En effet cette corrélation entre teneur en eau et $^{87}Sr/^{86}Sr$ est un argument fort en faveur de la contamination des ponces de Hrafntinnusker par une eau d'origine météorique.

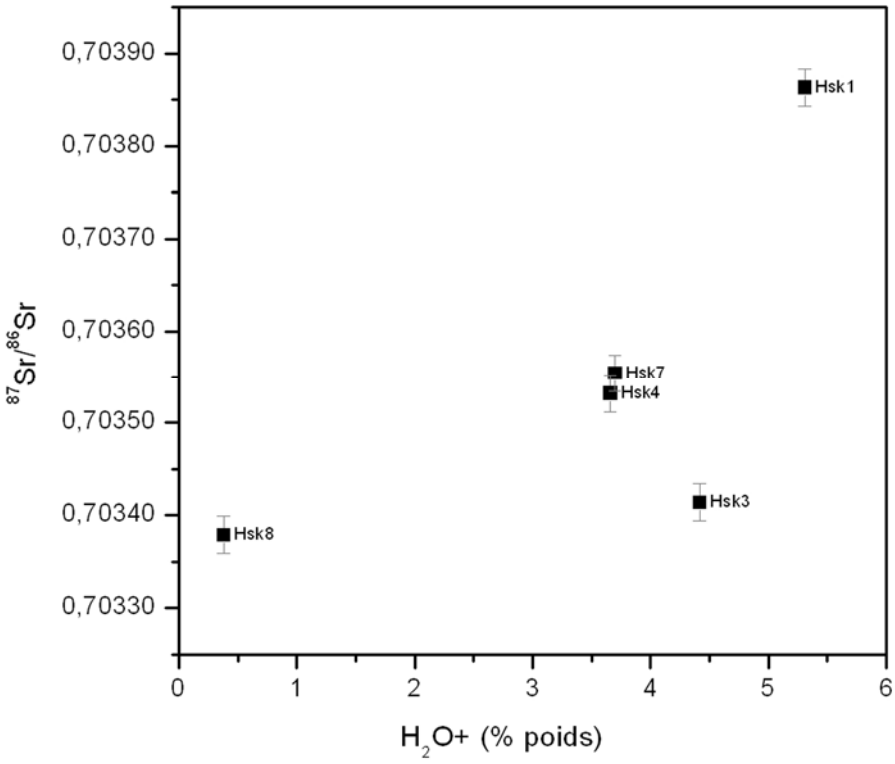

Figure III-4 : Diagramme montrant la corrélation entre le 87Sr/86Sr et l' H2O+ pour les échantillons de Hrafntinnusker.

Incorporation pré- ou post-éruptive de l'eau météorique

Si l'origine météorique de l'eau des ponces de Hrafntinnusker semble maintenant bien établie, il reste encore à déterminer si cette eau a été incorporée dans le système 1) avant la phase éruptive, c'est-à-dire au sein même de la chambre magmatique ou 2) après la phase éruptive par hydratation du verre constitutif de la ponce au sein même du dépôt de tephra.

Si l'on considère la première hypothèse, les fortes teneurs en eau des ponces résultent d'un processus de fragmentation (provoqué par l'exsolution des éléments volatils) incomplet qui se produit lors de la remontée du magma vers la surface. En effet, un magma rhyolitique ne peut contenir au grand maximum que 7,6 - 5,8 – 3,9 % poids d'eau à une pression de 3 - 2 - 1 kbar respectivement (Tamic et al., 2001). Le fait d'avoir jusqu'à 5,2 % poids d'eau dans les ponces implique qu'une grande quantité d'eau soit restée piégée dans le magma après le processus d'exsolution des éléments volatils, qui n'a donc pas pu se dérouler dans son intégralité. Cette déduction est cohérente avec le fait que les ponces de Hrafntinnusker possèdent une vésicularité très importante, qui atteste de la trempe du système en cours de fragmentation. En revanche l'obsidienne Hsk8 qui ne contient que 0,4 % poids d'eau, n'est absolument pas vésiculée, ce qui semble attester d'un dégazage complet du magma (tous les éléments volatils ont été intégralement extraits du liquide magmatique). Dans cette hypothèse,

l'ensemble des échantillons de Hrafntinnusker représenterait alors différents stades de dégazage du magma. Toutefois, la teneur maximale en eau de 5,2 % implique que la différenciation observée au sein des rhyolites de Hrafntinnusker ait eu lieu à une pression supérieure à 3 kbar (Tamic et al., 2001).

Dans le cas d'une hydratation pré-éruptive, il faut encore expliquer la manière dont l'eau météorique à pu s'intégrer au magma et ce au sein même du réservoir magmatique. Ce mécanisme a déjà été envisagé et proposé depuis longtemps par Shaw (1974) mais il reste un processus mal compris et très contesté par la communauté scientifique. En effet, comme cela a été discuté par Taylor & Sheppard (1986), il semble difficile, voire impossible, d'incorporer directement de l'eau de l'encaissant au cœur même du réservoir magmatique. La pression lithostatique étant plus importante dans le réservoir magmatique que dans les fractures de l'encaissant, tout transfert de fluide (par réseau de fractures) aura plutôt tendance à se faire du corps magmatique vers l'encaissant et non dans l'autre sens. L'eau pourrait éventuellement avoir été incorporée dans le magma par diffusion, mais les vitesses de diffusion sont très faibles et en conséquence, ce processus est trop lent pour avoir un impact significatif sur la composition de l'ensemble de la chambre magmatique. Un autre moyen d'intégrer de l'eau météorique dans le magma pourrait consister en une assimilation d'un encaissant hydraté. Toutefois, ce mécanisme nécessite un taux d'assimilation extrêmement important afin de pouvoir intégrer une quantité d'eau telle qu'après le processus de fragmentation (incomplet) il en reste encore jusqu'à 5,2 % poids. En conséquence, ce mécanisme d'hydratation au sein même de la chambre magmatique, ne semble pas être un processus simple et efficace.

Dans le cas d'une hydratation post-éruptive et étant donné qu'aucun minéral hydraté secondaire n'a été observé au sein des ponces de Hrafntinnusker, il convient impérativement de considérer un processus d'hydratation du verre. Poursuivant l'idée lancée par Friedman and Smith (1960), Anovitz et al., en se basant sur une approche expérimentale, ont travaillé sur une méthode de datation d'objets archéologiques en obsidienne ; l' « Obsidian hydration dating » (par ex. Anovitz et al., 1999; Riciputi et al., 2002; Anovitz et al., 2004). Le principe même de cette méthode repose sur la vitesse d'hydratation de l'obsidienne. Les données expérimentales montrent que dans un environnement où le taux d'humidité est de 100 %, la demi-vitesse d'hydratation de l'obsidienne peut atteindre 2,4 µm en 10 ka à une température de 4 – 5°C (Annovitz et al., 2006, communication personnelle). Il faut néanmoins noter que cette vitesse d'hydratation est extrêmement dépendante de la composition du verre et de la température. Dans le cas présent, ce qui nous intéresse est que sous les conditions climatiques

islandaises actuelles (4 - 5°C de moyenne annuelle), il est possible de saturer en eau des parois de verres de 4 - 6 µm d'épaisseur en 10 ka. Anovitz et al. (1999) ont également proposé que la saturation en eau des obsidiennes (qui ont fait l'objet de leur étude) pouvait atteindre jusqu'à 10 – 12 % poids, ce qui est plus du double de ce que l'on a mesuré dans les ponces de Hrafntinnusker.

La Figure III-3 illustre le fait que la ponce Hsk1 est plus vésiculée que Hsk7 et par conséquent que les parois de verre sont plus fines dans l'échantillon Hsk1 (~5 - 30 µm) que dans Hsk7 (~20 - 70 µm). Cette différence texturale entre ces échantillons peut simplement s'expliquer par le processus éruptif lui-même. En effet, au début de l'éruption, la pression de gaz et l'intensité éruptive sont les plus importantes, ce qui conduit naturellement à la formation des ponces les plus vésiculées (Hsk1). Au cours de cette phase éruptive, l'intensité du processus diminuant, les ponces formées seront de moins en moins vésiculées (jusqu'à Hsk7). Cette évolution texturale au sein du dépôt de Hrafntinnusker semble pouvoir expliquer le fait que pour un même temps d'exposition (~8 ka correspondant à l'âge estimé pour ces dépôts), le processus d'hydratation du verre sera plus important au sein des ponces les plus vésiculées c'est-à-dire celles ayant les parois de verre les plus fines. Il semble alors raisonnable de penser que plus on descend dans le dépôt de tephra et plus le processus d'hydratation post-éruptif sera conséquent.

L'obsidienne sommitale de Hrafntinnusker, qui ne présente aucune vésicularité n'est probablement affectée que de façon superficielle (les quelques premiers µm) par ce processus. L'échantillon (Hsk8) ayant été prélevé au cœur de la coulée n'est donc pas affecté par ce processus d'hydratation, conclusion qui est cohérente avec sa perte au feu mesurée qui n'est que de 0,4 % poids (H_2O+) et qui correspond probablement à l'eau juvénile. En conséquence, l'échantillon Hsk8 sera considéré comme représentatif de la série de Hrafntinnusker avant tout processus post-éruptif.

Interaction eau météorique - roche

Comme la teneur en eau des ponces est corrélée aux rapports $^{87}Sr/^{86}Sr$ mesurés, ces derniers seront utilisés afin de tenter de modéliser l'hydratation des ponces par de l'eau météorique en considérant un modèle de mélange. Hrafntinnusker se trouvant à environ 50 km de la côte Sud islandaise, il semble peu probable que l'eau de mer soit directement impliquée dans le processus d'hydratation du verre. Compte tenu de la géographie, il semble alors plus raisonnable de considérer une eau de pluie ou issue de la fonte de la neige.

Afin de modéliser le mélange (Équation 1) entre le verre des ponces et l'eau météorique, deux considérations ont été nécessaires. La neige prélevée sur le glacier Langjökull (Islande) contenant 2,32 ppm de Sr (Moune, 2006) est représentative de la neige islandaise actuelle et le $^{87}Sr/^{86}Sr$ initial des ponces de Hrafntinnusker est semblable à celui de Hsk8.

$$(^{87}Sr/^{86}Sr)_{mélange} = \frac{x.[Sr]_1.(^{87}Sr/^{86}Sr)_1 + (1-x).[Sr]_2.(^{87}Sr/^{86}Sr)_2}{x.[Sr]_1 + (1-x).[Sr]_2} \quad \textit{Équation 1}$$

$[Sr]_1$ et $[Sr]_2$: concentration en Sr des pôles 1 et 2 du mélange

$(^{87}Sr/^{86}Sr)_1$ et $(^{87}Sr/^{86}Sr)_2$: rapports isotopiques des pôles 1 et 2 du mélange

x : fraction du pôle 1

Approximation faite : l'abondance de ^{86}Sr est identique dans les deux pôles du mélange.

Deux approches ont été tentées : 1) la proportion eau/roche peut être estimée en considérant le $^{87}Sr/^{86}Sr$ et la teneur en Sr de la neige et 2) la teneur en Sr de l'eau peut être estimée en considérant celle en eau mesurée dans le verre.

Le Tableau III-3 indique les proportions eau/roche calculées pour chaque échantillon. Les ponces provenant de la base du dépôt de tephra ont interagit avec l'eau selon un rapport eau/roche d'environ 0,5, alors que celles situées au sommet ont interagit avec deux à trois fois moins d'eau (rapport eau/roche d'environ 0,15).

Echantillon	eau/roche
Hsk1	0,47
Hsk4	0,14
Hsk7	0,16
Hsk3	0,03

Tableau III-3: Rapport eau/roche permettant d'expliquer les 87Sr/86Sr mesurés dans chaque échantillon. Le 87Sr/86Sr initial des ponces = 0,70338, 87Sr/86Sr eau = 0,7091 ; teneur en Sr de l'eau (provenant de la neige)= 2,32 ppm (Moune, 2006).

Le Tableau III-4 donne la concentration en strontium calculée des eaux ayant possiblement interagit avec chaque échantillon. Pour cela il a été considéré que la quantité d'eau ayant réagi est égale à la perte au feu (H_2O+) de chaque échantillon.

Echantillon	Sr (ppm) calculé
Hsk1	20
Hsk4	9
Hsk7	10
Hsk3	1,5

Tableau III-4 : Concentration en Sr de l'eau ayant interagi avec les échantillons afin d'expliquer les 87Sr/86Sr mesurés en considérant que la proportion d'eau ayant interagit est égale à l'H2O+ mesuré dans chaque échantillon. Les 87Sr/86Sr considérés sont les mêmes que ceux présentés dans la légende du Tableau III-3.

En résumé, ces calculs amènent à envisager deux scénarii possibles : 1) l'eau météorique avait une composition constante et ce sont les rapports eau/roche qui ont varié, ceux-ci ayant pu être aussi importants que 0,5 ; 2) le rapport eau/roche a toujours été du même ordre de grandeur (de 0,03 à 0,06) et c'est la teneur en Sr de l'eau météorique qui a varié dans une vaste gamme de 1,5 à 20 ppm.

La dernière hypothèse semble la moins réaliste, en effet, il est très difficile d'imaginer la percolation d'eaux possédant des teneurs en Sr très différentes et ayant donc des origines différentes, et ce au sein d'un même dépôt de ponces. La première hypothèse quant à elle, est plus réaliste car elle envisage que l'eau a gardé une composition relativement constante et donc qu'elle avait une origine unique. Toutefois, cela implique qu'en base de dépôt le rapport eau/roche ait été très important (jusqu'à 0,5).

L'âge de la phase éruptive de Hrafntinnusker (8 ka) et la relativement faible répartition géographique des dépôts de ponces (Larsen, 2006, communication personnelle) permet de proposer un mode éruptif intermédiaire entre sous-glaciaire et purement aérien. En effet, cette période correspond à la déglaciation qui s'est produite à la fin du Pléistocène supérieur (10 ka), ce qui implique que l'éruption ne s'est vraisemblablement pas produite sous une couche de glace très importante. Une forte pression de glace (et/ou d'eau) permet d'inhiber le caractère explosif de l'éruption empêchant ainsi une grande dispersion des dépôts alors qu'une éruption purement aérienne engendre des dépôts de tephra peuvant être dispersés à des distances importantes du centre éruptif. En revanche, une fine couche de glace peut donner naissance à un mode éruptif intermédiaire, impliquant par là même une grande quantité d'eau d'origine météorique (neige ou glace fondue). Cette dernière étant intégrée au sein du dépôt de téphra, sera alors rapidement chauffée par les produits volcaniques comme cela a été décrit dans « la Vallée des 10 000 fumées » dans le parc national de Katmaï (Alaska ; par ex. Griggs, 1922) où en 1912 un épais dépôt de ponce (~200 m) a recouvert une vallée possédant un réseau hydrographique important (rivières, étangs, marais, neige). La température élevée du dépôt volcanique a permis de chauffer l'eau sous-jacente engendrant ainsi un réseau fumerolien qui est demeuré très actif pendant une dizaine d'années (par ex. Keith, 1991 et références incluses). Une augmentation de la température de l'eau piégée au sein du dépôt de Hrafntinnusker a pu permettre, par simple distillation, de concentrer le Sr, permettant ainsi de diminuer le rapport eau/roche nécessaire à l'explication des $^{87}Sr/^{86}Sr$ mesurés. De plus, l'élévation de température envisagée dans ce scénario permet également d'augmenter considérablement la vitesse du mécanisme d'hydratation du verre (par ex. Friedman and Smith, 1960; Anovitz et al., 2004). Dans ce cas, on peut considérer que la majeure partie de l'hydratation s'est déroulée dans un laps de temps assez court après la phase éruptive.

Se trouvant juste au dessus d'un niveau dans lequel circule actuellement de l'eau (Figure III-1), l'échantillon Hsk3 possède un $^{87}Sr/^{86}Sr$ bas compte tenu de son H_2O^+. En effet, sa teneur en eau (4,4 % poids) est cohérente avec l'ensemble des échantillons mais son $^{87}Sr/^{86}Sr$ est bien différent (0,70341, Figure III-4). La circulation d'eau actuelle à proximité de cet échantillon pourrait expliquer qu'il ait subi une histoire et une interaction eau/roche différentes de celles de l'ensemble des ponces du dépôt étudié, lui donnant ainsi un caractère unique.

Perte en Na_2O et U

La Figure III-5 montre que la teneur en eau est anti-corrélée avec celles en Na_2O et U. Comme cela a été proposé préalablement, le magma rhyolitique a résidé dans un réservoir magmatique dans lequel s'est produit une cristallisation fractionnée principalement de feldspath alcalin. Un tel processus est susceptible de diminuer efficacement la teneur en Na_2O du liquide résiduel. Afin d'expliquer la teneur de 3,04 % poids de Na_2O dans Hsk1 à partir de l'échantillon Hsk8, il faudrait imaginer 48 % de fractionnement d'albite pure. Un tel taux est 5 fois supérieur au taux de fractionnement estimé à partir des teneurs en Th (10 %). Considérant 10 % de fractionnement d'albite pure, la teneur en Na_2O de Hsk1 devrait donc être de l'ordre de 5.1 % poids. Il en découle qu'environ 2 % de Na_2O ont été perdus lors du processus d'hydratation. Il semble donc que le mécanisme d'hydratation ait été accompagné d'un processus de lessivage, grâce auquel les éléments les plus solubles en phase aqueuse tels que le sodium (par ex. Taylor and McLennan, 1985) ont été remobilisés. Cette perte de sodium permet de rendre compte de la diminution du caractère peralcalin des échantillons de Hsk en fonction de leur teneur en eau mais également en fonction de leur position au sein du dépôt de tephra. La perte de Na_2O est telle dans l'échantillon Hsk1 que ce dernier a une composition apparente sub-alcaline (Figure3 de la partie III-A-1).

Le même raisonnement peut être proposé afin d'expliquer les teneurs en U. En effet, le fractionnement de zircon permet de diminuer de façon considérable la teneur en U du liquide résiduel. Pour expliquer la teneur de 5,17 ppm d'U et un Th/U de 4,22 dans Hsk1 il faudrait imaginer plus de 0.5 % de zircon dans l'assemblage minéralogique fractionné (pour 10 % de fractionnement). Comme discuté et observé dans la partie précédente (partie III-A-1), la per-alcalinité des rhyolites de Hrafntinnusker ne milite pas en la faveur d'un fractionnement important de zircon. Il semble alors plus vraisemblable que la diminution des teneurs en U, qui est un élément très soluble en phase aqueuse (par ex. Taylor and McLennan, 1985) soit elle aussi et au moins pour partie due au processus de lessivage associé à celui d'hydratation.

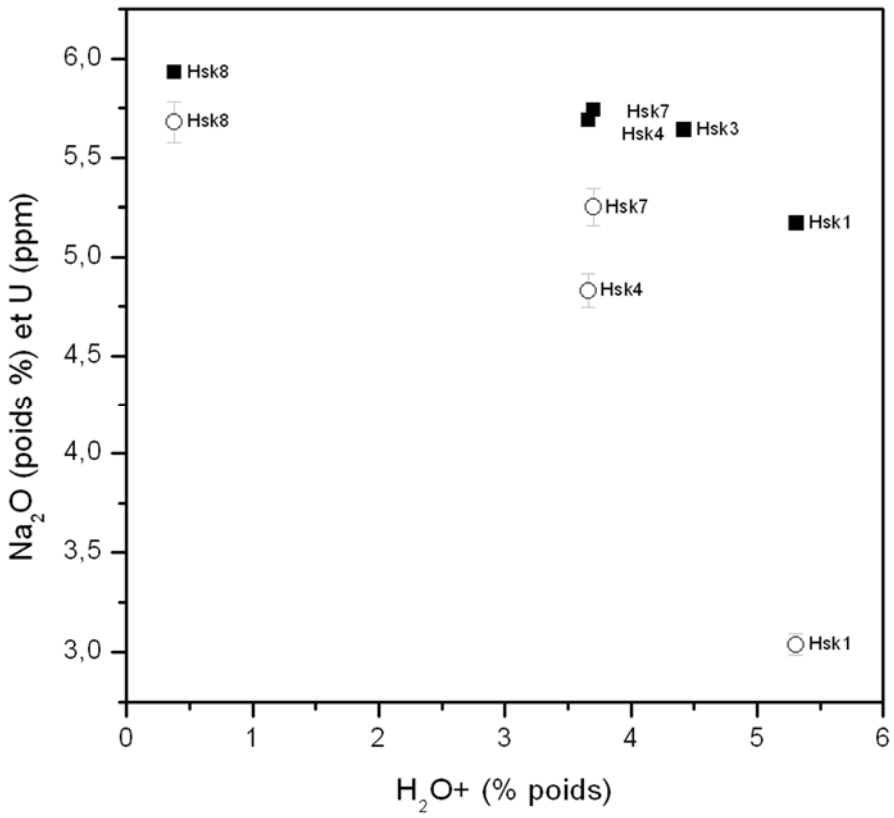

Figure III-5 : Diagramme montrant la baisse des teneurs en Na2O (ronds blancs) et U (carrés noirs) en fonction de celle en. H2O+ dans les échantillons de Hrafntinnusker.

En résumé, il apparaît que les dépôts de Hrafntinnusker proviennent de l'évolution d'une chambre magmatique finement stratifiée. Les laves situées dans la partie haute de la chambre (les plus différenciées) ont été émises les premières alors que la partie basse, la moins différenciée, a été mise en place seulement en fin de phase éruptive. Lors de cette phase éruptive, une certaine quantité de glace ou de neige fondue a été intégrée au sein du dépôt volcanique, permettant ainsi une hydratation du verre constitutif des ponces. Cette hydratation a été d'autant plus efficace que la température du dépôt était élevée et que les ponces étaient vésiculées. Ce mécanisme post-éruptif s'est aussi accompagné d'un lessivage des éléments les plus mobiles en phase aqueuse, tels que Na et U.

B. Variation temporelle de la genèse des roches acides d'Islande, Implications sur l'évolution géodynamique de l'Islande.

1. Article: "Silicic rock petrogenesis during the last 13 Ma, implications for the geodynamic evolution of Iceland", à soumettre.

Silicic rock petrogenesis during the last 13 Ma, implications for the geodynamic evolution of Iceland.

Martin, E.[1], Sigmarsson, O. [1,2]

1) Laboratoire Magmas et Volcans, OPGC - Université Blaise Pascal – CNRS, 5 rue Kessler, 63038 Clermont-Ferrand, France.

2) Institute of Earth Sciences, University of Iceland, 101 Reykjavik, Iceland.

E-mail: E.Martin@opgc.univ-bpclermont.fr

Keywords: silicic magma, petrogenesis mechanism, geodynamical context, rift jump, Iceland.

Abstract

In Iceland, the petrogenesis of silicic rocks is known to be closely linked to the thermal state of the crust, which in turn depends on the geodynamical environment. The dataset consists of felsic rocks from different volcanic systems whose ages range from 13 Ma until today. It allows addressing the problem of the temporal evolution of the mechanisms that generated silicic magmas and consequently, to trace and discuss the geodynamical evolution of Iceland through the last 13 Ma. Low Ba and Sr contents (~8.7 and ~1.2 ppm respectively) as well as Th > 9 ppm in silicic rocks appear as good tracer of fractional crystallisation process. On the other hand, low $\delta^{18}O$ (less than 5 ‰) in extrusive silicic rocks points to the role played by partial melting of the hydrated metabasaltic crust in their genesis. By contrast with $^{87}Sr/^{86}Sr$, the $^{143}Nd/^{144}Nd$ appears as an excellent marker of the source of the silicic magma. The highest $^{143}Nd/^{144}Nd$ (0.51303 to 0.51296) characterize a "rift zone" source-type, where felsic magmas are generated by partial melting of the basaltic Icelandic crust. The lowest $^{143}Nd/^{144}Nd$ (0.51290 to 0.51297) are typical of "off-rift" source-type, where magmas differentiated by fractional crystallisation of a basaltic magma far from the rift zone.

The spatio-temporal distribution of "rift zone" source-type samples allows reconstructing the position of the rift zone in course of time. For instance, in Snæfellsnes Peninsula, felsic magmas younger than 5.5 Ma have an "off-rift" signature and by contrast, samples older than 6.8 Ma, have typical "rift zone" geochemical characteristics. This evidences that before 6.8 Ma, silicic rocks were generated by crustal melting in a rift-zone and that after 5.5 Ma, they were produced by fractional crystallisation of basaltic magma in low geothermal gradient zone, far from the contemporaneous rift zone. This is interpreted in terms of the eastward rift jump, from Snæfellsnes towards the present Reykjanes rift zone between 7 and 5.5 Ma.

Introduction

In Iceland, the petrogenesis of recent silicic magmas is relatively well constrained and understood. Martin and Sigmarsson (2006) considered that the role played by each mechanism is closely linked to the geodynamical environment. Today, near the Iceland centre, the interaction between the rift zone and the plume centre gives rise to high

geothermal gradient, high enough to induce partial melting of the hydrated metabasaltic crust and thus to generate silicic magmas. On the other hand, far from the rift zone, the geothermal gradient is too low thus precluding much basalt crustal melting. In these conditions, fractional crystallisation is more efficient giving rise to off-rift silicic magmas. In other words, it seems that the knowledge of the petrogenesis of silicic lavas can provide reliable information about the geodynamical environment of its genesis and its position relative to the ridge system.

During the last 16 Ma, large amounts of silicic magmas erupted in Iceland (e.g. Walker, 1963). Until today, only single edifices were studied that were not integrated in a general spatio-temporal view of Iceland felsic magmatism. In this paper, we propose to extrapolate to older lavas our petrogenetic knowledge on young silicic magmas, in order to establish their spatio-temporal evolution. Our data set consists of silicic rocks located throughout the whole island and erupted from 13 Ma ago until today. The aim of this paper is to evaluate the petrogenesis processes of silicic magma and constrain the geodynamic evolution of Iceland during the last 13 Ma.

Geological setting and sample location

Iceland corresponds to an emerged segment of the mid-Atlantic ridge. This rift zone crosses the whole island from southwest, (RRZ = Reykjanes rift zone), to the North, (NIRZ = North Iceland rift zone) via a transform fault system called the mid-Iceland volcanic zone (MIVZ; Figure 1). Three active volcanic zones in off-rift context also exist and consist of the Snæfellsnes volcanic zone (SVZ) in western Iceland, the South Iceland volcanic zone (SIVZ), which is considered as the propagation of NIRZ) in South Central Iceland, and the Öræfi volcanic belt (OVB) in South East Iceland. Along these active zones, about 30 volcanic systems, mainly composed of a central volcano and its associated fissure swarm, have been recognized (Sæmundsson 1979). Silicic rocks are restricted to central volcanoes in contrast to basaltic magmas that erupted throughout the whole volcanic system. Many extinct volcanic systems were also recognized in Tertiary formations mainly in north western (Vestfirðir Peninsula) and Eastern Iceland (e.g. Sæmundsson 1979; Walker 1963).

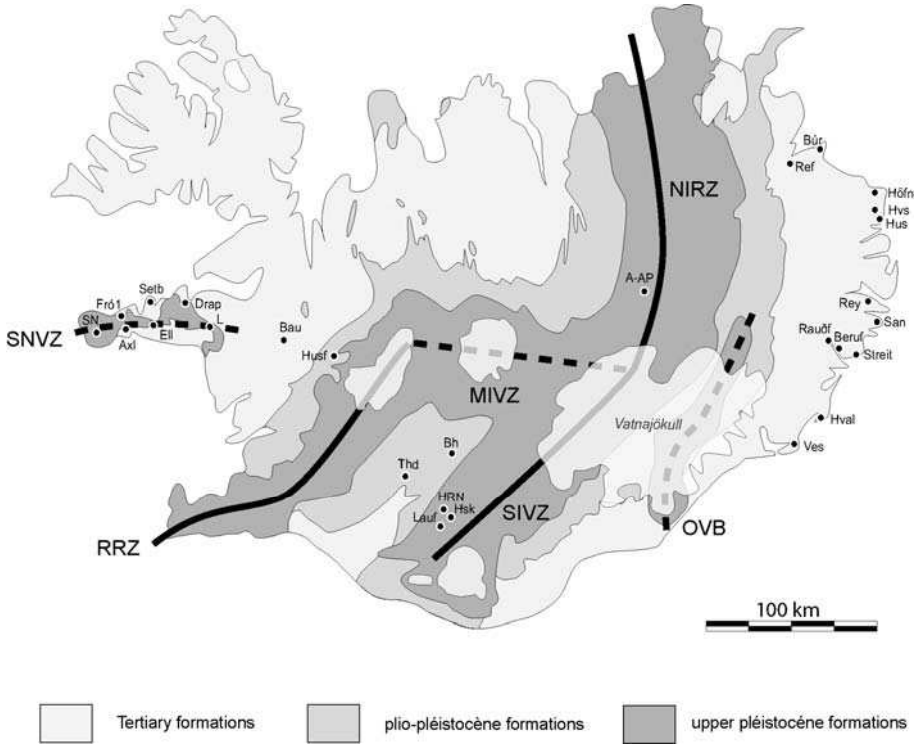

Figure 1: Map of Iceland showing sample locations. The Neovolcanic zones are the Snæfellsnes volcanic zone (SNVZ), Reykjanes rift zone (RRZ), Mid-Iceland volcanic zone (MIVZ), North-Iceland rift zone (NIRZ), South-Iceland volcanic zone (SIVZ) and the Öræfi volcanic belt (OVB). White areas correspond to the main glaciers.

The age repartition of volcanic formations through Iceland is due to the geodynamical evolution. Since several years, many authors, (e.g. Hardarson et al. 1997; Jóhannesson 1980; Sæmundsson 1979; Vink 1984)) demonstrated that, in Iceland the rift zone moves westward, relatively to the mantle plume centre, which is actually assumed to be located beneath the north-western part of Vatnajökull icecap (e.g. Eysteinsson and Gunnarsson 1995; Wolfe et al. 1997). They suggested that between 26 - 15 Ma ago, the rift zone was situated in the oldest tertiary formation, today located in NW Iceland. Around 15 Ma ago, the rift zone jumped to the East in a place close to the Snæfellsnes volcanic zone (SVZ) where it remained until around 7 Ma ago. At this time, the Holocene rift zone (RRZ – NIRZ) was formed by a new eastward rift jump. Finally, since 3 Ma the SIVZ is propagating southward the NIRZ, thus initiating a new rift zone that progressively replaces the RRZ (e.g. Hardarson et al. 1997; Jóhannesson 1980; Sæmundsson 1979).

Sample description

The dataset consists of felsic and mafic rocks sampled from different location in Iceland and (Figure 1) including volcanic system ages ranging from 13 Ma to present day (Table 1). Silicic and basic samples can be divided into intrusive and extrusive rocks (Table 1). Intrusive refers to millimetre- to centimetre-grained rocks having undergone a relatively slow cooling, long enough to allow the complete crystallisation of the magma. On the other hand, extrusive rocks contain few phenocrysts in a fine-grained groundmass if not completely quenched.

Intrusive silicic rocks mainly display granophyric texture and they consist of plagioclase + alkali-feldspar + quartz +clinopyroxene + Fe-Ti oxides assemblage together with subordinate amounts of accessory phases (zircon, monazite and apatite). In some samples, minor amounts of amphibole, biotite, chlorite and epidote can also be observed. The extrusive samples consist of obsidian, pumices or very fine-grained, which contain highly variable amounts of glass patches and phenocrysts. Their modal composition is the same as for intrusive rocks except quartz, epidote and chorite that are poorly expressed.

The intrusive basic samples consist of gabbros and are overwhelmingly composed of plagioclase + clinopyroxene + amphibole + Fe-Ti oxides ± interstitial alkali feldspar and quartz and accessory phases as zircon and apatite. As in intrusive silicic rocks, minor amount of chlorite and epidote can also be observed in some samples. Finally, extrusive basic rocks are mainly represented by basaltic lava flows or more rarely, as enclaves in silicic dykes or intrusions. They are made up of few phenocrysts of plagioclase and clinopyroxene into a groundmass composed of plagioclase, clinopyroxene and olivine together with Fe-Ti oxides and interstitial glass.

Minor amount of chlorite and epidote, referred as alteration minerals in Table 1, are quite common in intrusive rocks whereas these minerals are rare in extrusive ones. This is interpreted as the consequence of an efficient hydrothermalism activity during the cooling of the intrusive magmas. Optical microscopic observation of thin sections indicates that there is no correlation between loss on ignition (LOI) and the amount of alteration minerals. In addition, the major and trace element composition of high-LOI samples do not significantly differ from that of the other samples. These are the reasons why these samples, as Hval1a and Hval1b from Austurhorn, which contained the highest alteration minerals content, were nevertheless used in this study, nevertheless, they were taken with high precaution especially isotopic measurement interpretations.

Table 1: Volcanic system, ages, type of emplacement condition and rock types of samples from this study (see Figure 1).

Sample name	Age in Ma (Ref)	Volcanic System	Zone	Rock type	Proportion of Alteration minerals	Emplacement condition
SN-	~0.002 (1)	Snæfellsjökull	Snæfellsnes volcanic zone	pumices	-	Extrusive
L-	0.450 - 0.150 (2)	Ljósufjöll		domes and lava flows	-	Extrusive
Fró1	5.0 (3)	Fróðárheiði		granophyre	-	Intrusive
Ell1		Ellliði		granophyre	+	Intrusive
Axl1	4.7 (3)	Axlarhyrna		granophyre	+	Intrusive
Setb3	5.3 (3)	Setberg		dyke	+	Extrusive
Drap2	6.8 (3)	Drápuhlíðarfjall		lava flow	-	Extrusive
Husf-		Húsafell	West of Reykjanes rift zone	dyke and lava flow	-	Extrusive
Bau1	3.6 (3)	Baula		dome	-	Extrusive
Thd1	1.5 (3)	Thjórsárdalur	Between Reykjanes rift zone and south Iceland volcanic zone	obsidian	-	Extrusive
Bh1a	2.2 (3)	Búðarháls		dome	-	Extrusive
Hsk-	< 0.01(4)	Torfajökull	South Iceland volcanic zone	pumice and obsidian	-	Extrusive
Lauf and HRN-21					-	Extrusive
A2 and AP3	< 0.01(5)	Askja	North Iceland rift zone	dike and pumice	-	Extrusive
Gei-		Geitafell	Eastern Iceland	basaltic lava flow and	n.d.	Extrusive
Ves-	3.8 (6)	Vesturhorn		gabbro and granophyre	+	Intrusive
Hval-	6.5 – 7 (6)	Austurhorn		gabbro and granophyre	++	Intrusive
Rauðf1 and Beruf1	9.3 (6)	Breiðdalur		lava flow and dyke	-	Extrusive
Streit-	10.7 (6)	Álftafjörður		silicic dyke with mafic	-	Extrusive
San1, Rey3		Reyðarfjörður		domes	-	Extrusive
Hus1, Hvs1 and Höfn1	12.5 - 13.1 (6)	Borgarfjörður		Ignimbrites and dykes	-	Extrusive
Bur4		Fagridalur		lava flow	-	Extrusive
Ref1	13.1 (6)	Refsstaðir		dome	n.d.	Extrusive

Estimation of the proportion of alteration minerals: (-) less than 1%; (+) 1-5%; (++) 5-10% and (n.d.) not determined. (1)(Steinthorsson 1967); (2) (Guðmundsdóttir and Sigmarsson 2006); (3) Bosse and collaborators (2006; personal communication); (4) (Macdonald, et al. 1990); (5) (Sigvaldason 2002) (6) Paquette and collaborators (2006; personal communication).

Analytical techniques

Major and trace element compositions were both measured in "Laboratoire Magmas et Volcans" of (Clermont-Ferrand, France) and in ACME laboratories (Vancouver, Canada) using purified lithium tetraborate fusion of rock powder. The Th and U concentrations were measured by isotopic dilution method on a CAMECA TSN 206 mass spectrometer using a mixed 235U-230Th spike (Condomines et al., 1982). Analytical error is estimated at 0.5% (2σ) for Th and U concentrations. The Sr and Nd isotopes ratio were measured on Thermo-Finnigan TRITON mass spectrometer and normalized to 86Sr/88Sr = 0.1194 and 146Nd/144Nd= 0.7219. During this study, the $^{87}Sr/^{86}Sr$ of NBS-987 was equal to 0.710258 ±6 (2σ; n= 8) and $^{143}Nd/^{144}Nd$ of the AMES standard equal to 0.511960 ±4 (2σ; n=9). External error is about 2.10^{-5} (2σ) for both Sr and Nd isotopic ratios. For oxygen isotope measurements, 5-10 mg of whole rocks powder were reacted overnight with BrF_5 at 680°C in Ni reaction vessels (Clayton and Mayeda 1963). After conversion to CO_2 gas, the O isotope ratios were analyzed on a VG SIRA 10 dual inlet instrument at "Géosciences Rennes" and normalized to NBS-28 = 9.6‰ (the mean value of the NBS 28 found during the experiments was 9.36‰). Total analytical uncertainties on $\delta^{18}O$ are estimated at 0.15 ‰ based on duplicate analysis.

Results

Major and trace elements

Major and trace element compositions of silicic and associated basic samples are listed in Table 2 together with Sr, Nd and O isotopic ratios. In silicic samples SiO_2 ranges from 70 to 77 wt.% for rhyolites and 65 to 68 wt.% for trachytes and dacites (Figure 2). Rhyolites range from peralkaline (Hsk and L samples; Martin and Sigmarsson 2006) to sub alkaline (tholeiitic) compositions (Figure 2). All other samples have basaltic (SiO_2 = 44.5 - 50 wt.%) and intermediate (SiO_2 = 51.7 - 55 wt.%) composition (Figure 2). When compared with basic rocks, felsic samples are alkalis (Na_2O, K_2O)-richer whereas they are depleted in all other major elements.

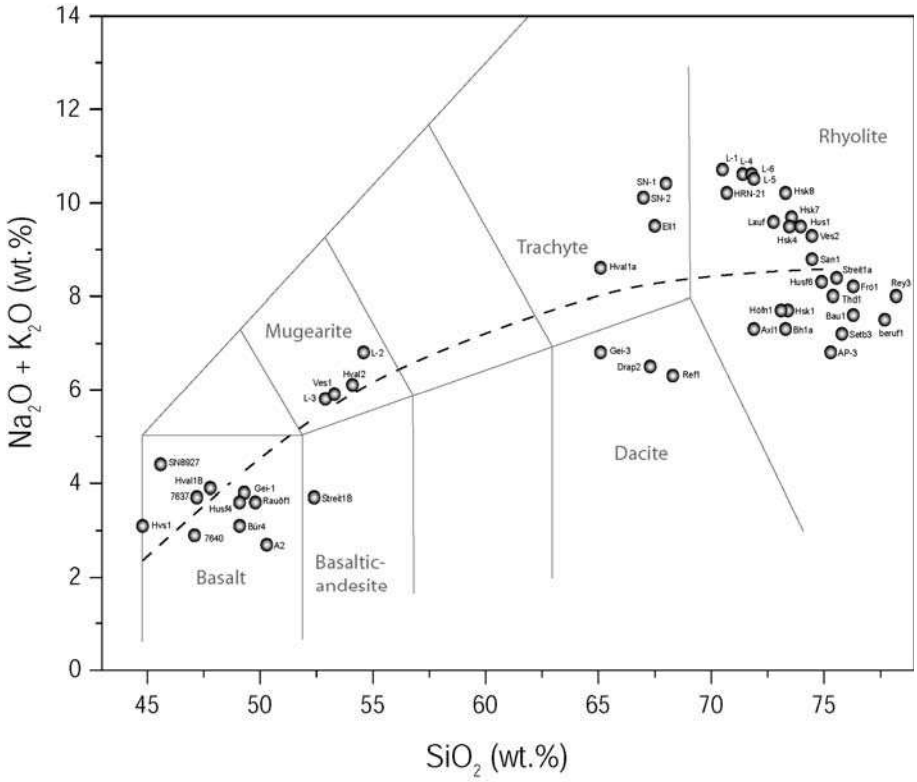

Figure 2: Total alkali vs. SiO2 diagram from Le Bas et al. (1986). The limit between alkalic and sub-alkalic field (dashed line) is that proposed by Miyashiro (1978). Silicic compositions range from trachytes to peralkaline rhyolites and from dacites to sub-alkaline (tholeiitic) rhyolites. Basic samples range from basalts to mugearite and basaltic andesite.

In a primitive mantle normalized multi-element diagram (Figure 3), basalts display patterns with a progressive enrichment in incompatible elements, except for Rb and Ba. When compared with basalts, dacites and trachytes are richer in all elements and do not show any Rb and Ba depletion. In addition, they display a slight negative anomaly in both Sr and Eu. Rhyolite compositions overlap the dacite and trachyte field even if some are Rb-, Nb- and LREE-richer. By contrast, all rhyolites have strong Ba, Sr and Eu anomalies.

Strongly incompatible elements, such as Th are perfectly correlated with the degree of differentiation. For instance, Th contents evolves from 7.34 to 26.3 ppm in rhyolites to 8.20 to 12.3 ppm in trachytes to 5.61 to 8.16 ppm in dacites to 2.35 to 6.16 ppm in intermediate rocks and finally to less than 2.69 in basalts (Table 2). Consequently, Th content is considered as an excellent marker of the degree of magmatic differentiation. The Th/U shows a wider variation range in silicic (2.94 to 4.63) than in basic (2.83 to 3.61) samples. It must be noted that, the highest Th/U from this study was measured in the sample Hval1a, which contain 5 – 10 % of

alteration minerals. Therefore, it is clear that this sample was affected by alteration processes that could result in an uranium loss.

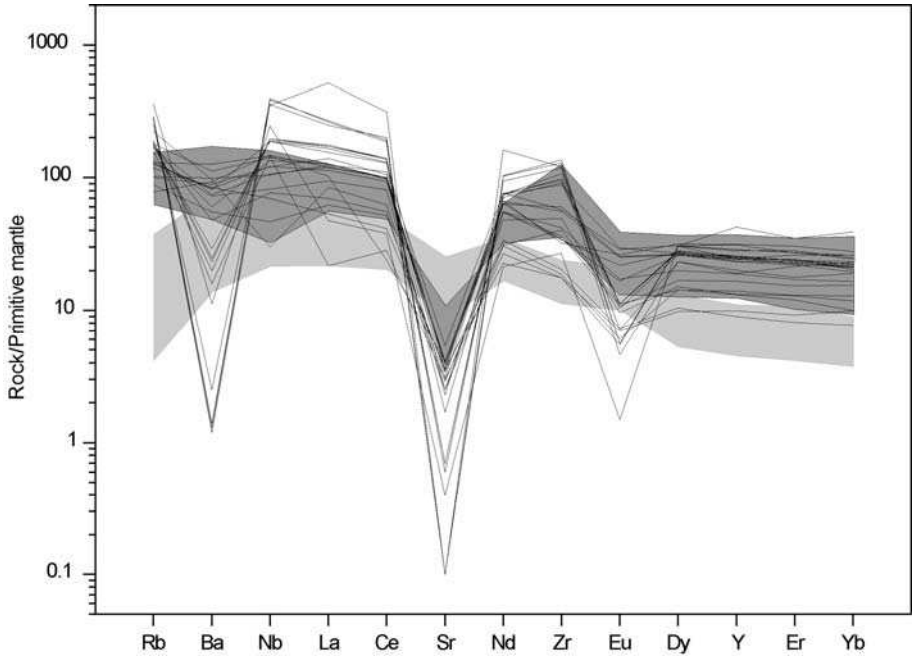

Figure 3: Primitive mantle normalized (Sun and McDonough 1989) multi-element diagram for silicic samples. The light and dark grey areas show the variation range for mafic (basaltic + mugearite + basaltic andesite) and dacitic + trachytic samples respectively. Compared to basaltic lavas, silicic samples are richer in all elements except for Ba, Sr and Eu that show strong negative anomalies.

Table 2 : Concentrations of Major and trace elements in weight % and ppm, respectively and Nd, Sr and O isotope compositions in samples of this study.

	SN-1	SN-2	Fró1	Axl1	Ell1	Setb3	Drap2	L1	L4	L5	L6	Bau1	Husf6	Thd1	Bh1a
SiO_2	65.6	64.9	75.8	69.0	67.0	74.5	65.6	70.0	71.6	71.3	71.5	75.2	74.2	70.1	71.0
TiO_2	0.31	0.38	0.20	0.31	0.62	0.26	0.55	0.25	0.22	0.21	0.21	0.10	0.17	0.16	0.21
Al_2O_3	14.9	15.1	12.7	12.2	14.5	12.5	12	13.6	13.1	12.7	12.8	12.8	12.7	11.8	13.8
Fe_2O_3	3.95	4.51	1.83	4.62	4.96	2.84	8.74	4.20	4.00	3.87	3.88	1.74	2.79	2.38	3.41
MnO	0.15	0.17	0.00	0.15	0.16	0.08	0.28	0.16	0.14	0.13	0.13	0.04	0.09	0.07	0.09
MgO	0.16	0.27	0.10	0.30	0.54	0.04	0.14	0.02	0.03	0.03	0.03	0.15	0.09	0.04	0.16
CaO	1.31	1.61	0.53	2.24	1.92	0.92	3.35	0.45	0.49	0.43	0.43	1.01	0.70	1.01	1.18
Na_2O	5.59	5.59	3.64	3.45	5.09	4.93	4.53	5.72	5.90	5.86	5.96	4.46	4.65	5.26	3.79
K_20	4.40	4.20	4.50	3.59	4.37	2.16	1.80	4.86	4.74	4.58	4.60	3.00	3.61	2.15	3.29
P_2O_5	0.06	0.08	0.03	0.04	0.11	0.03	0.09	0.05	0.02	0.02	0.02	0.02	0.03	0.02	0.03
H_2O-	0.38	0.3	0.4	0.6	0.1	0.0	0.5	0.1	0.1	0.1	0.2	0.2	0.2	1.7	1.0
H_2O+	2.72	2.1	0.8	3.7	0.9	0.7	0.9	0.2	0.0	0.2	0.2	0.4	0.7	4.8	2.2
total	99.5	99.1	100.6	100.2	100.3	99.0	98.9	99.6	100.2	99.4	100.0	99.1	99.9	99.6	100.1
Rb	98.7	91.3	114.5	81.4	101.2	49.4	38.4	*161.7*	*178.8*	*184.9*	*184.2*	75.2	81.4	107.8	63.6
Sr	83.3	118.5	36.1	95.4	148.9	87.3	176.5	*1.79*	*1.17*	*1.60*	*1.31*	76.2	83.6	73.7	66.0
Y	61.0	58.6	75.7	84.7	73.9	116.9	170.9	91.3	86.7	141.9	111.3	44.9	85.9	114.8	105.6
Zr	646.9	666.8	405.6	643.1	738.6	673.4	1433	1350	1320	1446	1524	197.6	468.4	381.6	621.0
Nb	117.6	113.9	100.7	92.9	138.3	105.4	81.0	251.1	253.6	274.8	281.7	49.8	86.4	76.1	85.6
Ba	1214	1216	779.1	839.5	964.3	650.0	418.8	17.7	8.7	9.5	9.3	589.9	580.2	519.9	622.5
La	87.5	85.0	86.7	80.5	71.4	81.8	64.4	353.4	170.4	184.8	180.4	36.6	77.8	82.4	96.1
Ce	177.5	172.6	176.6	169.6	149.6	177.6	149.7	552.8	355.8	340.4	329.5	73.5	166.1	177.8	186.3
Pr	19.4	19.0	20.4	19.9	16.4	21.7	20.0	68.4	37.0	39.5	40.0	8.05	19.7	20.6	21.9
Nd	69.3	68.1	74.9	75.5	64.8	85.4	87.6	219.1	127.7	138.8	140.1	30.7	74.8	86.3	90.0
Sm	13.0	12.7	14.5	15.3	12.6	18.87	22.4	34.3	22.9	26.9	27.1	6.84	15.6	18.3	18.4
Eu	2.51	2.75	1.82	3.19	2.68	4.29	6.68	1.18	0.77	0.95	0.95	1.17	2.88	3.67	4.24
Gd	11.2	10.9	11.9	13.5	10.9	18.1	24.1	20.9	15.9	19.7	19.6	6.32	13.5	17.1	15.6
Tb	1.75	1.71	2.00	2.31	1.96	3.07	4.23	3.10	2.73	3.63	3.64	1.14	2.35	3.04	2.85
Dy	10.9	10.7	12.4	14.5	12.3	19.5	27.6	17.1	17.2	22.6	22.5	7.20	14.7	20.0	19.3
Ho	2.30	2.24	2.59	3.04	2.71	4.09	5.98	3.16	3.66	4.75	4.63	1.63	2.99	4.27	4.14
Er	6.37	6.27	7.3	8.5	7.6	11.4	17.0	8.52	10.3	13.0	12.6	4.43	8.2	11.3	10.6
Tm	0.95	0.95	1.07	1.25	1.17	1.69	2.52	1.28	1.57	1.88	1.84	0.65	1.25	1.62	1.45
Yb	6.79	6.55	7.59	8.77	8.22	11.4	17.8	9.38	11.3	12.8	12.8	4.87	8.15	10.60	9.59
Lu	1.09	1.04	1.18	1.38	1.21	1.76	2.96	1.49	1.81	1.99	2.00	0.72	1.18	1.51	1.41
Hf	15.3	15.5	11.6	16.6	17.4	17.3	32.3	29.1	31.8	32.4	34.5	6.17	12.5	13.8	18.3
Ta	8.64	8.29	7.98	7.52	11.2	7.92	6.19	17.6	18.7	19.4	20.6	5.14	7.95	6.80	8.04
Pb	7.16	6.86	5.27	4.17	6.11	1.13	4.86	9.87	4.42	7.83	9.40	8.76	5.48	7.44	7.57
Th	*12.3*	*11.5*	*14.9*	*10.6*	*11.9*	*9.11*	*5.61*	*23.7*	*24.9*	*24.9*	*26.3*	*9.44*	*13.1*	*12.4*	*12.2*
U	*3.5*	*3.29*	*4.46*	*3.16*	*4.04*	*2.75*	*1.8*	*5.39*	*7.06*	*6.6*	*6.84*	*2.09*	*3.72*	*3.50*	*3.32*
Th/U	3.51	3.50	3.34	3.34	2.94	3.31	3.12	4.40	3.53	3.77	3.85	4.52	3.53	3.53	3.66
$^{87}Sr/^{86}Sr$	0.70338	0.70337	0.70414	0.70358	0.70342	0.70345	0.70320	0.70473	0.70435	0.70442	0.70463	0.70349	0.70355	0.70312	0.70338
$^{143}Nd/^{144}Nd$	0.51297	0.51296	0.51290	0.51290	0.51292	0.51295	0.51301	0.51291	0.51293	0.51292	0.51292	0.51300	0.51299	0.51302	0.51298
$\delta^{18}O$	5.1	4.9	1.0		0.9	0.1		6.3	6.2		5.8	4.8	5.1		
Age (Ma)	~0.002	~0.002	5.0	4.7	*4.8*	5.3	6.8	0.385	0.166	0.235	0.23	3.6		1.5	2.2
$[^{87}Sr/^{86}Sr]_i$	0.70338	0.70337	0.70350	0.70341	0.70329	0.70333	0.70314	0.70330	0.70331	0.70330	0.70330	0.70335		0.70303	0.70329

Underlined values indicate data obtained by isotope dilution mass spectrometry. The $(^{87}Sr/^{86}Sr)_0$ are calculated assuming $\lambda^{87}Rb = 1.42\times10^{-11}$ y^{-1}. Estimated ages are in italic.

(1) Sigmarsson et al. (1992b); (2) Carpentier (2003); (3) Hemond et al. (1993).

Table 2 (continued) :

	HRN-21	Lauf	Hsk8	Hsk7	Hsk4	Hsk3	Hsk1	AP-3	Gei-3	Ves2	Hval1a	beruf1	Streit1a	San1	Rev3	Hus1	Höfn1	Ref1
SiO_2	70.2	72.1	72.6	71.4	70.9		68.5	71.8	65.1	73.98	64.77	77.12	74.44	73.45	76.85	73.46	71.52	65.7
TiO_2	0.28	0.34	0.19	0.20	0.20		0.22	0.31	1.3	0.21	0.9	0.15	0.13	0.11	0.05	0.18	0.26	0.5
Al_2O_3	14.5	13.3	12.3	11.9	12.1		12.9	11.7	14.0	13.31	15	11.13	12.35	13.74	12.25	13.74	13.06	13.8
Fe_2O_3*	2.80	2.95	3.36	3.41	3.49		3.75	2.89	6.3	1.71	5.8	2.52	2.13	1.93	0.66	1.67	3.71	6.0
MnO	0.08	0.11	0.07	0.08	0.07		0.07	0.09	0.1	0.06	0.1	0.06	0.03	0.01	0.01	0.02	0.13	0.2
MgO	0.27	0.06	0.07	0.09	0.08		0.23	0.40	1.8	0.22	1.17	0.07	0.21	0.21	0.21	0.07	0.11	0.4
CaO	0.98	0.72	0.40	0.44	0.42		0.47	1.57	4.2	0.54	2.93	0.73	0.88	0.51	0.3	0.71	1.48	3.4
Na_2O	5.63	5.83	5.63	5.08	4.66		2.83	3.95	4.0	4.21	5.33	3.85	3.87	4.76	2.66	3.89	4.22	4.1
K_20	4.52	3.66	4.44	4.29	4.51		4.31	2.50	2.9	4.98	3.18	3.62	4.4	3.91	5.22	5.55	3.28	2.0
P_2O_5	0.10	0.03	0.02	0.03	0.03		0.03	0.11	0.3	0.03	0.26	0.02	0.02	0.01	0.01	0.02	0.03	0.1
H_2O-	0.2	0.1	0.2	0.3	0.4	0.9	0.9	0.2	0.1									
H_2O+	1.0	0.4	0.4	3.7	3.6	4.4	5.2	4.4	0.5	0.7	0.3	*0.6*	*1.5*	*1.2*	*1.7*	*0.6*	*2.0*	3.7
total	100.5	99.6	99.6	101.0	100.4		99.4	99.9	100.6	100	99.7	99.9	100.0	99.8	99.9	99.9	99.8	99.8
Rb	105.8	80.9	119.8	110.4	114.0		102.2	56.1	67.0	114.9	62	85.9	120.9	82.4	228.6	142.4	64.7	42.0
Sr	53.5	76.3	12.2	14.1	13.8		14.5	72.4	218.7	52.5	197.7	47.5	63.3	85.8	8.7	61.2	112.9	225.4
Y	60.2	107.3	116.9	111.4	115.9		112.2	63.8	56.5	59.8	71.1	110.2	128.3	143.3	193.6	40.9	130.1	91.9
Zr	551.0	989.2	1067.0	1026.3	1093.3		1189.3	449.2	408.7	210.2	937.4	386.1	197.2	359.7	300.8	229.8	641.3	692.5
Nb	95.7	133.4	140.3	133.5	140.2		135.6	33.2	23.5	54.7	45.1	58.2	103	103.8	175.1	21.4	74.6	46.2
Ba	421.4	573.2	172.4	203.2	163.8		139.5	385.6	337.6	335.5	619.2	508.5	111	884	79	674.6	690.6	363.7
La	87.1	106.1	120.6	113.9	118.1		118.4	42.7	38.7	47.8	58.8	64.8	14.9	70.2	32.6	58	85.3	57.0
Ce	174.4	228.8	246.8	232.0	242.4		247.5	91.6	87.6	98.9	129.7	143.4	50.2	42.6	67.2	110.5	196.2	125.6
Pr	18.4	25.8	28.1	26.3	27.7		27.6	10.7	10.8	11.43	15.88	17.81	7.55	21.54	8.77	12.51	24.95	16.1
Nd	64.8	100.9	102.0	96.2	100.8		100.8	42.0	43.8	41.5	64.7	73.9	36.3	90.7	28.8	45.8	103.5	66.2
Sm	12.6	20.8	21.5	20.2	21.4		21.3	9.58	10.1	10.2	14.6	16	13.7	21.7	10	8.2	22.9	15.9
Eu	1.61	4.95	1.88	1.74	1.89		1.89	1.89	2.2	1.03	3.68	2.8	0.93	4.42	0.25	1.22	4.83	4.6
Gd	10.1	17.0	18.5	17.4	18.6		18.4	8.29	8.3	9.32	12.4	16.45	16.21	21.62	12.37	7.28	21.64	16.3
Tb	1.78	3.07	3.33	3.12	3.33		3.24	1.62	1.5	1.85	2.24	2.97	3.27	3.81	2.98	1.25	3.68	2.8
Dy	11.0	19.8	20.6	19.5	20.7		20.2	10.4	9.4	10.52	12.85	19.1	22.38	23.31	22.57	7.7	22.74	16.8
Ho	2.24	4.19	4.19	3.94	4.22		4.07	2.19	1.9	2.03	2.59	3.77	4.32	4.7	5	1.36	4.48	3.3
Er	6.2	11.0	11.4	10.7	11.4		11.0	6.26	5.0	5.78	7.56	11.63	13.5	14.63	16.71	3.91	13.1	9.7
Tm	0.91	1.53	1.60	1.51	1.60		1.53	0.95	0.7	0.87	1.13	1.62	2.11	2.27	2.87	0.6	2.13	1.5
Yb	5.83	10.3	10.9	10.3	11.0		10.5	6.35	4.6	4.91	6.44	9.98	12.21	13.7	19.19	3.79	12.02	8.8
Lu	0.86	1.38	1.60	1.50	1.61		1.54	1.00	0.7	0.75	1.06	1.51	1.76	1.97	2.8	0.59	1.81	1.4
Hf	15.4	25.9	28.6	26.8	29.3		31.3	11.7	10.7	8.1	23	12.8	12	15.9	20.4	9	20.4	20.9
Ta	8.11	11.5	12.2	11.1	12.6		12.8	3.00	2.5	4.8	3.4	4.6	7.9	7.4	14.5	2.2	5.1	3.5
Pb	11.0	7.58	11.5	12.1	12.3		10.9	4.66	4.9									
Th	*17.6*	*13.9*	*20*	*19.7*	*20.3*	*21.4*	*21.9*	*7.34*	*8.16*	*9.88*	*8.20*	*8.59*	*12.1*	*8.69*	*17.9*	*14.42*	*8.66*	6.9
U	*5.09*	*4.22*	*5.96*	*5.77*	*5.73*	*5.68*	*5.2*	*2.14*	*2.28*	*2.48*	*1.77*	*2.55*	*3.84*	*2.73*	*5.81*	*3.60*	*2.43*	1.9
Th/U	3.46	3.28	3.36	3.41	3.54	3.77	4.21	3.43	3.58	3.99	4.63	3.37	3.15	3.18	3.07	4.01	3.56	3.63
$^{87}Sr/^{86}Sr$	0.70345	0.70332	0.70338	0.70355	0.70353	0.70341	0.70386	0.70324		0.70367	0.70357	0.70408	0.70624	0.70403	0.71752	0.70478	0.70380	
$^{143}Nd/^{144}Nd$	0.51296	0.51298	0.51298	0.51297	0.51297	0.51298	0.51297	0.51303		0.51302	0.513	0.51301	0.51300	0.51300	0.51300	0.51300	0.51302	
$\delta^{18}O$	3.7	2.4	3.9							-2.5	0.5	5.5				6.8		
Age (Ma)			<0.01	<0.01	<0.01	<0.01	<0.01	<0.01		3.7	7.0	9.3	10.7	(11.5)	(12)	13.1	(13)	13.1
$[^{87}Sr/^{86}Sr]_i$			0.70338	0.70355	0.70353	0.70341	0.70386	0.70324		0.70334	0.70348	0.70338	0.70540	*0.70358*	*0.70456*	0.70353	0.70349	

Table 2 (continued) :

	SN8927 (1) (2)	L2	L3	7640 (1) (2)	7637 (1) (2)	Husf4	A2 (3)	Gei-1	Ves1	Hval2	Hval1b	Rauðf1	Streit1b	Hvs1	Búr4
SiO_2	46.3	54.9	53.0	47.5	47.2	49.2	50.3	49.1	52.72	53.6	46.74	49.16	51.73	44.66	48.98
TiO_2	4.04	1.64	1.72	1.96	2.49	3.36	2.49	3.72	2.54	2.16	2.74	3.19	2.23	2.73	3.18
Al_2O_3	15	16	16	13	15	13	13	13	15.62	13.67	14.44	13.33	13.82	15.33	12.94
$Fe_2O_3^*$	15.4	9.04	9.33	11.4	12.4	15.3	15.9	16.1	10.51	13.29	13.43	16.07	12.15	16.11	15.77
MnO	0.22	0.21	0.20	0.16	0.18	0.26	0.24	0.24	0.2	0.28	0.18	0.23	0.23	0.2	0.21
MgO	5.17	3.89	4.83	11.2	6.81	4.92	5.24	4.83	3.5	2.57	6.49	4.21	5.64	7.19	5.47
CaO	10.2	7.41	8.77	11.9	11.8	9.48	9.6	8.58	6.89	6.16	9.67	8.56	9.05	10.07	9.67
Na_2O	3.35	4.18	3.61	2.27	2.95	3.04	2.2	3.01	4.32	4.28	3.07	3.11	2.85	2.78	2.76
K_20	1.11	2.66	2.20	0.67	0.76	0.57	0.48	0.78	1.53	1.79	0.77	0.4	0.79	0.27	0.37
P_2O_5	0.85	0.34	0.35	0.3	0.52	0.84	0.31	0.46	1.07	1.28	0.35	0.52	0.21	0.35	0.33
H_2O-	-	0.1	0.1	-	-	0.5	-	0.2							
H_2O+	-	-0.4	-0.1	-	-	0.4	-	1.2	*0.9*	*0.7*	*2.0*	*1.1*	*1.2*	*0.2*	*0.2*
total	101.4	100.3	100.2	100.8	100.0	101.2	99.9	101.0	99.8	99.8	99.9	99.9	99.9	99.9	99.9
Rb	23.4	*46.3*	*41.3*	15.6	14.5	20.6	11.0	15.7	33.2	42.3	21	24.6	25.5	2.7	7.9
Sr	546.0	*345.3*	*356.8*	368.0	398.0	269.6	187.0	342.8	574	426.7	370.2	296.4	221.1	403.9	265.3
Y	-	36.9	31.5	-	-	51.4	43.0	52.1	71.3	93.3	35.1	51.1	79.9	36.2	48.9
Zr	242.0	357.2	281.1	129.0	147.0	237.1	177.0	272.6	390.8	533.2	155.9	220	148	164.1	212.3
Nb	61.6	74.9	61.5	24.5	29.4	36.7	22.0	21.9	33.8	38.9	16.9	21.1	25	15.7	18.8
Ba	534.0	691.5	595.8	233.0	282.0	185.8	118.0	144.8	259.9	353.3	144.4	159.8	68.5	110.9	97.6
La	42.0	82.9	59.2	22.2	24.8	30.7	15.9	21.0	41.9	54.4	17.1	23.5	17.9	15.5	17.1
Ce	91.4	161.4	118.0	47.8	54.6	71.2	37.5	52.0	102.4	131.6	41.7	54.1	48.4	38.5	44
Pr	12.0	17.8	13.3	6.2	7.3	9.3	5.1	7.3	14.33	18.57	6.01	7.48	7.01	5.41	6.3
Nd	47.3	63.9	49.1	24.5	29.4	41.2	22.7	33.4	64.5	83.1	28.4	32.8	31.3	25.6	28.9
Sm	9.55	10.7	8.72	5.14	6.33	9.25	5.57	8.95	16	20.1	7.1	8	10.2	6.9	8
Eu	3.33	2.74	2.55	1.72	2.21	3.68	1.8	3.02	5.52	5.69	2.28	3.09	1.96	2.47	2.68
Gd	8.84	7.93	6.86	4.97	6.32	8.81	6.74	7.60	16.43	20.44	7.18	9.26	12.16	6.74	8.83
Tb	1.28	1.17	1.01	0.718	0.92	1.50	1.138	1.50	2.66	3.26	1.28	1.67	2.41	1.26	1.61
Dy	6.83	6.85	5.97	3.95	5.14	9.38	-	8.94	14.16	17.44	6.82	9.79	12.96	7.63	9.64
Ho	1.35	1.36	1.19	0.779	1.03	1.92	1.57	1.79	2.52	3.38	1.3	1.94	2.41	1.33	1.71
Er	3.51	3.62	3.18	2.05	2.69	4.80	4.67	4.47	6.92	9.09	3.57	5.26	7.1	3.68	5.08
Tm	0.50	0.51	0.46	0.30	0.40	0.65	0.65	0.62	0.86	1.2	0.47	0.71	1.03	0.55	0.75
Yb	3.2	3.52	3.06	1.87	2.46	4.06	4.24	3.95	5.15	6.91	2.45	4.37	5.36	2.84	4.16
Lu	0.49	0.59	0.48	0.28	0.38	0.60	0.62	0.56	0.76	1.06	0.38	0.73	0.86	0.5	0.64
Hf	5.37	7.69	6.34	3.03	3.5	5.60	-	6.81	10.6	13.4	4.4	6.7	4.9	4.5	6.3
Ta	3.82	5.45	5.20	-	-	4.59	-	1.86	2.7	2.7	1.3	1.8	1.9	1.2	1.5
Pb	-	2.79	2.72	-	-	1.93	-	1.23							
Th	*2.69*	*6.16*	*5.43*	*1.96*	*1.97*	*2.56*	1.45	*1.74*	*2.86*	*3.04*	*1.33*	*1.96*	*2.35*	*0.70*	*1.31*
U	*0.779*	*1.59*	*1.52*	*0.586*	*0.59*	*0.78*	0.41	*0.51*	*0.79*	*0.96*	*0.47*	*0.62*	*0.77*	*0.23*	*0.40*
Th/U	3.45	3.87	3.57	3.34	3.34	3.27		3.41	3.62	3.17	2.83	3.17	3.06	3.02	3.28
$^{87}Sr/^{86}Sr$	0.70336	0.70338	0.70347	0.70334	0.70330	0.70334	0.70320		0.70325	0.70343	0.70352	0.70330	0.70338	0.70344	0.70336
$^{143}Nd/^{144}Nd$	0.51297	0.51292	0.51291	0.51296	0.51295	0.51299	0.51300		0.51301	0.51299	0.51300	0.51303	0.51303	0.51302	0.51301
$\delta^{18}O$	5.3	5.7	5.8	5.4	5.2	4.1	3.2		2.3	-2.1				4.4	
Age (Ma)		0.15 - 0.45	0.15 - 0.45				<0.01		3.9	6.5	(7)	(9)	10.7	(12.5)	(12.5)
$[^{87}Sr/^{86}Sr]_i$	0.70336	0.70338	0.70347	0.70334	0.70330		0.70320		0.70324	0.70340	0.70350	0.70327	0.70333	0.70344	0.70334

O, Sr and Nd isotopes

The whole-rock δ18O-values show a wide range of variation in both silicic (6.8 to -2.5‰) and basic (5.4 to -2.1 ‰) magmas. The 143Nd/144Nd does not show significant differences between basic and silicic rocks from the same central volcano. It ranges from 0.51290 to 0.51303 in our sample suite. Samples from Snæfellsnes Peninsula (except Drap2) break free from others by their low 143Nd/144Nd values that show a restricted range from 0.51290 to 0.51297. The Snæfellsnes values, together with those from Öræfajökull (Prestvik et al. 2001; Sigmarsson et al. 2000) the lowest $^{143}Nd/^{144}Nd$ ratio ever measured in Iceland. By contrast, the $^{87}Sr/^{86}Sr$ show a wide variation, from 0.70320 to 0.70352 in basic samples and from 0.70312 to 0.71752 in silicic ones. The value of 0.71752 measured in Rey3 sample is by far the highest value ever measured in Iceland. When time-corrected, the initial $^{87}Sr/^{86}Sr$ range is reduced but remains wider in silicic (0.70303 to 0.70540) than in basic (0.70320 to 0.70350) magmas. All samples plot close to the Icelandic mantle array previously defined (Kokfelt et al. 2006) and references therein; Figure 4). Only Streit1a, Rey3 and Hsk1 have very high $[^{87}Sr/^{86}Sr]_i$ (0.70540, 0.70456 and 0.70386 respectively), which plot outside the mantle array and more reasonably reflect an open Sr isotopic system, which is likely due to meteoric water alteration or hydration.

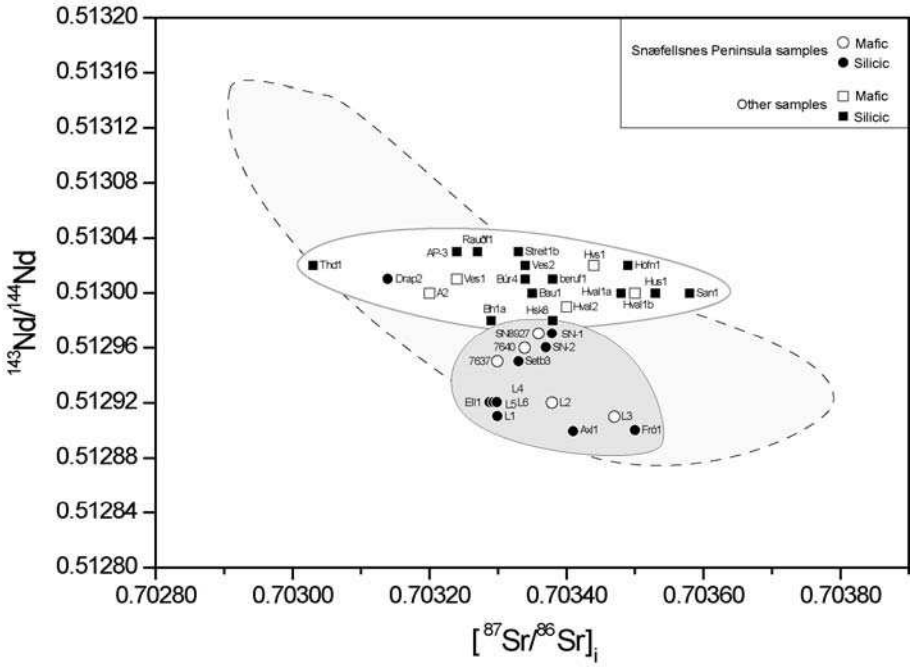

Figure 4 : $^{143}Nd/^{144}Nd$ vs. $[^{87}Sr/^{86}Sr]_i$ plot for both silicic and mafic samples. Light grey area represents the "rift zone" source type and the dark grey one, the "off-rift" source type (see the text for further discussion). The dashed limited area corresponds to the Iceland mantle array (Kokfelt et al. 2006).

Discussion

Role of the fractional crystallisation

Martin and Sigmarsson (2006) proposed that fractional crystallisation played a more or less important role in all silicic magma genesis. The role of fractional crystallisation appears to be amplified at the periphery of Iceland where the geothermal gradient is lower.

Ba and Sr depletion

The relative role of both fractional crystallisation and partial melting is illustrated in Figure 5 where both Ba (Ba*/Ba) and Sr (Sr*/Sr) anomalies are plotted against an incompatible element such as Rb. In the (Ba*/Ba) vs. Rb diagram, partial melting of a hydrated basalt defines a horizontal differentiation trend, which means that such partial melting is not efficient in producing Ba depletion. In contrast, such depletion is readily produced by high degrees of fractional crystallisation of feldspars leading to a much steeper trend in Figure 5. The two trends overlap at Rb < ~100 ppm, where most samples plot. However, several samples, Hsk-rhyolites, L-rhyolites, Streit1a and Rey3, show very high (Ba*/Ba) that cannot be explained by partial melting only. In other words, these samples can only be generated by high degrees of fractional crystallisation of a less differentiated magma. The (Sr*/Sr) vs. Rb diagram leads to the same conclusion even if the Sr depletion produced by high degrees of fractional crystallization is greater than for Ba ((Ba*/Ba) ~ 300 and (Sr*/Sr) ~ 4000). This is easily accounted by the fact that $D_{Sr}^{Plg/liq} >> D_{Ba}^{plg/liq}$ which results in a more compatible behaviour of Sr. Therefore, Sr anomalies allow a better estimation of the fractionation efficiency during the silicic magmas genesis than Ba anomalies. Based on Sr and Ba behaviour, it can be concluded that fractional crystallisation plays an important role in L- and Hsk-rhyolite genesis (Martin and Sigmarsson 2006) as well as in Rey3, Fró1 and Streit1a samples.

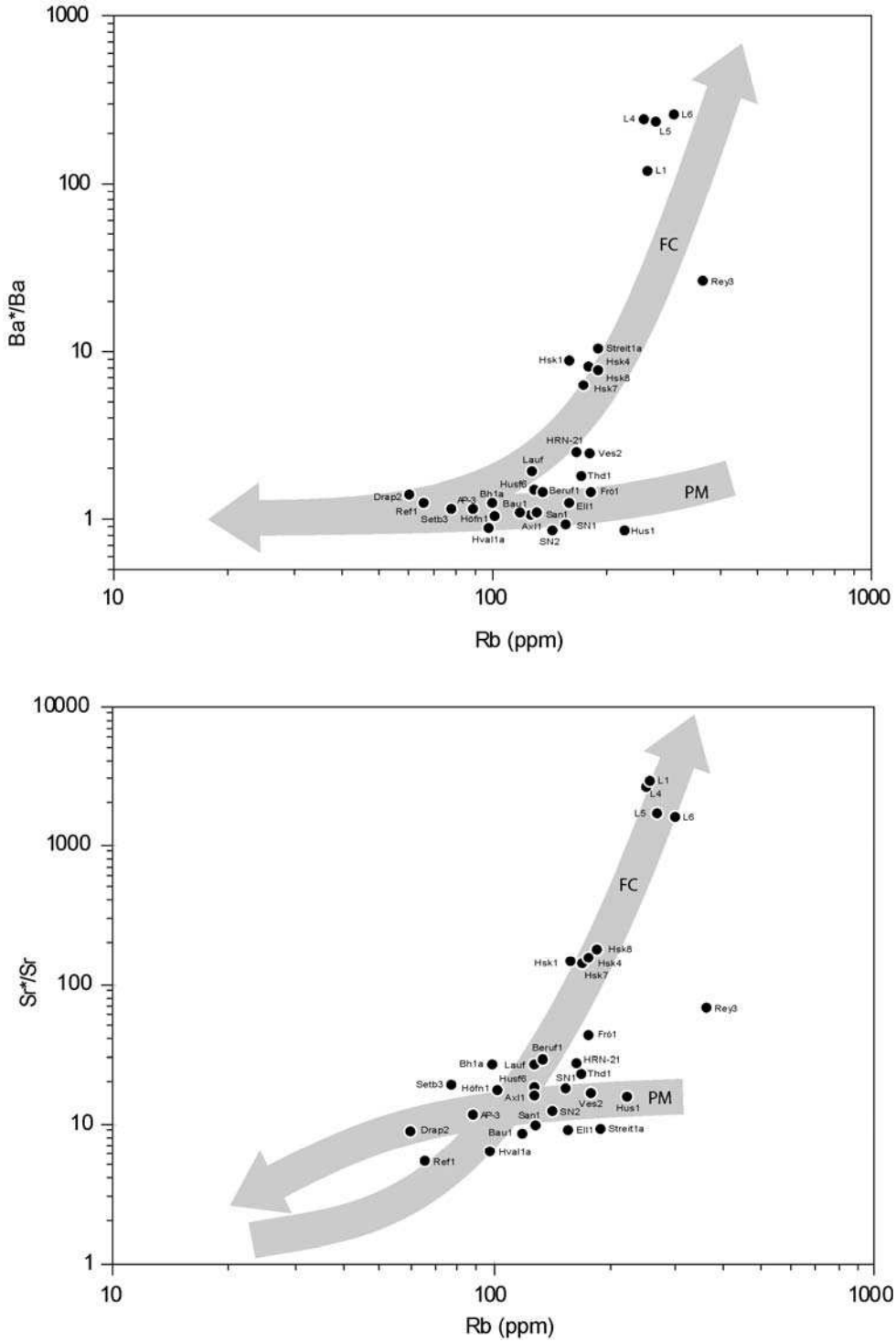

Figure 5: The Ba and Sr anomalies (Ba^*/Ba and Sr^*/Sr respectively) vs. Rb plotted in a logarithm scale diagram. The Ba* is defined as $10^{(Log[Rb]+Log[Nb])/2}$ and Sr* as $10^{(Log[Ce]+Log[Nd])/2}$ and all concentrations are normalized to primitive mantle values from Sun and McDounough 1989). The PM and FC arrow show the liquid evolution path generated by partial melting of the Iceland basaltic crust and fractional crystallisation of a basaltic magma respectively. See Martin and Sigmarsson (2006) for further discussion.

Constraints from Th concentrations

The Th provides a more accurate assessment of the role played by both mechanisms. Sigmarsson et al. (1992a; 1991) has measured Th concentration of 6.5 - 9 ppm in dacites generated by partial melting of the Iceland hydrated basaltic crust and of about 12 ppm in rhyolites produced by fractional crystallisation of these dacites. In Iceland, the basaltic crust contains about 1 - 1.5 ppm Th, as measured in tholeiitic lavas from the rift zone (e.g. Hemond et al. 1993). Consequently, assuming a perfect incompatible behaviour of Th during basalt melting, it appears that 10 to 20 % partial melting are required in order to derive dacites from basaltic crust composition. Magmas that contain more than 9 ppm Th should be produced by lower degrees of partial melting or by fractional crystallisation of less differentiated magma. The viscosity of a magma increases with its SiO_2 content (e.g. McBirney 1993) and therefore the lower degree of melting, the higher magma viscosity. In consequence, during partial melting, the extraction of small volumes (derived from low degree of melting) of differentiated magmas becomes difficult. The extraction of felsic liquids could be easier in case of fractional crystallisation, owing to gas filter process (e.g. Anderson et al. 1984; Sisson and Bacon 1999). Consequently, we will tentatively consider that Th > 9 ppm in silicic magmas reflects the prominent, if not exclusive, role played by fractional crystallisation.

The Figure 6 shows that only five silicic samples plot in the field of liquids produced by partial melting of the hydrated metabasaltic crust. The field for silicic melts produced by crustal partial melting has been estimated assuming 10 – 20 % partial melting of tholeiitic basalt with Th content ranging from 1 to 1.5 ppm and Th/U between 2.8 and 3.6. The variation range for Th/U corresponds to the variation observed in basalts from this study, which is considered as the extreme variation of the Icelandic crust. In most petrogenetic processes both Th and U have an incompatible behaviour, such that the Th/U ratio is not drastically modified. This does not remain true when accessory phases, such as zircon, monazite and allanite fractionate (Figure 6). For instance, $D_{Th/U}^{zircon/liq} < 1$ whereas $D_{Th/U}^{allanite/liq} >> 1$ and $D_{Th/U}^{monazite/liq} >> 1$ (e.g. Förster 1998; Mahood and Hildreth 1983).

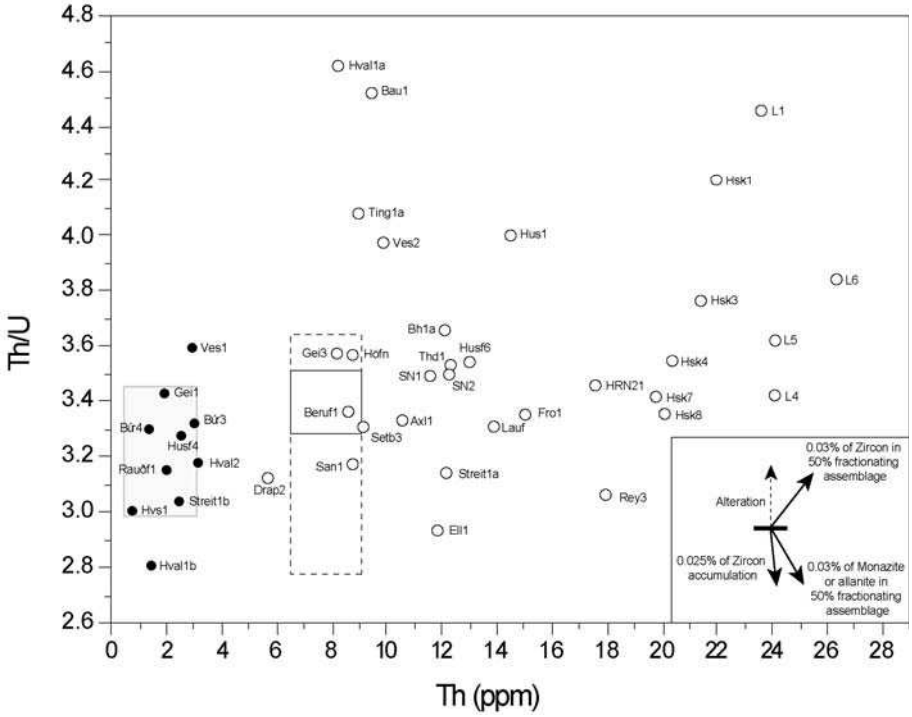

Figure 6: The Th/U vs. Th concentration in silicic (open circles) and mafic (filled circles) samples. Rectangle areas correspond to the variation range observed in basaltic samples (Th/U only) from Hekla, Krafla and Askja and contemporaneous dacites and rhyolites (Th and Th/U). These latter are most likely generated by partial melting of hydrothermal altered basaltic crust (Sigmarsson et al. 1992a; 1991). Dashed rectangle show the hypothetical range of Th/U in silicic melts produced by 10 – 20 % of partial melting of the basaltic crust, having Th/U similar to those of the mafic rocks measured in this study. Indicative illustration of the role played by accessory mineral phases and alteration process on the Th content and Th/U, are shown in the right corner.

The Figure 7 shows that in most samples, Zr is correlated with Th, which illustrates the highly incompatible behaviour of these two elements during the whole differentiation. Note however, that the Th variations are almost twice those for Zr (~20-30 vs. ~15 respectively) that underline the extreme incompatible character of Th, justifying its use as a differentiation index. The trend has 0.015 < Th/Zr < 0.025, and consequently all the samples plotting on it can be considered as representative of a magmatic evolution excluding important zircon fractionation. As $D_{Th}^{zircon/liq} << D_{Zr}^{zircon/liq}$, zircon fractionation would result in an increase of Th/Zr ratio, consequently, all samples with Th/Zr > 0.025 are likely to reflect zircon fractionation. For instance, samples Bau1, Ves2 and Hus1 have Th/Zr > 0.045, which attests important and efficient zircon fractionation. This conclusion is supported by their high Th/U (from 4.01 to 4.52; Figure 6). Samples Husf6, Fró1, HRN-21, Thd1 have 0.025<Th/Zr<

0.045 indicating a less efficient zircon fractionation, in agreement with their moderate Th/U (from 3.36 to 3.54).

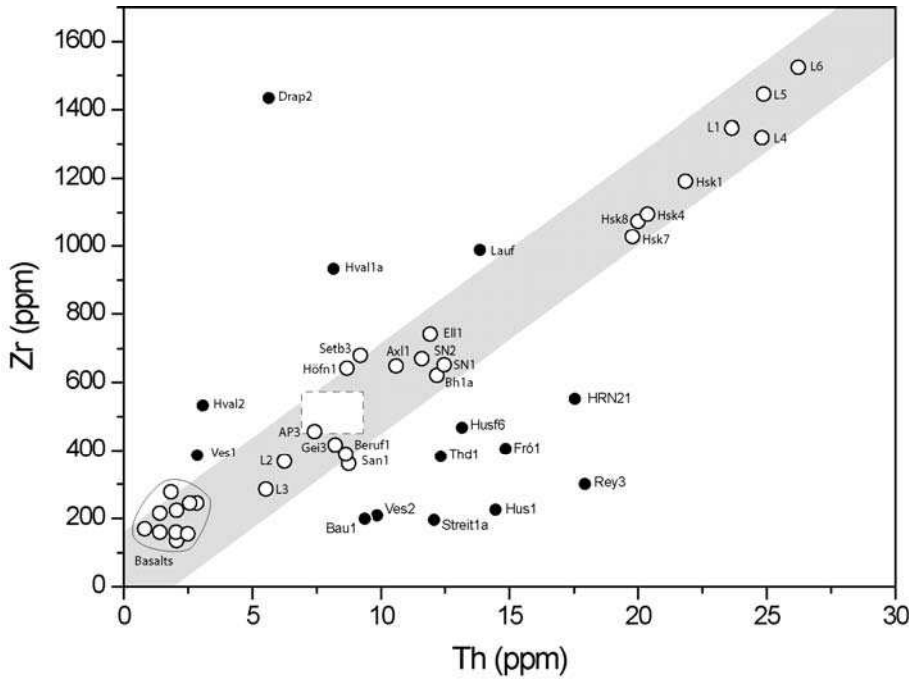

Figure 7: Diagram showing the Zr vs. Th concentrations. The correlation trend (grey area) defined by the open symbols corresponds to magmas that were insignificantly affected by zircon fractionation. Filled symbols show the magmas that have been highly affected by zircon fractionation (below the differentiation trend) or accumulation (above the differentiation trend). Dashed rectangle correspond to the composition range of the dacites and rhyolites obtained by partial melting of the Iceland crust from Hekla, Krafla and Askja (Sigmarsson et al. 1992a; 1991).

Samples Streit1a and Rey3 also have high Th/Zr (~0.06) but surprisingly they display Th/U as low as 3.15 and 3.07 respectively. Consequently, zircon fractionation alone is not able to account for these geochemical characteristics. Only mineral phases having $D_{Th/U}^{\text{mineral/liq}} >> 1$ such as monazite or allanite can, added to zircon, can account for both low Th/U and high Th/Zr. Monazite and allanite also have high LREE contents such that $D_{La}^{\text{mineral/liq}} < D_{Th}^{\text{mineral/liq}}$, therefore, the fractionation of these minerals should result in decreasing Th/La in the melt. The Figure 8 shows that the two samples, Streit1a and Rey3, have by far the highest Th/La and Th/Zr, which is interpreted as the result of important fractionation of both monazite (or allanite) and zircon. This is also in agreement with the low Th/U of these samples.

In contrast, sample Drap2 and to a less extent Hval1a and Lauf have low Th/Zr (< 0.015), which could indicate an accumulation of zircon during the differentiation process. The relatively low

Th/U measured in Drap2 and Lauf (3.12 and 3.28 respectively) are in agreement with this hypothesis. However, Hval1a has the highest Th/U measured in this study, which is in complete contradiction with the fact that it could be influence by zircon accumulation. As previously discussed, it is clear that the high Th/U from Hval1a is most likely due to an alteration process that results to an uranium loss, rather than a petrogenetic one.

It is quite clear that fractionation or accumulation of accessory mineral phases control the trace element ratios of even the most incompatible elements.

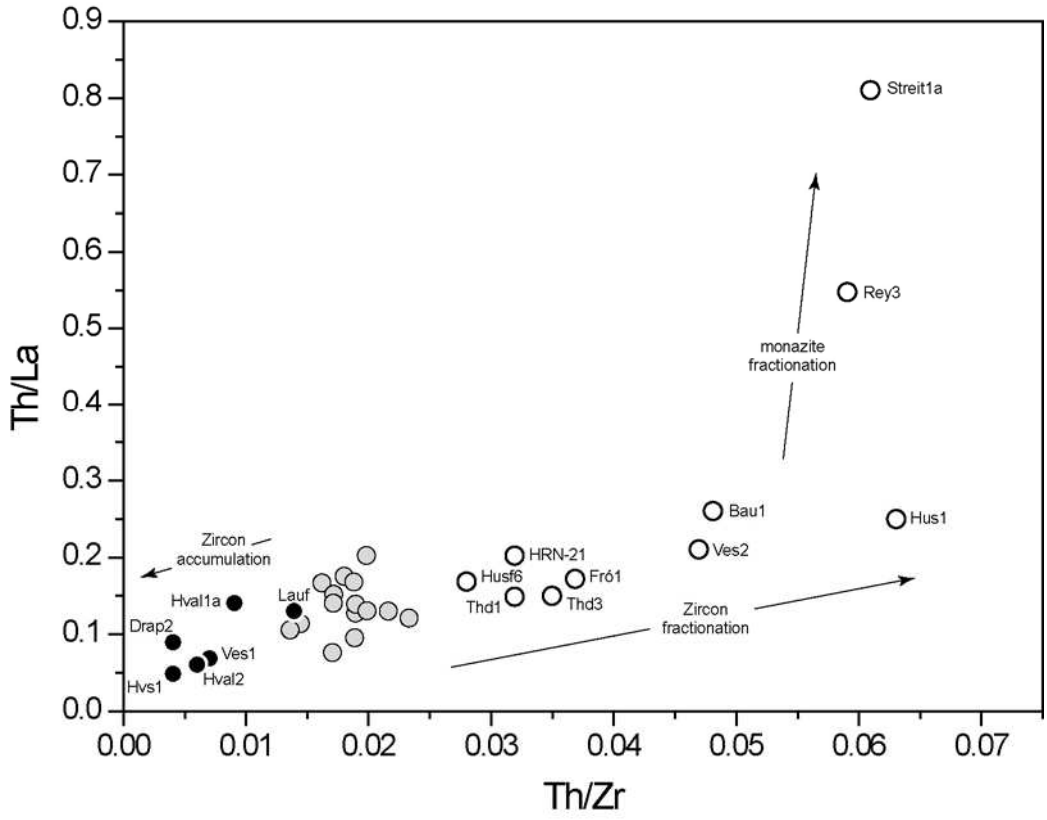

Figure 8: Th/La vs. Th/Zr diagram for silicic samples, displaying the role played by zircon and monazite fractionation or accumulation. Grey symbols show the samples that defined the differentiation trend in Figure 7. Open symbols correspond to samples affected by zircon and/or monazite fractionation. Filled symbols represent the magmas that have accumulated zircon.

Role of the partial melting

In Figure 5, most of silicic rocks plot where fractional crystallisation and partial melting trends overlap, thus making impossible to determine the petrogenetic mechanism from Rb-Ba-Sr systematic. However, oxygen isotopes often allow to infer the differentiation mechanism and especially role played by crustal partial melting (e.g. Nicholson et al. 1991; Sigmarsson et al. 1992a).

The Pálmason (1986) model suggests that the Iceland basaltic crust is generated in the rift zone. These basalts have a $\delta^{18}O$ of about 5 - 5.5 ‰ or lower (Gautason and Muehlenbachs 1998; Hémond et al. 1993; Sigmarsson et al. 1992b). In the rift system, efficient hydrothermalism leads to the crustal alteration at high temperature (300 - 400°C; Hattori and Muehlenbachs 1982), which results in a considerable decrease (about 1 – 3 ‰) of $\delta^{18}O$ (due to low fractionation of $^{18}O/^{16}O$ at high temperature). This hydrated basaltic crust progressively subsided through greenschist towards amphibolite facies conditions (e.g. Oskarsson et al. 1982), where it may reach anatexis and partially melt. Therefore, all silicic magmas generated by partial melting of the metabasaltic crust should have a low $\delta^{18}O$ ($\leq$ 5 ‰). In contrast, silicic magmas only generated by fractional crystallisation of basaltic melts, which are considered as having kept their original $\delta^{18}O$, should have the similar $\delta^{18}O$ as the cogenetic basalts or less than 1 ‰ higher ($\delta^{18}O$ ranging between 5 and 6.5 ‰).

The Figure 9 is a $\delta^{18}O$ vs. Th plot where Th content is used as differentiation index. Sigmarsson et al., 1991, 1992 demonstrated that dacitic magmas from Hekla, Krafla and Askja were generated by partial melting of the metabasaltic crust. These magmas show a wide $\delta^{18}O$ range from 5.3 to -0.2 ‰. The effect of subsequent fractional crystallisation would increase Th content without significantly changing the $\delta^{18}O$ of the silicic magmas. Samples from Ljósufjöll define a relatively flat trend typical of the fractional crystallisation of a basalt at the periphery of Iceland giving rise to per-alkaline rhyolites, with a maximum $\delta^{18}O$ increase of 1 ‰ (Martin and Sigmarsson 2006).

Samples as Beruf1 and Hval1a could be purely generated by partial melting whereas Husf6, Hsk8, Lauf, Ell1, Fró1 and in a less extent, Bau1 and Setb3 require subsequent fractional crystallisation in order to account for their high Th content. In the two intrusive samples, Hval2 and Ves2 that have the lowest $\delta^{18}O$ (< -2‰), hydrothermal circulation at high temperature could have decreased the $\delta^{18}O$ in sub-solidus conditions as discussed for Skaergaard intrusion (e.g. Taylor and Forester 1979). Samples Ves1, Hval1a, Ell1 and Fró1 (in addition to Hval2 and Ves2) are intrusive rocks and the presence of a minor content of minerals such as epidote and chlorite attests for hydrothermal activity during cooling. Therefore, low $\delta^{18}O$ in intrusive rocks could be either due to melting of metabasaltic crust or sub-solidus alteration. Consequently, if $\delta^{18}O$ is an efficient marker of partial melting in extrusive felsic magmas (as Hsk8 or Lauf), it must be used very carefully for intrusive rocks, due to their possible hydrothermal alteration.

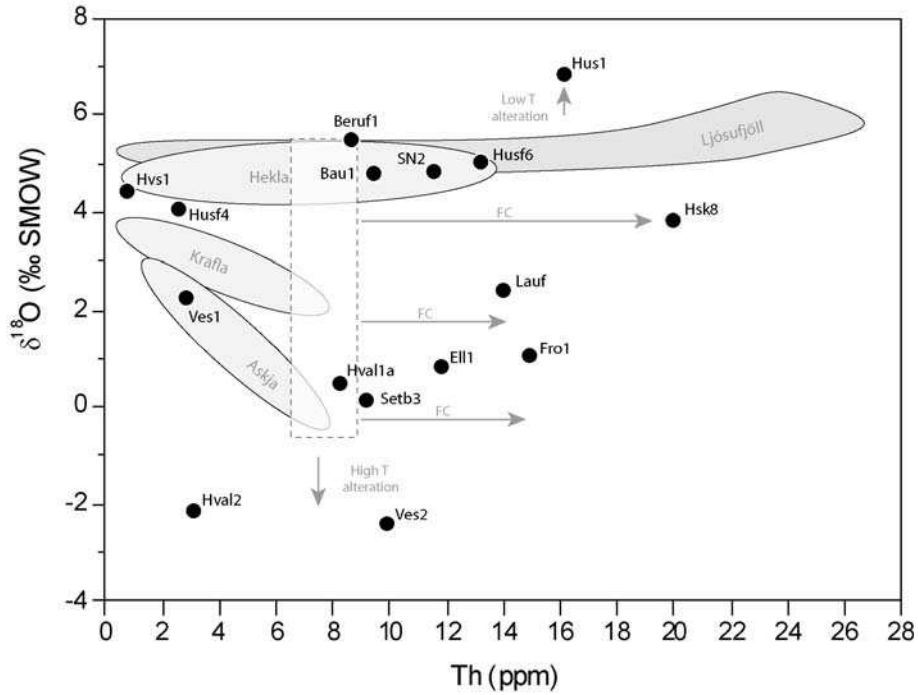

Figure 9: $\delta^{18}O$ vs. Th plot for samples from this study. The dark grey area represents the fractional crystallisation evolution as defined in Ljósufjöll (Martin and Sigmarsson 2006). The light grey areas show the magmatic evolution of Hekla, Krafla and Askja volcanoes and the dashed rectangle corresponds to compositional range of dacites and rhyolites obtained by crustal melting, from the same volcanoes (Sigmarsson et al. 1992a; 1991). Arrows show the effect of fractional crystallisation (FC) and alteration under high and low temperature (T).

Sample Hus1 has the highest $\delta^{18}O$ (6.8 ‰), which precludes an origin by partial melting. Considering a maximum increase of 1 ‰ during fractional crystallisation, the parental basalt should have had a minimum $\delta^{18}O$ of 5.8 ‰, which appears outside the range estimated for Icelandic mantle $\delta^{18}O$ (5 – 5.5 ‰; Gautason and Muehlenbachs 1998; Hemond et al. 1993; Sigmarsson et al. 1992b). Therefore, neither fractional crystallisation of a basaltic magma nor crustal partial melting are likely to account for its high $\delta^{18}O$. However, low temperature alteration, close to the surface, is able to slightly increase $\delta^{18}O$ (due to high fractionation of $^{18}O/^{16}O$ at low temperature).

Samples Beruf1, Bau1 and Husf6 $\delta^{18}O$ can be explained either by partial melting of a basaltic crust having a "high" $\delta^{18}O$ (~ 5 ‰), as suggested for Hekla volcano (Sigmarsson et al. 1992a) or by fractional crystallisation of a basaltic magma such as for Ljósufjöll central volcano (Martin and Sigmarsson 2006). Taken together, oxygen isotopes reveal the origin of most extrusive silicic samples of this study.

Source of the silicic magmas

The Figure 4 shows that all samples have $^{87}Sr/^{86}Sr$ ranging from about 0.70312 to 0.70358 in agreement with the Icelandic mantle array previously defined (Kokfelt et al. 2006) and references therein). However, as clearly observed in samples Streit1a, Rey3 and Hsk1, Sr-isotope behaviour is very sensitive to alteration or hydration processes especially so in silicic rocks with very low Sr content. For this reason, $^{87}Sr/^{86}Sr$ is not a good tracer for silicic magma source. In contrast, Nd-isotopes appear to be insignificantly affected by weak alteration processes and consequently, they can be considered as better markers of the magmatic source

The Figure 4 as well as Figure 10 show that $^{143}Nd/^{144}Nd$ in both felsic and basic rocks is correlated to geography. Samples from Snæfellsnes (except Drap2) have the lowest $^{143}Nd/^{144}Nd$, (0.51290 to 0.51297) whereas all the others, including rift zone sample as AP-3, have significantly higher values, (0.51296 to 0.51303). Carpentier (2003) and Kokfelt et al. (2006) observed a similar behaviour in Holocene basalts. They described a symmetrical increase of $^{143}Nd/^{144}Nd$ towards the rift zone, with the lowest values in Snæfellsnes Peninsula and Öræfarjökull central volcano. Therefore, silicic magmas independently of their age have two different sources linked to present day geodynamical environment. The high $^{143}Nd/^{144}Nd$ ($\geq$ 0.51297) lavas define a "rift zone" source-type and the low $^{143}Nd/^{144}Nd$ ($\leq$ 0.51298) are referred as "off-rift" source-type. However, as Nd-isotopes are not significantly fractionated during magmatic processes, the $^{143}Nd/^{144}Nd$ of silicic rocks is the same as that of their basaltic source whatever the differentiation process is.

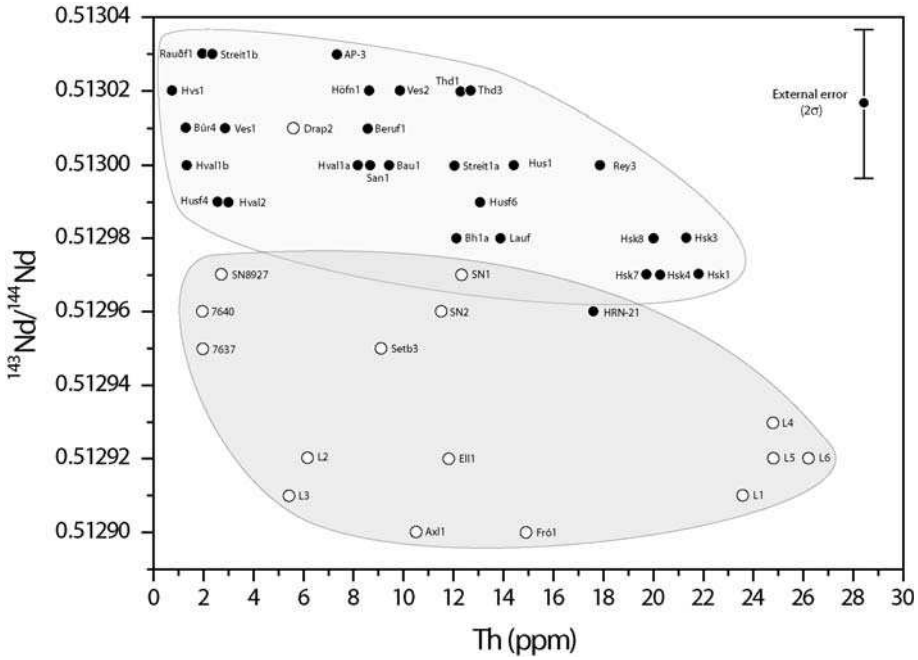

Figure 10: $^{143}Nd/^{144}Nd$ vs. Th concentration in samples from Snæfellsnes Peninsula (open circles) and all other locations sampled in this study (filled circle). The light and grey areas are the same as in Figure 4. The error bar (2σ) correspond to the external error.

Martin and Sigmarsson (2006) proposed that the source of silicic magmas is mainly controlled by the thermal state of the crust. Near central Iceland, rift and plume systems interact resulting in sufficiently high geothermal gradients to induce the partial melting of the hydrated metabasaltic crust. Possibly subsequent fractional crystallisation can take place. In the "off-rift" context (far from the rift zone and Iceland centre), geothermal gradient is not high enough to allow crustal melting and felsic magmas are generated by fractional crystallisation of basalts with eventually small amount of crustal assimilation. Based on these interpretations, silicic rocks with high $^{143}Nd/^{144}Nd$ ("rift zone" source type) were generated by partial melting of the basaltic crust, which had also been generated in a rift zone. On the other hand, felsic magmas with low $^{143}Nd/^{144}Nd$ were most likely formed by fractional crystallisation of contemporaneous related basalts in off-rift context.

All samples from the East and West Iceland have a "rift zone" signature, which is interpreted as reflecting an origin by partial melting of the metabasaltic crust in a rift zone environment. This observation leads to the conclusion that the volcanic systems that contain silicic magmas formed close to the ridge system were subsequently drifted away from the rift zone by the North-Atlantic spreading motion. For instance, all samples located in eastern Iceland were likely generated close to eastern part of the NIRZ and then progressively drifted

to the East. Samples as Husf6 and Bau1 were most likely generated in the western part of the RRZ and then drift to the West whereas Thd1 followed a symmetrical path, in the eastern part of the RRZ.

The Dacite Drap2, from Snæfellsnes Peninsula is the unique silicic rocks from this area that have a "rift zone" source-type whereas all others have typical "off-rift" characteristics. Among Snæfellsnes samples, Drap2 is also the oldest one with an age of 6.8 Ma (Table 1), all the other samples are younger than 5.3 Ma. Therefore, about 7 Ma ago, the Snæfellsnes Peninsula was still in a rift zone environment, which is recorded in the Nd-isotope composition of Drap2. In stark contrast, samples Fró1 and Setb3 dated at 4.95 and 5.27 Ma respectively, record an "off-rift" Nd-signature. This leads to the conclusion that the rift jump towards its present day position took place between 7 Ma and 5.5 Ma.

The Drap2 dacite has been generated in rift zone environment and thus by partial melting of an hydrated basaltic crust. This dacite contains 5.6 ppm of Th, which indicates a degree of partial melting of the metabasaltic crust of around 22 %. As observed today between the RRZ and the SIVZ, the rift jump process is not an instantaneous mechanism but rather a process that develop over few Ma. During this transition, both old and new rift zones coexist. Similarly, the high geothermal gradient of the rift zone does not immediately decrease and the crust does not instantly turn cold as it is today beneath Lósufjöll central volcano, it progressively cools. Today, the positive thermal anomaly under the northwest Snæfellsnes Peninsula is assumed to be a remnant of the extinct rift zone influence (e.g. Flóvenz and Saemundsson 1993), which implies that the thermal state of the crust is still influenced by this rift zone 6 - 7 Ma after its extinction. As the rift zone activity has progressively decreased in Snæfellsnes, the basaltic crust progressively cooled and the changed in silicic magma genesis progressively turned from crustal partial melting to fractional crystallisation. It is assumed that intermediate processes as Assimilation Fractional Crystallisation (AFC) could have played an important role during the few Ma that followed the Snæfellsnes rift zone extinction. Unfortunately, the error bars on $^{143}Nd/^{144}Nd$ compared with the variation range of data set is too high to allow a detailed record of the transition in petrogenesis mechanisms.

The samples from Torfajökull central volcano (Hsk-samples, HRN-21 and Lauf) and sample Bh1a are all located on or close to the SIVZ and display Nd-isotope signatures intermediate between "rift zone" and "off-rift" types (Figure 10). The SIVZ is considered as the propagation of the NIRZ in South central Iceland and therefore corresponds to a transitional geodynamical context between an "off rift" and a "rift zone" context. Martin and

Sigmarsson (2006) have proposed that silicic rocks from Torfajökull were generated by partial melting of the Iceland metabasaltic crust followed by fractional crystallisation. In this scheme, the Torfajökull silicic magmas should have a typical "rift zone" Nd-isotopic signature. Surprisingly, in Figure 10, these rocks have $^{143}Nd/^{144}Nd$ intermediate between "rift" and "off-rift" types, which induces that the metabasaltic crust beneath Torfajökull have an intermediate Nd-isotope signature. The first consequence is that these samples cannot result from RRZ activity, in which case, they should have recorded a typical "rift zone" signature, such as Tdh1, Husf6 and Bau1. On the other hand, SIVZ is a propagating rift zone and consequently it cannot be considered as mature as the NIRZ and the RRZ. During the initiation and the propagation of a rift zone, as observed in the SIVZ, the composition of basaltic magmas shows typical alkali affinities and in course of time, they become progressively tholeiitic via transitional compositions. Therefore, the Nd-isotopic signature of Torfajökull magmas reflects the transitional characteristics of the basaltic source. In conclusion, we propose that the Torfajökull silicic magmas as well as Bh1a sample were formed by partial melting of the basaltic crust generated in the immature SIVZ rift zone, since 3 Ma and not generated few Ma ago in the RRZ. Assuming the model of Pálmason (1986), this 3 Ma old immature crust has probably not subsided very deeply and therefore the partial melting of such a crust occurred more likely in its upper part rather than in the lower one.

Conclusion

The exceptional geodynamical context of Iceland allows the assessment of silicic magma genesis in an oceanic environment. Partial melting of the hydrated metabasaltic crust and fractional crystallisation of basaltic magmas are the two main processes whereas intermediate mechanism such as AFC can also take place. Martin and Sigmarsson (2006) proposed that the petrogenesis mechanism is strongly controlled by the thermal state of the crust. In rift zone, ridge and plume systems interaction results in high geothermal gradients, which is high enough to induce the partial melting of the hydrated metabasaltic crust. Far from there, in off-rift environment, geothermal gradient is too low, thus precluding crustal melting and privileging the fractional crystallisation of basaltic magmas. Consequently, this detailed study on Icelandic silicic rocks allows the reconstruction of the petrogenesis mechanisms and therefore of the geodynamical environment. In other words, this study leads to spatio-temporal evolution of silicic petrogenesis mechanisms and Icelandic geodynamical environment.

The main conclusions of this work are 1) As clearly observed in Eastern Iceland, most of Icelandic silicic rocks were generated by partial melting of the hydrated basaltic crust in the rift zone. Subsequently to their genesis, they drifted far from their genesis location due to plate spreading. 2) The Snæfellsnes area has a "rift zone" signature for samples older than 5.5 Ma and "off-rift" signature for more recent rocks. This change is interpreted as resulting from an eastward rift relocation between 7 and 5.5 Ma. From ~15 to 7 Ma the rift was passed through the Snæfellsnes Peninsula and generated silicic rocks having, "rift zone" signature, by crustal melting. Between 7 and 5.5 Ma the rift zone jumped eastward forming the present RRZ. Since this time, silicic rocks from Snæfellsnes are generated by fractional crystallisation of basaltic magmas with decreasing crustal assimilation with time. 3) In the Torfajökull area felsic magmas were most likely generated by partial melting of the hydrated metabasaltic crust (Martin and Sigmarsson 2006). However, their Nd isotopic signature is intermediate between "rift zone" and "off-rift" one. Due to rift propagation environment, this transitional character (also observed in major and trace elements) induce that the melted crust beneath Torfajökull central volcano was recently (<3 Ma) generated in the SIVZ itself and not in the RRZ few Ma ago.

References

Anderson AT, George JR, Swihart H, Artioli G, Geiger CA (1984) Segregation vesicles, Gas filter-pressing, and igneous differentiation. J. Geol. 92:55-72

Carpentier M (2003) Variabilité géochimique des basaltes Holocène islandais. In, vol. Université Blaise Pascal, Clermont Ferrand, p 53

Clayton R, N., Mayeda TK (1963) The use of bromine pentafluoride in the extraction of oxygen from oxides and silicates for isotopic analysis. Geochim. Cosmochim. Acta 27:43-52

Eysteinsson H, Gunnarsson K (1995) Maps of gravity, bathymetry and magnetics for Iceland and surroundings. In, vol. Orkustofnun, National Energy Authority, Geothermal division,

Flóvenz ÓG, Saemundsson K (1993) Heat flow and geothermal processes in Iceland. Tectonophysics 225:123-138

Förster H-J (1998) The chemical composition of the REE-Y-Th-U-rich accessory minerals in peraluminous granites of the Erzgebirge-Fichtelgebirge region, Germany, PartI: The monazite-(Ce)-brabantite solid solution series. Amer. Mineral. 83:259-272

Gautason B, Muehlenbachs K (1998) Oxygen isotopic fluxes associated with high-temperature processes in the rift zones of Iceland. Chem. Geol. 145:275-286

Guðmundsdóttir IS, Sigmarsson O (2006) Highest measured strontium isotope ratios in Icelandic rocks: Rb and Sr systematics in Ljósufjöll volcanics, Snæfellsnes peninsula In: Natural Science Symposium, vol., Reykjavik

Hardarson BS, Fitton JG, Ellam RM, Pringle MS (1997) Rift relocation-a geochemical and geochronological investigation of a paleo-rift in northwest Iceland. Earth Planet. Sci. Lett. 153:181-196

Hattori K, Muehlenbachs K (1982) Oxygen isotope ratios of the Icelandic crust. J. Geophys. Res. 87:6559-6565

Hemond C, Arndt NT, Lichtenstein U, Holfmann AW, Oskarsson N, Steinthorsson S (1993) The heterogeneous Iceland plume: Nd-Sr-O isotopes and traces element constraints. J. Geophys. Res. 98:15833-15850

Jóhannesson H (1980) Jarðlagaskipan og þróun rekbelta á Vesturlandi. Náttúrufræðingurinn 50:13-31

Kokfelt TF, Hoernle K, Hauff F, Fiebig J, Werner R, Gabre-Schönberg D (2006) Combined trace element and Pb-Nd-Sr-O isotope evidence for recycled oceanic crust (upper and lower) in the Iceland mantle plume. J. Petrol.:1-45

Le Bas MJ, Le Maitre Rw, Streckeisen A, Zanettin B (1986) A chemical classification of volcanic rocks based on the total alkali-silica diagram. J. Petrol. 22:745-750

Macdonald R, McGarvie DW, Pinkerton H, Smith RL, Palacz ZA (1990) Petrogenetic evolution of the Torfajökull volcanic complex, Iceland I. Relation between the magma types. J. Petrol. 31:461-481

Mahood G, Hildreth W (1983) Large partition coefficients of trace elements in high-silica rhyolites. Geochim. Cosmochim. Acta 47:11-30

Martin E, Sigmarsson O (2006) Geographical variations of silicic magma origin in Iceland: the case of Torfajökull, Ljósufjöll and Snæfellsjökull volcanoes. Contrib. Mineral. Petrol. accepted

McBirney AR (1993) Igneous petrology, vol. Jones and Bartlett Publishers, Boston, p 508

Miyashiro A (1978) Nature of alkalic volcanic rock series. Contrib. Mineral. Petrol. 66:91-104

Nicholson H, Condomines M, Fitton JG, Fallick AE, Grönvold K, Rogers G (1991) Geochemical and isotopic Evidence for Crustal Assimilation Beneath Krafla, Iceland. J. Petrol. 32:1005-1020

Oskarsson N, Sigvaldason GE, Steinthorsson S (1982) A dynamic model of rift zone petrogenesis and the regional petrology of Iceland. J. Petrol. 23:28-74

Pálmason G (1986) Model of crustal formation in Iceland and application to submarine mid-ocean ridges. In: Vogt PR, Tucholke BE (eds) The Geology of North America, vol The Western North Atlantic Region. Geological Society of America, Boulder, pp 87-97

Prestvik T, Goldberg S, Karlsson H, Grönvold K (2001) Anomalous strontium and lead-isotope signatures in the off-rift Öraefajökull central volcano in south-east Iceland, Evidence for enriched endmember(s) of the Iceland mantle plume? Earth Planet. Sci. Lett. 190:211-220

Sæmundsson K (1979) Outline of geology of Iceland. Jökull 29:7-28

Sigmarsson O, Condomines M, Fourcade S (1992a) A detailed Th, Sr and O isotope study of Hekla: differentiation processes in an Icelandic volcano. Contributions to Mineralogy and Petrology 112:20-34

Sigmarsson O, Condomines M, Fourcade S (1992b) Mantle and crustal contribution in the genesis of recent basalts from off-rift zones in Iceland: constraints from Th, Sr and O isotopes. Earth Planet. Sci. Lett. 110:149-162

Sigmarsson O, Hémond C, Condomines M, Fourcade S, Oskarsson N (1991) Origin of silicic magma in Iceland revealed by Th isotopes. Geology 19:621-624

Sigmarsson O, Karlsson HR, Larsen G (2000) The 1996 and 1998 subglacial eruptions beneath the Vatnajökull ice sheet in Iceland: contrasting geochemical and geophysical inferences on magma migration Bull. volcanol. 61:468-476

Sigvaldason GE (2002) Volcanic and tectonic processes coinciding with glaciation and crustal rebound: an early Holocene rhyolitic eruption in the Dynjujöll volcanic centre and the formation of the Askja caldera, north Iceland. Bull. volcanol. 64:192-205

Sisson TW, Bacon CR (1999) Gas-driven pressing in magmas. Geology 27:613-616

Steinthorsson S (1967) Tvær nýjar C^{14}-aldursákvarðanir á ökulögum úr Snæfellsjökli Náttúrufræðingurinn 37:236-238

Sun SS, McDonough WF (1989) Chemical and isotopic systematics of oceanic basalts: Implications for the mantle composition and processes. In: Magmatism in the Ocean Basin, vol 42. Geol. Soc. Sp. Publi., pp 313-345

Taylor JHP, Forester RW (1979) An oxygen and hydrogen isotope study of the Skaergaard intrusion and its country rocks: a description of a 55-My old fossil hydrothermal system. J. Petrol. 20:355-419

Vink GE (1984) A hotspot model for Iceland and the Vøring plateau. J. Geophys. Res. 89:9949-9959

Walker GPL (1963) The Breiddalur central volcano, Eastern iceland. Quart J. geol. Soc. Lond. 119:29-63

Wolfe CJ, Bjarnason IT, VanDecar SC, Solomon SC (1997) Seismic structure of the Iceland mantle plume. Nature 385:245-247

2. Evolution géodynamique des volcans centraux Est-Islandais depuis 12 - 13 Ma

Organisation spatio-temporelle des formations volcaniques

Des roches magmatiques de composition basique et acide provenant de différents systèmes volcaniques de l'Est de l'Islande ont été datées selon la méthode K-Ar sur roche totale (Moorbath et al., 1968) ou U-Th-Pb in situ sur zircon (Paquette, 2006, communication personnelle). Les résultats de ces datations sont résumés dans le Tableau III-5.

Nom du volcan central	Ages (Ma)	Méthode analytique
Refsstaðir	13,1	1
Borgarfjörður	12,5 – 13,1	1
Barðsnes	*12,5*	*2*
Reyðarfjörður	*11,9*	*2*
Þingmúli	*9,5*	*2*
Breiðdalur	9,3	1
Álftafjörður	10,7	1
Austurhorn	7,0 – 6,5 – *6,6*	1-*2*
Vesturhorn	3,7 – 3,9 – *6,6*	1-*2*

Tableau III-5 : âges obtenus sur des roches provenant des volcans centraux de l'Est de l'Islande. 1 : méthode U-Th-Pb in-situ sur zircon, (Paquette 2006, communication personnelle) et 2 : méthode K-Ar sur roche totale, (Moorbath et al., 1968)

La Figure III-6, reporte les âges des volcans centraux en fonction de leur localisation géographique (latitude et longitude). Il apparaît clairement que l'âge de ces volcans est corrélé à leur position géographique. En effet, plus on se dirige vers le Nord-Est et plus les formations volcaniques sont anciennes. Seul l'échantillon Ref1 provenant du volcan central de Refsstaðir n'est pas cohérent avec cette tendance générale. Si ce dernier suivait la tendance générale, il devrait être plus jeune ou bien se trouver beaucoup plus à l'Est par rapport à sa position actuelle.

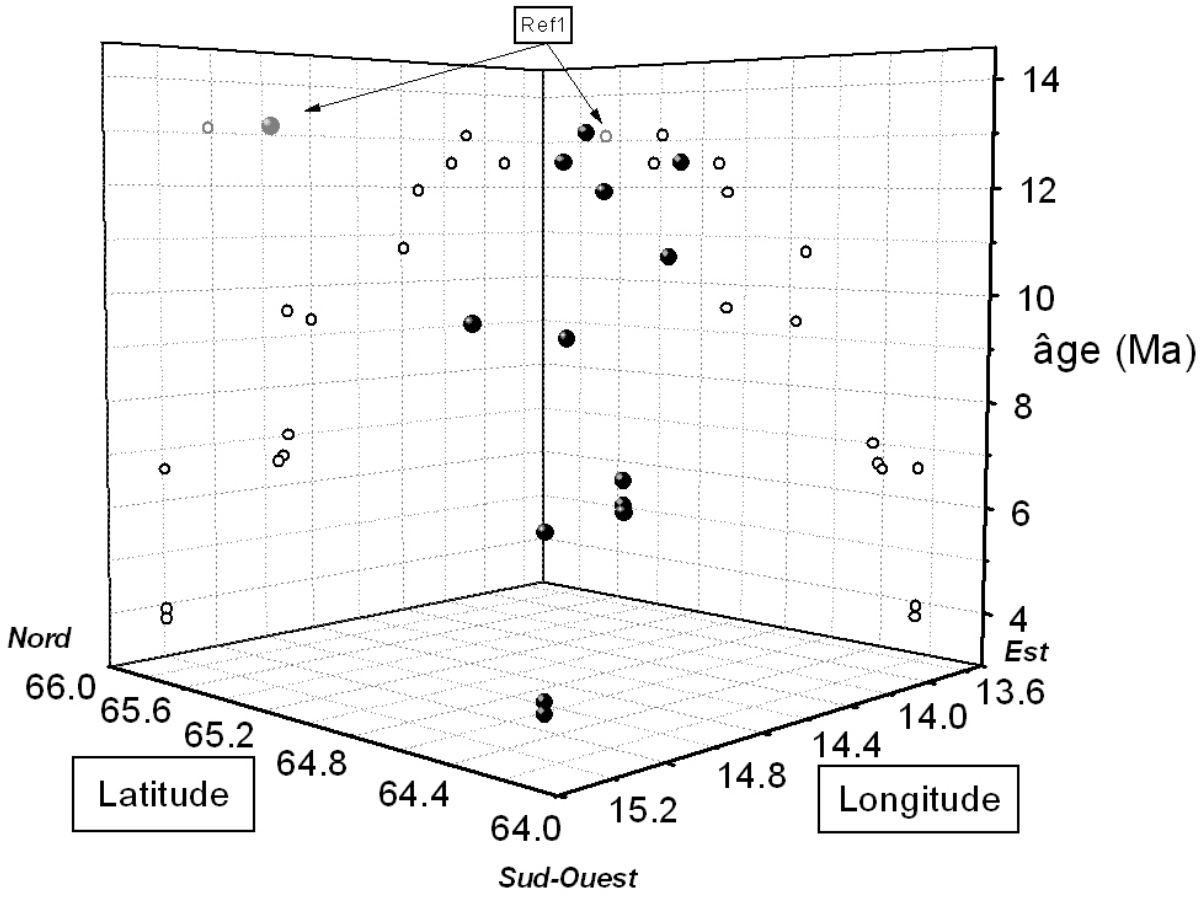

Figure III-6 : Age vs. latitude (en °Nord) et longitude (°Ouest) d'échantillons provenant de différents volcans centraux de l'Est de l'Islande. Les symboles pleins représentent les échantillons selon les trois dimensions alors que les cercles vides représentent les projections sur les plans N-S (latitude) vs. âge et E-O (longitude) vs âge.

Afin d'essayer d'expliquer cette anomalie, la position géographique des systèmes volcaniques lors de leur formation a été évaluée, en considérant la dérive due à l'écartement des plaques de part et d'autre des zones de rift au cours des 13 derniers Ma, le but étant d'estimer le contexte géodynamique dans lequel ils se sont mis en place.

Relocalisation des volcans centraux

Le modèle de formation de la croûte islandaise proposé par Pálmason (1973; 1986 ; Figure I-2) , considère que les roches se formant à proximité de la North Iceland Rift Zone (NIRZ) s'écartent et forment des lignes isochrones parallèles à cette zone de rift. En estimant une demi-vitesse d'ouverture de la ride médio-Atlantique constante d'environ 1 cm/an suivant la direction l05°N (Sæmundsson, 1979; Vogt et al., 1980; Nunns, 1983; DeMets et al., 1990; Sigmundsson et al., 1995; Sella et al., 2002) et en supposant qu'aucune subsidence n'est active, il est alors supposé qu'une roche qui a 10 Ma s'est mise en place à

environ 100 km à l'Ouest de sa position actuelle. Il est ainsi possible de déterminer la position géographique approximative qu'occupait chaque système volcanique au moment de sa formation.

Afin de réaliser cette reconstruction, il a été nécessaire de considérer que : 1) les âges des roches mesurés (Tableau III-5) sont représentatifs de ceux de l'ensemble de l'édifice qui les contient ; 2) la vitesse et la direction d'ouverture au sein de la NIRZ sont restées constantes au cours du temps et ce en tout point de zone de rift.

Les résultats de la relocalisation des systèmes volcaniques sont illustrés dans la Figure III-7 ; elle permet de diviser l'Est de l'Islande en trois zones d'évolution différentes :

Au centre, les volcans centraux de Barðsnes, Reyðarfjörður, Þingmúli et Breiðdalur se seraient formés au sein de la partie Est de la NIRZ (à 10 - 25 km du centre de la zone de rift). Une telle localisation est en accord avec le modèle de Pálmason (1973; 1986; Figure I-2) car les roches se formant dans la partie Est de la zone de rift seront décalées vers l'Est sans subir de subsidence importante, ce qui permettra aux systèmes volcaniques de rester en sub-surface lors de leur dérive et donc d'être aujourd'hui à l'affleurement dans les fjords Est islandais.

Au Sud, les volcans centraux de Vesturhorn et Austurhorn se seraient quant à eux formés à 35 - 45 km à l'Est du centre de la NIRZ. Cette distance est plus grande (double) que celle estimée pour les systèmes volcaniques précédents. Une explication pourrait être que la vitesse d'écartement des plaques au niveau de la NIRZ n'était pas la même en tous points de la ride. En effet Hofton and Foulger (1996) ont mesuré dans le Sud-Est de l'Islande, entre 1987 et 1992, des vitesses de déplacement de surface plus importantes et plus orientées vers le sud que celles mesurées à l'Est de l'île. En supposant cette différence de vitesse d'expansion comme représentative de celle opérant durant ces derniers Ma, il est alors possible de considérer que les systèmes volcaniques du Sud se sont également formés dans la partie Est de la NIRZ, dans une zone ou la demi-vitesse d'expansion de la ride était plus importante et où le déplacement s'opérait localement vers le SSE au lieu de l05°N.

Au Nord, le volcan central de Borgarfjörður occupe une position cohérente avec une formation dans la partie Est de la NIRZ au même titre que tous les volcans dont il a été discuté précédemment. En revanche, celui de Refsstaðir apparaît s'être formé à environ 40 km à l'Ouest de la NIRZ, ce qui est incohérent avec sa position actuelle à l'Est de la NIRZ. Effectivement, un système volcanique formé à l'Ouest de la zone de rift dérivera vers l'Ouest et non vers l'Est. Il apparaît alors que le système volcanique de Refsstaðir n'a pu aucunement se former dans la partie Est de la NIRZ.

Implications pour l'évolution géodynamique de l'Est de l'Islande

Dans un premier temps, le fait que les volcans centraux actuellement localisés au Sud et au centre Est de l'Islande sont cohérents avec une formation au niveau de la NIRZ, est en parfait accord avec les données géochimiques relatives aux roches acides de ces mêmes volcans. En effet, il a été montré dans la Partie III-B-1 que les roches magmatiques acides provenant des volcans des fjords Est ont une signature isotopique du Nd de type « zone de rift ». Ceci implique qu'elles aient été engendrées dans une zone de rift par fusion de la croûte basaltique amphibolitisée. Etant donné que les volcans étudiés et formés dans la NIRZ ont des âges qui peuvent être aussi anciens que 12,5 Ma, il est possible d'émettre l'hypothèse que la NIRZ est active depuis au moins 12,5 Ma. Cette conclusion est en accord avec les résultats de Jancin et al. (1985) qui, à partir d'une étude sur la partie Ouest de la NIRZ, arrivent à la conclusion qu'une « proto-NIRZ » devait exister il y a 12 Ma, au même titre que Oskarsson et al. (1985) qui ont proposé une initiation de la NIRZ il y a environ 20 Ma.

Enfin, à l'image du volcan central de Refsstaðir, il semble que la partie NE de l'Islande n'a pas pu se former dans la partie Est de la NIRZ. Cette partie NE se serait alors formée plus à l'Ouest, comme par exemple au niveau de la ride de Kolbeinsey (KR). Ce ne serait qu'ensuite, par le jeu des failles transformantes de Tjörnes (TFZ), que cette partie aurait été décalée d'environ 20 - 40 km vers l'Est. Cette hypothèse a aussi l'avantage d'expliquer la flexure observée dans le tracé des lignes isochrones dans l'Est de l'Islande (Figure III-7), flexure qui est parfaitement dans l'alignement de la TFZ. Ce scénario est conforté par les conclusions de l'étude faite sur le volcan central de Fagridalur par Geirsson (1993) et qui propose lui aussi que ce volcan se soit formé au niveau de la ride de Kolbeinsey.

La reconstitution illustrée par la Figure III-7 permet de visualiser l'évolution géodynamique de l'Est de l'Islande depuis 12 Ma.

- Il y a 12 - 13 Ma, seule la partie centrale de la NIRZ était active et c'est elle qui a donné naissance aux systèmes volcaniques de Barðsnes et Reyðarjörður, alors qu'à la même période ceux de Refsstaðir et Fagridalur se forment dans la partie Sud Est de la ride de Kolbeinsey. Les volcans centraux de Njarðvik et Borgarfjörður ont le même âge que ceux de Refsstaðir et de Fagridalur, alors qu'ils sont localisés de 20 à 50 km plus à l'Est. Leur position initiale estimée est cohérente avec celle de la NIRZ actuelle ce qui permet de penser qu'ils se sont formés sur le prolongement Nord de la NIRZ.
- Entre 12 et 6 Ma, le système de failles transformantes de Tjörnes (TFZ) décale d'environ 20 - 40 km vers l'Est la partie Nord Est de l'Islande actuelle. Il en résulte que les

édifices volcaniques formés dans cette zone, vont se retrouver décalés à l'est de la NIRZ. Cette conclusion est en accord avec les résultats de Young et al. (1985) qui ont proposé que l'activité de la TFZ aurait généré un décalage d'une vingtaine de kilomètre entre 10 et 7 Ma. Ensuite, la NIRZ commence à se propager progressivement 1) vers le Nord donnant naissance aux discontinuités stratigraphiques des formations volcaniques (coulées de laves) de part et d'autres de la partie septentrionale de la NIRZ actuelle (e.g. Sæmundsson, 1979) et 2) vers le sud en engendrant des volcans de plus en plus méridionaux. Dans ce contexte, et comme l'ont déjà suggéré Furman et al. (1992b) à partir de données géochimiques et structurales, les systèmes volcaniques d'Austurhorn et de Vesturhorn pourraient résulter de l'activité de la partie Sud de la NIRZ en cours de propagation. Garcia et al. (2003) ont étudié des échantillons provenant du Nord de l'Islande et ont conclu à la formation de la NIRZ il y a environ 8 Ma. Compte tenu de leur jeu de données, il semblerait en effet plus approprié de penser que la partie Nord et non nécessairement l'intégralité de la NIRZ se soit initiée il y a environ 8 Ma, ce qui serait parfaitement cohérent avec le scénario proposé ici.

- A 6 Ma, la NIRZ possède une configuration très proche de celle que nous connaissons de nos jours. Toutefois, ce n'est que 3 Ma plus tard que la SIVZ apparaitra comme la propagation de la NIRZ vers le Sud (e.g. Sæmundsson, 1979; Oskarsson et al., 1985). Ce mécanisme de propagation de la zone de rift vers le Sud apparaît comme étant très semblable à celui qui se serait produit vers le Nord il y a environ 8 Ma.

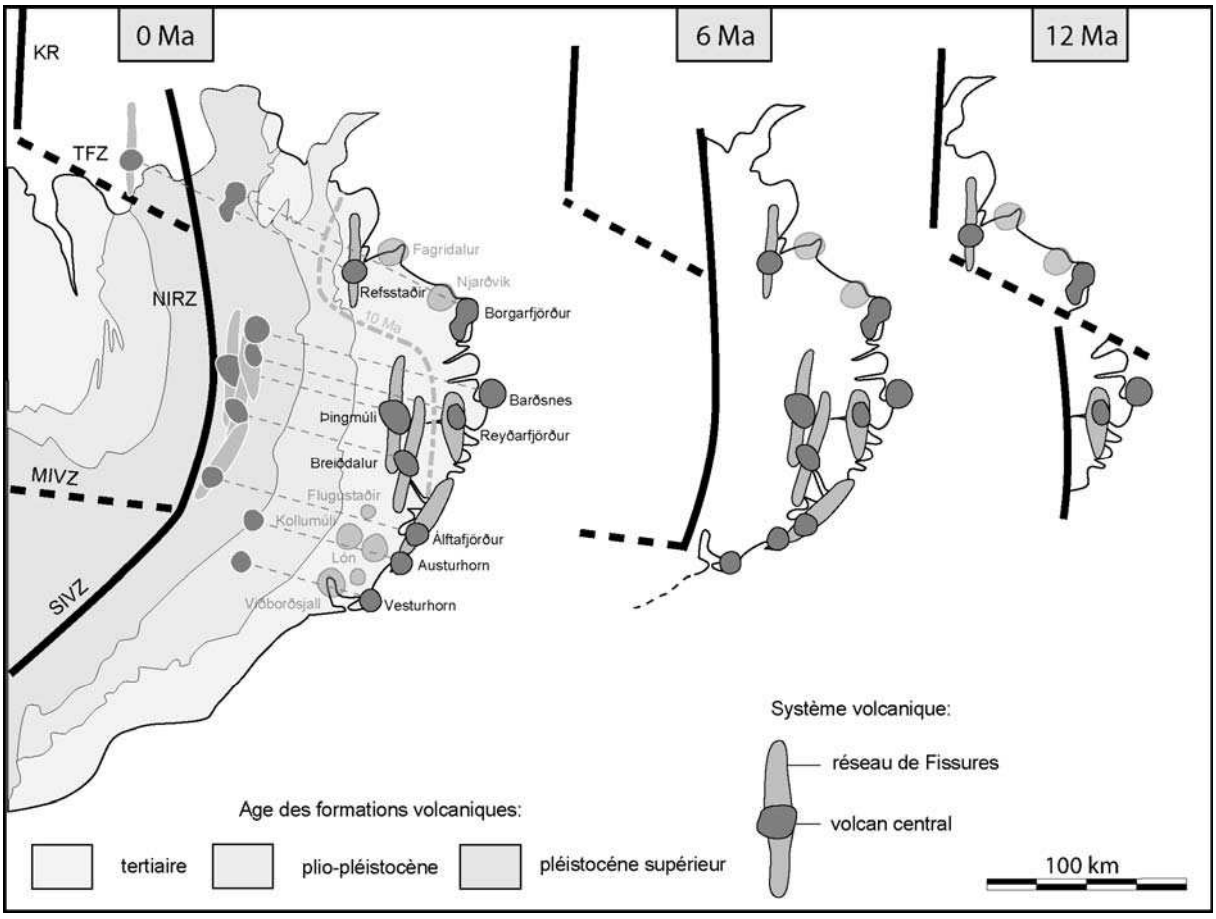

Figure III-7 : Reconstitution géodynamique de l'Est de l'Islande depuis 12 Ma. Les segments en pointillés gris illustrent la dérive des systèmes volcaniques depuis leur mise en place en considérant une demi-vitesse d'écartement de 1 cm/an. La ligne discontinue grise correspond à l'isochrone 10 Ma. KR : Kolbeinsey Ridge, TFZ : Tjörnes Fracture Zone, NIRZ : North Iceland Rift Zone, MIVZ : Mid-Iceland Volcanic Zone, SIVZ : South Iceland Volcanic Zone.

3. Modèle d'évolution géodynamique de l'Islande

Largeur énigmatique de l'Islande

Un modèle d'évolution géodynamique, afin d'être le plus réaliste possible, doit pouvoir expliquer l'une des plus grandes énigmes de l'Islande : sa largeur (par ex. Walker, 1975; Walker, 1976; Pálmason, 1981; Bott, 1985; Helgason, 1985).

Comme cela a été discuté par Foulger (2006), l'Islande fait environ 500 km dans sa plus grande largeur. D'autre part, les roches les plus anciennes sont datées à 16 Ma pour l'Ouest et à 13 Ma pour l'Est (par ex. Moorbath et al., 1968) ; Paquette et al., 2006, communication personnelle). Lorsque l'on considère un modèle de ride simple et unique, ayant une demi-vitesse d'ouverture de 1 cm/an (10 km/Ma ; par ex. Sæmundsson, 1979; Vogt et al., 1980; Nunns, 1983; DeMets et al., 1990; Sigmundsson et al., 1995; Sella et al., 2002) la

largeur maximale calculée pour l'Islande est seulement de 290 km ((16 Ma ×10 km/Ma) + (13.1Ma×10 km/Ma) = 160 + 130 km). Il en découle que les 210 km de croûte islandaise «excédentaires» ne sont pas expliqués par ce modèle et qu'ils ont nécessairement été formés antérieurement à 16 Ma. Toutefois la nature de ce morceau de croûte plus ancien que 16 Ma n'est pas connue, il pourrait s'agir d'un segment de croûte océanique aussi bien que d'une croûte continentale. Cependant, les données géochimiques disponibles permettent d'exclure une origine principalement continentale et en conséquence, ce segment crustal ne peut être que d'origine océanique. En effet, les rapports isotopiques du Sr et du Nd mesurés en Islande par exemple, ont des valeurs mantelliques et aucunement continentales. Foulger (2006) propose que cette croûte ait un âge maximum compris entre 26,5 et 37 Ma. En effet, si elle s'est formée symétriquement de part et d'autre de la ride, 10,5 Ma lui ont suffit pour atteindre une largeur de 210 km à raison d'une vitesse d'ouverture de 2 cm/an. En revanche si cette croûte s'est formée au sein d'une seule et même plaque, 21 Ma auront été nécessaire (210 km / 1 cm.an^{-1}). Lorsque l'on ajoute ces 10,5 Ma ou 21 Ma aux 16 Ma de l'âge maximum des roches islandaises, ont en déduit que les 210 km de croûte « excédentaire » ont commencé à se former entre 26,5 et 37 Ma.

En revanche les âges de 140-240 Ma mesurés sur des zircons de Hvítserkur (Nord-Est Islande ; Paquette et al., in prep) ne peuvent pas provenir de matériaux océaniques. Ils sont interprétés comme provenant de lambeaux de croûte continentale coincés sous le Nord-Est de l'Islande dans le prolongement du microcontinent de Jan Mayen.

Un autre moyen de rendre compte de la largeur actuelle de l'Islande consisterait à envisager une vitesse d'expansion supérieure à 2 cm.an^{-1}. Cette solution a déjà été envisagée pour le Nord de l'Islande par Garcia et al. (2003) qui ont proposé une vitesse de près de 3 cm/an. Un calcul simple montre que la largeur actuelle de l'Islande (500 km) pourrait être obtenue en 13-16 Ma à condition toutefois que la vitesse d'expansion soit de l'ordre de 3,4 cm/an. Cependant, de telles vitesses d'ouverture (> 3 cm/an) sont en contradiction avec les vitesses d'ouverture des zones de rift islandais qui sont de l'ordre de 2 cm/an, et aussi très supérieures à la vitesse moyenne d'ouverture de la ride médio-Atlantique Nord (~2 cm/an; Sæmundsson, 1979; Vogt et al., 1980; Nunns, 1983; DeMets et al., 1990; Sigmundsson et al., 1995; Sella et al., 2002). D'autre part, il semble difficile d'imaginer la manière dont la lithosphère océanique, dont la vitesse d'ouverture dans l'ensemble de l'Atlantique Nord est de l'ordre de 2 cm/an, pourrait mécaniquement accommoder des vitesses de plus de 3 cm/an à l'échelle de l'Islande.

Modèle proposé

La Figure III-8 illustre l'évolution géodynamique de l'Islande. Cette reconstitution repose sur 3 contraintes principales :

1) La largeur de l'Islande peut être expliquée par le « piégeage » d'un morceau d'une ancienne croûte océanique.

2) La répartition des pendages et des âges des empilements basaltiques résulte à la fois l'accrétion de la croûte islandaise elle-même et du recouvrement de l'ancienne croûte « piégée » par les formations magmatiques générées au niveau des zones de rift (processus d'accrétion-recouvrement).

3) C'est le mouvement relatif de la ride médio-océanique et du panache islandais qui permet de rendre compte de la distribution géographique des zones de rift éteintes de l'Ouest de l'Islande (par ex. Sæmundsson, 1979; Jóhannesson, 1980; Hardarson et al., 1997).

- Entre 20 et 15 Ma, le centre du panache mantellique préalablement situé sous la zone de rift du Nord-Ouest de l'Islande, se déplace vers l'ESE et initie la création de la zone de rift de Snæfellsnes-Skagi (à l'Est ; Hardarson et al., 1997). Durant cette période de transition, le panache mantellique alimente simultanément les deux zones de rift. De ce saut de ride résulte le « piégeage », entre les deux zones de rift, d'un morceau d'une ancienne croûte océanique de largeur D.
- Il y a 15 Ma, suite à la dérive continue du panache, la distance entre son centre et la ride Nord-Ouest de l'Islande devient trop grande pour que cette zone de rift puisse continuer à être « alimentée ». Par conséquent, elle « s'éteint » (Hardarson et al., 1997), et toute l'activité volcanique se concentre alors au niveau de la zone de rift de Snæfellsnes-Skagi.
- Aux alentours de 13 Ma, le panache mantellique qui s'éloigne toujours de plus en plus en direction de l'ESE initie la naissance d'une nouvelle zone de rift (future NIRZ) à une distance D' de l'axe Snæfellsnes-Skagi. Ici aussi le saut de rift s'accompagne du « piégeage » d'un segment d'une ancienne croûte océanique de telle manière que D + D' = 210 km.
- Entre 12 et 10 Ma, les extrêmes Ouest et Est de l'Islande actuelle sont déjà formés. La partie Nord-Est de l'Islande actuelle est alors générée entre la ride de Kolbeinsey et le prolongement de la NIRZ. Le centre du panache mantellique alimente ces deux principales zones de rift ainsi que la zone septentrionale qui correspond à la transition entre la ride de Kolbeinsey et la NIRZ. Une telle configuration rejoint l'idée développée par Bourgeois et al. (2005) qui suggèrent une large zone de rift (~200 km de large) dans laquelle l'activité

volcanique se serait concentrée sur ses bordures Est et Ouest. La formation de la croûte islandaise est alors assurée par le processus d'accrétion-recouvrement.

- Aux environ de 7 Ma, la distance entre le centre du panache et la zone de rift de Snæfellsnes-Skagi devient si importante que cette dernière « s'éteint » et devient inactive (cf. partie III-B-1). A partir de ce moment là, l'activité volcanique va essentiellement se concentrer au niveau de la NIRZ et de la RRZ. Cette dernière, créée dans le prolongement de la ride de Reykjanes, est reliée à la NIRZ par la MIVZ.

- Depuis 3 Ma, la SIVZ représente la propagation de la NIRZ vers le Sud (par ex. Sæmundsson, 1979; Oskarsson et al., 1985) où elle remplace progressivement la RRZ. L'activité de la SIVZ va permettre par accrétion-recouvrement la formation de la partie Sud-est de l'Islande.

- Actuellement le centre du panache islandais est localisé sous la partie Nord-est du glacier Vatnajökull, c'est-à-dire à l'intersection de la NIRZ, MIVZ et SIVZ. Ceci permet alors une concentration de l'activité volcanique au sein de la NIRZ et de la SIVZ, en n'excluant toutefois pas un volcanisme actif localisé sur la Péninsule de Snæfellsnes.

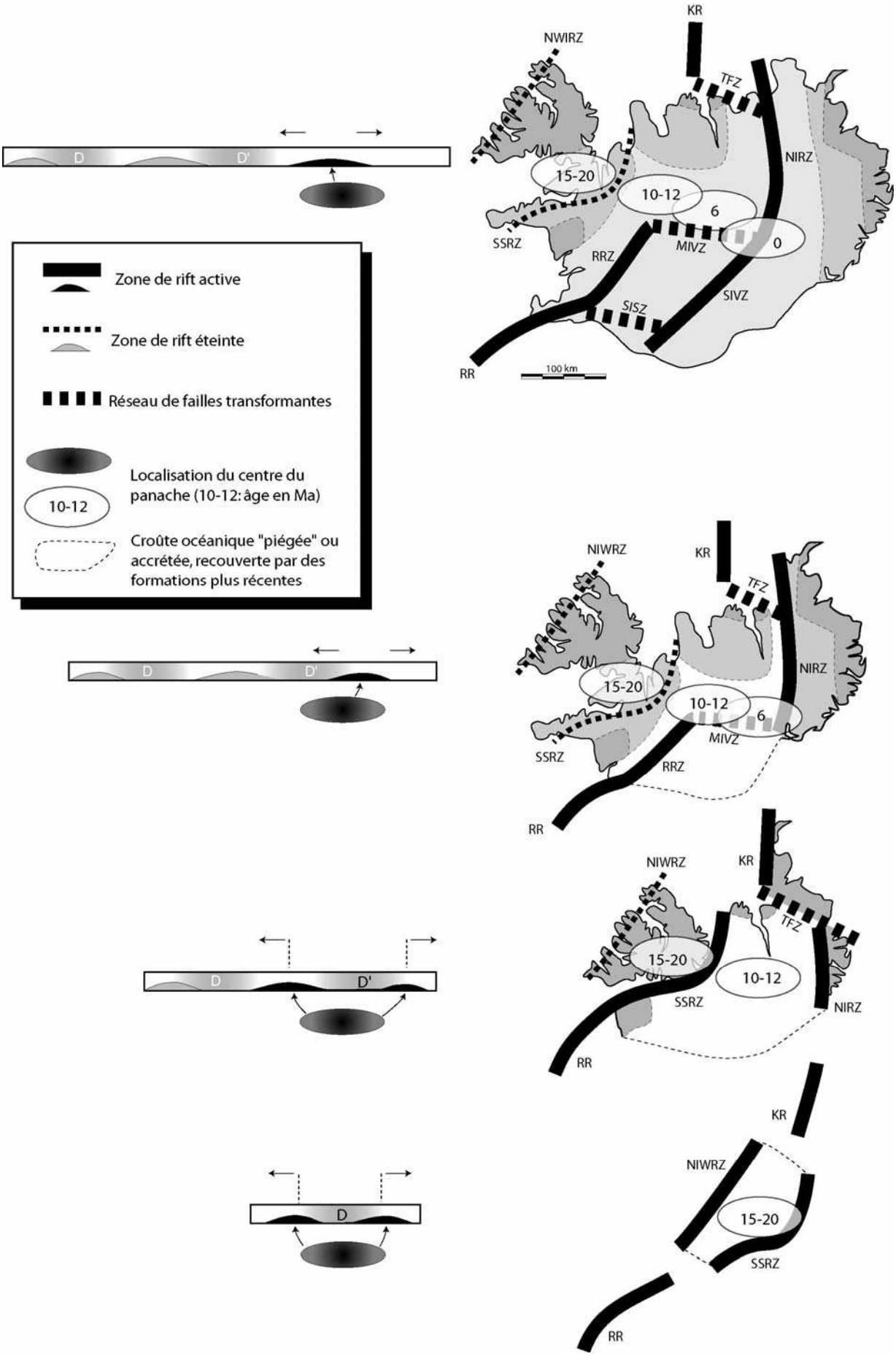
KR
NWIRZ
TFZ
NIRZ
15-20
10-12
6
0
SSRZ
RRZ
MIVZ
SISZ
SIVZ
RR
100 km
D
D'
Zone de rift active
Zone de rift éteinte
Réseau de failles transformantes
Localisation du centre du panache (10-12: âge en Ma)
10-12
Croûte océanique "piégée" ou accrétée, recouverte par des formations plus récentes
NIWRZ
KR
TFZ
NIRZ
15-20
10-12
6
MIVZ
SSRZ
RRZ
RR
NIWRZ
KR
TFZ
15-20
10-12
SSRZ
NIRZ
RR
D
D'
KR
NIWRZ
15-20
SSRZ
RR
D

Figure III-8 : Reconstitution de l'évolution géodynamique de l'Islande. La vitesse d'expansion considérée est de 2 cm/an. D+D'= 210 km d'ancienne croûte océanique « piégée ». Voir la discussion dans le texte pour de plus amples discussions. Ride médio-atlantique : KR = Kolbeinsey Ridge et RR = Reykjanes Ridge; Zones de rift actif, et d'activité volcanique et sismique : NIRZ = North-Iceland Rift Zone ; RRZ = Reykjanes Rift Zone ; MIVZ = Mid-Iceland Volcanic Zone ; SIVZ = South-Iceland Volcanic Zone; TFZ = Tjörnes Fracture Zone et SISZ = South-Iceland Seismic Zone. Zones de rift éteintes : NWIRZ = North-West-Iceland Rift Zone et SSRZ = Snæfellsnes-Skagi Rift-Zone.

Evolution future

Les principales caractéristiques géologiques actuellement observables en Islande sont bien expliquées par un mouvement de dérive relatif du panache mantellique par rapport à la ride médio-atlantique. En envisageant que ce mouvement relatif se poursuive pendant encore quelques millions d'années, il semble possible de prédire quelle sera l'évolution géodynamique future de l'Islande. En effet, à l'aplomb du centre du panache, la zone de rift se décale (par sauts successifs) dans le temps pour accommoder le déplacement relatif du point chaud par rapport à la ride médio-Atlantique. Ceci explique la position actuelle du rift, anormalement décalé vers l'Est par rapport à l'ensemble de la ride médio-Atlantique. Tout se passe donc comme si le panache « retenait » de plus en plus la zone de rift vers l'Est. De toute évidence dans quelques millions d'années, le panache se sera encore déplacé vers l'Est de telle sorte que sa position deviendra tellement excentrée par rapport à l'ensemble de la ride médio-Atlantique qu'il ne pourra plus la « retenir ». Ainsi le panache islandais sera dissocié de la ride et se retrouvera en position intra-plaque océanique à l'image de celui d'Hawaii. Un tel scénario a déjà été observé au cours de l'évolution du plateau océanique de Kerguelen. Ce dernier qui se trouvait à l'aplomb de la ride SE indienne il y a ~40 Ma, se trouve actuellement en position intra-plaque (Gautier et al., 1990).

Chapitre IV : Genèse de la croûte continentale primitive : rôle des plateaux océaniques

En Islande, l'interaction entre la ride médio-Atlantique et le point chaud constitue un environnement géodynamique exceptionnel dont résulte la formation de volumes exceptionnellement importants (10%) de roches magmatiques acides, et ce en plein milieu océanique. Ces roches magmatiques de composition acide, du fait de leur relativement faible densité possèdent une grande flottabilité, ce qui fait que contrairement aux roches de la croûte océanique, elles sont difficilement recyclables dans le manteau. Ces caractéristiques font que l'Islande pourrait être considéré comme la nucléation d'un continent. En effet, plusieurs auteurs (par ex. Marsh et al., 1991; Sigmarsson et al., 1991) ayant étudié et discuté le mode de genèse de ces roches acides ont émis l'hypothèse que l'Islande puisse être un analogue actuel du mode de genèse de la proto-croûte continentale terrestre, à l'Archéen voire même à l'Hadéen.

En effet, le modèle le plus communément admis pour l'origine de la croûte continentale primitive terrestre est la fusion hydratée des basaltes de la croûte océanique entrant en subduction (par ex. Martin, 1986; Condie, 1989; Rollinson, 1997; Albarède, 1998; Barth et al., 2002a; Barth et al., 2002b; Foley et al., 2002; Martin and Moyen, 2002; Kamber et al., 2003). Le chapitre précédent a déjà permis de montrer que la majorité des roches acides islandaises sont issues de la fusion hydratée du plateau océanique islandais. Dans les deux cas c'est la fusion hydratée d'un basalte qui est supposée être à l'origine de ces roches de type continental.

En se basant sur une compilation des données géochimiques disponibles des roches acides des trois plus grands plateaux océaniques du monde, l'Islande, Hawaii et Kerguelen, ce chapitre va tenter de comparer celles-ci de façon directe avec les TTG de la croûte continentale primitive. Le but de ce chapitre sera de discuter du rôle des plateaux océaniques dans la genèse de la croûte continentale primitive et plus particulièrement sur la viabilité d'un modèle de type « islandais » comme un analogue à la formation de la proto-croûte continentale et comme alternative possible au modèle de subduction.

A. Le modèle « islandais » est-il un analogue de la formation de la croûte continentale primitive ?

1. Article : “Can Iceland be a modern analogue of Earth’s early continental crust? “, à soumettre

Can Iceland be a modern analogue of Earth's early continental crust?

Martin E.[1], Martin H.[1] and Sigmarsson O. [1,2]

1) Laboratoire Magmas et Volcans, OPGC - Université Blaise Pascal – CNRS, 5 rue Kessler, 63038 Clermont-Ferrand, France.

2) Institute of Earth Sciences, University of Iceland, 101 Reykjavik, Iceland.

E-mail: E.Martin@opgc.univ-bpclermont.fr

Abstract

A study of the major and trace element patterns of silicic rocks from modern oceanic plateaus shows that they are drastically different compared to Archaean TTG ones, thus demonstrating that they generated through contrasted mechanisms and/or sources. In most oceanic plateaus, felsic magmas differentiated by fractional crystallization of basalts. However, due to the interaction between mantle plume and mid-Atlantic ridge that induce abnormally high geothermal gradients, most of felsic magmas from Iceland are produced by partial melting of a partially hydrated oceanic crust. Nevertheless, this melting takes place at shallow depths and is unable to generate TTG-like magmas. This is probably due to the lack of an efficient hydration of the lower part of Iceland thick crust. Therefore, data suggest that the early Earth continental crust could not be significantly generated in oceanic plateau environments. However, subduction of oceanic plateaus could account for the episodic increase of the continental crust growth during the whole Earth history.

Introduction

Today, the continental crust has the average composition of granodiorite, which due to its buoyancy prevents its significant recycling into the mantle. Contrarily to core formation that probably took place in less than 50Ma (Yin et al., 2002; Kleine et al., 2004), the continental crust extraction from the mantle is a slow continuous but irregular process that started 4.4 Ga ago and that continues today (Albarède, 1998; Condie, 1998; Wilde et al., 2001; Cavosie et al., 2005). Presently, most juvenile crust is generated in subduction environment where intermediate to felsic magmas are produced, either by melting of fluid

metasomatised peridotite or by directed melting of the subducted slab. These magmas can subsequently evolve and differentiate by fractional crystallisation and crustal contamination. If subduction geodynamic environment is the most favourable for juvenile crust genesis, felsic magmas are also generated in oceanic plateaus, such in Iceland, Hawaii and Kerguelen. There, petrogenetic mechanisms are the fractional crystallisation of basaltic magmas or the melting of the hydrated basaltic crust (e.g. Marsh et al., 1991; Cousens et al., 2003; Gagnevin et al., 2003; Martin and Sigmarsson, 2006a; Shamberger and Hammer, 2006). Since many years, several authors proposed that, during Archaean or Hadean times, in plate tectonics environments dominated by plume dynamics (Smithies et al., 2005), the primitive continental crust could have formed in an Iceland-like geodynamic environment (e.g. Marsh et al., 1991; Sigmarsson et al., 1991).

The purpose of this paper consists of 1) establishing the geochemical signature of felsic rocks generated in oceanic plateau environment, 2) comparing them to the composition of the Archaean crust and 3) discussing the possible role played by oceanic plateaus in early continental crust genesis.

Geochemical characteristics

Oceanic plateaus

Today, plume activity results in the genesis of Large Igneous Provinces (LIP; or oceanic plateaus), which composition is mainly basaltic with minor amounts of felsic magmas. These later are well recognized in the biggest emerged oceanic plateaus such as Iceland, Hawaii and Kerguelen. Hawaii is a typical intra-plate plateau, located in the middle of the Pacific plate. By contrast, Iceland has an exceptional position at a plate boundary, where the mantle plume interacts with the mid-Atlantic ridge. If today the Kerguelen plateau is located in the middle of the Antarctic plate, its situation was different ~40 Ma ago when it was located on the South East Indian Ridge (e.g. Gautier et al., 1990).

These three oceanic plateaus are overwhelmingly composed of tholeiitic to alkalic basalts whereas felsic rocks only appear in much subordinated amounts. Nevertheless, in Iceland, the volume of silicic rocks is abnormally high (10 % of the emitted lavas) which is interpreted as reflecting the unusual geodynamic environment where high geothermal gradients result of the interaction between the mantle plume and the mid-Atlantic ridge (e.g. Marsh et al., 1991).

In Iceland, silicic magmas range from tholeiitic (dacite and rhyolite) to alkaline (rhyolite and trachyte), whereas Hawaii and Kerguelen are dominated by alkaline felsic rocks (trachyte, phonolite and rhyolite). In a normative Qz-Or-(An+Ab)-Ne diagram (Figure 1), Hawaii and most of Kerguelen rocks plot close to the Or-(An+Ab) line or even in the Ne-bearing rock domain; by contrast, all Iceland samples have normative Qz > 10%.

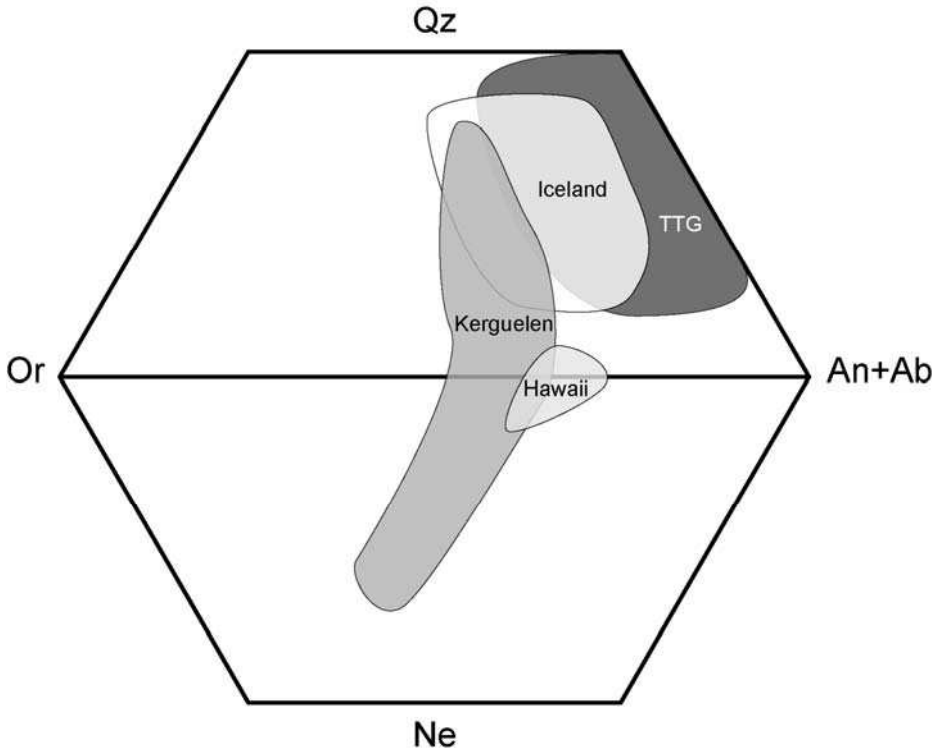

Figure 1 : CIPW normative quartz – orthoclase – anorthite + albite – nepheline (Qz-Or-(An+Ab)-Ne) diagram, showing the composition of Archaean TTG and felsic rocks from Iceland, Hawaii and Kerguelen.

The Table 1 shows that all felsic rocks from oceanic plateaus are characterized by SiO_2 > 60 % with moderately high (Fe_2O_3 + MgO + MnO + TiO_2) contents (from 4.4 to 5.5 %). However, all display low Mg# (~ 0.2). They are alkali-rich (8 % < Na_2O + K_2O < 12 %) with relatively high K_2O/Na_2O (from 0.6 up to 0.9). Iceland felsic magmas slightly differ from Hawaii and Kerguelen by the fact that they have a higher Mg#; they are alkali-poorer and consequently SiO_2 -richer (Table 1).

Table 1: Average major and trace element composition of primitive continental crust (Archaean TTG) and felsic rocks from oceanic plateaus of Iceland, Hawaii and Kerguelen.

	Archaean TTG			Iceland			Hawaii			Kerguelen		
	Mean	*CI*	*n*	Mean	*CI*	*n*	Mean	*CI (2σ)*	*n*	Mean	*CI*	*n*
SiO_2	68.8	*0.2*	*1104*	69.2	*0.4*	*434*	62.6	*0.5*	*47*	62.8	*0.7*	*99*
Al_2O_3	15.5	*0.1*	*1104*	14.1	*0.2*	*424*	18.4	*0.6*	*46*	17.4	*0.5*	*99*
Fe_2O_3*	3.24	*0.09*	*1104*	4.11	*0.21*	*434*	3.85	*0.95*	*47*	3.39	*0.50*	*99*
MnO	0.05	*0.00*	*1030*	0.12	*0.01*	*424*	0.28	*0.02*	*36*	0.13	*0.01*	*99*
MgO	1.25	*0.05*	*1103*	0.63	*0.05*	*402*	0.48	*0.06*	*37*	0.41	*0.07*	*99*
CaO	3.15	*0.07*	*1104*	2.04	*0.11*	*370*	1.32	*0.36*	*47*	1.23	*0.16*	*99*
Na_2O	4.67	*0.05*	*1104*	4.91	*0.12*	*433*	7.50	*0.21*	*47*	6.29	*0.27*	*99*
K_2O	1.92	*0.05*	*1104*	3.15	*0.12*	*434*	4.27	*0.36*	*46*	5.65	*0.24*	*99*
TiO_2	0.38	*0.01*	*1104*	0.66	*0.05*	*250*	0.52	*0.04*	*36*	0.45	*0.05*	*99*
P_2O_5	0.14	*0.01*	*934*	0.08	*0.01*	*383*	0.15	*0.03*	*36*	0.13	*0.03*	*99*
Mg#	0.43			0.23			0.20			0.19		
Rb	65.0	*2.8*	*981*	90.1	*4.6*	*161*	132	*4*	*24*	132	*21*	*43*
Sr	489	*14*	*996*	108	*11*	*179*	29.9	*5.5*	*23*	60.7	*25.6*	*43*
Y	11.5	*1.1*	*788*	93.6	*6.1*	*158*	68.7	*6.3*	*24*	43.3	*5.9*	*43*
Zr	156	*8*	*858*	650	*49*	*160*	847	*33*	*24*	767	*130*	*43*
Nb	7.1	*0.4*	*545*	99.0	*9.1*	*140*	126	*4*	*24*	114	*18*	*43*
Ba	713	*34*	*866*	500	*35*	*168*	392	*52*	*23*	261	*156*	*39*
La	31.1	*1.9*	*629*	81.7	*7.4*	*120*	71.4	*6.0*	*23*	106	*15*	*28*
Ce	57.8	*3.6*	*655*	172	*14*	*127*	138	*10*	*20*	204	*29*	*28*
Nd	22.7	*1.5*	*537*	78.1	*6.1*	*108*	62.9	*6.2*	*22*	75.5	*9.2*	*28*
Sm	3.49	*0.22*	*527*	17.1	*1.1*	*110*	11.5	*1.6*	*16*	13.6	*2.0*	*28*
Eu	0.91	*0.04*	*525*	2.85	*0.26*	*110*	2.81	*0.31*	*16*	1.81	*0.48*	*28*
Gd	2.43	*0.13*	*517*	15.2	*1.1*	*66*	9.87	*1.29*	*15*	12.0	*3.8*	*7*
Tb	0.33	*0.02*	*350*	2.73	*0.17*	*108*	1.62	*0.22*	*16*	1.45	*0.23*	*22*
Dy	1.66	*0.12*	*260*	16.7	*1.5*	*40*	10.2	*1.2*	*15*	10.4	*4.3*	*7*
Er	0.79	*0.07*	*229*	9.50	*0.93*	*42*	5.98	*0.66*	*15*	5.70	*2.67*	*7*
Yb	0.66	*0.04*	*507*	8.97	*0.56*	*98*	5.88	*0.59*	*16*	4.51	*0.69*	*28*
Lu	0.13	*0.01*	*411*	1.35	*0.08*	*110*	0.95	*0.09*	*16*	0.64	*0.07*	*21*
Hf	3.95	*0.32*	*223*	18.8	*1.5*	*92*	18.8	*1.7*	*16*	20.6	*2.9*	*21*
Ta	0.78	*0.14*	*201*	7.63	*0.86*	*91*	7.76	*0.63*	*15*	8.50	*2.13*	*21*
Th	6.73	*0.60*	*420*	12.7	*0.9*	*135*	8.84	*0.41*	*23*	22.8	*6.9*	*21*
U	1.46	*0.16*	*280*	3.57	*0.33*	*91*	1.94	*0.34*	*15*	5.29	*1.67*	*20*
V	47.9	*2.9*	*408*	18.8	*5.3*	*63*	5.75	*1.36*	*16*	2.54	*1.21*	*15*
Cr	37.8	*3.3*	*573*	9.27	*2.66*	*95*	6.26	*1.91*	*23*	3.60	*0.66*	*12*
Ni	18.7	*1.6*	*531*	7.82	*1.46*	*101*	8.19	*2.80*	*21*	7.78	*1.58*	*19*

Oceanic plateaus compositions are compiled from GEOROC database (http://georoc.mpch-mainz.gwdg.de/georoc/).n: number of compiled values and CI: Confidence Interval in 2σ.

REE contents are high (La_N > 250 and Yb_N >20) resulting in moderately fractionated patterns (6 < $(La/Yb)_N$ < 15) with slight negative Eu anomaly (Figure 2A). When, plotted in a primitive mantle normalized multi-element diagram (Figure 2B), all oceanic plateau felsic lavas display high contents in most trace element, except for Ba, Sr and Ti that draw very strong negative anomalies. Transition element contents are generally low (Ni < 8.2 ppm, Cr <

10 ppm, V < 18 ppm; Table 1), however silicic lavas from Hawaii and Kerguelen have transition element content systematically lower than in their Icelandic equivalents.

Classically, felsic rocks in oceanic plateaus, as in Hawaii and Kerguelen, are considered as generated by high degrees of fractional crystallisation of basaltic magma (e.g. Cousens et al., 2003; Gagnevin et al., 2003; Shamberger and Hammer, 2006), which accounts for their high incompatible element content. Fractional crystallisation is also a powerful process for depleting residual liquid in highly compatible elements, which is perfectly consistent with the very low transition element contents. In addition, the strong negative anomalies in Ba, Sr and Eu are indicative of large-scale feldspar fractionation. Due to its peculiar geodynamic environment, it has been proposed that in Iceland, together with subsequent fractional crystallisation, partial melting of hydrated basalts have played an important role in felsic magma genesis (Martin and Sigmarsson, 2006a, references therein). The role of partial melting is supported by higher transition element content (as well as slightly higher Mg#) in Iceland compared to Hawaii and Kerguelen. There, the lower alkali content could reflect the implication of the peculiar mantle source, which generates less alkaline basalt and consequently felsic magmas, than in other oceanic plateaus. The bigger amounts of silicic rocks in Iceland, relatively to others oceanic plateaus, points that partial melting is a more efficient process than fractional crystallisation in generating felsic magmas.

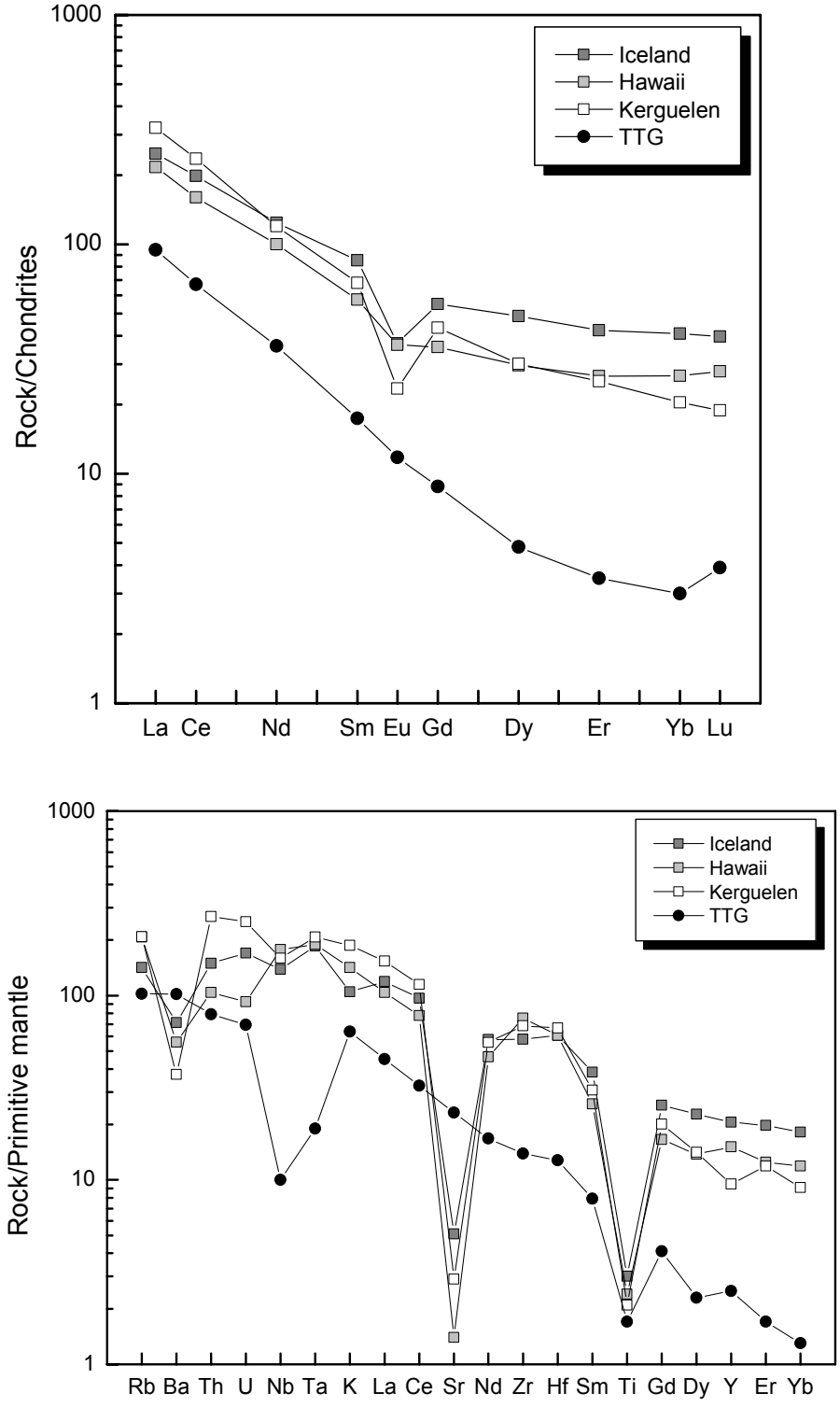

Figure 2: A) Chondrite-normalized (Nakamura, 1974) Rare Earth Element and B) Primitive mantle-normalized (Sun and McDonough, 1989) multi-element diagrams comparing the average Archaean continental crust composition (TTG) with those of oceanic plateaus of Iceland, Hawaii and Kerguelen.

Archaean TTG

The database used for this study contains 1104 analyses of Archaean TTG whose ages range from 4.0 up to 2.5 Ga. These plutonic rocks have trondhjemitic affinities (Martin, 1987; Martin et al., 2005) and in the Figure 1 they plot along the Q-(An+Ab) side of the diagram, thus demonstrating their relative poverty in normative Or.

TTG are characterized by SiO_2 contents > 60% with moderately high (Fe_2O_3 + MgO + MnO +TiO_2) contents (4.9 %). The Mg# is high for silicic magmas (0.43) and their alkali content is moderate ($Na_2O + K_2O$ = 6.6%) with low K_2O/Na_2O (0.4; Table 1).

TTG are LREE rich (La_N ~100) but HREE contents are very low (Yb_N ~3.2) with a typical concave shape, it results in strongly fractionated pattern $(La/Yb)_N$ ~30) with no Eu anomaly (Figure 2A). In a primitive mantle normalized multi-element diagram (Figure 2B), TTG display a quite regular pattern except for a strong negative anomaly in Nb and Ta and to a less extent in Ti. Transition element contents are relatively high for felsic magmas (Ni ~19 ppm, Cr ~38 ppm, V ~ 48 ppm).

Most researchers consider that TTG were generated by partial melting of hydrated basalt. In such a case, (1) the basalt was previously underplated beneath a thickened crust (Arndt, 1992; Rudnick, 1995; Albarède, 1998) and partially melted due to mantle plume activity or (2) the basalt corresponds to a subducted hot oceanic slab that melted instead of dehydrated (Martin, 1986; Condie, 1989; Rollinson, 1997; Albarède, 1998; Barth et al., 2002a; Barth et al., 2002b; Foley et al., 2002; Martin and Moyen, 2002; Kamber et al., 2003). Recently, Kamber et al. (2002) and Kleinhanns et al. (2003) also proposed that TTG generated in a subduction environment but by extensive fractional crystallization of a basaltic magma.

The genetic models proposed for oceanic plateaus also refer to either large-scale fractional crystallisation of basaltic magmas or partial melting of a hydrated basaltic crust. This is the reason why TTG will be compared with oceanic plateaus felsic magmas.

Discussion

Comparison TTG-Oceanic plateaus

Na_2O and K_2O

The alkali content in oceanic plateaus is very high (Na2O + K2O ~ 11.8 %) when compared with TTG (6.6 %). This is interpreted in terms of both degree of melting and source composition. Martin and Sigmarsson (2006b) showed that the composition of felsic melts (i.e. K2O/ Na2O) is primarily controlled by the composition of the parental magma. In mantle plume environment the basaltic precursors are already alkali rich, which combined with low degrees of differentiation can easily generate alkali-rich felsic magmas (Na2O + K2O > 11 %). TTG, considered as generated by 20 to 30 % melting of a tholeiite (Martin, 1987) would logically produce alkali-poorer differentiated magmas. In Iceland where basalts result from interaction between ridge and plume activity, the felsic magma alkali contents are intermediate between typical oceanic plateau and TTG (Na2O + K2O ~ 8.1 %).

HREE

The HREE show a stark contrast between Archaean TTG where average YbN ~3.2, whereas in oceanic plateaus felsic magmas YbN >20. Since many years, it has been demonstrated that in the Archaean TTG, the low HREE contents are due to garnet fractionation possibly associated with hornblende (Condie, 1986; Martin, 1987; Rapp et al., 1991; Wolf and Wyllie, 1994, among others). Indeed, in intermediate to felsic magmas, garnet has $D_{Yb}^{grt/liq} \approx 20$ and hornblende $D_{Yb}^{hbd/liq} \approx 2$ whereas all other major mineral phases have $D_{Yb}^{\min/liq} << 1$. In addition, the concave HREE-end of TTG is also accounted by the fractionation of these minerals. Consequently, in oceanic plateaus, the systematically high HREE contents in felsic rocks demonstrate that garnet was not a residual or cumulative phase during the differentiation processes. Whatever could be the mechanism of felsic rock genesis in oceanic plateaus, it can be concluded that contrarily to Archaean TTG, this mechanism took place at shallow depth, out of the garnet stability field.

Ba, Sr and Eu

In oceanic plateaus, felsic rocks also differ from Archaean TTG by their strong negative anomalies in Ba, Sr and Eu, which point to the prominent role played by fractional crystallisation of plagioclase to K-feldspar (Martin and Sigmarsson, 2006a). Indeed, fractional crystallisation is by far a more efficient process than partial melting able to impoverish the

liquid in compatible elements. In addition, the stability of plagioclase during the genesis of these rocks supports the assumption that, contrarily to Archaean TTG, they were generated at shallow depth.

Transition elements and Mg#

In most intermediate and felsic magmas, transition elements and Mg have a strong compatible behaviour and consequently, as for Ba, Sr and Eu, fractional crystallisation will be a more powerful magma impoverisher process than partial melting. Accordingly, the low transition element content and Mg# in all oceanic plateaus felsic rocks also supports their genesis by fractional crystallisation. However, in Iceland, transition element contents as well as Mg#, are not as low as in Hawaii and Kerguelen, which could reflect the more important role played by partial melting mechanisms. In Archaean TTG both Mg# and transition element contents are significantly greater than in oceanic plateaus. This could also support the hypothesis of their genesis mainly through partial melting mechanisms. However, most TTG have Mg# and transition element contents higher than those determined in experimental high-pressure melting of basaltic material, which is interpreted in terms of interaction of TTG parental magma with mantle peridotite (e.g. Maury et al., 1996; Rapp et al., 1999; Smithies, 2000; e.g. Martin and Moyen, 2002). By contrast, the low contents of these elements in oceanic plateaus felsic rocks preclude any interaction with ultramafic material.

Nb and Ta anomalies

Another big difference consists in the strong Nb-Ta negative anomaly in Archaean TTG, which is totally lacking in oceanic plateaus. In TTG, as well as in modern adakites, this anomaly is generally considered as reflecting the fractionation of Fe-Ti oxides and more particularly rutile (Foley et al., 2002; Rapp et al., 2003; Schmidt et al., 2004; Xiao et al., 2006). Here too, the presence of residual or cumulative rutile during differentiation processes points to pressures greater than 12 kbars.

Role played by oceanic plateaus in continental crust genesis

Obviously, Archaean TTG and magmas generated today in oceanic plateau environment have very contrasted composition, which indicate different petrogenetic mechanisms and/or sources. Indeed, the HREE depletion in Archaean TTG as well as their Ti, Nb and Ta negative anomalies point to the differentiation of both garnet and rutile, which

implies a deep source (P > 12 kbar). The lack of these geochemical characteristics and the strong Ba, Sr and Eu negative anomalies, indicates that felsic magmas from oceanic plateaus are generated in feldspar stability conditions, thus demonstrating a shallow depth differentiation. Similarly, in Archaean TTG, the high transition element contents and high Mg# values are interpreted as reflecting interactions between TTG melts and peridotite (e.g. Schiano et al., 1995; Maury et al., 1996; Rapp et al., 1999; Smithies, 2000; e.g. Martin and Moyen, 2002). These imply that the magmatic source is located at great depth; under a mantle slice thick enough for that significant interactions can take place. The transition element paucity and the low Mg# in felsic magmas from oceanic plateaus preclude any interaction with mantle peridotite and thus are consistent with shallow petrogenesis.

In all aspects, the modern oceanic plateaus environments, if able to produce small amounts of felsic magmas are unable to give rise to Archaean TTG composition. The best evidence in favour of the Archaean subduction model is that today, when Archaean-like thermal regimes are created in subduction environments, TTG-like magmas (adakites) are generated (Martin, 1986; Defant and Drummond, 1990; Drummond and Defant, 1990; Martin, 1999). By contrast, even when in exceptional high thermal conditions, comparable to Archaean ones are present in oceanic plateaus environment, as in Iceland, no TTG-like magma is generated. Consequently, present felsic magmatism in oceanic plateau cannot be considered as modern analogue of Archaean magmatism.

Oceanic plateaus crustal thickness could be as high as 40 km as expected in Iceland (Kaban et al., 2002, and references therein). Therefore, garnet and rutile should be stable in lower part of the thick oceanic plateaus. The lack of HREE, Ti, Ta and Nb depletions in silicic magmas lead to the conclusion that, petrogenestic mechanisms and more particularly the most efficient one, crustal partial melting, take place at high crustal level, out of the garnet and rutile stability field. In addition, it could be suggested that, the depth of crustal melting could also be controlled by water availability, or by the degree of crustal alteration (hydration). Indeed, basalts, generated in a rift system could have suffered hydrothermal alteration, whereas underplated basalts should mostly remain dry. This assumption could be corroborated by the fact that in Kerguelen, deep enclaves are re-equilibrated under granulite facies conditions, which indicates a water-poor environment (Grégoire et al., 1998). It appears that in Iceland, the high rift zone hydrothermal activity is not efficient enough to hydrate the 30 - 40 km deep crust. Therefore, it could be proposed that, according to the Pálmason (1986) model, the lower crust is generated by subsidence of the partially hydrated lava piles from the

central part of the rift zone during its drifting away, but that the subsidence is too slow to maintain significant water content in the lower crust.

If Archaean continental crust cannot have been generated in an oceanic plateau environment, it could therefore be considered that during Hadean times, when plume tectonics has been considered as a dominant process (Smithies et al., 2005), early "proto-continental crust" could result from melting of a thick oceanic plateau environment. It must be noted that, even when transposed to Early Earth this mechanism does not provide a reliable process able to hydrate the lower part of a thick oceanic plateau. Recently, zircon crystals, extracted from Jack Hills meta-quartzites in Australia gave ages ranging from 4.4 to 4.0 (Wilde et al., 2001; Cavosie et al., 2004; Cavosie et al., 2005), which demonstrate that continental crust developed and grew all along Hadean times. Moreover, the REE content of these zircons, shows that the host magmas were LREE-enriched and HREE-depleted (Wilde et al., 2001), similarly to Archaean TTG. In the same way, *Type-1* zircons from Jack Hills have the same REE patterns as Acasta gneiss ones that are TTG in composition (Hoskin, 2005). Consequently, very probably Jack Hills zircons crystallised in TTG-type felsic magma. Based on a Hf isotope study of these zircons, Harrison et al. (2005) concluded that both continental crust genesis and plate tectonics began during the first 100-150 Ma of Earth history. Consequently, it also seems that the early (4.4 Ga) continental crust was already TTG in composition with a geochemical signature clearly different from that observed in felsic magmas generated in modern oceanic plateaus environments.

Does this mean that oceanic plateaus never played any significant role in continental crust genesis? Today, in some peculiar environments, oceanic plateaus are subducted. For instance, in Ecuador, the Carnegie ridge, which is generated by the Galapagos hot spot activity, is subducted under the South American plate since 5 Ma (Gutscher et al., 2000; Sallares and Charvis, 2003). There, the volcanic activity is more important than in other parts of Andes and results in larger arc and adakite generation (Samaniego et al., 2002; Bourdon et al., 2003; Samaniego et al., 2005; Hidalgo et al., 2007). It seems that increase of magmatic activity can result from basaltic oceanic plateau subduction.

Throughout the whole Earth history, crustal growth proceeded by super-events (i.e. 3.8, 2.7, 1.8, 1.1 and 0.5 Ga), each typically lasting 250 to 350 Ma (Condie, 1993; McCulloch and Bennet, 1993). Several authors consider that mantle plume activity could be responsible for the periodicity of Earth crustal production (Stein and Hofmann, 1994; Albarède, 2006).

Albarède (1998) proposed that oceanic plateaus, when entering in subduction are able to undergo partial melting and to generate continental crust. As subduction of oceanic plateaus corresponds to a significant increase of the volume of warm basalt subducted, it logically results that the volume of juvenile continental crust also significantly increases, resulting in an episodic crustal growth.

Conclusion

Iceland, with abnormally high thermal regime is probably the modern oceanic plateau that best fits the Early Earth conditions; however, it appears unable to give rise to TTG-like magmas. Consequently, Iceland cannot be regarded as a modern analogue of Earth proto-crust genesis environment. This is probably mainly due to the lack of efficient processes able to hydrate the lower part of a thick crust. Whatever it is, felsic magmatism in oceanic plateaus always remains a largely subordinated mechanism when compared with the efficiency of subduction. However, oceanic plateaus, when subducted, could be responsible of the episodic increase of the continental crust growth during the earth history.

References

Albarède, F., 1998. The growth of continental crust. Tectonophysics, 296: 1-14.

Albarède, F., 2006. The formation of the crust of the rocky planets and the mineral environment of the origin of life. In: M. Gargaud, P. Claeys and H. Martin (Editors), Lectures in Astrobiology. Springer, Heidelberg, pp. 75-102.

Arndt, N.T., 1992. Rate and mechanism of continent growth in the Precambrian. In: S. Maruyama (Editor), Evolving Earth Symposium, Okazaki, pp. 38-41.

Barth, M.G., Foley, S.F. and Horn, I., 2002a. Partial melting in Archaean subduction zones: constraints from experimentally determined trace element partition coefficients between eclogitic minerals and tonalitic melts under upper mantle conditions. Precambrian Research, 113: 323-340.

Barth, M.G., Rudnick, R.L., Carlson, R.W., Horn, I. and McDonough, W.F., 2002b. Re---Os and U---Pb geochronological constraints on the eclogite-tonalite connection in the Archean Man Shield, West Africa. Precambrian Research, 118(3-4): 267-283.

Bourdon, E., Eissen, J.-P., Gutscher, M.-A., Monzier, M., Hall, M.L. and Cotten, J., 2003. Magmatic response to early aseismic ridge subduction: the Ecuadorian margin case (South America). Earth and Planetary Science Letters, 205(3-4): 123-138.

Cavosie, A.J., Valley, J.W., Wilde, S.A. and E.I.M.F., 2005. Magmatic [delta]18O in 4400-3900 Ma detrital zircons: A record of the alteration and recycling of crust in the Early Archean. Earth and Planetary Science Letters, 235(3-4): 663-681.

Cavosie, A.J., Wilde, S.A., Liu, D., Weiblen, P.W. and Valley, J.W., 2004. Internal zoning and U-Th-Pb chemistry of Jack Hills detrital zircons: a mineral record of early Archean to Mesoproterozoic (4348-1576 Ma) magmatism. Precambrian Research, 135: 251-279.

Condie, K.C., 1986. Origin and early growth rate of continents. Precambrian Research, 32: 261-278.

Condie, K.C., 1989. Plate tectonics and crustal evolution. Pergamon, Oxford, 476 pp.

Condie, K.C., 1993. Chemical composition and evolution of the upper continental crust: contrasting results from surface samples and shales. Chemical Geology, 104: 1-37.

Condie, K.C., 1998. Episodic continental growth and supercontinents: a mantle avalanche connection? Earth and Planetary Science Letters, 163(1-4): 97-108.

Cousens, B.L., Clague, D.A. and Sharp, W.D., 2003. Chronology, chemistry, and origin of trachytes from Hualalai volcano, Hawaii. Geochemistry Geophysics Geosystems, 4: Paper number 2003GC000560.

Defant, M.J. and Drummond, M.S., 1990. Derivation of some modern arc magmas by melting of young subducted lithosphere. Nature, 347: 662-665.

Drummond, M.S. and Defant, M.J., 1990. A model for trondhjemite-tonalite-dacite genesis and crustal growth via slab melting: Archaean to modern comparisons. Journal of Geophysical Research, 95: 21503-21521.

Foley, S.F., Tiepolo, M. and Vannucci, R., 2002. Growth of early continental crust controlled by melting of amphibolite in subduction zones. Nature, 417: 637-640.

Gagnevin, D., Ethien, R., Bonin, B., Moine, B., Féraud, G., Gerbe, M.C., Cottin, J.Y., Michon, G., Tourpin, S., Mamias, G., Perrache, C. and Giret, A., 2003. Open-system processes in the genesis of silica-oversaturated alkaline rocks of the Rallier-du-Baty peninsula, Kerguelen archipelago (Indian ocean). Journal of Volcanology and Geothermal Research, 123: 267-300.

Gautier, I., Weis, D., Mennessier, J.-P., Vidal, P., Giret, A. and Loubet, M., 1990. Petrology and geochemistry of the Kerguelen archipelago basalts (South Indian ocean): evolution of the mantle sources from ridge to intraplate position. Earth and Planetary Science Letters, 100: 59-76.

Grégoire, M., Cottin, J.Y., Giret, A., Mattielli, N. and Weis, D., 1998. The meta-igneous granulite xenoliths from Kerguelen archipelago: evidence of a continent nucleation in an oceanic setting. Contribution to Mineralogy and Petrology, 133: 259-283.

Harrison, M.T., Blichert-toft, J., Müller, W., Albarede, F., Holden, P. and Mojzsis, S.J., 2005. Heterogeneous Hadean hafnium: Evidence of continental crust at 4.4 to 4.5 Ga. Science, 10.1126: 1-4.

Hidalgo, S., Monzier, M., Martin, H., Chazot, G., Eissen, J.-P. and Cotten, J., 2007. Adakitic magmas in the Ecuadorian Volcanic Front: Petrogenesis of the Iliniza Volcanic Complex (Ecuador). . Journal of Volcanic and Geothermal Research: in press.

Hoskin, P.W.O., 2005. Trace-element composition of hydrothermal zircon and the alteration of Hadean zircon from the Jack Hills, Australia. Geochimica et Cosmochimica Acta, 69(3): 637-648.

Kaban, M.K., Flóvenz, Ó.G. and Pálmason, G., 2002. Nature of the crust-mantle transition zone and the thermal state of the upper mantle beneath Iceland from gravity modelling. Geophys. J. Int., 149: 281-299.

Kamber, B.S., Collerson, K.D., Moorbath, S. and Whitehouse, M.J., 2003. Inheritance of early Archaean Pb-isotope viariability from long-lived Archarean protocrust. Contributions to Mineralogy and Petrology, 145: 25-46.

Kamber, B.S., Ewart, A., Collerson, K.D., Bruce, M.C. and Mc Donald, G.A., 2002. Fluid-mobile trace element constraints on the role of slab melting and implications for Archaean crustal growth models. Contribution to Mineralogy and Petrology, 144: 38-56.

Kleine, T., Mezger, K., Palme, H. and Munker, C., 2004. The W isotope evolution of the bulk silicate Earth: constraints on the timing and mechanisms of core formation and accretion. Earth and Planetary Science Letters, 228(1-2): 109-123.

Kleinhanns, I.C., D., K.J. and Kamber, B.S., 2003. Importance of water for Archaean granitoid petrology: a comparative study of TTG and potassic granitoids from Barberton Mountain and, South Africa. Contribution to Mineralogy and Petrology, 145: 377-389.

Marsh, B.D., Gunnarsson, B., R., C. and Carmody, R., 1991. Hawaiian basalt and Icelandic rhyolite: Indicators of differentiation and partial melting. International Journal of Earth Sciences, 80: 481-510.

Martin, E. and Sigmarsson, O., 2006a. Geographical variations of silicic magma origin in Iceland: the case of Torfajökull, Ljósufjöll and Snæfellsjökull volcanoes. Contribution to Mineralogy and Petrology, accepted.

Martin, E. and Sigmarsson, O., 2006b. Segregation veins formed by in-situ differentiation of tholeiitic lavas from Reykjanes (Iceland), Lanzarote (Canary Islands) and Masaya (Nicaragua). Contribution to Mineralogy and Petrology, submitted.

Martin, H., 1986. Effect of steeper Archean geothermal gradient on geochemistry of subduction-zone magmas. Geology, 14: 753-756.

Martin, H., 1987. Petrogenesis of Archaean trondhjemites, tonalites and granodiorites from eastern Finland: major and trace element geochemistry. Journal of Petrology, 28(5): 921-953.

Martin, H., 1999. The adakitic magmas: modern analogues of Archaean granitoids. Lithos, 46(3): 411-429.

Martin, H. and Moyen, J.-F., 2002. Secular changes in TTG composition as markers of the progressive cooling of the Earth. Geology, 30(4): 319-322.

Martin, H., Smithies, R.H., Rapp, R., Moyen, J.-F. and Champion, D., 2005. An overview of adakite, tonalite-trondhjemite-granodiorite (TTG), and sanukitoid: relationships and some implications for crustal evolution. Lithos, 79: 1-24.

Maury, R.C., Sajona, F.G., Pubellier, M., Bellon, H. and Defant, M.J., 1996. Fusion de la croûte océanique dans les zones de subduction/collision récentes : l'exemple de Mindanao (Philippines). Bulletin de la Société Géologique de France, 167(5): 579-595.

McCulloch, M.T. and Bennet, V.C., 1993. Evolution of the early Earth: constraints from ^{143}Nd-^{142}Nd isotopic systematics. Lithos, 30: 237-255.

Nakamura, n., 1974. Determination of REE, Ba, Fe, Mg, Na and K in carbonaceous and ordinary chondrites. Geochimica Cosmochimica Acta, 38: 757-775.

Pálmason, G., 1986. Model of crustal formation in Iceland and application to submarine mid-ocean ridges. In: P.R. Vogt and B.E. Tucholke (Editors), The Geology of North America. Geological Society of America, Boulder, pp. 87-97.

Rapp, R.P., Shimizu, N. and Norman, M.D., 2003. Growth of early continental crust by partial melting of eclogite. Nature, 425: 605 - 609.

Rapp, R.P., Shimizu, N., Norman, M.D. and Applegate, G.S., 1999. Reaction between slab-derived melts and peridotite in the mantle wedge: experimental constraints at 3.8 GPa. Chemical Geology, 160: 335-356.

Rapp, R.P., Watson, E.B. and Miller, C.F., 1991. Partial melting of amphibolite/eclogite and the origin of Archaean trondhjemites and tonalites. Precambrian Research, 51: 1-25.

Rollinson, H., 1997. Eclogite xenoliths in west African kimberlites as residues from Archaean granitoid crust formation. Nature, 389: 173-176.

Rudnick, R.L., 1995. Making continental crust. Nature, 378: 571-577.

Sallares, V. and Charvis, P., 2003. Crustal thickness constraints on the geodynamic evolution of the Galapagos Volcanic Province. Earth and Planetary Science Letters, 214: 545-559.

Samaniego, P., Martin, H., Monzier, M., Robin, C., Fornari, M., Eissen, J.-P. and Cotten, J., 2005. Temporal Evolution of Magmatism in the Northern Volcanic Zone of the Andes: The Geology and Petrology of Cayambe Volcanic Complex (Ecuador). J. Petrology, 46(11): 2225-2252.

Samaniego, P., Martin, H., Robin, C. and Monzier, M., 2002. Transition from calc-alkalic to adakitic magmatism at

Cayambe volcano, Ecuador: Insights into slab melts and mantle wedge interactions. Geology, 30(11): 967-970.

Schiano, P., Clochiatti, R., Shimizu, N., Maury, R.C., Jochum, K.P. and A.W., H., 1995. Hydrous, silica-rich melts in the sub-arc mantle and their relationships with erupted arc lavas. Nature, 377: 595-600.

Schmidt, M.W., Dardon, A., Chazot, G. and Vannucci, R., 2004. The dependence of Nb and Ta rutile-melt partitioning on melt composition and Nb/Ta fractionation during subduction processes. Earth and Planetary Science Letters, 226(3-4): 415-432.

Shamberger, P.J. and Hammer, J.E., 2006. Leucocratic and Gabbroic xenoliths from Hualai volcano, Hawaii. Journal of Petrology, 47: 1785-1808.

Sigmarsson, O., Hémond, C., Condomines, M., Fourcade, S. and Oskarsson, N., 1991. Origin of silicic magma in Iceland revealed by Th isotopes. Geology, 19: 621-624.

Smithies, R.H., 2000. The Archaean tonalite-trondhjemite-granodiorite (TTG) series is not an analogue of Cenozoic adakite. Earth and Planetary Science Letters, 182: 115-125.

Smithies, R.H., Van Kranendonk, M.J. and Champion, D.C., 2005. It started with a plume - early Archaean basaltic proto-continental crust. Earth and Planetary Science Letters, 238(3-4): 284-297.

Stein, M. and Hofmann, A.W., 1994. Mantle plumes and episodic crustal growth. Nature, 372: 63-68.

Sun, S.S. and McDonough, W.F., 1989. Chemical and isotopic systematics of oceanic basalts: Implications for the mantle composition and processes., Magmatism in the Ocean Basin. Geol. Soc. Sp. Publi., pp. 313-345.

Wilde, S.A., Valley, J.W., Peck, W.H. and Graham, C.M., 2001. Evidence from detrital zircons for the existence of continental crust and oceans on the Earth 4.4 Ga ago. Nature, 409: 175-178.

Wolf, M.B. and Wyllie, P.J., 1994. Dehydration-melting of amphibolite at 10 Kbar: the effects of temperature and time. Contribution to Mineralogy and Petrology, 115: 369-383.

Xiao, Y., Sun, W., Hoefs, J., Simon, K., Zhang, Z., Li, S. and Hofmann, A.W., 2006. Making continental crust through slab melting: Constraints from niobium-tantalum fractionation in UHP metamorphic rutile. Geochimica et Cosmochimica Acta, 70(18): 4770-4782.

Yin, Q., Jacobsen, S.B., Yamashita, K., Blichert-Toft, J., Telouk, P. and Albarède, F., 2002. A short timescale for terrestrial planet formation from Hf-W chronometry of meteorites. Nature, 418(6901): 949-952.

Conclusion générale

L'objectif de ce travail consistait à essayer de mieux contraindre les processus pétrogénétiques ainsi que les conditions de mise en place du magmatisme acide en Islande, ceci dans le but de discuter la viabilité du « modèle islandais » en tant qu'analogue actuel de l'environnement de genèse de la croûte continentale terrestre primitive.

Les principaux résultats et conclusions sont les suivants :

1) Les veines de ségrégation qui se forment au sein même des coulées de laves ont permis d'étudier de façon globale et quasi-complète le mécanisme de cristallisation fractionnée de basaltes tholéiitiques. Il a ainsi été mis en évidence 1) le rôle important du processus de « gas-filter pressing » dans la genèse et la mise en place des magmas différenciés ; ce mécanisme permet d'isoler et de concentrer des fractions de magma différencié dans des vésicules ou veines dites « de ségrégation » et 2) le contrôle de la composition des magmas différenciés par la composition du magma parent. Par exemple, la cristallisation fractionnée d'un magma basaltique possédant un faible K_2O/Na_2O (<0,1) engendrera des liquides de composition trondhjémitique, alors que pour un K_2O/Na_2O élevé (>0,2) il donnera naissance à des liquides de type granitique. En d'autres termes, un petit changement de composition du magma parent pourra produire des magmas différenciés de composition très contrastée.

2) Du point des compositions en éléments majeurs, il est parfaitement possible de rendre compte de la composition des roches acides d'Islande par la cristallisation fractionnée des magmas basaltiques contemporains qui leur sont associés au sein du même système volcanique.

3) Cependant, l'utilisation du comportement des éléments en traces et des isotopes montre que contrairement à ce qui avait été conclu avec les éléments majeurs, un autre mécanisme que la cristallisation fractionnée a dans la plupart des cas joué un rôle important. En effet il apparaît qu'en Islande, la pétrogenèse des laves acides holocènes est contrôlée par l'état thermique de la croûte. A proximité du centre de l'île, là où le centre du panache mantellique interagit avec la ride médio-Atlantique, le gradient géothermique est élevé, de telle sorte que la température du solidus d'un basalte hydraté soit franchie. Ceci se traduit par la fusion partielle de la croûte basaltique partiellement hydratée, générant ainsi le

magmatisme acide localisé à proximité du centre de l'île, dont fait parti Torfajökull qui est le système volcanique présentant le plus grand volume de magmas acides émis. Ce mécanisme n'exclut toutefois pas une cristallisation fractionnée subséquente. En revanche, dans les zones périphériques de l'île (ex : péninsule de Snæfellsnes, système volcanique d'Öræfajökull), l'influence thermique de la ride et du panache mantellique est amoindrie, ne permettant plus à la croûte partiellement hydratée de franchir la température de son solidus. Des magmas acides sont aussi engendrés dans ces zones périphériques, mais la modélisation géochimique a montré qu'ils sont principalement, si ce n'est exclusivement, engendrés par cristallisation fractionnée de magmas basaltiques.

4) Le rapport $^{143}Nd/^{144}Nd$ s'est révélé être un excellent marqueur du contexte géodynamique dans lequel les magmas acides ont été générés. En effet, les magmas basaltiques actuels produits au sein de la zone de rift possèdent un $^{143}Nd/^{144}Nd > 0,51297$ alors que ceux formés loin de la zone de rift ont un $^{143}Nd/^{144}Nd < 0,51297$. En se basant sur ce seul critère, il apparaît que la majeure partie des roches acides d'Islande possède une signature isotopique du Nd de type « zone de rift » ($^{143}Nd/^{144}Nd > 0,51297$). Ceci implique donc qu'ils se sont formés à partir de basaltes, eux-mêmes mis en place au sein de la zone de rift. Comme cela a déjà été montré, les gradients géothermiques au niveau des zones de rift induisent la fusion de la croûte partiellement hydratée, comme le processus majeur de genèse des magmas acides. Il est alors conclu que toutes les roches acides possédant un $^{143}Nd/^{144}Nd > 0,51297$ sont issues de la fusion partielle de la croûte basaltique au sein d'une zone de rift. En revanche toutes les roches acides de la péninsule de Snæfellsnes ayant moins de 7 Ma et celles du système volcanique d'Öræfajökull ont un $^{143}Nd/^{144}Nd < 0,51297$, indiquant une genèse à partir de magmas basaltiques eux-mêmes formés loin de la zone de rift. De telles conditions impliquent alors une origine principalement par cristallisation fractionnée.

5) En considérant que le $^{143}Nd/^{144}Nd$ est un bon marqueur de l'environnement de genèse des laves (« zone de rift » ou « hors-rift »), et connaissant l'âge de ces mêmes laves, il est possible de discuter de l'évolution géodynamique de l'Islande. Par exemple, cette approche a permis de confirmer qu'il y a 6-7 Ma, la ride médio-Atlantique a sauté de la Péninsule de Snæfellsnes vers sa position actuelle au sein de la Péninsule de Reykjanes. En effet, les roches acides de plus de 7 Ma provenant de la péninsule de Snæfellsnes possèdent un $^{143}Nd/^{144}Nd > 0,51297$, témoignant d'un contexte de « zone de rift », alors que les laves

plus récentes (< 5,5 Ma) ont un $^{143}Nd/^{144}Nd < 0,51297$, marqueur d'un contexte franchement hors-zone de rift depuis 5,5 Ma.

6) Les roches acides de l'Est de l'Islande, âgées de 4 à 13 Ma, présentent toutes une signature isotopique du Nd cohérente avec une origine par fusion crustale au sein d'une zone de rift. Un modèle simple de fonctionnement de la ride médio-Atlantique Nord (demi-vitesse d'ouverture d'environ 1cm / an avec une orientation de 105°N) montre que, lors de leur édification, les systèmes volcaniques de l'Est de l'Islande se trouvaient dans la partie Est de la « North Iceland Rift Zone » (NIRZ) actuelle. Une telle configuration implique que la formation de la NIRZ ait été initiée il y a au moins 12,5 Ma. En revanche, la partie Nord-Est de l'Islande a des âges incohérents avec une formation au sein de la NIRZ. En conséquence, il semble préférable de considérer 1) qu'elle se soit formée au sein de la partie Est de la ride de Kolbeinsey à partir de 13 Ma et 2) qu'ensuite, par le jeu des failles transformantes de Tjörnes (TFZ), cette partie ait été décalée vers l'Est (entre 12 et 6 Ma), trouvant ainsi sa place dans l'Est de l'île.

7) Un modèle global d'évolution géodynamique de l'Islande a été proposé. Celui-ci permet en particulier de rendre compte de l'une des plus grandes énigmes islandaises qui est la largeur actuelle de l'île. Le modèle proposé est basé sur un mécanisme d'accrétion-recouvrement associé à des sauts de ride eux-mêmes induits par le mouvement relatif de la ride médio-Atlantique et du centre du panache mantellique islandais.

8) L'étude des rhyolites peralcalines de Hrafntinnusker (Torfajökull) a permis de mettre en évidence : 1) que ces roches acides sont issues de la fusion partielle de la croûte basaltique hydrothermalement altérée et produite au sein de la SIVZ (South Iceland Volcanic-Zone) ; 2) que ce magma a résidé dans une chambre magmatique dans laquelle les processus de cristallisation fractionnée et probablement de « gas-filter pressing » ont permis une fine stratification compositionnelle et enfin 3) qu'un processus post-éruptif d'hydratation du verre constitutif des ponces associé à du lessivage a joué un rôle important dans l'évolution de la composition isotopique ($^{87}Sr/^{86}Sr$), des éléments traces (U) et des majeurs (Na_2O, H_2O).

9) L'Islande est le plateau océanique qui compte tenu de l'interaction ride - panache mantellique possède des gradients géothermiques anormalement élevés. Ces derniers ont fait que cette île a longtemps été considérée comme un possible analogue du contexte

géodynamique de genèse de la croûte continentale primitive. Malgré ce régime thermique exceptionnel, les laves acides n'ont pas une composition de TTG typique de la croûte continentale archéenne. Il en est conclu que des volumes significatifs de croûte continentale primitive n'ont pas pu se former par différenciation intra-plateaux océaniques. En effet, malgré la grande épaisseur de la croûte islandaise, les magmas acides sont systématiquement formés hors du champ de stabilité du grenat et du rutile, c'est-à-dire dans le domaine de stabilité du plagioclase, impliquant des processus pétrogénétiques (principalement la fusion partielle) à faible profondeur. Il semble que le facteur limitant la profondeur de fusion soit le taux d'hydratation de la croûte. En effet, la croûte basaltique ne peut être partiellement fondue que si elle est hydratée. Si tel était le cas en base de croûte islandaise, les magmas acides issus de la fusion crustale auraient vraisemblablement des compositions de TTG. Le fait de ne former des magmas acides qu'à faible profondeur (domaine de stabilité du plagioclase) implique que la croûte n'est fusible, donc hydratée, que dans sa partie supérieure. Malgré une activité hydrothermale importante en Islande, il semble néanmoins que ce mécanisme ne soit pas suffisant pour hydrater la base de la croûte.

10) Au cours de l'histoire de la Terre, il semble malgré tout que les plateaux océaniques aient pu jouer un rôle important dans la genèse de la croûte continentale. En effet, lorsqu'ils sont entraînés dans une subduction, les plateaux océaniques constituent un apport important de matériel potentiellement fusible. Les accélérations cycliques de la vitesse de croissance crustale pourraient alors correspondre à des périodes où de grands volumes de plateaux océaniques sont formés et à terme subductés.

Cette étude a permis de mettre en évidence le caractère atypique du magmatisme acide d'Islande. Classiquement, dans les autres plateaux océaniques émergés (par ex. Hawaii, Kerguelen), les roches acides 1) sont en faible proportion relativement aux magmas basaltiques et 2) résultent quasi-exclusivement de la cristallisation fractionnée d'un magma parent basaltique.

Un environnement exceptionnel où ride médio-océanique et panache mantellique interfèrent est capable d'induire des gradients géothermiques tel que la fusion partielle d'une croûte basaltique hydratée est possible. D'autre part un environnement de ride médio-océanique, de par son hydrothermalisme intense, est capable d'hydrater efficacement une croûte basaltique. L'Islande, regroupant ces deux paramètres à la fois, est actuellement le lieu unique où la fusion de la croûte basaltique est possible en contexte de plateau océanique.

D'autre part, en Islande, le volume de roches acides représente près de 10 % de laves émises en surface, ce qui ne résulte pas d'un épiphénomène. Il apparaît par conséquent qu'en termes de productivité des mécanismes pétrogénétiques, le modèle « islandais » est plus efficace que le modèle « classique » de plateau océanique. Ceci pourrait provenir du fait que le mécanisme de fusion partielle, régissant le modèle « islandais », affecte des basaltes hydratés (croûte altérée) et donc à température de solidus « basse », alors que la cristallisation fractionnée, régissant le modèle « classique », affecte des basaltes essentiellement anhydres (issus de la fusion du manteau), donc à température de solidus « élevée ». Ceci implique qu'en contexte de plateau océanique et pour des conditions thermiques identiques, la fusion d'un basalte (hydraté) va produire des volumes plus importants de magmas acides que la cristallisation fractionnée d'un basalte (anhydre).

Références bibiographiques

A

Albarède, F., 1998. The growth of continental crust. Tectonophysics, 296: 1-14.

Albarède, F., 2006. The formation of the crust of the rocky planets and the mineral environment of the origin of life. In: M. Gargaud, P. Claeys and H. Martin (Editors), Lectures in Astrobiology. Springer, Heidelberg, pp. 75-102.

Andersen, D.J., Lindsley, D.H. and Davidson, P.M., 1993. QUILF: a PASCAL program to assess equilibria among Fe- Mg-Ti oxides, pyroxenes, olivine, and quartz. Computers in Geosciences, 19: 1333-1350.

Anderson, A.T., George, J.R., Swihart, H., Artioli, G. and Geiger, C.A., 1984. Segregation vesicles, Gas filter-pressing, and igneous differentiation. Journal of Geology 92: 55-72.

Anovitz, L.M., Elam, J.M., Riciputi, L.R. and Cole, D.R., 1999. The failure of obsidian hydration dating: sources, implications and new directions. Journal of Archaeological Science, 26: 735-752.

Anovitz, L.M., Elam, J.M., Riciputi, L.R. and Cole, D.R., 2004. Isothermal time-series determination of the rate of diffusion of water in Pachuca obsidian. Archaeometry, 46: 301-326.

Arndt, N.T., 1992. Rate and mechanism of continent growth in the Precambrian. In: S. Maruyama (Editor), Evolving Earth Symposium, Okazaki, pp. 38-41.

B

Bacon, C.R. and Hirschmann, M.M., 1988. Mg/Mn partitioning as a test for equilibrium between coexisting Fe-Ti oxides. American Mineralogist, 73: 57-61.

Barker, F., 1979. Trondhjemites: definition, environment and hypothesis of origin. In: F. Barker (Editor), Trondhjemites, Dacites and Related Rocks. Elsevier, Amsterdam, pp. 1-12.

Barth, M.G., Foley, S.F. and Horn, I., 2002a. Partial melting in Archaean subduction zones: constraints from experimentally determined trace element partition coefficients between eclogitic minerals and tonalitic melts under upper mantle conditions. Precambrian Research, 113: 323-340.

Barth, M.G., Rudnick, R.L., Carlson, R.W., Horn, I. and McDonough, W.F., 2002b. Re---Os and U---Pb geochronological constraints on the eclogite-tonalite connection in the Archean Man Shield, West Africa. Precambrian Research, 118(3-4): 267-283.

Bindeman, I.N., Davis, A.M. and Drake, M., J., 1998. Ion microprobe study of plagioclase-basalt partition experiments at natural coàncentration levels of trace elements. Geochimica Cosmochimica Acta, 62: 1175-1193.

Blundy, J. and Cashman, K., 2001. Ascent-driven crystallisation of dacite magmas at Mount St Helens, 1980-1986. Contribution to Mineralogy and Petrology, 140: 631-650.

Bott, M.H.P., 1985. Plate tectonic evolution of the Iceland transverse ridge and adjacent regions. Journal of Geophysical Research, 90: 9953-9960.

Bottinga, Y. and Weill, D., 1970. Densities of liquid silicate systems csalculated from partial molar volumes of oxide components. American Journal of Science, 269: 169-182.

Bourdon, E., Eissen, J.-P., Gutscher, M.-A., Monzier, M., Hall, M.L. and Cotten, J., 2003. Magmatic response to early aseismic ridge subduction: the Ecuadorian margin case (South America). Earth and Planetary Science Letters, 205(3-4): 123-138.

Bourgeois, O., Dauteuil, O. and Hallot, E., 2005. Rifting above a mantle plume: structure and development of the Iceland Plateau. Geodinamica Acta, 18: 59-80.

Boyet, M., Blichert-Toft, J., Rosing, M., Storey, M., Télouk, P. and Albarède, F., 2003. ^{142}Nd evidence for early earth differentiation. Earth and Planetary Science Letters, 214: 427-442.

Brugger, C.R., Johnston, A.D. and Cashman, K.V., 2003. Phase relations in silicic systems at one-atmosphere pressure. Contributions to Mineralogy and Petrology, 146: Contributions to Mineralogy and Petrology356-369.

C

Cantagrel, F. and Pin, C., 1994. Major, minor and rare-earth element determinations in 25 rock standards by ICP-atomic emission spectrometry. Geostandards Newsletter, 18: 123-138.

Carlson, R.W., 1994. Mechanisms of earth differentiation: consequences for the chemical structure of the mantle. Reviews of geophysics, 32: 337-361.

Carlson, R.W. and Lugmair, G.W., 1988. The age of ferroan anorthosite 60025: oldest crust on a young moon. Earth and Planetary Science Letters, 90: 119-130.

Carmichael, I.S.E., 1964. The petrology of Thingmuli, a tertiary volcano in Eastern Iceland. Journal of Petrology, 5: 435-460.

Caroff, M., Maury, R.C., Cotten, J. and Clement, J.-P., 2000. Segregation structures in vapor-differentiated basaltic flows. Bulletin of volcanology, 62: 171-187.

Carpentier, M., 2003. Variabilité géochimique des basaltes Holocène islandais, Université Blaise Pascal, Clermont Ferrand, 53 pp.

Carr, M.J., Rose, W.I. and Stoiber, R.E., 1982. Andesites: orogenic andesites and related rocks, Central america. Wiley, New-York, pp. 149-166.

Cavosie, A.J., Valley, J.W., Wilde, S.A. and E.I.M.F., 2005. Magmatic [delta]18O in 4400-3900 Ma detrital zircons: A record of the alteration and recycling of crust in the Early Archean. Earth and Planetary Science Letters, 235(3-4): 663-681.

Cavosie, A.J., Wilde, S.A., Liu, D., Weiblen, P.W. and Valley, J.W., 2004. Internal zoning and U-Th-Pb chemistry of Jack Hills detrital zircons: a mineral record of early Archean to Mesoproterozoic (4348-1576 Ma) magmatism. Precambrian Research, 135: 251-279.

Clayton, R., N. and Mayeda, T.K., 1963. The use of bromine pentafluoride in the extraction of oxygen from oxides and silicates for isotopic analysis. Geochimica Cosmochimica Acta, 27: 43-52.

Condie, K.C., 1986. Origin and early growth rate of continents. Precambrian Research, 32: 261-278.

Condie, K.C., 1989. Plate tectonics and crustal evolution. Pergamon, Oxford, 476 pp.

Condie, K.C., 1993. Chemical composition and evolution of the upper continental crust: contrasting results from surface samples and shales. Chemical Geology, 104: 1-37.

Condie, K.C., 1998. Episodic continental growth and supercontinents: a mantle avalanche connection? Earth and Planetary Science Letters, 163(1-4): 97-108.

Condomines, M., 1981. Chronologie et géochimie du volcanisme récent: l'apport du déséquilibre rédioactif $^{230}Th/^{238}U$, Université Paris VII, 282 pp.

Condomines, M., Tanguy, J.C., Kieffer, G. and Allègre, C.J., 1982. Magmatic evolution studied gy 230Th-238U disequilibrium and trace element systematics: the Etna case. Geochimica Cosmochimica Acta, 46: 1397-1416.

Cousens, B.L., Clague, D.A. and Sharp, W.D., 2003. Chronology, chemistry, and origin of trachytes from Hualalai volcano, Hawaii. Geochemistry Geophysics Geosystems, 4: Paper number 2003GC000560.

D

Defant, M.J. and Drummond, M.S., 1990. Derivation of some modern arc magmas by melting of young subducted lithosphere. Nature, 347: 662-665.

Defant, M.J., Richerson, M., De Boer, J.Z., Stewart, R.H., Maury, R.C., Bellon, H., Drummond, M.S., Feigenson, M.D. and Jackson, T.E., 1991. Dacite genesis via both slab melting and differentiation : petrogenesis of La Yeguada volcanic complex, Panama. Journal of Petrology, 32: 1101-1142.

DeMets, C., Gordon, R.G., Argus, D.F. and Stein, S., 1990. Current plate motions. Geophys. J. Int., 101: 425-478.

Drake, M.J. and Weill, D.F., 1975. Partition of Sr, Ba, Ca, Y, Eu^{2+}, Eu^{3+} and other REE between plagioclase feldspar and magmatic liquid: an experimental study. Geochimica Cosmochimica Acta, 39: 689-712.

Drummond, M.S. and Defant, M.J., 1990. A model for trondhjemite-tonalite-dacite genesis and crustal growth via slab melting: Archaean to modern comparisons. Journal of Geophysical Research, 95: 21503-21521.

E

Eysteinsson, H. and Gunnarsson, K., 1995. Maps of gravity, bathymetry and magnetics for Iceland and surroundings. Orkustofnun, National Energy Authority, Geothermal division.

F

Flóvenz, Ó.G. and Saemundsson, K., 1993. Heat flow and geothermal processes in Iceland. Tectonophysics, 225: 123-138.

Foley, S.F., Tiepolo, M. and Vannucci, R., 2002. Growth of early continental crust controlled by melting of amphibolite in subduction zones. Nature, 417: 637-640.

Förster, H.-J., 1998. The chemical composition of the REE-Y-Th-U-rich accessory minerals in peraluminous granites of the Erzgebirge-Fichtelgebirge region, Germany, PartI: The monazite-(Ce)-brabantite solid solution series. American Mineralogist, 83: 259-272.

Foulger, G.R., 2006. Older crust underlies Iceland. Geophys. J. Int, 165:672-676

Friedman, I. and Smith, R., 1960. A new dating method using obsidian: Part I, the development of the method. American Antiquity, 25: 476-522.

Frost, B.R. and Lindsley, D.H., 1992. Equilibria among Fe-Ti oxides, pyroxens, olivine, and quartz: Part II. Application. American Mineralogist, 77: 1004-1020.

Furman, T., Frey, F.A. and Meyer, P.S., 1992a. Petrogenesis of evolved basalts and rhyolites at Austurhorn, Southeastern Iceland: the role of fractional crystallisation. Journal of Petrology, 33: 1405-1445.

Furman, T., Meyer, P.S. and Frey, F.A., 1992b. Evolution of Icelandic central volcanoes: evidence from the Austurhorn intrusion, southeastern Iceland. Bulletin of volcanology, 55: 45-62.

G

Gagnevin, D., Ethien, R., Bonin, B., Moine, B., Féraud, G., Gerbe, M.C., Cottin, J.Y., Michon, G., Tourpin, S., Mamias, G., Perrache, C. and Giret, A., 2003. Open-system processes in the genesis of silica-oversaturated alkaline rocks of the Rallier-du-Baty peninsula, Kerguelen archipelago (Indian ocean). Journal of Volcanology and Geothermal Research, 123: 267-300.

Garcia, S., Arnaud, N.O., Angelier, J., Françoise, B. and Homberg, C., 2003. Rift jump process in northern Iceland sinc 10 Ma from $^{40}Ar/^{39}Ar$ geochronology. Earth and Planetary Science Letters, 214: 529-544.

Gautason, B. and Muehlenbachs, K., 1998. Oxygen isotopic fluxes associated with high-temperature processes in the rift zones of Iceland. Chemical Geology, 145: 275-286.

Gautier, I., Weis, D., Mennessier, J.-P., Vidal, P., Giret, A. and Loubet, M., 1990. Petrology and geochemistry of the Kerguelen archipelago basalts (South Indian ocean): evolution of the mantle sources from ridge to intraplate position. Earth and Planetary Science Letters, 100: 59-76.

Gee, M.A.M., Thirlwal, M.F., Taylor, R.N., Lowry, D. and Murton, B.J., 1998. Crustal processes: Major control on Reykjanes Peninsula lava chemistry, SW Iceland. Journal of Petrology, 39: 819-839.

Geirsson, K., 1993. Pétrologie d'une série tholéiitique complète: le volcan central de Fagridalur, nord-est de l'Islande, Université Pierre et Marie Curie, Paris, 217 pp.

Ghiorso, M.S. and Sack, R.O., 1995. Chemical mass transfer in magmatic processes. 4. A revised and internally consistent thermodynamic model for the interpolation of liquid-

solid equilibria in magmatic systems at elevated temperatures and pressures. Contributions to Mineralogy and Petrology, 119: 197-212.

Goff, F., 1996. Vesicle cylinders in vapor-differentiated basalt flows. Journal of Volcanology and Geothermal Research, 71: 167-185.

Govindaraju, K., 1994. 1994 Compilation of working values and sample description for 383 geostandards. Geostandards Newsletter, 18(Special issue): 1-158.

Grégoire, M., Cottin, J.Y., Giret, A., Mattielli, N. and Weis, D., 1998. The meta-igneous granulite xenoliths from Kerguelen archipelago: evidence of a continent nucleation in an oceanic setting. Contribution to Mineralogy and Petrology, 133: 259-283.

Griggs, R.F., 1922. The Valley of Ten Thousand Smokes. National Geographic Society, Washington, 340 pp.

Gruau, G., Rosing, M. and Bridgwater, R.C.O.G., 1996. Resetting Sm-Nd systematics during metamorphism of >3.7 Ga rocks: implications for isotopic models of early earth differentiation. Chem. Geol., 133: 225-240.

Guðmundsdóttir, I.S. and Sigmarsson, O., 2006. Highest measured strontium isotope ratios in Icelandic rocks: Rb and Sr systematics in Ljósufjöll volcanics, Snæfellsnes peninsula Natural Science Symposium, Reykjavik.

Gudmundsson, A., 1995. Infrastructure and mechanics of volcanic systems in Iceland. Journal of Volcanology and Geothermal Research, 64: 1-22.

Gunnarsson, B., Marsh, B.D. and Taylor, J.H.P., 1998. Generation of Icelandic rhyolites: silicic lavas from the Torfajökull central volcano. Journal of Volcanology and Geothermal Research, 83: 1-45.

Günther D, Frischknecht R, Frischknecht CA, Frischknecht H, Frischknecht HJ, Frischknecht K (1997) Capabilities of an Argon Fluoride 193 nm excimer laser ablation inductively coupled plasma mass spectrometry microanalysis of geological materials. J Anal At Spectrom 12: 939-944

H

Hardarson, B.S., Fitton, J.G., Ellam, R.M. and Pringle, M.S., 1997. Rift relocation-a geochemical and geochronological investigation of a paleo-rift in northwest Iceland. Earth and Planetary Science Letters, 153: 181-196.

Harrison, M.T., Blichert-toft, J., Müller, W., Albarede, F., Holden, P. and Mojzsis, S.J., 2005. Heterogeneous Hadean hafnium: Evidence of continental crust at 4.4 to 4.5 Ga. Science, 10.1126: 1-4.

Hattori, K. and Muehlenbachs, K., 1982. Oxygen isotope ratios of the Icelandic crust. Journal of Geophysical Research, 87: 6559-6565.

Helgason, J., 1985. Shifts of the plate boundary in Iceland: some aspectes of Tertiary volcanism. Journal of Geophysical Research, 90: 10084-10092.

Helz, R.T., 1980. Crystallization history of Kilauea Iki lava lake as seen in drill core recovered in 1967-1979. Bull. Volcanol., 43: 675-701.

Helz, R.T., Kirschenbaum, H. and Marinenko, J.W., 1989. Diapiric transfer of melt in Kilauea Iki lava lake, Hawaï: a quick, efficient process of igneous differenciation. Geological Society of America Bulletin, 101: 578-594.

Hemond, C., Arndt, N.T., Lichtenstein, U., Holfmann, A.W., Oskarsson, N. and Steinthorsson, S., 1993. The heterogeneous Iceland plume: Nd-Sr-O isotopes and traces element constraints. Journal of Geophysical Research, 98: 15833-15850.

Hidalgo, S., Monzier, M., Martin, H., Chazot, G., Eissen, J.-P. and Cotten, J., 2007. Adakitic magmas in the Ecuadorian Volcanic Front: Petrogenesis of the Iliniza Volcanic Complex (Ecuador). . Journal of Volcanic and Geothermal Research: in press.

Hoernle, K. and Schmincke, H.U., 1993. The petrology of the tholeiites through melilite nephelinites on Gran Canaria, Canary Islands: crystal fractionation, accumulation and depths of melting. Journal of Petrology, 34: 573-597.

Hofmann, A.W., 1988. Chemical differentiation of the Earth: the relationship between mantle, continental crust, and oceanic crust. Earth and Planetary Science Letters, 90: 297-314.

Hofton, M.A. and Foulger, G.R., 1996. Post-rifting anelastic deformation around the spreading plate boundary, north-Iceland:1. Modeling of the 1987-1992 deformation field using a viscoelastic Earth structure. Journal of Geophysical Research, 101: 25403-25421.

Hoskin, P.W.O., 2005. Trace-element composition of hydrothermal zircon and the alteration of Hadean zircon from the Jack Hills, Australia. Geochimica et Cosmochimica Acta, 69(3): 637-648.

J

Jahn, B.M., 1997. Géochimie des granitoïdes archéens et de la croûte
primitive. In: R. Hagemann and M. Treuil (Editors), Introduction à la Géochimie et ses Applications. Editions Thierry Parquet., pp. 357-393.

Jackson SE, Pearson NJ, Griffin WL, Belousova EA (2004) The application of laser ablation-inductively coupled plasma-mass spectrometry to in situ U–Pb zircon geochronology. Chem Geol 211, 1-2: 47-69

Jakobsson, S.P., 1972. Chemistry and distribution pattern of recent basaltic rocks in iceland. Lithos, 5: 365-386.

Jakobsson, S.P., Jonsson, J. and Shido, F., 1978. Petrology of the Western Reykjanes Peninsula, Iceland. Journal of Petrology, 19: 669-705.

Jancin, M., Young, K.D. and Voight, B., 1985. Stratigraphy and K/Ar ages across the west flank of the northeast Iceland axial rift zone, in relation to the 7 Ma volcano_tectonic reorganization of Iceland. Journal of Geophysical Research, 90: 9961-9985.

Jochum, K.P., Stoll, B., Herwig, K., Willbold, M., Hofmann, A.W., Amini, M., Aarburg, S., Abouchami, W., Hellebrand, E., Mocek, B., Raczek, I., Stracke, A., Alard, O., Bouman, C., Becker, S., Dücking, M., Brätz, H., Klemd, R., De Bruin, D., Canil, D., Cornell, D., De Hoog, C.-J., Dalpé, C., Danyushevsky, L., Eisenhauer, A., Gao, Y., Snow, J.E., Groschopf, N., Günther, D., Latkoczy, C., Guillong, M., Hauri, E.H., Höfer, H.E., Lahaye, Y., Horz, K., Jacob, D.E., Kasemann, S.A., Kent, A.J.R., Ludwig, T., Zack, T., Mason, P.R.D., Meixner, A., Rosner, M., Misawa, K., Nash, B.P., Pfänder, J., Premo, W.R., Sun, W.D., Tiepolo, M., Vannucci, R., Vennemann, T., Wayne, D. and Woodhead, J.D., 2006. MPI-DING reference glasses for in situ microanalysis: New reference values for element concentrations and isotope ratios. Geochemistry Geophysics Geosystems, 7: Paper number 2005GC001060.

Johannes, W. and Holtz, F., 1996. Petrogenesis and experimental petrology of granitic rocks. Springer-Verlag, Berlin Heidelberg, 335 pp.

Jóhannesson, H., 1980. Jarðlagaskipan og þróun rekbelta á Vesturlandi. Náttúrufræðingurinn, 50: 13-31.

Jóhannesson, H. and Saemundsson, K., 1998. Geological map of Iceland. 1:500 000. Bedrock geology. Icelandic Institute of Natural History, Reykjavík.

Jónasson, K., 1994. Rhyolite volcanism in the Krafla central volcano, north-east Iceland. Bulletin of Volcanology, 56: 516-528.

K

Kaban, M.K., Flóvenz, Ó.G. and Pálmason, G., 2002. Nature of the crust-mantle transition zone and the thermal state of the upper mantle beneath Iceland from gravity modelling. Geophys. J. Int., 149: 281-299.

Kamber, B.S., Collerson, K.D., Moorbath, S. and Whitehouse, M.J., 2003. Inheritance of early Archaean Pb-isotope viariability from long-lived Archarean protocrust. Contributions to Mineralogy and Petrology, 145: 25-46.

Kamber, B.S., Ewart, A., Collerson, K.D., Bruce, M.C. and Mc Donald, G.A., 2002. Fluid-mobile trace element constraints on the role of slab melting and implications for Archaean crustal growth models. Contribution to Mineralogy and Petrology, 144: 38-56.

Keith, T.E.C., 1991. Fossil and active fumeroles in the 1912 reuptive deposits, Valley of Ten Thousand Smokes, Alaska. Journal of Volcanology and Geothermal Research, 45: 227-254.

Kleine, T., Mezger, K., Palme, H. and Munker, C., 2004. The W isotope evolution of the bulk silicate Earth: constraints on the timing and mechanisms of core formation and accretion. Earth and Planetary Science Letters, 228(1-2): 109-123.

Kleinhanns, I.C., D., K.J. and Kamber, B.S., 2003. Importance of water for Archaean granitoid petrology: a comparative study of TTG and potassic granitoids from Barberton Mountain and, South Africa. Contribution to Mineralogy and Petrology, 145: 377-389.

Kokfelt, T.F., Hoernle, K., Hauff, F., Fiebig, J., Werner, R. and Gabre-Schönberg, D., 2006. Combined trace element and Pb-Nd-Sr-O isotope evidence for recycled oceanic crust (upper and lower) in the Iceland mantle plume. Journal of Petrology: 1-45.

L

Lacasse, C., Sigurdsson, H., Carey, S.N., Jóhannesson, H., Thomas, L.E. and Rogers, N.W., 2006. Bimodal volcanism at the Katla subglacial caldera, Iceland: insight into geochemistry and pertogenesis of rhyolitic magmas. Bulletin of volcanology, in press.

Le Bas, M.J., Le Maitre, R.w., Streckeisen, A. and Zanettin, B., 1986. A chemical classification of volcanic rocks based on the total alkali-silica diagram. Journal of Petrology, 22: 745-750.

Leeman, W.P., Ma, M.S., Murali, A.V. and Schmitt, R.A., 1978. Empirical estimation of magnetite/liquid distribution coefficients for some transition elements - A correction. Contribution to Mineralogy and Petrology, 65: 269-272.

Ludwig KR (2001) User manual for Isoplot/Ex rev. 2.49. A geochronological toolkit for Microsoft Excel. Berkeley Geochronology Center Special Publication n°1a, 56 p

M

Macdonald, R., McGarvie, D.W., Pinkerton, H., Smith, R.L. and Palacz, Z.A., 1990. Petrogenetic evolution of the Torfajökull volcanic complex, Iceland I. Relation between the magma types. Journal of Petrology, 31: 461-481.

Mahood, G. and Hildreth, W., 1983. Large partition coefficients of trace elements in high-silica rhyolites. Geochimica Cosmochimica Acta, 47: 11-30.

Marsh, B.D., 2002. On bimodal differentiation by solidification front instability in basaltic magmas, part 1: Basic mechanics. Geochimica Cosmochimica Acta, 66: 2211-2229.

Marsh, B.D., Gunnarsson, B., R., C. and Carmody, R., 1991. Hawaiian basalt and Icelandic rhyolite: Indicators of differentiation and partial melting. International Journal of Earth Sciences, 80: 481-510.

Martin, E. and Sigmarsson, O., 2005. Trondhjemitic and granitic melts formed by fractional crystallization of an olivine tholeiite from Reykjanes Peninsula, Iceland. Geological Magazine, 142(6): 651-658.

Martin, E. and Sigmarsson, O., 2006a. Geographical variations of silicic magma origin in Iceland: the case of Torfajökull, Ljósufjöll and Snæfellsjökull volcanoes. Contribution to Mineralogy and Petrology, accepted.

Martin, E. and Sigmarsson, O., 2006b. Segregation veins formed by in-situ differentiation of tholeiitic lavas from Reykjanes (Iceland), Lanzarote (Canary Islands) and Masaya (Nicaragua). Contribution to Mineralogy and Petrology, submitted.

Martin, E. and Sigmarsson, O., 2006c. Segregation veins in tholeiitic lavas: implications for the formation of silicic magmas in Iceland and for the genesis of primitive continental crust on the earth., Raunvísindaþing, Reykjavík.

Martin, H., 1986. Effect of steeper Archean geothermal gradient on geochemistry of subduction-zone magmas. Geology, 14: 753-756.

Martin, H., 1987. Petrogenesis of Archaean trondhjemites, tonalites and granodiorites from eastern Finland: major and trace element geochemistry. Journal of Petrology, 28(5): 921-953.

Martin, H., 1999. The adakitic magmas: modern analogues of Archaean granitoids. Lithos, 46(3): 411-429.

Martin, H. and Moyen, J.-F., 2002. Secular changes in TTG composition as markers of the progressive cooling of the Earth. Geology, 30(4): 319-322.

Martin, H., Smithies, R.H., Rapp, R., Moyen, J.-F. and Champion, D., 2005. An overview of adakite, tonalite-trondhjemite-granodiorite (TTG), and sanukitoid: relationships and some implications for crustal evolution. Lithos, 79: 1-24.

Maury, R.C., Sajona, F.G., Pubellier, M., Bellon, H. and Defant, M.J., 1996. Fusion de la croûte océanique dans les zones de subduction/collision récentes : l'exemple de Mindanao (Philippines). Bulletin de la Société Géologique de France, 167(5): 579-595.

McBirney, A.R., 1993. Igneous petrology. Jones and Bartlett Publishers, Boston, 508 pp.

McCulloch, M.T. and Bennet, V.C., 1993. Evolution of the early Earth: constraints from ^{143}Nd-^{142}Nd isotopic systematics. Lithos, 30: 237-255.

McCulloch, M.T. and Bennett, V.C., 1993. Evolution of the early Earth: constraints from ^{143}Nd-^{142}Nd isotopic systematics. Lithos, 30: 237-255.

McGarvie, D.W., 1984. Torfajökull: a volcano dominated by magma mixing. Geology, 12: 685-688.

McGarvie, D.W., Macdonald, R., Pinkerton, H. and L., S.R., 1990. Petrogenetic evolution of the Torfajökull volcanic complex, Iceland II. The role of magma mixing. Journal of Petrology, 31: 461-481.

Miyashiro, A., 1978. Nature of alkalic volcanic rock series. Contribution to Mineralogy and Petrology, 66: 91-104.

Mojzsis, S.J., Harrison, M.T. and Pidgeon, R.T., 2001. Oxygen-isotope evidence from ancient zircons for liquid water at the Earth's surface 4,300 Myr ago. Nature, 409: 178-181.

Moorbath, S., Sigurdsson, H. and Goodwin, R., 1968. K-Ar ages of the oldest exposed rocks in Iceland. Earth and Planetary Science Letters, 4: 197-205.

Morse, S.A., 1980. Basalts and phase diagrams. Springer-Verlag, New-York.

Moune, S., 2006. Trace element degassing and enrichment in the eruptive plume of the 2000 eruption of Hekla volcano, Iceland. Geochimica Cosmochimica Acta, 70 461-479

N

Nakamura, n., 1974. Determination of REE, Ba, Fe, Mg, Na and K in carbonaceous and ordinary chondrites. Geochimica Cosmochimica Acta, 38: 757-775.

Nicholson, H., Condomines, M., Fitton, J.G., Fallick, A.E., Grönvold, K. and Rogers, G., 1991. Geochemical and isotopic Evidence for Crustal Assimilation Beneath Krafla, Iceland. Journal of Petrology, 32: 1005-1020.

Nunns, A.G., 1983. Plate tectonic evolutionof the Greenland-Scotland ridge and surronding regions. In: M.H.P. Botts, S. Saxov, M. Talwani and J. Thiede (Editors), Structure and Development of the Greenland-Scotland Ridge. Plenum Press, New-York and London.

O

O'Nions, R.K. and Gronvold, K., 1973. Petrogenetic relationships of acid and basic rocks in Iceland: Sr-isotopes and rare-earth elements in late and postglacial volcanics. Earth and Planetary Science Letters, 19: 397-409.

Oskarsson, N., Sigvaldason, G.E. and Steinthorsson, S., 1982. A dynamic model of rift zone petrogenesis and the regional petrology of Iceland. Journal of Petrology, 23: 28-74.

Oskarsson, N., Steinthorsson, S. and Sigvaldason, G.E., 1985. Iceland geochemical anomaly: origin, volcanotectonics, chemical fractionation and isotope evolution of the crust. Journal of Geophysical Research, 90: 10011-10025.

P

Pálmason, G., 1973. Kinematics and heat flow in a volcanic rift zone, with application to Iceland. Geophys. J.R. Astr. Soc., 33: 451-481.

Pálmason, G., 1981. Crustal rifting and related thermomechanical processes in the lithosphere beneath Iceland. Geol. Rundsh, 70: 244-260.

Pálmason, G., 1986. Model of crustal formation in Iceland and application to submarine mid-ocean ridges. In: P.R. Vogt and B.E. Tucholke (Editors), The Geology of North America. Geological Society of America, Boulder, pp. 87-97.

Philpotts, A.R., 1979. Silicate liquid immiscibility in tholeiitic basalts. Journal of Petrology, 20: 99-118.

Philpotts, A.R., Carroll, M. and Hill, J.M., 1996. Crystal-mush compaction and the origin of pegmatitic segregation sheets in a thick flood-basalt flow in the mesozoic Hartford basin, Connecticut. Journal of Petrology, 34: 811-836.

Pin, C., Briot, D., Bassin, C. and Poitrasson, F., 1994. Concomitant separation of strontium and samarium-neodynium for isotopic analysis in silicate samples, based on specific extraction chromatography. Analytical Chimica Acta, 298: 209-217.

Prestvik, T., Goldberg, S., Karlsson, H. and Grönvold, K., 2001. Anomalous strontium and lead-isotope signatures in the off-rift Öraefajökull central volcano in south-east Iceland, Evidence for enriched endmember(s) of the Iceland mantle plume? Earth and Planetary Science Letters, 190: 211-220.

Puffer, J.H. and Horter, D.L., 1993. Origin of pegmatitic segregation veins within flood basalts. Geological Society of America Bulletin, 105: 738-748.

R

Rapp, R.P., Shimizu, N. and Norman, M.D., 2003. Growth of early continental crust by partial melting of eclogite. Nature, 425: 605 - 609.

Rapp, R.P., Shimizu, N., Norman, M.D. and Applegate, G.S., 1999. Reaction between slab-derived melts and peridotite in the mantle wedge: experimental constraints at 3.8 GPa. Chemical Geology, 160: 335-356.

Rapp, R.P., Watson, E.B. and Miller, C.F., 1991. Partial melting of amphibolite/eclogite and the origin of Archaean trondhjemites and tonalites. Precambrian Research, 51: 1-25.

Rayleigh, J.W.S., 1896. Theorical considerations respecting the separation of gases by diffusion and similar processes. Philos. Mag., 42: 77-107.

Reese, C.C., Solomatov, V.S. and Moresi, L.N., 1999. Non-newtonian stagnant lid convection and magmatic resurfacing on Venus. Icarus, 139: 67-80.

Riciputi, L.R., Elam, J.M., Anovitz, L.M. and Cole, D.R., 2002. Obsidian diffusion dating by Secondary Ion Mass Spectrometry: a test using results from Mound 65, Chalco, Mexico. Journal of Archaeological Science, 29: 1055-1075.

Rollinson, H., 1997. Eclogite xenoliths in west African kimberlites as residues from Archaean granitoid crust formation. Nature, 389: 173-176.

Rudnick, R.L., 1995. Making continental crust. Nature, 378: 571-577.

Ruffet, G., Féraud, G., Ballèvre, M. and Kiénast, J.R., 1995. Plateau ages and excess argon on phengites: a 40Ar-39Ar laser probe study of alpine micas (Sesia Zone). Chemical Geology, 121: 327-343.

Ruffet, G., Gruau, G., Ballèvre, M., Féraud, G. and Philippot, P., 1997. Rb-Sr and 40Ar-39Ar laser probe dating of HP phengites (Sesia zone, Western Alps): underscoring of excess argon and new crystallization age constraints. Chemical Geology 141: 1-18.

S

Sæmundsson, K., 1979. Outline of geology of Iceland. Jökull, 29: 7-28.

Sallares, V. and Charvis, P., 2003. Crustal thickness constraints on the geodynamic evolution of the Galapagos Volcanic Province. Earth and Planetary Science Letters, 214: 545-559.

Samaniego, P., Martin, H., Monzier, M., Robin, C., Fornari, M., Eissen, J.-P. and Cotten, J., 2005. Temporal Evolution of Magmatism in the Northern Volcanic Zone of the Andes: The Geology and Petrology of Cayambe Volcanic Complex (Ecuador). J. Petrology, 46(11): 2225-2252.

Samaniego, P., Martin, H., Robin, C. and Monzier, M., 2002. Transition from calc-alkalic to adakitic magmatism at Cayambe volcano, Ecuador: Insights into slab melts and mantle wedge interactions. Geology, 30(11): 967-970.

Saunders, A.D., Fitton, J.G., Kerr, A.C., Norry, M.J. and Kent, R.W., 1997. The North Atlantic Igneous Province. In: J.J. Mahoney and M.F. Coffin (Editors), Large Igneous Provinces: Continental, Oceanic, and Planetary Volcanism. Geophysical Monograph. American Geophysical Union Washington DC., pp. 45-93.

Schiano, P., Clochiatti, R., Shimizu, N., Maury, R.C., Jochum, K.P. and A.W., H., 1995. Hydrous, silica-rich melts in the sub-arc mantle and their relationships with erupted arc lavas. Nature, 377: 595-600.

Schilling, J.G., 1973. Iceland mantle plume: geochemical study of Reykjanes ridge. Nature, 242: 465.

Schmidt, M.W., Dardon, A., Chazot, G. and Vannucci, R., 2004. The dependence of Nb and Ta rutile-melt partitioning on melt composition and Nb/Ta fractionation during subduction processes. Earth and Planetary Science Letters, 226(3-4): 415-432.

Schmidt, M.W. and Poli, S., 1998. Experimentally based water budgets for dehydrating slabs and consequences for arc magma generation. Earth and Planetary Science Letters, 163(1-4): 361-379.

Sella, G.F., Dixon, T.H. and Mao, A., 2002. REVEL: A model for recent plate velocities from space geodesy. Journal of Geophysical Research, 107: 1-32.

Shamberger, P.J. and Hammer, J.E., 2006. Leucocratic and Gabbroic xenoliths from Hualai volcano, Hawaii. Journal of Petrology, 47: 1785-1808.

Shaw, H.P., 1972. Viscosities of magmatic silicate liquids: an empirical method of prediction. American Journal of Science, 272: 870-893.

Shaw, H.R., 1974. Diffusion of H_2O in granitic liquids, I. experimental data; II mass transfer in magma chambers. In: A.W. Hofmann, B.J. Giletti, H.S. Yoder JR and R.A. Yund (Editors), Geochemical Transport and Kinetics. Carnegie Inst. Washington Publ., Washington, pp. 139-170.

Shimizu, N. and Kushiro, I., 1975. Partitioning of Rare-Earth Elements between Garnet and Liquid at High-Pressures - Preliminary Experiments. Geophysical Research Letters 2 413-416.

Sigmarsson, O., Carn, S. and Carracedo, J.C., 1998. Systematics of U-series nuclides in primitive lavas from the 1730-36 eruption on Lanzarote, Canary Islands and implications for the role of garnet pyroxenites during oceanic basalt formations. Earth and Planetary Science Letters, 162: 137-151.

Sigmarsson, O., Condomines, M. and Fourcade, S., 1992a. A detailed Th, Sr and O isotope study of Hekla: differentiation processes in an Icelandic volcano. Contributions to Mineralogy and Petrology, 112: 20-34.

Sigmarsson, O., Condomines, M. and Fourcade, S., 1992b. Mantle and crustal contribution in the genesis of recent basalts from off-rift zones in Iceland: constraints from Th, Sr and O isotopes. Earth and Planetary Science Letters, 110: 149-162.

Sigmarsson, O., Hémond, C., Condomines, M., Fourcade, S. and Oskarsson, N., 1991. Origin of silicic magma in Iceland revealed by Th isotopes. Geology, 19: 621-624.

Sigmarsson, O., 1999. Segregation veins in Surtsey lavas, Iceland, and implications for volatile-liquid transfer processes during magma differentiation. Université Blaise Pascal, Clermont-Ferrand.

Sigmarsson, O., Karlsson, H.R. and Larsen, G., 2000. The 1996 and 1998 subglacial eruptions beneath the Vatnajökull ice sheet in Iceland: contrasting geochemical and geophysical inferences on magma migration Bulletin of volcanology, 61: 468-476.

Sigmundsson, F., Einarsson, P., Bilham, R. and Sturkell, E., 1995. Rift transform kinematics in south Iceland: deformation from Global Positionning System measurements 1986 to 1992. Journal of Geophysical Research, 100: 6235-6248.

Sigurdsson, H., 1977. Generation of icelandic rhyolites by melting of plagiogranites in the oceanic layer. Nature, 269: 28-28.

Sigurdsson, H. and Sparks, R.S.J., 1981. Petrology of Rhyolitic and Mixed Ejecta from the 1875 Eruption of Askja, Iceland. Journal of Petrology, 22: 41-84.

Sigvaldason, G.E., 2002a. Volcanic and tectonic processes coinciding with glaciation and crustal rebound: an early Holocene rhyolitic eruption in the Dyngjufjöll volcanic centre and the formation of the Askja caldera, north Iceland. Bulletin of volcanology, 64: 192-205.

Sigvaldason, G.E., 2002b. Volcanic and tectonic processes coinciding with glaciation and crustal rebound: an early Holocene rhyolitic eruption in the Dynjujöll volcanic centre and the formation of the Askja caldera, north Iceland. Bulletin of volcanology, 64: 192-205.

Sisson, T.W. and Bacon, C.R., 1999. Gas-driven pressing in magmas. Geology, 27: 613-616.

Sleep, N., 1994. Martian plate tectonics. Journal of Geophysical Research, 99: 5639-5655.

Smithies, R.H., 2000. The Archaean tonalite-trondhjemite-granodiorite (TTG) series is not an analogue of Cenozoic adakite. Earth and Planetary Science Letters, 182: 115-125.

Smithies, R.H., Van Kranendonk, M.J. and Champion, D.C., 2005. It started with a plume - early Archaean basaltic proto-continental crust. Earth and Planetary Science Letters, 238(3-4): 284-297.

Sotin, C., 2005. Thermal evolution of the earth during the first billion years. In: M. Gargaud, B. Barbier, H. Martin and J. Reisse (Editors), Lectures in Astrobiology. Springer-Verlag, pp. 167-196 (in press).

Spera, F.J., 2000. Physical properties of magma. In: H. Sigurdsson (Editor), Encyclopedia of volcanoes. Academic press, London, pp. 171-190.

Stein, M. and Hofmann, A.W., 1994. Mantle plumes and episodic crustal growth. Nature, 372: 63-68.

Steinthorsson, S., 1967. Tvær nýjar C^{14}-aldursákvarðanir á ökulögum úr Snæfellsjökli Náttúrufræðingurinn, 37: 236-238.

Stormer, J.C. and Nicholls, J., 1978. XLFRAC: a program for interactive testing of magmatic differentiation models. Computer Geoscience, 87: 51-64.

Sun, S.S. and McDonough, W.F., 1989. Chemical and isotopic systematics of oceanic basalts: Implications for the mantle composition and processes., Magmatism in the Ocean Basin. Geol. Soc. Sp. Publi., pp. 313-345.

T

Tamic, n., Behrens, H. and Holtz, F., 2001. The solubility of H_2O in rhyolitic melts in equilibrium with a mixed CO_2-H_2O fluid phase. Chemical Geology, 174: 333-347.

Tatsumi, Y., 1989. Migration of fluid phase and genesis of basalt magma in subduction zones. Journal of Geophysical Research, 94: 4697-4707.

Taylor, J.H.P. and Forester, R.W., 1979. An oxygen and hydrogen isotope study of the Skaergaard intrusion and its country rocks: a description of a 55-My old fossil hydrothermal system. Journal of Petrology, 20: 355-419.

Taylor, J.H.P. and Sheppard, S.M.F., 1986. Igneous rocks:I. Processes of isotopic fractionation and isotope systematics. In: J.W. Valley, J.H.P. Taylor and J.R. O'Neil (Editors), Reviews in Mineralogy, volume16: Stable isotopes in high temperature geological processes. Mineralogical society of Amercia.

Taylor, S.R. and McLennan, S.M., 1985. The continental crust: its composition and evolution: An examination of the geochemical record preserved in sedimentary rocks. Blackwell Scientific Publications, Oxford.

Thordarson, T. and Hoskuldsson, A., 2002. Iceland. Classic Geology in Europe 3. Terra Publishing, Harpenden, Hertfordshire.

Thordarson, T. and Self, S., 1998. The Roza member, Columbia basalt group: a gigantic pahoehoe lava flow field formed by endogenous processes? Journal of Geophysical Research, 103: 27411-27445.

Tiepolo M (2003) In situ Pb geochronology of zircon with laser ablation-inductively coupled plasma-sector field mass spectrometry. Chem Geol 14192: 1-19

V

Vervoort, J.D., Patchett, P.J., Gehrels, G.E. and Nutman, A.J., 1996. Constraints on early Earth differentiation from hafnium and neodymium isotopes. Nature, 379: 624-627.

Vink, G.E., 1984. A hotspot model for Iceland and the Vøring plateau. Journal of Geophysical Research, 89: 9949-9959.

Vogt, P.R., Johnson, G.L. and Kristjánsson, L., 1980. Morphology and magnetic anomalies north of Iceland. J. Geophys., 47: 67-80.

W

Wager, L.R. and Brown, G.M., 1967. Layered igneous rocks, San Fransisco.

Walker, G.P.L., 1963. The Breiddalur central volcano, Eastern iceland. Quart J. geol. Soc. Lond., 119: 29-63.

Walker, G.P.L., 1975. Excess spreading axes and spreading rate in iceland. Nature, 255: 468-470.

Walker, G.P.L., 1976. Spreading rate in Iceland. Nature, 261: 75-76.

Walker, J.A., 1989. Caribbean are tholeiites. Journal of Geophysical Research, 94: 10539-10548.

Wallace, P. and Anderson, A.T., 2000. Volatiles in magmas. In: H. Sigurdsson (Editor), Encyclopedia of volcanoes. Academic press., London.

Warren, P.H., 1985. The magma ocean concept and lunar evolution. Annual Review of Earth Planetary Science, 13: 201-240.

Watson, E.B., 1979. Zircon saturation in felsic liquids: experimental results and applications to trace element geochemistry. Contribution to Mineralogy and Petrology, 70: 407-419.

White, R.S., McKenzie, D. and O'Nions, R.K., 1992. Oceanic crustal thikness from seismic measurements and rare earth element inversions. Journal of Geophysical Research, 97: 19683-19715.

Wiedenbeck, M., Allé, P., Corfu, F., Griffin, W.L., Meier, M., Oberli, F., von Quadt, A., Roddick, J.C., and Spiegel, W., (1995). Three natural zircon standards for U-Th-Pb, Lu-Hf, trace element and REE analyses. Geostand. Newsl. 19/1, 1-23.

Wilde, S.A., Valley, J.W., Peck, W.H. and Graham, C.M., 2001. Evidence from detrital zircons for the existence of continental crust and oceans on the Earth 4.4 Ga ago. Nature, 409: 175-178.

Winkler, H.G.F., 1974. Petrogenesis of metamorphic Rocks. Springer Verlag, New york, 320 pp.

Wolf, M.B. and Wyllie, P.J., 1994. Dehydration-melting of amphibolite at 10 Kbar: the effects of temperature and time. Contribution to Mineralogy and Petrology, 115: 369-383.

Wolfe, C.J., Bjarnason, I.T., VanDecar, S.C. and Solomon, S.C., 1997. Seismic structure of the Iceland mantle plume. Nature, 385: 245-247.

Wood, D.A., 1978. Major and trace element variations in the tertiary lavas of eastern Iceland and their significance with respect to the Iceland geochemical anomaly. Journal of Petrology, 19: 393-436.

Wyllie, P.J. and Sekine, T., 1982. The formation of mantle phlogopite in subduction zone hybridization. Contributions to Mineralogy and Petrology, 79(4): 375-380.

X

Xiao, Y., Sun, W., Hoefs, J., Simon, K., Zhang, Z., Li, S. and Hofmann, A.W., 2006. Making continental crust through slab melting: Constraints from niobium-tantalum fractionation in UHP metamorphic rutile. Geochimica et Cosmochimica Acta, 70(18): 4770-4782.

Y

Yin, Q., Jacobsen, S.B., Yamashita, K., Blichert-Toft, J., Telouk, P. and Albarède, F., 2002. A short timescale for terrestrial planet formation from Hf-W chronometry of meteorites. Nature, 418(6901): 949-952.

Young, K.D., Jancin, M., Voight, B. and Orkan, N.I., 1985. Transform deformation of the tertiary rocks along the Tjörnes fracture zone, north central Iceland. Journal of Geophysical Research, 90: 9986-10010.

Z

Zindler, A., Hart, S.R., Frey, F.A. and Jakobsson, S.P., 1979. Nd and Sr isotope ratios and rare earth element abundances in Reykjanes Peninsula basalts: evidence for mantle heterogeneity beneath Iceland. Earth and Planetary Science Letters, 45: 249-262.

Annexes

Annexe 1 : Description et localisation des échantillons

Région	*Nom de l'échantillon*	*Localisation (cf. carte)*	*Type de roche*	*Paragenèse*
Þjórsárdalur	Thd1	64°07.75N 19°49.46W	Dyke rhyolitique	Phénocristaux (3%): plagioclase (65%) + clinopyroxène (35%) Matrice vitreuse (97%) : contenant de nombreux nucléi et petits cristaux (50%) de plagioclase (30%) + clinopyroxène (18%) + minéraux opaques (2%)
Búðarháls	Bh1a	64°14.10N 19°22.12W	Dôme rhyolitique	Rares phénocristaux de plagioclase (2%) Microlithe : plagioclase (75%) + verre (20%) + minéraux opaques (5%) ± carbonates ± quartz
Hrafntinnusker	Hsk1 Hsk3 Hsk4 Hsk7	63°55.56 19°10.73W	Ponces rhyolitiques	Densité importante de vésicules, chacune bordée de parois vitreuses
	Hsk8	63°55.82N 19°11.30W	Obsidienne rhyolitique	Verre comprenant des nucléi ou petits cristaux de plagioclase + minéraux opaques ± clinopyroxène
Laufafell	Lauf	63°54.68N 19°20.93W	Obsidienne rhyolitique	Phénocristaux (5%) : plagioclase (80%) + clinopyroxène altéré (20%) Matrice vitreuse (95%) : verre (85%) + plagioclase (12%) + clinopyroxène (3%) ± zircon ± apatite
Húsafell	Husf4	64°45.83 20°44.97W	Coulée de basalte	Micro-phénocristaux (15%) : plagioclase (70%) + clinopyroxène (30%) + minéraux Microlithe (85%) : plagioclase (40%) + clinopyroxène (40%) + verre (10%) + minéraux opaques (10%)

Région	*Nom de l'échantillon*	*Localisation (cf. carte)*	*Type de roche*	*Paragenèse*
Baula	Bau1	64°51.00N 21°27.58W	Dôme rhyolitique	Phénocristaux (5%) : plagioclase (90%) + clinopyroxène (10%) Micro-phénocristaux de plagioclase (20%) Microlithe (75%) : plagioclase + verre + quartz (90-95%) + minéraux opaques (5-10%)
Drápuhlíðarfjall	Drap2	64°59.57N 22°43.77W	Dacite	Rares phénocristaux de plagioclase et olivine idingsitisées Microlithe : plagioclase (45%) + clinopyroxène (25%) + verre (10%) + orthopyroxene ± oxydés (15%) + minéraux opaques (5%) ± apatite ± zircon
Setberg	Setb3	64°57.50N 23°12.62W	Dyke rhyolite	Pas de phénocristaux Vésicules remplies de quartz (18%) + carbonates (2%) Microlithe (80%): feldspath (80%) + épidote (10%) + verre (15%) ± zircon
Fróðárheiði	Fro1	64°53.95N 23°33.27W	Granophyre	Feldspath alcalin (65%) + quartz (30%) présentant souvent des textures micrographiques + minéraux opaque (5%) ± zircon
Axlarhýrna	Axl1	64°49.86N 23°27.67W	Granophyre	Feldspath alcalin ±perthitique (65%) + quartz (30%) présentant souvent des textures micrographiques + carbonate (5%) ± zircon et apatite
Lýsuhóll	Ell1	64°50.79N 23°12.59W	Granophyre	Feldspath alcalin (60%) + quartz (25%) présentant souvent des textures micrographiques + amphibole ±chloritisée (13%) + épidote (2%) ± zircon et apatite

Région	*Nom de l'échantillon*	*Localisation (cf. carte)*	*Type de roche*	*Paragenèse*
Vesturhorn	Ves1	64°15.63N 14°59.63W	Gabbro	Plagioclase (25-30%) + feldspath alcalin (15%) + quartz (15%) présentant souvent des textures micrographiques + amphibole ±chloritisée (15%) + clinopyroxène (15%) + minéraux opaques (5-10%) + chlorite (3%) + biotite (3%) + épidote (1%) ± zircon, apatite
	Ves2		Granophyre	Feldspath alcalin ±perthitique et ±altéré (53%) + quartz (40%) présentant souvent des textures micrographiques + minéraux opaques (4%) + biotite peu chloritisée (3%) ± zircon, apatite
Hvalnesskriður	Hval2	64°26.35N 14°30.19W	Gabbro	Feldspath alcalin ±altéré (35%) + plagioclase ±altéré (25%) + quartz (20%) + amphibole ±chloritisée (15%) + minéraux opaques (5%) ± épidote et zircon
	Hval1a	64°26.35N 14°30.19W	Granophyre contenant des enclaves basaltiques (Hval1b)	Plagioclase (65%) + amphibole (15%) + chlorite (5-10%) + minéraux opaques (5-10%) ± épidote, zircon, apatite
	Hval1b		Enclaves basaltiques dans le granophyre Hval1a	Plagioclase (40%) + clinopyroxènes (30%) + minéraux opaques (10%) + biotite (10%) + chlorite (5%) + épidote (5%)
Búr	Búr4		Coulée Basaltique	Rares phénocristaux de plagioclase et clinopyroxène Microlithe : plagioclase (50%) + clinopyroxène (40%) + minéraux opaques (5-10%) + verre (2-3%)

Région	*Nom de l'échantillon*	*Localisation (cf. carte)*	*Type de roche*	*Paragenèse*
Streitishvarf	Stretit1a	64°43.85N 13°59.29W	Dyke rhyolitique contenant des enclaves basaltiques (Streit 1b)	Phénocristaux (10%) : feldspath + quartz Microlithe (90%) : feldspath > quartz (90%) + minéraux opaques (10%) ± zircon
	Streit1b		Enclaves basaltiques du dyke rhyolitique Streit1a	Rares phénocristaux de plagioclase déstabilisé Micro-phénocristaux (30%) Plagioclase (65%) + clinopyroxène (45%) Microlithe (70%) : plagioclase + clinopyroxène + minéraux opaques + verre
Rauðafell	Rauðf1	64°48.39N 14°30.31W	Dyke basaltique	Rares micro-phénocristaux de Plagioclase (50%) + clinopyroxène (50%) Microlithe : plagioclase (60%) + clinopyroxène (25%) + minéraux opaques (10%) + verre (5%)
Berufjörður	Beruf1	64°45.99N 14°24.21W	Rhyolite	Micro-phénocristaux (4%) : plagioclase ± clinopyroxène ± minéraux opaques Microlithe (96%) : feldspath > quartz (96%) + minéraux opaques (4%) ± zircon
Sandfell	San1	64°52.66N 13°52.66W	Rhyolite intrusive	Phénocristaux (5%) : plagioclase (60%) + agglomérats de quartz (30%) + minéraux opaques (10%) Microlithe (95%) : quartz + feldspath (97%) + minéraux opaques (3%)
Reyðarfjörður	Rey3	64°58.86N 13°53.23W	Rhyolite	Pas de phénocristaux Feldspath + quartz (95%) + minéraux opaques (5%)
Refsstaður	Ref1	65°40.15N 14°48.40W	Rhyolite altérée intrusive	Phénocristaux (10%) : plagioclase (60%) + clinopyroxène (40%) Matrice vitreuse dévitrifiée principalement en feldspath et quartz ± zircon
Húsavík	Hus1	65°23.67N 13°41.16W	Ignimbrite rhyolitique	Verre ± dévitrifié : plagioclase + quartz ± clinopyroxène

Région	*Nom de l'échantillon*	*Localisation (cf. carte)*	*Type de roche*	*Paragenèse*
Hvítserkur	Hvs1	65°25.75N 13°45.59W	Dyke basaltique	Matrice oxydée (opaque ; 70%) + Plagioclase (20%) + clinopyroxène (3-5%) + olivine altérée (5-10%)
Höfn	Höfn1	65°32.18N 13°45.39W	Dyke rhyolitique	Pas de phénocristaux Quartz + feldspath (90%) + minéraux opaques (5%) + carbonate (5%)

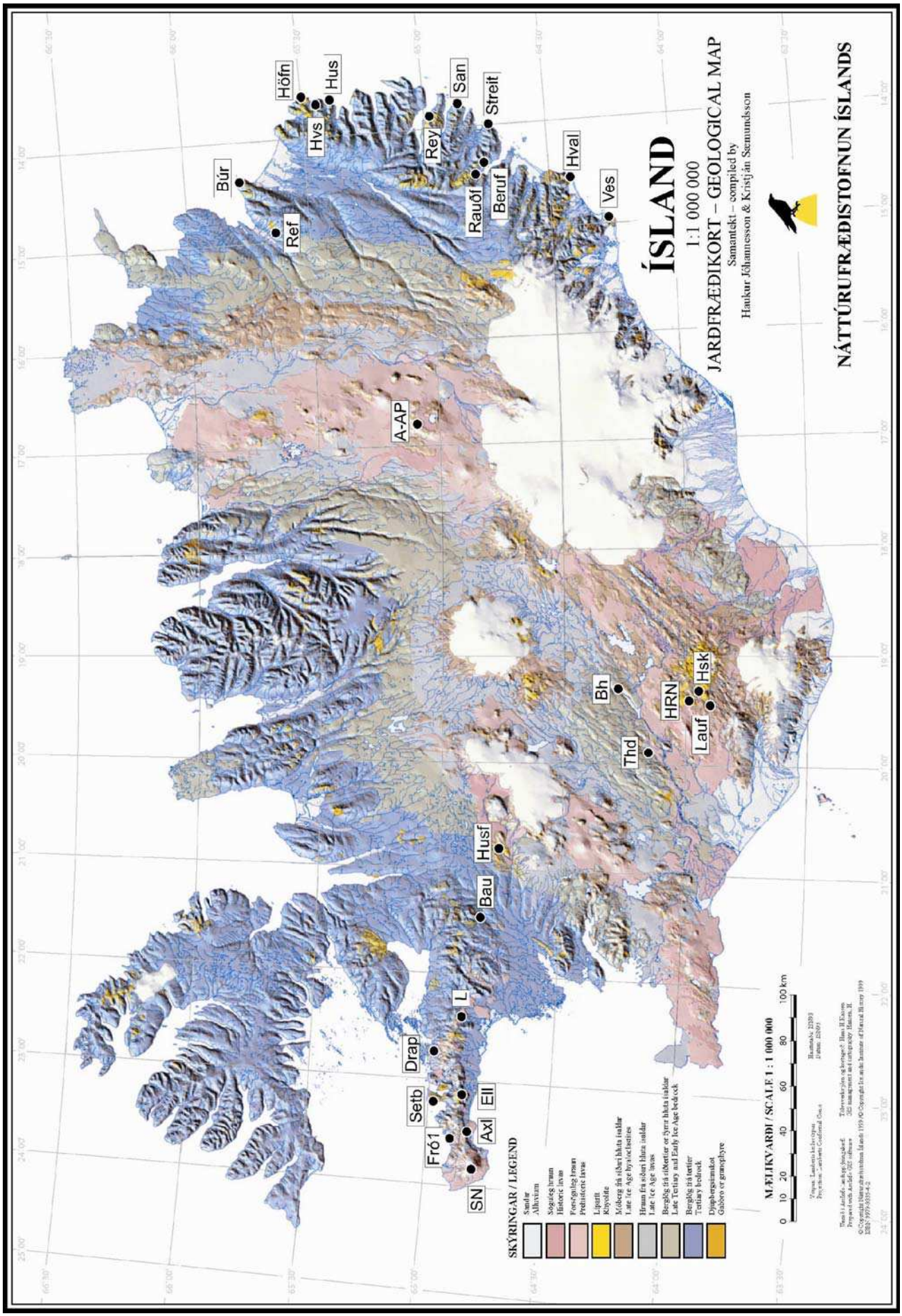
ÍSLAND
1:1 000 000
JARÐFRÆÐIKORT – GEOLOGICAL MAP
Samantekt – compiled by
Haukur Jóhannesson & Kristján Sæmundsson
NÁTTÚRUFRÆÐISTOFNUN ÍSLANDS
SKÝRINGAR / LEGEND
MÆLIKVARÐI / SCALE 1 : 1 000 000
Höfn
Hus
Hvs
Búr
Rey
San
Streit
Ref
Rauðf
Beruf
Hval
Ves
A-AP
Husf
Bau
L
Drap
Setb
Ell
Fró1
Axl
SN
Bh
Thd
HRN
Hsk
Lauf

Voici des photos prises au microscope optique de quelques échantillons représentatifs de l'ensemble de ceux décrit précédemment.

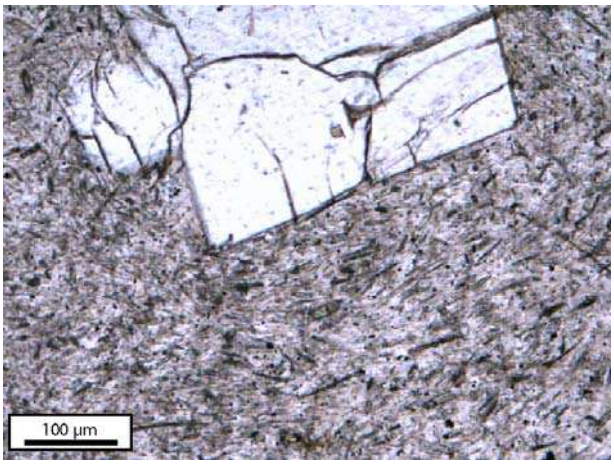

Thd1 :

Phénocristal de plagioclase dans une matrice vitreuse contenant de nombreux nucléi de plagioclase, clinopyroxène et minéraux opaques.

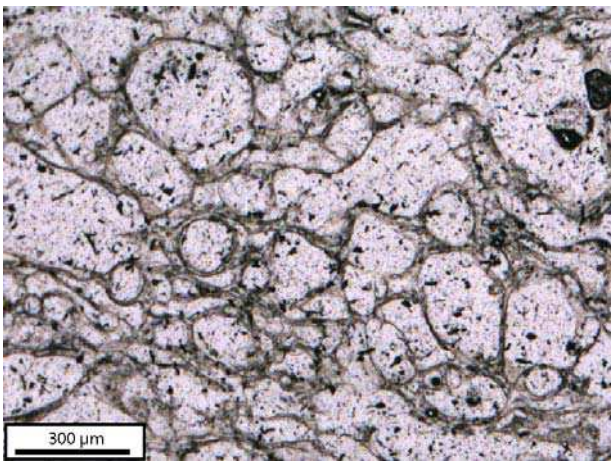

Hsk3 :

Ponce présentant une densité de vésicule importante, chacune délimitées par une fine paroi de verre totalement aphyrique.

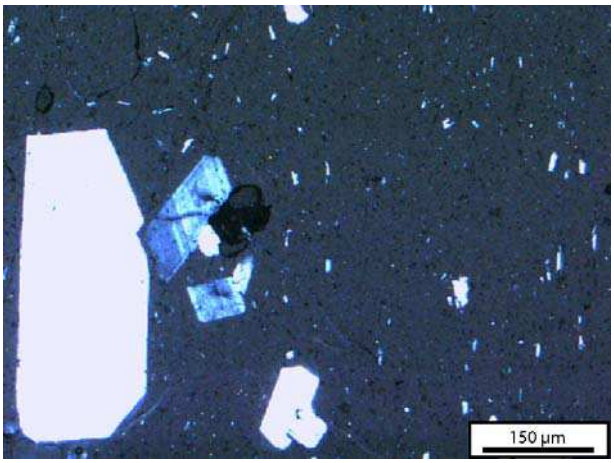

Lauf :

Phénocristaux de plagioclase dans une matrice vitreuse à faible densité de cristaux.

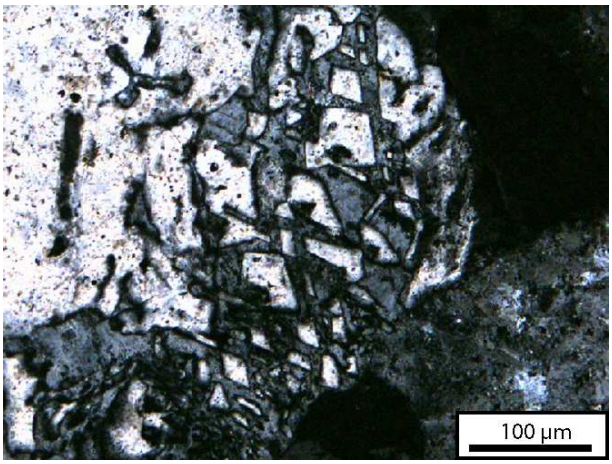

Fro1 :

Texture micrographique (intercroissance de feldspath et quartz).

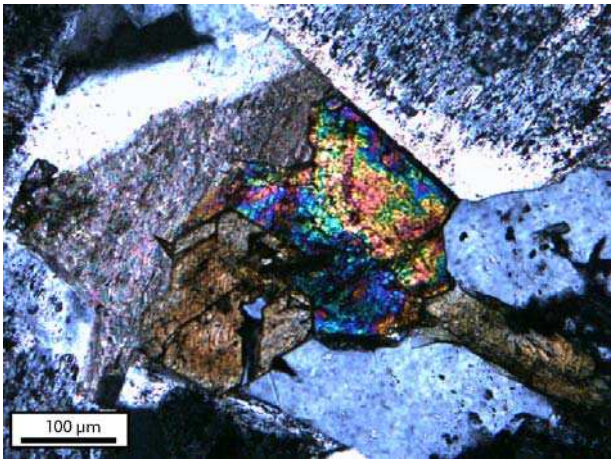

Ell1 :

Cristal d'épidote (présentant une teinte de biréfringence élevée) accompagnée d'amphibole dans une texture grenue principalement composée de feldspath et quartz.

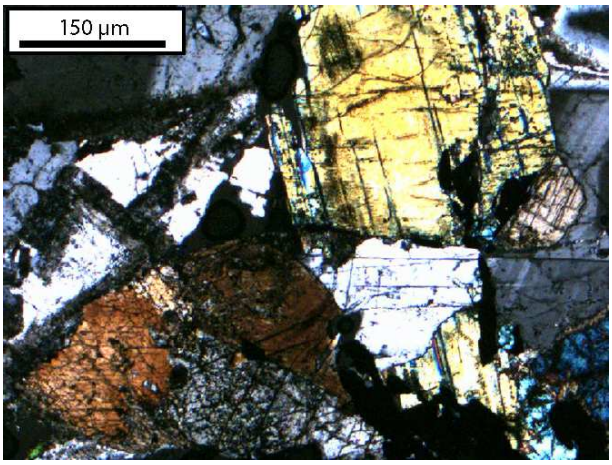

Ves1 :

Texture grenue composée de feldspath, quartz, amphibole et clinopyroxène.

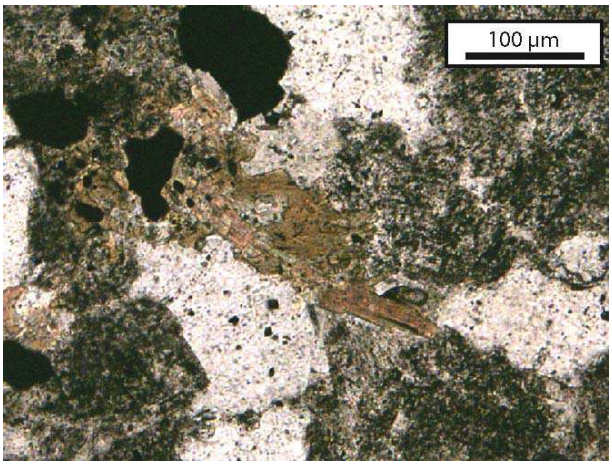

Ves2 :

Cristaux de biotite dans une texture grenue principalement composée de feldspath et quartz.

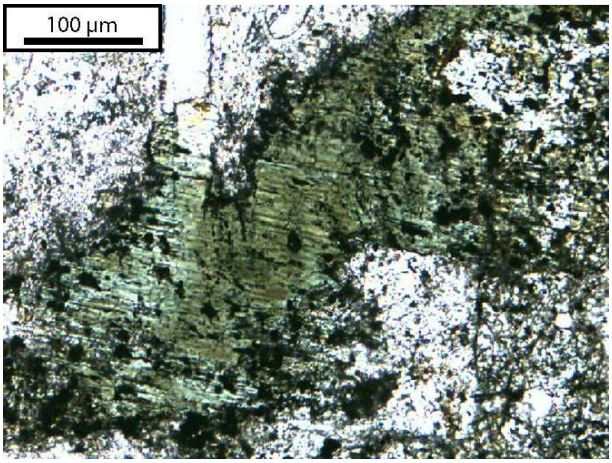

Hval2 :

Cristal de chlorite remplaçant le plus souvent l'amphibole.

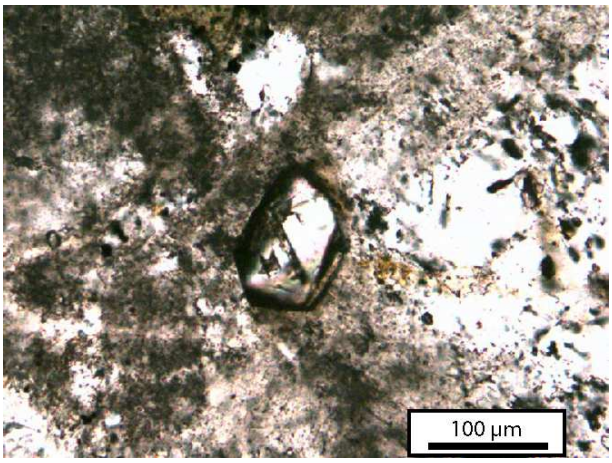

Hval2 :

Cristal de zircon

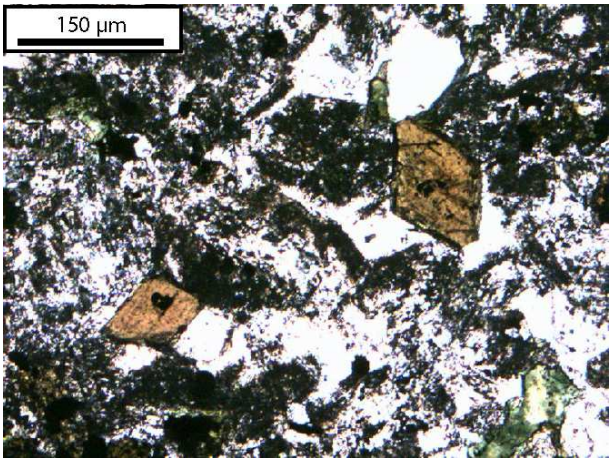

Hval1a :

Quelques cristaux d'amphibole et de chlorite dans une matrice principalement composée de plagioclase et minéraux opaques.

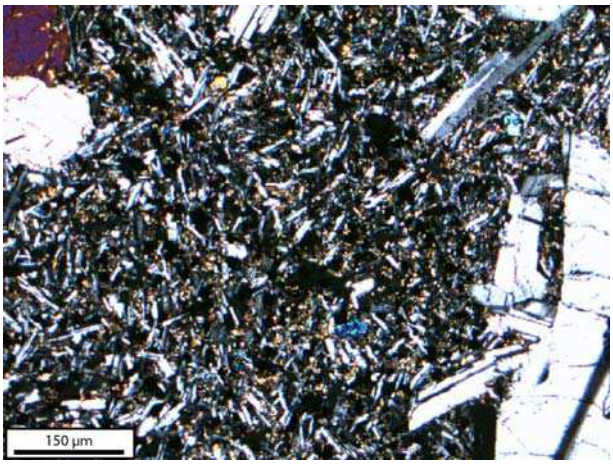

Bur4 :

Texture et composition minéralogique classique d'une coulée basaltique.

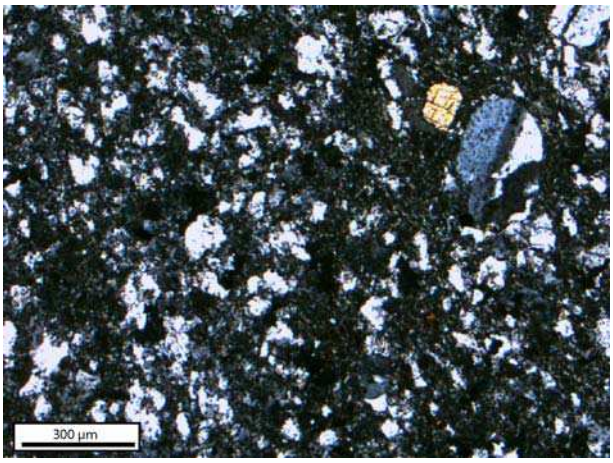

Beruf1 :

Quelques phénocristaux de plagioclase et clinopyroxène dans une matrice finement cristallisée et principalement composée de feldspath, quartz et de verre.

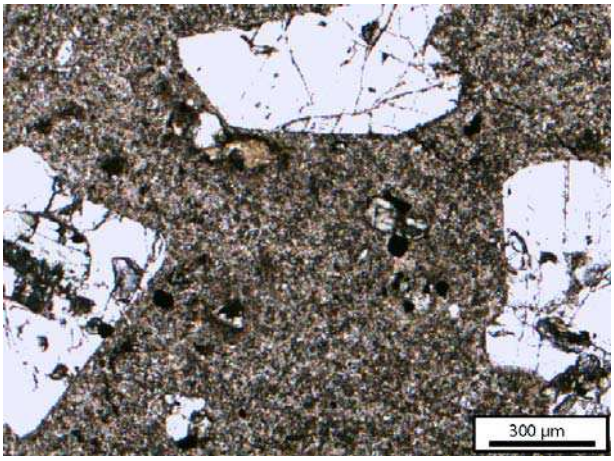

Ref1 :

Phénocristaux de plagioclase dans une matrice vitreuse plus ou moins dévitrifiée.

Annexe 2 : Protocole d'analyse des éléments majeurs et en trace

Principe de la méthode

La méthode d'attaque par fusion alcaline des échantillons permet de transformer l'échantillon en « perle » de magma et de mettre ce dernier quasi instantanément en solution. Les teneurs en éléments majeurs et traces sont ensuite respectivement analysés par ICP-AES et ICP-MS.

Attaque par fusion alcaline

- Mélanger dans des creusets en graphite 100 mg d'échantillon avec 300 mg de fondant (tétrataborate de lithium, $LiBO_3$).
- Placer le creuset dans un four à induction magnétique (1100°C) pendant 5 minutes.
- Verser la « perle » en fusion dans une solution composée de 50 mL de HNO_3 (1M) et 40 µL de HF (29M).
- Laisser agiter jusqu'à ce que tout soit bien dissous.

Mesure des éléments majeurs

Les analyses faites sur un ICP-AES ULTIMA C Jobin-Yvon ont permis d'établir un facteur de dilution totale de l'échantillon optimum qui est de 2000. Afin d'arriver à ce facteur de dilution, une aliquote de la solution précédemment obtenue, de 4 mL est prélevée et diluée dans 12 mL d'H_2O.

Le nébuliseur utilisé est un Sea Spray (Glass Expansion), la chambre de nébulisation est de type cyclonique et enfin un humidificateur d'argon est utilisé afin de minimiser la précipitation de sels qui pourraient éventuellement boucher le nébuliseur.

Des standards internationaux tels que le BR, GH, BHVO-1 et DRN-1 (Govindaraju, 1994) sont utilisés pour calibrer la machine. Un blanc (fondant de $LiBO_3$), GH (pour Si, Na et K) et BR (Al, Fe, Mn, Mg, Ca, Ti et P) sont utilisés pour étalonner la machine. Le passage de DRN-1 tous les 3-4 échantillons permet de normaliser les valeurs obtenues à celles admises comme références afin d'annuler tout effet de dérive de l'ICP-AES. Enfin 8 A-THO et 10 BHVO-1 ont été passé comme inconnu dans différentes sessions d'analyse afin d'estimer l'erreur externe de la machine (Tableau 1).

	Moyenne A-THO	erreur externe (2σ) %	A-THO de référence (1)	Moyenne BHVO-1	erreur externe (2σ) %	BHVO-1 de référence (2)
SiO2	75.1	*0.4*	75.6	49.4	*0.3*	49.9
TiO2	0.24	*1.9*	0.255	2.82	*0.3*	2.71
Al_2O_3	11.9	*1.5*	12.2	13.5	*0.3*	13.8
Fe_2O_3*	3.7	*1.0*	3.62	12.3	*0.3*	12.3
MnO	0.10	*1.7*	0.106	0.17	*1.2*	0.17
MgO	0.097	*9.3*	0.103	7.33	*0.3*	7.2
CaO	1.64	*4.5*	1.7	11.4	*0.4*	11.4
NaO	4.28	*1.8*	3.75	2.30	*0.9*	2.3
K_20	2.59	*2.6*	2.64	0.53	*1.8*	0.52
P_2O_5	0.03	*18.5*	0.025	0.28	*1.2*	0.27

Tableau 1: Erreurs externes de l'ICP-AES estimées à partir de A-THO (n=8) et BHVO-1 (n=10). (1) Jochum et al (2006) et (2) Govindaraj (1994)

Mesure des éléments traces

Les analyses faites sur un ICP-MS VG PQ2+ ont permis d'établir un facteur de dilution totale de l'échantillon optimum qui est de 6500. Afin d'arriver à ce facteur de dilution, une aliquote de la solution précédemment obtenue, de 1 mL est prélevée et diluée dans 12 mL de standard interne composé de 10 ppb de Mo, In, Re, Bi et Rh ainsi que de 70 ppb de Ge.

L'ICP-MS est équipé d'un nébuliseur concentrique (glass expansion) d'une chambre de nébulisation de type Scott et enfin d'une torche Fassel.

La calibration du spectromètre se fait à partir du standard interne (10 ppb de Mo, In, Re, Bi et Rh ainsi que 70 ppb de Ge) et du standard externe BR (Govindaraju, 1994). Le passage de BR tous les 3-4 échantillons permet de normaliser les valeurs obtenues à celle admises comme références, ce qui annule tout effet de dérive potentielle de l'ICP-MS. Enfin BHVO-1 (Govindaraju, 1994) a été passé comme inconnu au cours de chaque session d'analyses permettent d'estimer l'erreur externe du spectromètre (Tableau 2).

	Moyenne BHVO-1	*erreur externe (2σ)*	BHVO-1 de référence
Rb	9.55	*3.6*	11.0
Sr	387.6	*0.8*	403
Y	27.1	*0.4*	27.6
Zr	166.3	*1.4*	179
Nb	16.2	*1.1*	19.0
Ba	128.2	*1.0*	139
La	15.3	*1.5*	15.8
Ce	37.3	*0.8*	39.0
Pr	5.26	*1.0*	5.70
Nd	24.1	*0.8*	25.2
Sm	6.11	*2.2*	6.20
Eu	2.27	*11.8*	2.06
Gd	5.55	*11.2*	6.40
Tb	0.90	*2.9*	0.96
Dy	5.25	*1.7*	5.20
Ho	1.00	*1.1*	0.99
Er	2.43	*1.7*	2.40
Tm	0.31	*0.8*	0.33
Yb	1.97	*1.4*	2.02
Lu	0.29	*3.1*	0.29
Hf	4.31	*1.2*	4.38
Ta	1.19	*13.2*	1.23
Pb	2.42	*19.6*	2.60
Th	1.29	*2.6*	1.08
U	0.42	*3.4*	0.42

Tableau 2 : Erreurs externes de l'ICP-MS estimée à partir du standard international BHVO-1 (n=3). (1) Govindaraju (1994).

Tous les échantillons provenant de l'ouest, sud et centre de l'Islande ont été analysés au Laboratoire Magmas et Volcans (LMV) de Clermont-Ferrand, suivant les conditions analytiques ci-dessus alors que ceux provenant de l'est de l'Islande ont été analysés par le laboratoire ACME (Vancouver, Canada) suivant la même méthode. Dans un souci de comparaison, il a été inséré un échantillon acide et un basique déjà analysés au LMV dans la série envoyée au laboratoire ACME (Tableau 3). Ces échantillons sont A-THO et B-THO ; A-THO (Jochum et al., 2006) est une obsidienne rhyolitique bien connue car utilisée comme standard pour les teneurs en U et Th obtenue par dilution isotopique et B-THO qui provient du même échantillon (même poudre de roche totale) que le standard international BIR (Govindaraju, 1994) dont la composition est parfaitement connue.

	A-THO ref	A-THO LMV	A-THO ACME	BIR ref	BIR LMV	B-THO ACME
SiO_2	**75.6**	75.13	74.18	**47.8**	46.3	47.19
TiO_2	**0.255**	0.24	0.25	**0.96**	0.93	0.93
Al_2O_3	**12.2**	11.91	12.14	**15.3**	15.3	15.62
$Fe_2O_3^*$	**3.62**	3.66	3.79	**11.4**	11.2	11.19
MnO	**0.106**	0.10	0.09	**0.17**	0.17	0.16
MgO	**0.103**	0.10	0.10	**9.68**	10.9	10.49
CaO	**1.7**	1.64	1.78	**13.2**	13.4	12.79
Na_2O	**3.75**	4.28	4.44	**1.75**	1.59	1.68
K_20	**2.64**	2.59	2.78	*0.03*	0.05	0.04
P_2O_5	**0.025**	0.03	0.03	*0.05*	0.03	0.02
total	**100.0**	**99.7**	**99.6**	**100.4**	**100.0**	**100.1**
Rb	**65.3**	64.4	64.20	**0.25**	0.31	<.5
Sr	**94.1**	96.0	104.65	**108**	113	119.6
Y	**94.5**	103.1	106.85	**16**	17	16.3
Zr	**512**	526.3	506.20	*15.5*	15.3	14.2
Nb	**62.4**	56.8	55.95	*0.6*	0.56	0.5
Ba	**547**	574.0	568.4	*7*	6.7	8.7
La	**55.6**	55.3	61.60	**0.62**	0.64	1.0
Ce	**121**	125.2	135.25	**1.95**	1.99	2.2
Pr	**14.6**	15.8	16.71	**0.38**	0.41	0.46
Nd	**60.9**	62.5	68.40	**2.5**	2.4	2.8
Sm	**14.2**	15.0	15.80	**1.1**	1.1	1.3
Eu	**2.76**	2.6	3.22	**0.54**	0.52	0.52
Gd	**15.3**	15.8	16.10	**1.85**	1.92	2.11
Tb	**2.51**	2.8	3.02	**0.36**	0.37	0.5
Dy	**16.2**	16.1	18.64	**2.5**	2.5	2.54
Ho	**3.43**	3.5	3.78	**0.57**	0.57	0.55
Er	**10.3**	9.8	11.60	**1.7**	1.6	2
Tm	**1.52**	1.6	1.79	**0.26**	0.24	0.27
Yb	**10.5**	10.3	10.88	**1.65**	1.67	1.63
Lu	**1.54**	1.5	1.71	**0.26**	0.27	0.28
Hf	**13.7**	13.0	16.5	**0.6**	0.6	<.5
Ta	**3.9**	4.2	4.15	*0.04*	0.03	<.1
Th	**7.4**	7.2	8.70	*0.03*	0.02	<.1
U	**2.37**	2.4	2.60	*0.01*	0.01	<.1

Tableau 3 : Valeurs de A-THO et B-THO/BIR obtenues au LMV (Clermont-Ferrand, France), au laboratoire ACME (Vancouver, Canada) et les valeurs de référence internationale de A-THO (Jochum et al., 2006) et BIR (Govindaraju, 1994). Les valeurs en gras sont les valeurs certifiées des standards.

Les analyses en éléments majeurs sont relativement comparables entre les analyses faites au LMV et celles faites au laboratoire ACME. En effet, la moyenne des écarts aux valeurs de références (Equation 1) est de 5,6 % (LMV) et 8 % (ACME) pour le standard A-THO. En ce qui concerne le standard BIR et ne considérant pas les teneurs en K_2O et P_2O_5 (non certifiées), la moyenne des écarts aux valeurs de références sont de 3,9 % (LMV) et 3,7 % (ACME).

$$Ecart(\%) = \frac{C_{(Lab)} - C_{(Std)}}{C_{(Std)}} \times 100$$ *Équation* 1

$C_{(Lab)}$ *: Teneurs analysé dans le laboratoire considéré d'un standard.*

$C_{(Std)}$ *: Teneurs de référence du standard*

Contrairement aux éléments majeurs, les éléments en trace présentent des valeurs sensiblement différentes selon le labo d'analyse. La Figure 1 permet de visualiser très clairement le fait que les analyses en éléments trace faites au LMV sont systématiquement plus proches des valeurs de référence que celles faites au laboratoire ACME. En ce qui concerne le standard A-THO, les analyses faites au LMV sont systématiquement inférieures à 10 % d'écart et présentent une moyenne de 4,3 %, alors que celles faites au laboratoire ACME peuvent aller jusqu'à 20 % d'écart aux valeurs de référence et présente une moyenne de 11,2 %. Pour ce qui est du standard BIR/B-THO, les analyses faites au LMV sont systématiquement inférieures à 8 % d'écart aux valeurs de références avec une moyenne de 3,6 %, alors que celles faites au laboratoire ACME ont une moyenne des écarts à 14,7 % avec des écarts importants pour des éléments comme le La, Tb et le Ba. Il est également à noter que des éléments comme le Th, Rb et Ta analysé au LMV, ayant des faibles teneurs dans le BIR, présentent des écarts aux valeurs de références de l'ordre de 25 - 30 %. Mais pour ces mêmes éléments plus l'U et l'Hf, les teneurs sont inférieures au seuil de détection du laboratoire ACME.

Afin d'envisager un facteur de correction permettant de remettre les mesures faites au laboratoire ACME sur celles faites au LMV, pour les roches acides d'une part et pour les roches basique d'une autre part, il aurait été bon de choisir un basalte de référence moins appauvri, comme le BHVO-1 et le faire analyser plusieurs fois dans chaque laboratoire.

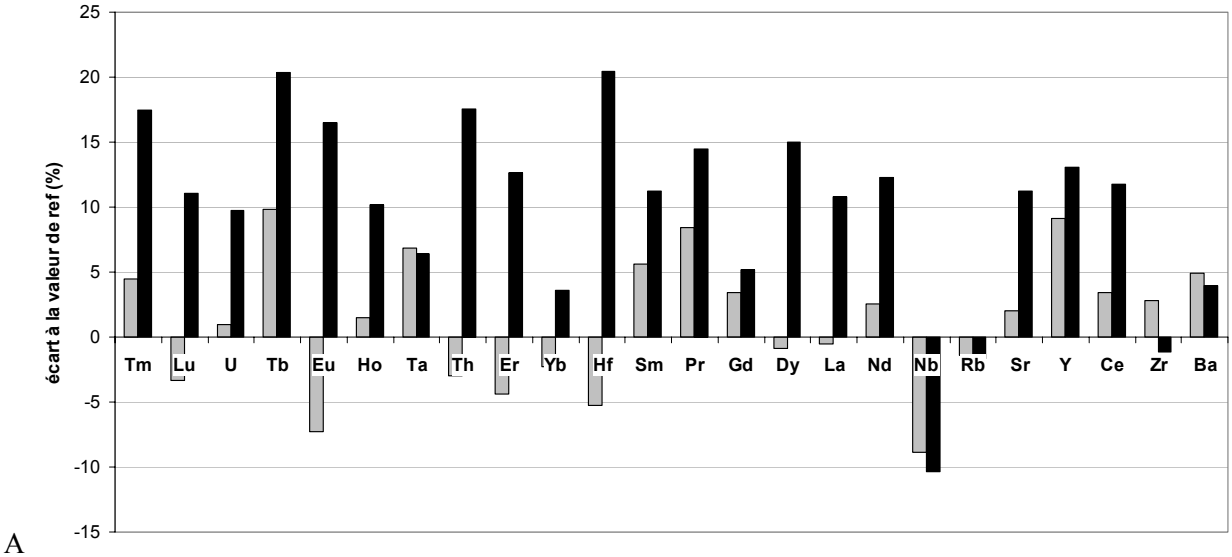

A

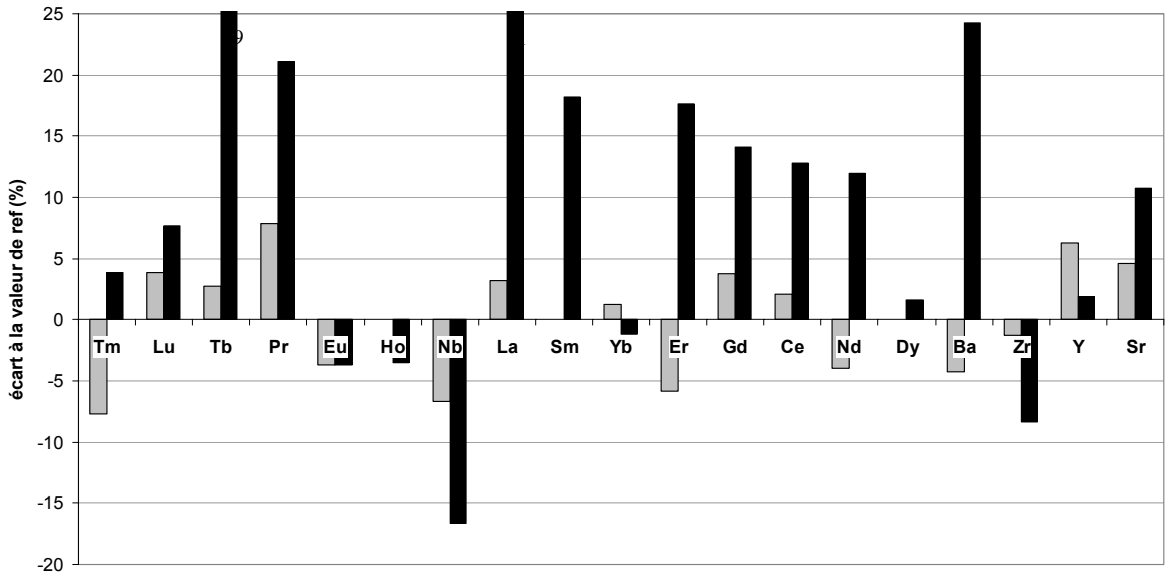

B

Figure 1 : Graphique permettant de comparer les teneurs mesurées au LMV (Clermont-Ferrand ; gris) et au laboratoire ACME (Vancouver ; noir). Les éléments sont classés par ordre de concentration dans le standard considéré. ***A*** *: A-THO ;* ***B*** *: BIR/B-THO.*

Annexe 3 : Protocole d'analyse de l'U et Th par dilution isotopique

Principe de la méthode

Afin d'obtenir, le plus précisément possible la concentration d'un élément dans un échantillon, on ajoute un traceur. Ce dernier est très enrichi en un isotope, peu abondant dans la nature, de l'élément considéré (spike de concentration connue). Afin de minimiser les erreurs sur les rapports U/Th mesurés, on utilise un traceur mixte très enrichi en ^{235}U et ^{230}Th (0.3537ppm de ^{235}U, 0.7827ppm de ^{230}Th soit un ^{238}U/^{235}U de 0.05764 et un de ^{232}Th/^{230}Th de 0.1949. Par spectrométrie de masse, on mesure un rapport isotopique de l'élément choisit (pour l'U : ^{235}U/^{238}U et pour le Th : ^{230}Th/^{232}Th). Les teneurs en U et Th sont alors calculées en appliquant la formule de la dilution isotopique (exemple pour les teneurs en Uranium):

$$\left[^{238}U\right]_{Ech} = \frac{238}{235} \times \frac{\left[^{235}U\right]_T . m_T}{m_{Ech}} \times \frac{1 - \left(\frac{^{238}U}{^{235}U}\right)_T . \left(\frac{^{235}U}{^{238}U}\right)_{Mes}}{\left(\frac{^{235}U}{^{238}U}\right)_{Mes} - \left(\frac{^{235}U}{^{238}U}\right)_{Ech}}$$

m_T et m_{Ech} : masses de traceur et d'échantillon mesurés.

$\left[^{235}U\right]_T$ et $\left(\frac{^{238}U}{^{235}U}\right)_T$: concentration de 235U et rapport isotopique d'U dans le traceur.

$\left(\frac{^{235}U}{^{238}U}\right)_{Ech}$: rapport isotopique dans l'échantillon (=1/137,88).

$\left(\frac{^{235}U}{^{238}U}\right)_{Mes}$: rapport isotopique mesuré avec le spectromètre de masse.

Connaissant l'abondance isotopique naturelle de ^{238}U (99,2742%) et du ^{232}Th (considéré égale à 100%), il est facile de convertir les concentrations isotopiques précédemment calculées en concentrations élémentaires (U et Th). De même qu'il est possible de convertir le rapport de teneurs U/Th en rapport d'activités en suivant la relation suivante :

$$(^{238}\text{U}/^{232}\text{Th}) = 3{,}056 \times {}^{238}\text{U}/^{232}\text{Th} = 3{,}034 \times \text{U/Th}$$

Attaque acide

Le protocole suivant est calibré pour 100 mg d'échantillon :

- Ajouter le traceur mixte à l'échantillon dans un bécher en téflon.
- Attaque par 0,5 mL de $HClO_4$, 1 mL HCl (6M) et 2 mL HF (50%) à 60°C dans le bécher fermé jusqu'à obtention d'une solution limpide.
- Evaporer à 60°C jusqu'à évaporation de l' $HClO_4$.
- Ajouter de 2 mL l'H_3BO_3 et laisser agir à 60°C dans le bécher fermé jusqu'à obtention d'une solution limpide.
- Evaporer à sec.
- Reprendre avec 1 mL de HCl (6M).
- Attaque en bombe.
- Evaporer à sec.
- Reprendre dans 1 mL de HNO_3 (7M).
- Evaporer à sec.
- L'échantillon est finalement repris dans 1 mL de HNO_3 (7M) puis centrifuger afin de ne conserver que la partie parfaitement limpide.

Séparation

Afin de séparer le Th et l'U, les colonnes 5 mL AG1X8 dans un premier temps puis afin de parfaitement purifier la fraction Th-U les colonnes 1 mL AG1X8 ont été utilisées.

- 5 mL AGX8 :
- Resédimenter en H_2O et laver les colonnes avec un réservoir de HNO_3 (1M).
- Préconditionner les colonnes avec 2x3 mL de HNO_3 (7M).
- Charger l'échantillon repris dans 1 mL de HNO_3 (7N).
- Rincer les colonnes avec 2x2 mL puis 4 mL de HNO_3 (7N).
- Récupérer l'U avec 6 mL d'H_2O dans le bécher d'attaque.
- Récupérer dans le même bécher le Th avec 6 mL de HCl (6M).
- Evaporer à sec les solutions contenant le Th et l'U.
- 1 mL AGX8 :
- Resédimenter en H_2O et laver les colonnes avec un réservoir de HNO_3 (1M).
- Préconditionner les colonnes avec 2x1 mL de HNO_3 (7M).
- Charger la fraction de Th et d'U repris dans 300 µL de HNO_3 (7N).
- Rincer les colonnes avec 2x1 mL de HNO_3 (7N).

- Récupérer l'U avec 2 mL d'H_2O dans le bécher d'attaque.
- Récupérer dans le même bécher le Th avec 2 mL de HCl (6M).
- Evaporer à sec les solutions contenant le Th et l'U.

Dépôt sur filament

En vue d'un passage sur le spectromètre de masse CAMECA TSN 206:

- La fraction de Th et d'U est reprise dans 5 µL de HCl (3M).
- Des filaments triples en Rhénium sont utilisés et 1,25 µL de la fraction précédemment reprise est chargé sur chaque filament latéral.

Spectromètre de masse

Le spectromètre utilisé est un CAMECA TSN 206. A température croissante, les teneurs en U et Th (sous forme métal ou oxyde) sont successivement mesurées. Le passage de plusieurs dupliqués ont permis d'établir l'erreur externe maximum de la machine qui est de 0,5 % (2σ) pour les deux éléments considéré. Enfin le passage régulier du standard A-THO (Jochum et al., 2006) permet de vérifier la qualité et la reproductibilité des mesures faites ainsi que de la fiabilité du traceur mixte utilisé. Les valeurs de A-THO obtenues au cours de cette étude (5 passages) sont de U=2,236 ± 0,0047 (2σ) et Th=7,47 ± 0,01 (2σ).

Annexe 4 : Protocole d'analyse des rapports isotopiques de l'oxygène, du strontium et du néodyme

Mesure du $\delta^{18}O$

Les mesures ont été faites au laboratoire « Géosciences Rennes » sous la tutelle de Serge Fourcade.

Principe de la méthode

L'oxygène est extrait de la roche grâce à une attaque de cette dernière par du penta fluorure de brome (BrF_5). Une fois extrait, les isotopes de l'oxygène sont mesurés sur un spectromètre de masse. Enfin, le rapport d'isotope $^{18}O/^{16}O$ est exprimé sous la forme de $\delta^{18}O$, de la façon suivante

$$\delta^{18}O = \frac{\left(^{18}O/_{16}O\right)_{échantillon} - \left(^{18}O/_{16}O\right)_{SMOW}}{\left(^{18}O/_{16}O\right)_{SMOW}} \times 1000$$

Formule utilisée pour calculer le $\delta^{18}O$ (‰) d'un échantillon. SMOW=Standard Mean Ocean Water.

Extraction

Les isotopes de l'oxygène ont été analysés sur des poudres de roches totales (5 à 10 mg). Les échantillons ont été attaqués selon la méthode de (Clayton and Mayeda, 1963) dans des tubes de nickel mis sous pression de BrF_5 à 680°C pendant une nuit. Le O_2 est alors extrait de la roche, il sera ensuite purifié puis converti en CO_2 par le biais d'une barre en graphite chauffée et disposée dans une chambre dite de conversion. L'oxygène est finalement piégé en fin de ligne sous la forme CO_2 dans une ampoule qui sera ensuite directement fixée sur le spectromètre de masse.

Spectromètre de Masse

Le rapport d'isotope $^{18}O/^{16}O$ est alors mesuré à partir du gaz CO_2 extrait précédemment sur un spectromètre de masse VG SIRA 10 dual inlet instrument. Le standard NBS-28 (qui suit toute la procédure au même titre que les échantillons) est utilisé afin de calibrer l'ensemble de la procédure. Ce standard international est attaqué dans des tubes différents à chaque fois afin d'intégrer l'erreur due au choix du tube de nickel pour l'attaque de tel ou tel échantillon. Au cours de cette étude, la valeur du $\delta^{18}O$ pour le NBS-28 mesuré à été de 9,36 ±0,07‰ (2σ ; n=5). Enfin toutes les mesures, sont normalisées à une valeur du NBS-28 de 9,6‰. Le

standard Circé 93 (verre basaltique de MORB; qui n'est pas un standard international mais qui permet un suivit, à long terme, de la procédure) est passé au cours de ces séries afin de s'assurer de la calibration de la procédure.

L'erreur externe de l'ensemble de la procédure (extraction + mesure au spectromètre de masse) a été établit à partir de duplicata. Tous les échantillons ont été analysés 2 fois et la valeur moyenne de cette erreur externe est de 0,07‰ avec une valeur maximale de 0,15‰.

Mesure de $^{86}Sr/^{88}Sr$ et $^{146}Nd/^{144}Nd$.

Principe de la méthode

La séparation du Sr et Nd se fait à partir d'une même attaque, par une méthode de chromatographie sur résine échangeuse d'ions. 100 à 150 mg d'échantillon en poudre sont attaqué selon la teneur en Sr et Nd. Il est nécessaire d'utiliser 150 mg si la concentration en Sr ou Nd est inférieure à 20 ppm.

Attaque acide

Le protocole suivant est calibré pour 100 mg d'échantillon :

- Attaque par 1 mL de $HNO_{3con.}$ et 2 mL de HF (29M) à 50-70°C pendant 24h dans un bécher en téflon fermé.
- Ajouter 2 mL de HNO_3 (7M) et 200 µL de $HClO_4$ après l'ouverture du bécher.
- Evaporer à sec.
- Reprendre avec 5 mL de HCl (6M) à 50-70°C jusqu'à obtenir une solution parfaitement limpide.
- Attaque en bombe.
- Evaporer à sec.
- Reprendre avec 1 mL de $HNO_{3con.}$.
- Evaporer à sec.
- L'échantillon est finalement repris dans 1,5 mL de HNO_3 (2M) (ou 2 mL de HCl (1,25M) si passage sur colonnes AG50X4) puis centrifugé afin de ne conserver que la partie la plus limpide. Si besoin est, le gel résiduel peut être attaqué à l'H_3BO_3 afin de tout parfaitement mettre en solution.

Séparation

Pour les échantillons les plus riches en fer, un passage sur colonnes AG50X4 (2mL) a été effectué.

- Resédimenter et laver les colonnes.
- Préconditionner les colonnes avec 2 x 2 mL de HCl (1,25M).
- Charger l'échantillon repris dans 2mL de HCl (1,25M).
- Rincer les colonnes avec 0,5 mL suivit de 3 à 6 mL de HCl (1,25M).
- Récupérer dans le bécher d'attaque, les TR avec 2 x 2,5 mL de HNO_3 (5M) / HF (0,1M).
- Evaporer à sec.

Afin se séparer le Sr et les Terres Rares (TR), les colonnes Sr-Spec, qui ne retiennent que le Barium et le Strontium et les colonnes TRU-Spec, qui ne retiennent que les TR et l'Uranium (U) ont été utilisées (Pin et al., 1994).

- Resédimenter et laver les colonnes avec un réservoir de HNO_3 (0,05M).
- Préconditionner les colonnes avec 2 x 0,5 mL de HNO_3 (2M).
- Mettre les colonnes Sr-Spec au dessus des TRU-Spec.
- Charger l'échantillon repris dans 1,5 mL de HNO_3 (2M) en 3 x 0,5 mL.
- Rincer des colonnes avec 2 x 0,5 mL de HNO_3 (2M).
- Séparer des colonnes
- Récupérer le Sr avec 2 mL de HNO_3 (0,05M), après avoir passé 3 mL de HNO_3 (7M) puis 0.5 mL de HNO_3 (2M) sur les colonnes Sr-Spec.
- Récupérer les TR avec 2 mL de HNO_3 (0,05M), après avoir passé 3 mL de HNO_3 (2M) sur les colonnes TRU-Spec.
- Evaporer à sec les solutions contenant le Sr et de celles contenant les TR.

Afin de séparer le Nd des TR préalablement séparés, les colonnes Ln-Spec (360 mg) ont été utilisées.

- Préconditionner les colonnes avec 3 x 100 µL (0,25M) sur les colonnes TRU-Spec.
- Charger la fraction de TR reprise dans 100 µL de HCl (0,25M).
- Rincer les colonnes avec 2 x 100 µL (afin de bien reprendre toute la fraction de TR) puis avec 2,9 mL de HCl (0,25M).

- Récupérer le Nd avec 2,5 mL de HCl (0,25M).
- Evaporer à sec.

Dépôt sur filament

En vue d'un passage sur le spectromètre de masse Thermo-Finnigan TRITON :

- Charger 0,5 µg de Sr (repris dans de l'eau acidulée) avec une goûte de H_3PO_4 (3M) préalablement déposée sur un filament de tungstène.
- Charger 0,5 µg de Nd (repris dans de l'eau acidulée) avec une goûte de H_3PO_4 (1M) préalablement déposée sur un filament de tungstène.

Spectromètre de masse

Le spectromètre utilisé est un Thermo-Finnigan TRITON. Pour chaque échantillon deux filaments sont utilisés. Le dépôt de Sr ou de Nd sur le premier et le second sera l'ionisateur.

Mesure de $^{87}Sr/^{86}Sr$ et $^{143}Nd/^{144}Nd$: Les corrections de fractionnement de masse ont été faite en prenant les rapports suivant $^{86}Sr/^{88}Sr = 0,1194$ et $^{146}Nd/^{144}Nd= 0,7219$. Les standards NBS987 (pour le $^{87}Sr/^{86}Sr$) et AMES (pour le $^{146}Nd/^{144}Nd$) sont passé en début et en fin de chaque session d'analyse afin de s'assurer de la reproductibilité des analyses faites au cours de chacune d'elle. Les valeurs moyennes obtenues au cours de cette étude pour le NBS987 et le AMES sont respectivement de 0,710258 ± 5,9 (2σ ; n=8) et 0,511960 ± 3,5 (2σ ; n=9). Les valeurs obtenues pour chaque échantillon ont été normalisées par rapport aux valeurs admises des standards qui sont de 0,71025 et 0,51197 pour le NBS987 et le AMES respectivement. Le passage de plusieurs dupliqués ont permis d'établir l'erreur externe de la machine qui est de l'ordre de 2.10^{-5} (2σ) pour les mesures de $^{87}Sr/^{86}Sr$ et $^{143}Nd/^{144}Nd$.

Annexe 5 : Attaque en bombe

Principe de la méthode

Lors de cette étude les roches analysées (essentiellement les roches acides), contiennent plus ou moins des minéraux accessoires tels que le zircon. Ces derniers résistent à une attaque acide classique telles celles utilisées pour mesurer les teneurs en U-Th et les rapports isotopiques du Sr et Nd. Afin de dissoudre intégralement ces minéraux résiduels, on les attaque à l'HF au sein d'une bombe en téflon. Cette méthode, conditionne ces minéraux sous pression (quelques bars) de vapeur d'HF à haute température (210-230°C).

Attaque acide

- Centrifuger la solution souhaitée (échantillon en HCl 6M) afin de ne conserver que la fraction non dissoute.
- Dans des petits piluliers en téflon, reprendre cette fraction résiduelle avec 25 µL de $HNO_{3conc.}$ et 100 µL de HF (29M).
- Remplir le fond de la bombe avec 5 mL de HF (29M).
- Mettre la bombe dans une étuve à 210-230°C pendant 30h.
- Sortir la bombe de l'étuve et laisser refroidir complètement.
- Verser 20 µL de $HClO_4$ dans les piluliers.
- Evaporer à sec
- Reprendre la fraction sèche avec le même acide (HCl 6M) que celui dans lequel baigne tout le reste de la solution dans le bécher d'attaque.

Annexe 6 : Datations Ar-Ar et U-Th-Pb

Méthodes utilisées

Une collaboration avec Valérie Bosse (LMV de Clermont Ferrand) et Gilles Ruffet (laboratoire « Géosciences Rennes ») a été établie afin de dater les échantillons par la méthode Ar-Ar sur roches totales. De même une collaboration avec Jean Louis Paquette (LMV de Clermont Ferrand) et de Massimo Tiepolo (CNR de Pavi) a également été initiée afin de dater les zircons contenus dans les roches de l'Est de l'Islande par la méthode U-Th-Pb.

Voici un tableau résumant les données obtenues :

Echantillon	Age (en Ma)	Méthode utilisée
Thd2	1.49 ±0.11	
Thd3	1.72 ±0.04	
Setb1	5.20 ±0.08	
Setb3	5.27 ±0.18	
Bau1	3.55 ±0.03	Ar-Ar (±1σ)
Fró1	4.95 ±0.09	
Drap2	6.79 ±0.07	
Bh1a	2.22 ±0.13	
Axl1	4.69 ±0.07	
Ves 2	3.7±0.1	
Ves1	3.9±0.1	
Hval1a	7.0±0.4	
Hval2	6.5±0.1	
Beruf1	9.3±0.4	U-Pb (±2σ) sur zircon
Streit1a	10.7±0.2	
Hus1	13.1 ±0.2	
Ref1	13.1±0.3	
Hvs2	12.5	

La méthode Ar-Ar

Les spectres d'âge présentés ci-dessus ont été obtenus sur des fragments de roches totales soigneusement triés pour éliminer les phénocristaux. Les échantillons ont été irradiés au sein du réacteur nucléaire McMaster (Hamilton, Canada) en position 5 C. L'échantillon moniteur utilisé est une sanidine (ACs-2) dont l'âge est 1.186 ± 0.006 Ma.

Les analyses ont été ensuite effectuées sur une ligne d'extraction équipée d'un laser CO_2 Synrad et connectée au spectromètre de masse en phase gazeuse (MAP215). La procédure de chauffage s'effectue par paliers de température successifs (Ruffet et al., 1995; Ruffet et al., 1997). Les blancs sont mesurés tous les 3 paliers et soustraits des fractions de gaz analysées.

Les âges plateaux sont indiqués à 1 σ et définis pour au moins trois étapes successives représentant au minimum 70% de l'^{39}Ar dégazé et concordantes avec l'âge intégré du segment de plateau considéré.

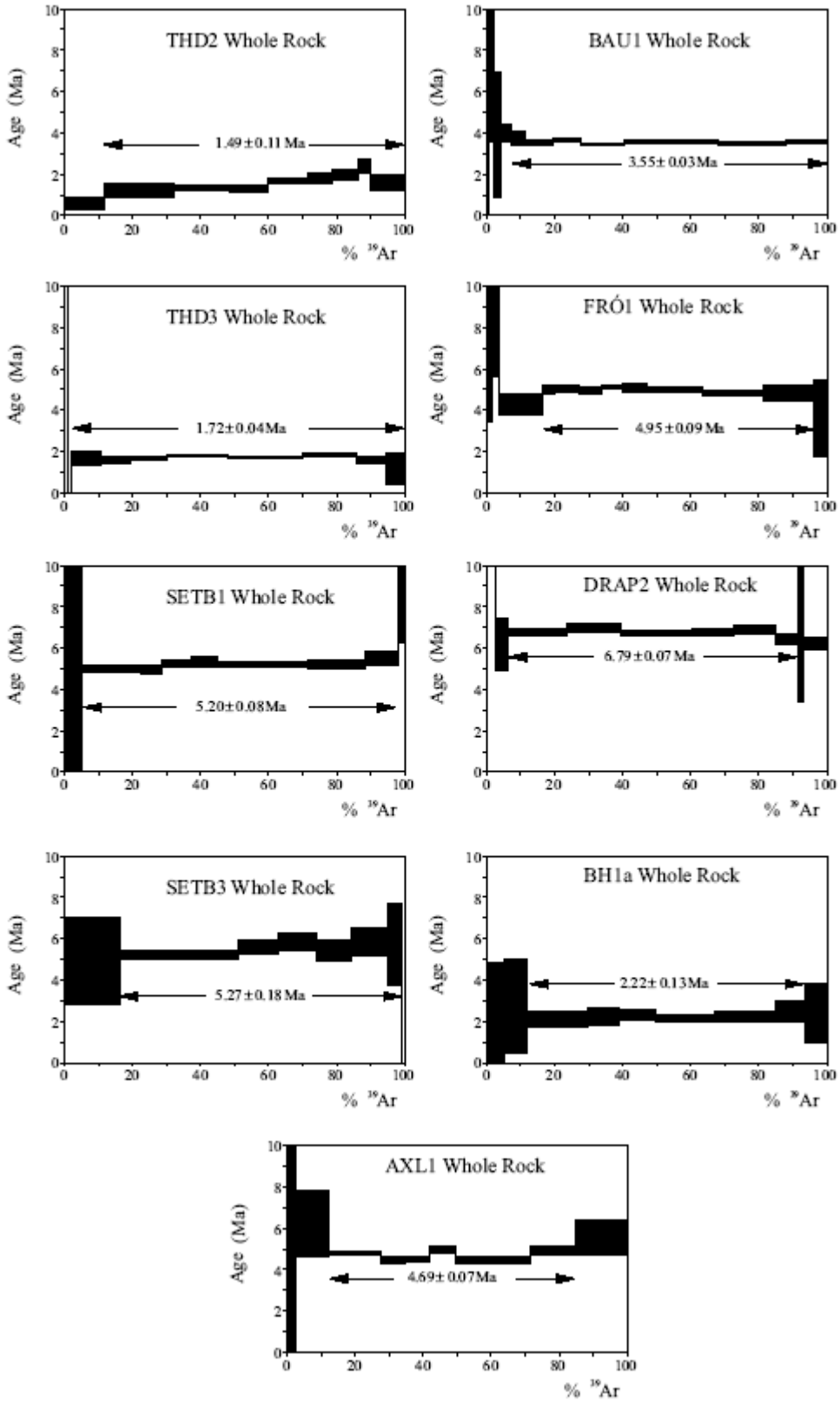
THD2 Whole Rock
1.49±0.11 Ma
BAU1 Whole Rock
3.55±0.03Ma
THD3 Whole Rock
1.72±0.04Ma
FRÓ1 Whole Rock
4.95±0.09 Ma
SETB1 Whole Rock
5.20±0.08Ma
DRAP2 Whole Rock
6.79±0.07 Ma
SETB3 Whole Rock
5.27±0.18 Ma
BH1a Whole Rock
2.22±0.13Ma
AXL1 Whole Rock
4.69±0.07Ma
Age (Ma)
% 39Ar

La méthode U-Th-Pb

Les datations U-Th-Pb ont été réalisées grâce à un dispositif d'ablation laser Compex Microlas Excimer ArF de longueur d'onde 193 nm (Günter et al., 1997) couplé à un ICP-MS haute résolution Element II de Thermo-Finnigan. Afin d'optimiser le rapport signal/bruit de fond dans des zircons récents, un diamètre de faisceau de 50µm a été choisi pour cette étude. Pour les mesures de géochronologie, l'appareil est configuré en basse résolution. L'alignement et la calibration de l'appareil avant analyse sont réalisés avec le verre de référence NIST 610. L'acquisition des mesures est effectuée selon Tiepolo (2003). Les masses 202Hg, 204(Pb+Hg), 206Pb, 207Pb, 208Pb 232Th et 238U sont mesurées successivement, chaque balayage durant approximativement 165 ms. La mesure de 202Hg permet de corriger l'interférence isobarique de 204Hg sur 204Pb et ainsi de pouvoir estimer la présence de Pb commun. Le signal de ^{235}U est calculé à partir de ^{238}U sur la base du rapport $^{238}U/^{235}U= 137.88$. Chaque analyse consiste en une mesure du bruit de fond durant 1 min suivie par environ 30 s d'ablation. Afin d'assurer des mesures justes et précises, les effets du fractionnements sont corrigés par standardisation externe (Jackson et al., 2004) en utilisant le standard 91500 (Wiedenbeck et al ., 1995) par séries de 4 mesures de standards encadrant 10 inconnus. La réduction des données est effectuée par le logiciel GLITTER® (Macquarie Research Ltd, 2001) et les âges sont calculés avec Isoplot/Ex 2.49 (Ludwig, 2001).

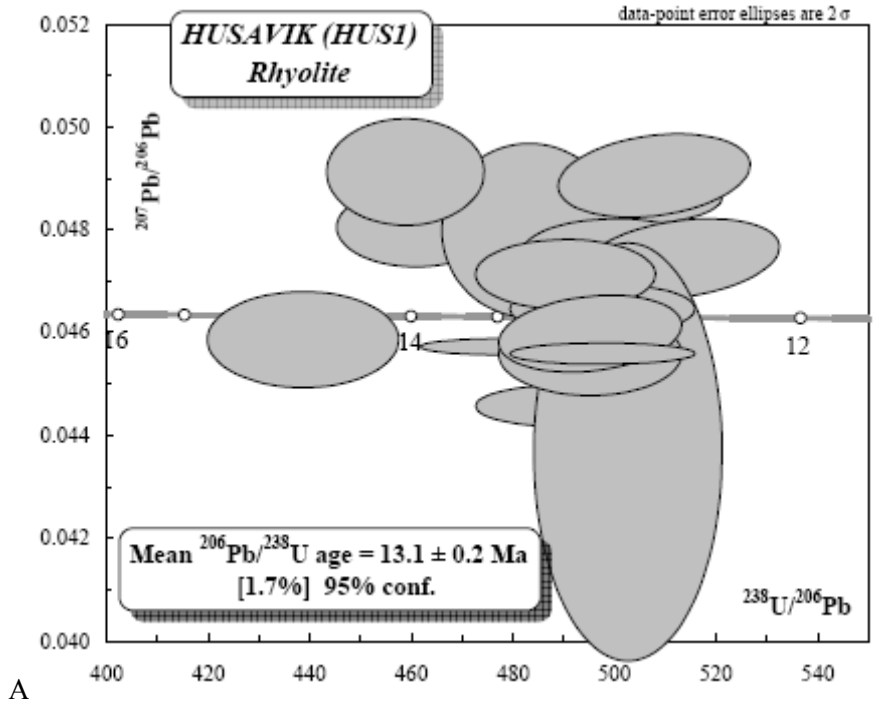

A

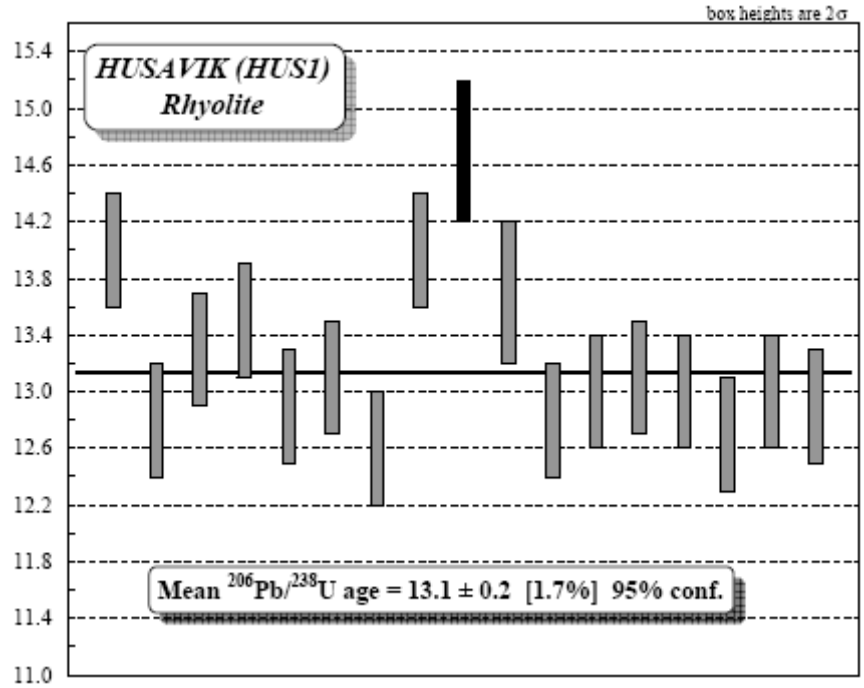

B

Les âges U-Th-Pb peuvent être présentés sous la forme de concordia (A) ou d'histogramme de fréquence (B).

Annexe 7 : Photos de terrain

Deux campagnes de terrain ont été effectuées pour l'échantillonnage de cette thèse. La première s'est déroulée en Août 2004 dans la partie Ouest et Sud de l'Islande alors que la seconde expédition s'est faite en Août 2005 et a consisté en l'échantillonnage de l'Est de l'île.

Dôme rhyolitique de Baula.

Hrafntinnusker :

les géologues face à l'immensité de leur rationalisme.

Torfajökull vu du Mont Hrafntinnusker.

Dôme de Laufafell surmonté de sa coulée d'obsidienne.

Dyke rhyolitique de Setberg… Merci Benji pour l'échelle.

Campement dans le petit fjord de Husavik où à été prélevé l'échantillon Hus1.

Mont de Hvítserkur (Hvs2) entrecoupé de ses dykes basaltiques (Hvs1).

Virkisvík :

Coulée basaltique Búr4 surmontant l'ignimbrite de Búr.

Dyke rhyolitique (Streit1a) et ses enclaves basiques (Streit1b) de Streitishvarf.

« Net-veined complex » de Hvalnesskriður. Granophyre trachytique (Hval1a) contenant de nombreuses enclaves basiques (Hval 1b).

Gabbro de Hvalnesviti (Hval2).

Intrusion de Vesturhorhn où ont été prélevés Ves1 et Ves2.

Ces campagnes de terrain n'auraient jamais pu aussi bien se passer sans la présence des personnes et des ambiances suivantes.

Gudrun Larsen et Bergrún Óladóttir au campement près de Hrafntinnusker.

Kristján Geirsson revient sur son terrain de thèse afin de nous guider quelques jours.

Diner sur table et chaises taillées à même le gabbro bourré de zircon, au grand bonheur des géochronologues Valérie Bosse et Jean Louis Paquette.

Encore un p'tit café à l'arrière du 4x4 de Thor Thordarsson.

« Ye er Vikingur !!! »

Voici à quoi doit se livrer une étudiante Islandaise pour se faire respecter de l'un de ses supérieurs.

Enfin, voici ce que la beauté de l'Islande peut nous infliger.

Résumé

Une approche principalement géochimique élémentaire (éléments majeurs et en trace) et isotopique ($^{87}Sr/^{86}Sr$, $^{143}Nd/^{144}Nd$ et $\delta^{18}O$) a été menée afin de déterminer et de quantifier les mécanismes de genèse des magmas acides d'Islande. Ceci afin d'en discuter les implications quand à l'évolution géodynamique de l'île. Les résultats principaux de cette thèse sont les suivants :

Tout au long de l'histoire de l'Islande, la plupart des roches acides ont été engendrées par fusion de la croûte métabasaltique au niveau de la zone de rift, là où l'interaction du point chaud avec la ride médio-atlantique est la plus importante. En effet, de cette interaction résulte un gradient géothermique élevé, tel que le solidus de la croûte basaltique partiellement hydratée est franchi. Néanmoins, en périphérie de l'île (comme actuellement, dans la Péninsule de Snæfellsnes et dans le système volcanique d'Öræfajökull), loin du centre du panache mantellique et de la zone de rift, le gradient géothermique est plus faible, ne permettant plus de dépasser la température du solidus hydraté des métabasaltes. Une telle situation privilégie la formation de magma acide par cristallisation fractionnée (incluant éventuellement un faible taux d'assimilation crustale).

Ayant établi un lien entre la composition chimique des laves acides et l'environnement géodynamique de leur genèse, et à condition d'avoir déterminé leur âge, il est alors possible de procéder à une reconstitution de l'évolution géodynamique de l'Islande. Le modèle proposé se base sur le fait que la ride médio-Atlantique dérive relativement au centre du panache mantellique et sur un mécanisme d' « accrétion-recouvrement » qui explique le mieux la largeur anormalement élevée de l'île.

Enfin, à l'image de l'Islande, les plateaux océaniques, peuvent donner naissance à une quantité significative (jusqu'à 10%) de magma acide, c'est-à-dire d'un matériel potentiellement constitutif de la croûte continentale, et ce en domaine océanique. Une comparaison a été effectuée entre les compositions de ces roches « continentales » formées au sein des plateaux océaniques récents et celles de la croûte continentale primitive (TTG). Il en résulte que malgré un environnement thermique islandais proche de celui qui devait régner au début de l'histoire de la terre, les plateaux océaniques récents n'engendrent pas de magmas ayant la composition de la croûte continentale terrestre primitive. Il est alors conclu que les plateaux océaniques n'ont pas été un environnement géodynamique ayant pu jouer un rôle majeur dans la genèse de la croûte primitive et que le. « Modèle Islandais » n'est donc pas un analogue aux conditions de formation de la croûte continentale primitive.

Abstract

An elementary (major and trace elements) and isotopic ($^{87}Sr/^{86}Sr$, $^{143}Nd/^{144}Nd$ and $\delta^{18}O$) geochemical study has been achieved in order to determine and to quantify the petrogenetic mechanisms that gave rise to silicic magmas in Iceland. The target of this approach consists not only of understanding the genesis of these magmas but also in addressing their significance in terms of Iceland geodynamic evolution. The main results of this thesis are as follows:

In course of Iceland history, most of the silicic rocks appear to have been generated by partial melting of the hydrated metabasaltic crust in a rift zone environment. In this place, the interaction between hot spot and mid-oceanic ridge is important resulting in a geothermal gradient high enough to exceed the solidus temperature of the partially hydrated basaltic crust. However, at the periphery of the island (i.e. Snæfellsnes Peninsula and Öræfajökull volcanic system), far from both the mantle plume centre and the rift-zone, the geothermal gradient is lower, precluding to step over the solidus temperature of hydrated metabasalts. This situation favoured the genesis of silicic magmas by fractional crystallisation (with possibly slight crustal assimilation).

The link that exists between the composition of silicic rocks and the geodynamic environment of their genesis has been used together with age determination in order to establish the time-space geodynamic evolution of Iceland. The proposed model is based on the fact that mid-Atlantic ridge migrate relatively to the plume centre and on the "accretion - over lapping" mechanism that best accounts for the abnormally great width of Iceland.

Iceland demonstrates that oceanic plateaus can give rise to significant volumes (towards 10%) of silicic magmas; in other words, it can be a potential environment for continental crust genesis in a purely oceanic environment. A comparison between these "continental" rock compositions from recent oceanic plateaus and primitive continental crust one (TTG) shows that, in spite of the Icelandic high geothermal gradients, which are assumed to be similar to the early Earth ones, modern oceanic plateaus cannot generate magmas having the primitive continental crust composition. Thus, it is concluded that oceanic plateau environment has not played a significant role, in the primitive continental crust genesis. Consequently, the "Iceland model" is not a modern analogue of the environment where proto-continental crust formed.